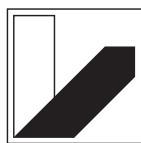


Dissertation

Construction Principles for Semilocal Density Functionals with Balanced Nonlocality

Timo Lebeda



**UNIVERSITÄT
BAYREUTH**

Construction Principles for Semilocal Density Functionals with Balanced Nonlocality

Von der Universität Bayreuth
zur Erlangung des Grades eines
Doktors der Naturwissenschaften (Dr. rer. nat.)
genehmigte Abhandlung

von

Timo Lebeda

aus Stuttgart

1. Gutachter: Prof. Dr. Stephan Kümmel
2. Gutachter: Prof. Dr. Johannes Margraf
3. Gutachter: Prof. Dr. Stefano Pittalis

Tag der Einreichung: 16. Dezember 2024

Tag des Kolloquiums: 11. Februar 2025

Abstract

The quest to understand nature and the search for new materials have always been at the heart of the natural sciences. Nowadays, the understanding of biological systems and the design of new materials is routinely guided, complemented or even made possible by computer simulations of their electronic structure. The aim of this thesis is to improve these computer simulations by improving the underlying theory. The central question we need to ask ourselves for this purpose is: What are the requirements for the computational method?

The electronic structure is determined by the laws of quantum mechanics. Biological systems are often large, and in order to find the best material for a given application, many candidate materials, often solids, have to be screened. Therefore, our computational method must be fast and capable of handling many electrons at once. In this setting, density functional theory is usually the method of choice.

For the practical application of density functional theory, one crucial approximation must be made that determines both the accuracy and the computational effort: the density functional approximation to the exchange-correlation energy. For the study of large biological systems or for high-throughput materials screening, only the computationally most efficient density functionals, the so-called semilocal functionals, are generally feasible.

Topical problems such as catalysis often exhibit surfaces or interfaces that require an accurate description of different types of systems, particularly of both molecules and solids. For charge separation in photocatalytic water splitting or in solar cells, the size of the band gap is of crucial importance. Weak interactions are often decisive for the stability of biological systems and layered materials, as well as for the binding of ligands to a surface. Consequently, we strive for a semilocal density functional with sufficient accuracy for molecules and solids, band gaps and energetic bonds, including weak bonds. Finding out what is crucial for a density functional to achieve this, and ultimately designing one that does so, is the quest of this thesis.

To this end, I first recall the relevant concepts of density functional theory: the fundamentals of density functional theory, the traditional semilocal density functionals and their limitations, and finally, why the class of orbital-dependent meta-Generalized Gradient Approximations (meta-GGAs) is suitable for the goal of this thesis (their orbital dependence is the key to describe nonlocal properties). Subsequently, I investigate which requirements a meta-GGA must fulfill in order to provide an accurate description of band gaps in the first step, of band gaps *and* energetic bonds in the second step, and third of weakly interacting systems.

First, I demonstrate that the orbital dependence of meta-GGAs is the key to predict the right band gaps for the right reason, that is, by including the derivative discontinuity with proper size. In the course of this study, I refine the construction principle for a sizeable derivative discontinuity in meta-GGAs. Next, in investigating what is required to combine accuracy for band gaps and energetic binding, I find that the construction principle for a sizeable derivative discontinuity leads to a strong repulsion between weakly interacting systems. Therefore, I next

investigate what is decisive for the description of weakly interacting systems with meta-GGAs. From this I deduce a second construction principle that ensures a proper description of the short- and intermediate-range Van der Waals interactions. Thus, I now have two construction principles that allow to control these two types of nonlocality in the density functional approximation.

To combine these findings in a new meta-GGA, I complement the established design strategy for nonempirical density functionals with the two construction principles for appropriate nonlocality and propose the design strategy of “enhancement factor engineering”. However, combining the two construction principles in a nonempirical meta-GGA contradicts the usual treatment of the gradient expansion for slowly varying densities. Consequently, I revisit the gradient expansion in meta-GGAs and demonstrate how a so far unexplored degree of freedom in the gradient expansion enables a more balanced treatment, and in particular the fulfillment of the two construction principles.

Finally, I combine all these insights, i.e., the construction principles for proper nonlocality, the design strategy of enhancement factor engineering, and the balanced treatment of the gradient expansion, to develop a nonempirical meta-GGA that combines state-of-the-art accuracy for band gaps, energetic bonding, and weak interactions at a very attractive computational cost.

Kurzdarstellung

Das Bestreben, die Natur zu verstehen, und die Suche nach neuen Materialien stehen schon immer im Mittelpunkt der Naturwissenschaften. Heutzutage wird das Verständnis biologischer Systeme und die Entwicklung neuer Materialien routinemäßig durch Computersimulationen ihrer elektronischen Struktur angeleitet, ergänzt oder sogar erst ermöglicht. Ziel der vorliegenden Arbeit ist es, diese Computersimulationen durch Verbesserung der zugrunde liegenden Theorie zu verbessern. Die zentrale Frage, die wir uns zu diesem Zweck stellen müssen, lautet: Was sind die Anforderungen an die rechnergestützte Berechnungsmethode?

Die elektronische Struktur wird durch die Gesetze der Quantenmechanik bestimmt. Biologische Systeme sind oft groß, und um das beste Material für eine bestimmte Anwendung zu finden, müssen viele in Frage kommende Materialien, oft Feststoffe, gescreent werden. Daher muss unsere rechnergestützte Methode schnell sein und viele Elektronen auf einmal behandeln können. In diesem Setting ist die Dichtefunktionaltheorie in der Regel die Methode der Wahl.

Für die praktische Anwendung der Dichtefunktionaltheorie muss eine entscheidende Näherung vorgenommen werden, die sowohl die Genauigkeit als auch den Rechenaufwand bestimmt: die Dichtefunktionalnäherung an die Austausch-Korrelationsenergie. Für die Untersuchung großer biologischer Systeme oder für das Hochdurchsatz-Screening von Materialien kommen in der Regel nur die rechnerisch effizientesten Dichtefunktionale, sogenannte semilokale Funktionale, in Frage.

Aktuelle Probleme wie die Katalyse weisen häufig Oberflächen oder Grenzflächen auf, die eine genaue Beschreibung verschiedener Systemtypen, insbesondere von Molekülen und Festkörpern, erfordern. Für die Ladungstrennung in der photokatalytischen Wasserspaltung oder in Solarzellen ist die Größe der Bandlücke von entscheidender Bedeutung. Schwache Wechselwirkungen sind oft entscheidend für die Stabilität biologischer Systeme und geschichteter Materialien, sowie für die Bindung von Liganden an eine Oberfläche. Daher streben wir nach einem semilokalen Dichtefunktional mit ausreichender Genauigkeit für Moleküle und Festkörper, Bandlücken und energetische Bindungen, einschließlich schwacher Bindungen. Herauszufinden, was für ein Dichtefunktional entscheidend ist, um dies zu erreichen, und schließlich ein Funktional zu entwerfen, das dies tut, ist das Ziel dieser Dissertation.

Zu diesem Zweck rufe ich zunächst die dafür relevanten Konzepte der Dichtefunktionaltheorie in Erinnerung: die Grundlagen der Dichtefunktionaltheorie, die traditionellen semilokalen Dichtefunktionale und wann sie an ihre Grenzen kommen, und schließlich, warum die Klasse der orbitalabhängigen *meta-Generalized Gradient Approximations* (meta-GGAs) für das Ziel dieser Dissertation geeignet ist. Anschließend untersuche ich, welche Anforderungen ein meta-GGA erfüllen muss, um eine genaue Beschreibung von Bandlücken im ersten Schritt, von Bandlücken *und* energetischen Bindungen im zweiten Schritt und drittens von schwach wechselwirkenden Systemen zu ermöglichen.

Zunächst zeige ich, dass die Orbitalabhängigkeit von meta-GGAs der Schlüssel zur Vorhersage der richtigen Bandlücken aus dem richtigen Grund ist, nämlich durch Einbeziehung der sogenannten *derivative discontinuity* mit der richtigen Größe. Im Rahmen dieser Untersuchung verfeinere ich das Konstruktionsprinzip für eine große *derivative discontinuity* in meta-GGAs. Im nächsten Schritt, der Untersuchung der Voraussetzung für die Kombination von Genauigkeit für Bandlücken und energetische Bindungen, stelle ich fest, dass das Konstruktionsprinzip für eine beträchtliche *derivative discontinuity* zu einer starken Abstoßung zwischen schwach wechselwirkenden Systemen führt. Daher untersuche ich als nächstes, wie meta-GGAs eine Beschreibung schwach wechselwirkender Systeme ermöglichen können. Daraus leite ich ein zweites Konstruktionsprinzip ab, das eine korrekte Beschreibung der Van-der-Waals Wechselwirkungen im Nah- und Mittelbereich gewährleistet. Somit habe ich nun zwei Konstruktionsprinzipien, die es ermöglichen, diese beiden Arten von Nichtlokalität in der Dichtefunktionalnäherung zu kontrollieren.

Um diese Erkenntnisse in einem neuen meta-GGA zu kombinieren, ergänze ich die etablierte Konstruktionsstrategie für nicht-empirische Dichtefunktionale um die beiden Konstruktionsprinzipien für geeignete Nichtlokalität und schlage die Konstruktionsstrategie des “enhancement factor engineering” vor. Allerdings steht die Kombination der beiden oben genannten Konstruktionsprinzipien in einem nicht-empirischen meta-GGA im Widerspruch zur üblichen Behandlung der Gradientenentwicklung für langsam veränderliche Dichten. Daher überprüfe ich die Gradientenentwicklung in meta-GGAs und zeige, wie ein bisher unerforschter Freiheitsgrad in der Gradientenentwicklung eine ausgewogenere Behandlung ermöglicht, sowie insbesondere die Erfüllung der beiden Konstruktionsprinzipien.

Schließlich kombiniere ich all diese Erkenntnisse, d.h. die Konstruktionsprinzipien für angemessene Nichtlokalität, die Konstruktionsstrategie des enhancement factor engineering und die ausbalancierte Behandlung der Gradientenentwicklung, um ein nicht-empirisches meta-GGA zu entwickeln, das modernste Genauigkeit für Bandlücken, energetische Bindung und schwache Wechselwirkungen zu sehr attraktiven Rechenkosten vereint.

Contents

Abstract	v
Kurzdarstellung	vii
1 Introduction	1
I Concepts of Density Functional Theory	5
2 Fundamentals of Density Functional Theory	7
3 Traditional Semilocal Functionals	11
3.1 Local Density Approximation	11
3.2 Generalized Gradient Approximation	11
3.3 Limitations of LDA and GGA	12
3.3.1 Self-Interaction	12
3.3.2 Derivative Discontinuity	13
3.3.3 Consequences	14
4 Orbital-Dependent Semilocal Functionals	19
4.1 Meta-Generalized Gradient Approximations	19
4.2 Different treatments of meta-GGAs	20
4.2.1 The Optimized Effective Potential and the Krieger-Li-Iafrate Approximation	21
4.2.2 Generalized Kohn-Sham schemes	22
4.3 Ultranonlocality from meta-GGAs	25
II A Guide for the Publications	27
5 Towards combined Accuracy for Band Gaps and Energetic Bonds from meta-GGAs	29
5.1 Accurate Band Gaps for the Right Reason	30
5.2 Accurate Band Gaps and Improved Energetic Bonds	32
5.3 Understanding van der Waals Interactions in meta-GGAs	34
5.4 Enhancement Factor Engineering: Density Functionals based on Insights from Mathematics, Physics, and Chemistry	38

5.5	The General Form of the Gradient Expansion for Meta-GGAs	40
6	A new meta-GGA that combines Accuracy for Band Gaps and Energetic Bonds	43
	Bibliography	47
	List of Publications	63
III	Publications	65
	Publication 1	
	Right band gaps for the right reason at low computational cost with a meta-GGA	67
	Publication 2	
	Exact exchange-like electric response from a meta-generalized gradient approximation: A semilocal realization of ultranonlocality	89
	Publication 3	
	First steps towards achieving both ultranonlocality and a reliable description of electronic binding in a meta-generalized gradient approximation	105
	Publication 4	
	A meta-Generalized Gradient Approximation that describes weak interactions in addition to bond energies and band gaps	123
	Publication 5	
	Balancing the Contributions to the Gradient Expansion: Accurate Binding and Band Gaps with a Nonempirical Meta-GGA	141
	Acknowledgments	171
	Eidesstattliche Versicherung	173

CHAPTER 1

Introduction

It is generally accepted that our planet earth is heating up and that we as humans need to take action to keep this global warming in a manageable range [ipc23]. The main driver of global warming is the release of greenhouse gases from the consumption of fossil fuels to generate heat and electricity. To reduce the consumption of fossil fuels, we need to generate more heat and electricity from renewable sources, e.g., through more efficient solar cells, and reduce our consumption of heat and energy, especially in industrial processes.

The key to increasing the efficiency of solar cells and industrial catalysis or the capacity of batteries for storing “green” energy, are novel materials that are specifically designed for their respective purpose [KLJ⁺20, HYB⁺20, SD21, DV21, ESL⁺22]. Just as important as efficiency is the search for cheaper and more sustainable materials that can replace critical ingredients such as lithium [NYBA18, HL19, CMDN20] or lead [ZHL⁺18]. Nowadays, new materials, including the above mentioned so-called energy materials, are often predicted computationally using a combination of high-throughput materials screening and advanced computational quantum mechanical simulations [LCdJ⁺21, RZ22]. Both of these steps require methods that combine high computational efficiency with sufficient accuracy.

Consequently, the subject of the present thesis is the fundamental validation and improvement of existing computational methods, and ultimately the introduction of a new method, all of which aim to provide sufficient accuracy for many important applications at a very attractive computational cost. While the present thesis is therefore mainly concerned with the rather abstract development of new computational methods in the field of quantum mechanics, the resulting methods are already available [SCM24a, SCM24b, LSOM24] in large program packages for large-scale simulations and material predictions or will be available with the next release [VAS24, SCM25].

Due to its favorable balance between accuracy and computational cost, Density Functional Theory (DFT) has become very popular for electronic structure calculations. Fundamentally based on the Hohenberg-Kohn theorem [HK64] and widely applicable through the Kohn-Sham formalism [KS65], DFT circumvents the enormous numerical effort necessary for solving the many-body Schrödinger equation directly. In particular for these achievements, Walter Kohn was awarded his share of the Nobel prize in 1998 [Koh99]. Instead of the many-body wavefunction, DFT is based on the electronic density as its main variable.

Although DFT is exact in principle, a crucial approximation must be made in practical DFT calculations, namely for the so-called exchange-correlation energy as a functional of the

electronic density. Already the earliest and simplest Density Functional Approximations (DFAs), the Local Density Approximation (LDA) [HK64] and the Generalized Gradient Approximation (GGA) [Bec86, PY86] showed great success in solid state physics and chemistry. However, these computationally very efficient approximations have well-known limitations, see, e.g., Ref. [KK08]. A particularly profound limitation is that these traditional semilocal DFAs are unable to predict properties that require so-called ultranonlocality, e.g., the band gaps of solids, for fundamental reasons [PL83, SS83, SS85, Per85], as we discuss in detail in Chapter 3.

Historically, this shortcoming of the traditional semilocal density functionals was first addressed by applying so-called self-interaction corrections [Per79, PZ81]. While these substantially improve over LDA and GGA for ultranonlocal properties [PZ81], self-interaction corrected density functionals come at a significantly increased computational cost [PRSP15] and are often hampered by their limited accuracy for chemical bonds [VS04]. More successful in this regard was the mixing of semilocal DFAs with a fraction of so-called exact exchange, the DFT equivalent of the Fock energy, which led to the class of hybrid functionals [Bec93a, Bec93b] (see also Ref. [KK08]). However, the evaluation of the exact exchange energy is, especially for large or periodic systems, even more computationally demanding. Therefore, computationally cheaper ways to include a proper description of ultranonlocality are strongly desirable. On-top empirical methods can achieve this in certain cases [Kul15]. However, a nonempirical density functional would offer much more reliability and transferability [GCDV24].

Although they have been around for over 35 years [Bec88], only the last decade has shown that the class of meta-Generalized Gradient Approximations (meta-GGAs) can provide the required ultranonlocality [YPSP16, PYB⁺17, AK19, KBM23]. In addition, meta-GGAs offer another type of nonlocality: they can incorporate the short-and intermediate-range van der Waals interactions [ZT06, MFH10, SRZ⁺16, YKC19]. At the same time, meta-GGAs offer an overall higher accuracy than LDA and GGA and remain comparable to LDA and GGA in terms of computational effort [SRZ⁺16]. This makes meta-GGAs a very attractive choice for materials modeling.

In practice, however, this is impaired by the fact that so far no *single* meta-GGA achieves an accurate description of both energetic bonds, including weak bonds, and ultranonlocal properties, e.g., band gaps. The aim of the present thesis is therefore to find out whether this is possible at all, what would be crucial in a meta-GGA to achieve this, and if possible, to construct a meta-GGA that does so.

This thesis consists of three parts. In Part I, we introduce and discuss the concepts of DFT relevant to this work: The fundamentals of DFT in Chapter 2, the traditional semilocal functionals LDA and GGA in Chapter 3, and finally the orbital-dependent semilocal meta-GGAs in Chapter 4. In Part II, we outline the results of the five publications that make up Part III. In Chapter 5, we analyze in detail what is required in meta-GGAs to achieve state-of-the-art accuracy for ultranonlocal properties in the first step [Pub1, Pub2], for band gaps and energetic bonds in the second step [Pub3], and for weakly interacting systems in the third step [Pub4]. Based on the findings from these analyses, we refine the established design strategy for nonempirical meta-GGAs [Pub5, Pub4]. Additionally, we demonstrate how a so

far unexplored degree in the gradient expansion for slowly varying densities allows for a more balanced treatment in meta-GGAs [Pub5]. Finally, in Chapter 6 we combine all our findings and insights to ultimately construct a best-of-both-worlds meta-GGA and demonstrate that it indeed achieves state-of-the-art accuracy for both energetic bonds, including weak bonds, and band gaps.

Part I

Concepts of Density Functional Theory

CHAPTER 2

Fundamentals of Density Functional Theory

Within the Born-Oppenheimer approximation [BO24], the electronic structure of materials is determined by the electronic many-body Schrödinger equation [Sch26]. However, the computational demand to solve the Schrödinger equation encounters a so-called exponential wall with respect to the number of electrons in the system [Koh99]. An elegant way to circumvent this exponential wall was found by Hohenberg and Kohn in 1964 [HK64]. They showed by means of the variational principle that instead of solving the Schrödinger equation for the wavefunction, the electron density n can also be used as the central variable. The latter reduces the number of spatial variables for a three-dimensional system of N electrons from $3N$ to 3. The Hohenberg-Kohn theorem in particular states that the many-body wavefunction and thus every ground-state property is a unique functional of the ground-state density. The electronic ground-state density n is in principle determined as the minimizer of the total energy $E[n]$, i.e., by the variational equation

$$\frac{\delta}{\delta n(\mathbf{r})} \left[E[n] - \mu \left(\int n(\mathbf{r}) \, d^3r - N \right) \right] = 0, \quad (2.1)$$

where μ is a Lagrange multiplier of the subsidiary condition that enforces the correct particle number. As important as the Hohenberg-Kohn proof of existence is a practicable formalism for calculating the density. To this end, the total energy can be written as a functional of the density in the form

$$E[n] = T[n] + \int v_{\text{ext}}(\mathbf{r})n(\mathbf{r}) \, d^3r + E_{\text{H}}[n] + E_{\text{r}}[n], \quad (2.2)$$

where T is the kinetic energy, v_{ext} the external potential, E_{H} the Hartree energy, and E_{r} the residual. While v_{ext} is determined by the system under study (in particular the nuclei), E_{H} stems from the classical Coulomb energy and reads (we use atomic units throughout)

$$E_{\text{H}}[n] = \frac{1}{2} \iint \frac{n(\mathbf{r})n(\mathbf{r}')}{|\mathbf{r} - \mathbf{r}'|} \, d^3r \, d^3r'. \quad (2.3)$$

In contrast, the explicit density dependence of $T[n]$ and $E_{\text{r}}[n]$ is not known and needs to be approximated in practice. Since finding good approximations to $T[n]$ is difficult, DFT is usually used in the Kohn-Sham formalism [KS65]. The latter maps the interacting many-body Schrödinger equation onto a system of non-interacting single-particle Schrödinger equations that generates the same electronic density. The resulting so-called Kohn-Sham equations read

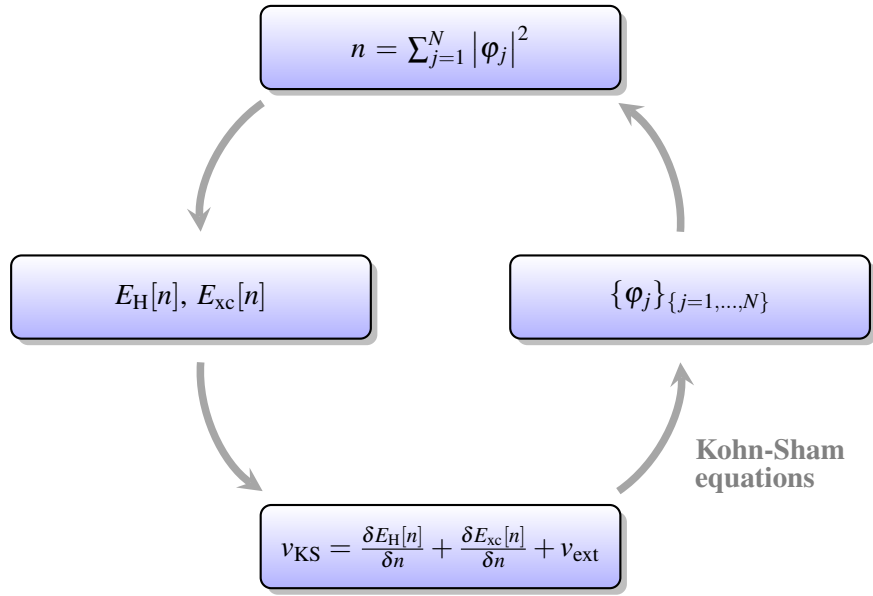


Figure 2.1: The Kohn-Sham self-consistent cycle: A first guess for the orbitals $\{\varphi_j\}$ yields the electronic density. From this, the Hartree and exchange-correlation energy functionals are obtained. Taking the functional derivatives leads to an approximate Kohn-Sham potential. Solving the Kohn-Sham equations with this approximate potential yields a new set of orbitals. This procedure is repeated until self-consistence is achieved. Thus, the orbitals depend implicitly on the density via the Kohn-Sham equations.

(for the sake of simplicity, we neglect the spin in the following)

$$\left(-\frac{1}{2}\nabla^2 + v_{\text{KS}}(\mathbf{r})\right)\varphi_i(\mathbf{r}) = \varepsilon_i\varphi_i(\mathbf{r}). \quad (2.4)$$

Their solutions $\{\varphi_i\}_{i=1,\dots,N}$ are called Kohn-Sham orbitals, v_{KS} is the Kohn-Sham potential (to be defined below), and $\{\varepsilon_i\}_{i=1,\dots,N}$ are the Kohn-Sham eigenvalues. The kinetic energy is now approximated by the kinetic energy of the non-interacting system

$$T_s[n] = T_s[\{\varphi_j[n]\}] = -\frac{1}{2}\sum_{j=1}^N \int \varphi_j^*(\mathbf{r})\nabla^2\varphi_j(\mathbf{r})\,d^3r. \quad (2.5)$$

T_s depends implicitly on the density via the Kohn-Sham orbitals, as we illustrate in Fig. 2.1. Consequently, the total energy of Eq. (2.2) is replaced by

$$E[n] = T_s[n] + \int v_{\text{ext}}(\mathbf{r})n(\mathbf{r})\,d^3r + E_{\text{H}}[n] + E_{\text{xc}}[n], \quad (2.6)$$

where the residual E_{xc} is called the exchange-correlation (xc) energy. Finally, the Kohn-Sham potential reads

$$v_{\text{KS}} = v_{\text{H}} + v_{\text{ext}} + v_{\text{xc}}, \quad (2.7)$$

where the Hartree potential v_H and the exchange-correlation potential v_{xc} are obtained as functional derivatives from the respective energy functionals via

$$v_H(\mathbf{r}) = \frac{\delta E_H[n]}{\delta n(\mathbf{r})}, \quad v_{xc}(\mathbf{r}) = \frac{\delta E_{xc}[n]}{\delta n(\mathbf{r})}. \quad (2.8)$$

In practice, the Kohn-Sham equations (2.4) are solved iteratively, as illustrated in Fig. 2.1. This formalism has the advantage that the kinetic energy of the non-interacting system T_s is a reasonable approximation to the kinetic energy of the interacting system. Thus, only the density dependence of the relatively small contribution $E_{xc}[n]$ needs to be approximated. Nevertheless, $E_{xc}[n]$ is often decisive, e.g., for chemical bonding. Unfortunately, although the Hohenberg-Kohn theorem [HK64] guarantees the existence of an exchange-correlation functional that yields the exact ground-state density, its proof is not constructive. Consequently, finding suitable approximations for $E_{xc}[n]$ is the holy grail of DFT and also the main concern of the present thesis.

The exchange-correlation energy is often further split into an exchange and a correlation part. This is motivated by the following formal definition of the exchange part, the so-called exact exchange energy (for which it is necessary to explicitly denote the spins)

$$E_x^{\text{exact}}[n] = -\frac{1}{2} \sum_{\sigma=\uparrow,\downarrow} \sum_{i,j=1}^{N_\sigma} \iint \frac{\varphi_{i\sigma}^*(\mathbf{r}) \varphi_{i\sigma}(\mathbf{r}') \varphi_{j\sigma}^*(\mathbf{r}') \varphi_{j\sigma}(\mathbf{r})}{|\mathbf{r} - \mathbf{r}'|} d^3r d^3r'. \quad (2.9)$$

The remainder $E_{xc} - E_x^{\text{exact}}$ is then defined as the correlation energy. The correlation energy can be further split into a long-range part, sometimes called the static correlation, and a more local component, the dynamical correlation [MNH96, HC01]. In practice, it is often advantageous to approximate the dynamical correlation by a semilocal correlation functional and the combination of exact exchange and static correlation by a semilocal exchange functional for three reasons [NNH96, GSB97, Cre01, MCH02, KK08]. First, the evaluation of the double integral in Eq. (2.9) is computationally demanding. Second, good approximations for the static correlation are hard to find and computationally even more demanding. Third, there are certain similarities between the exact exchange energy and the static correlation. Therefore, approximating their sum by a semilocal functional often leads to good results due to cancellation of errors [PSTS08, KK08].

Despite their formal similarity, the (Kohn-Sham) exact exchange energy is different from the Fock energy of Hartree-Fock theory, because in Eq. (2.9) the Kohn-Sham orbitals are used. Moreover, for a given approximation of the exchange-correlation energy, one can uniquely determine its exchange part via uniform density scaling to the high-density limit [Lev91].

CHAPTER 3

Traditional Semilocal Functionals

3.1 Local Density Approximation

The simplest approximation to $E_{xc}[n]$ is to use the exchange-correlation energy of a homogeneous electron gas also for inhomogeneous systems, which leads to the Local Density Approximation (LDA) [HK64, KS65]. The exchange energy of a homogeneous electron gas is known analytically [DG90]:

$$E_x^{\text{LDA}}[n] = A_x \int n^{4/3}(\mathbf{r}) d^3r \quad (3.1)$$

with $A_x = -(3/4)(3/\pi)^{1/3}$. The correlation energy of a homogeneous electron gas is known analytically only for certain limits [PW92]. However, it was calculated very accurately using Quantum Monte Carlo (QMC) simulations [CA80] and several parametrizations of this data exist [VWN80, PZ81, PW92]. Even though the density is clearly not uniform in real systems, the LDA has often been found to yield accurate predictions of experimental results, see, e.g., Ref. [KK08] and references therein. Nevertheless, the LDA systematically and significantly overestimates atomization energies [PA82] and underestimates bond lengths [PA82] and band gaps [PL83].

3.2 Generalized Gradient Approximation

A natural extension of the LDA is to include the gradient expansion for slowly varying densities [PK03] that we discuss in detail in Section 5.5. However, direct use of the second-order gradient expansion as the next systematic correction for slowly-varying densities results in spurious positive correlation energies for atoms [MB68] and worsens E_{xc} in general. This issue is solved by considering Generalized Gradient Approximations (GGAs) of the form

$$E_{xc}^{\text{GGA}}[n] = A_x \int n^{4/3} F_{xc}^{\text{GGA}}[n, \nabla n] d^3r, \quad (3.2)$$

where the enhancement factor F_{xc} accounts for the local enhancement of the exchange-correlation energy with respect to the LDA. That is, $F_{xc} = 1$ everywhere leads back to the LDA. In nonempirical density functionals, F_{xc} is constructed based on the gradient expansion and further known properties of the exact functional [PBE96, PK03, SRP15, KLP23], see also Section 5.4. Although GGAs represent a significant improvement over the LDA, e.g., in terms of atomization

energies and bond lengths [PBE96, PK03], both share several fundamental limitations.

3.3 Limitations of LDA and GGA

At the heart of many of the problems encountered with LDA and GGA are the presence of self-interaction and the absence of a derivative discontinuity in the exchange-correlation energy [KK08, CMSY12]. Both of these issues are interlinked and their wide-reaching consequences are often influenced by both. Nevertheless, we first introduce the concepts of self-interaction and derivative discontinuity separately before discussing their consequences together.

3.3.1 Self-Interaction

The origin of the self-interaction lies in the fact that the classical Coulomb interaction implies the Hartree-like energy

$$\frac{1}{2} \sum_{\substack{i,j \\ i \neq j}}^N \iint \frac{|\varphi_i(\mathbf{r})|^2 |\varphi_j(\mathbf{r}')|^2}{|\mathbf{r} - \mathbf{r}'|} d^3r d^3r', \quad (3.3)$$

which becomes the Hartree energy of equation (2.3) only if the terms with $i = j$ are added to the sum. These supernumerary ($i = j$)-terms in equation (2.3) resemble an artificial interaction of each orbital with itself. This has immediate consequences in real systems. Most prominently, in one-electron systems the Hartree energy does not vanish, while there clearly should be no electron-electron interaction at all [PZ81].

In the exact exchange-correlation functional this spurious self-interaction is exactly compensated for by the exchange part, Eq. (2.9). Thus, for any one-electron density n_{1e} the exact exchange-correlation functional satisfies the conditions [PZ81]

$$E_H[n_{1e}] + E_{xc}[n_{1e}] = 0, \quad (3.4)$$

$$E_c[n_{1e}] = 0. \quad (3.5)$$

A DFA that violates condition (3.4) is said to suffer from "one-electron self-interaction". Semilocal DFAs do not possess the nonlocality inherent to the Hartree energy and are therefore unable to exactly compensate for this spurious self-interaction. For LDA and GGA, the situation is even worse: they introduce an additional self-interaction in their correlation part, as the latter does not vanish in one-electron regions. That is, they violate condition (3.5). This spurious self-interaction of the correlation part is referred to as "self-correlation". As a consequence of violating the conditions (3.4) and (3.5), LDA and GGA suffer from a self-interaction error [PZ81, KKP04, PRSP15]. We discuss in Chapter 4, how more advanced semilocal DFAs can reduce the self-interaction error by resolving the issue of self-correlation and reducing the one-electron self-interaction.

In the Literature also the term "many-electron self-interaction" appears [MSCY06, RPC⁺06]. This, however, describes a separate issue [RPC⁺07, SK16], namely the straight-line condition

discussed in the next section, compare also Ref. [KK20].

3.3.2 Derivative Discontinuity

The discovery of the derivative discontinuity of the exchange-correlation energy dates back to 1982, when the Hohenberg-Kohn theorem was extended to non-integer particle numbers [PPLB82]. This extension is mathematically necessary to properly define the variational equation (2.1) and the functional derivative $\delta E[n]/\delta n$. To this end, consider an integer $N_0 \in \mathbb{N}_0$ and let $0 < \eta < 1$. Then, the energy functional is generalized to non-integer particle numbers $N = N_0 + \eta$ using the constrained search formalism [Lev79, Val80, PPLB82], in which the total energy is minimized with respect to number-conserving variations of the density. Consequently, the ground state energy is the lowest energy that a statistical mixture of the pure $N - 1$ and N electron ground states can attend. This yields

$$E(N) = (1 - \eta)E(N_0) + \eta E(N_0 + 1). \quad (3.6)$$

Obviously, $E(N)$ is piecewise linear between integer particle numbers, which implies the so-called straight-line condition for DFAs [PPLB82]. It is the deviation from this straight-line condition that is sometimes referred to as the many-electron self-interaction error mentioned in the previous section.

The piecewise linearity of $E(N)$ implies that $E(N)$ is continuously differentiable everywhere except for integer particle numbers. There, its slope changes discontinuously, giving rise to

$$\Delta_g = \lim_{\eta \rightarrow 0^+} \left(\left. \frac{\partial E}{\partial N} \right|_{N_0 + \eta} - \left. \frac{\partial E}{\partial N} \right|_{N_0 - \eta} \right). \quad (3.7)$$

Δ_g carries the following physical meaning [PYB⁺17]. Consider the removal of an electron from the N_0 -particle system. This requires the energy

$$I(N_0) = E(N_0 - 1) - E(N_0), \quad (3.8)$$

which is called the ionization potential. On the other hand, the energy required to add an electron to the system is the electron affinity

$$A(N_0) = E(N_0) - E(N_0 + 1). \quad (3.9)$$

Comparison of Eqs. (3.6)–(3.9) shows that Δ_g equals the fundamental gap $I - A$, i.e.,

$$\Delta_g = I(N_0) - A(N_0). \quad (3.10)$$

In order to gain further insights, we analyze which parts of the energy functional $E[n]$ contribute to the discontinuity on the right-hand side of Eq. (3.7), and thus to the fundamental gap. To this

end, reconsider the Kohn-Sham partitioning of the total energy, Eq. (2.6). Obviously, the terms

$$\frac{\delta E_{\text{H}}[n]}{\delta n(\mathbf{r})} = v_{\text{H}}(\mathbf{r}) \quad \text{and} \quad \frac{\delta \int v_{\text{ext}}(\mathbf{r}')n(\mathbf{r}') d^3r'}{\delta n(\mathbf{r})} = v_{\text{ext}}(\mathbf{r})$$

are continuous in the density. Therefore, the discontinuity at integer particle numbers must result from the contributions of T_{s} and E_{xc} . Consequently, the fundamental band gap splits into [PL83, SS83]

$$\begin{aligned} \Delta_{\text{g}} &= \lim_{\eta \rightarrow 0^+} \left(\left. \frac{\delta T_{\text{s}}[n]}{\delta n(\mathbf{r})} \right|_{N_0+\eta} - \left. \frac{\delta T_{\text{s}}[n]}{\delta n(\mathbf{r})} \right|_{N_0-\eta} \right) + \lim_{\eta \rightarrow 0^+} \left(\left. \frac{\delta E_{\text{xc}}[n]}{\delta n(\mathbf{r})} \right|_{N_0+\eta} - \left. \frac{\delta E_{\text{xc}}[n]}{\delta n(\mathbf{r})} \right|_{N_0-\eta} \right) \\ &=: \Delta_{\text{KS}} + \Delta_{\text{xc}}. \end{aligned} \quad (3.11)$$

Here, the contribution due to the noninteracting kinetic energy T_{s} is called the Kohn-Sham gap Δ_{KS} , as it corresponds to the energy difference between the lowest unoccupied (LU) and the highest occupied (HO) Kohn-Sham eigenvalue at integer electron number [KK08],

$$\Delta_{\text{KS}} = \varepsilon_{N_0+1}(N_0) - \varepsilon_{N_0}(N_0) = \varepsilon_{\text{LU}} - \varepsilon_{\text{HO}}. \quad (3.12)$$

The second term in Eq. (3.11), Δ_{xc} , is the derivative discontinuity [PL83, SS83]. It is well established that the derivative discontinuity is non-vanishing for the exact functional [PL83, Per85, GSS86] and has significant physical consequences [PL83, Per85, GSS86, MK05, GMR06b, GMR06a, YCMS12, PYB⁺17, YPSP16, AGC⁺23]. In particular, Eqs. (2.8) and (3.11) imply that the derivative discontinuity causes a spatially uniform jump in the exchange-correlation potential when the particle number crosses an integer [PPLB82, PL83, SS83],

$$\lim_{\eta \rightarrow 0^+} \left(\left. v_{\text{xc}}(\mathbf{r}) \right|_{N_0+\eta} - \left. v_{\text{xc}}(\mathbf{r}) \right|_{N_0-\eta} \right) = \Delta_{\text{xc}}. \quad (3.13)$$

Thus, an infinitesimally small change of the density at any point \mathbf{r} can lead to a finite global change of the potential v_{xc} . To distinguish this type of nonlocality from the nonlocality inherent to the Hartree energy, the nonlocality associated with the derivative discontinuity is often referred to as ultranonlocality [Pub2]. For LDA and GGA, the second term in Eq. (3.11) vanishes, because in both $E_{\text{xc}}[n]$ depends continuously on the density. Therefore, these traditional semilocal DFAs lack the derivative discontinuity and the physics it conveys.

3.3.3 Consequences

Underestimation of band gaps

An important consequence of the missing derivative discontinuity is that LDA and GGA systematically underestimate the band gaps, i.e., fundamental gaps, of solids [PL83]. Figure 3.1 illustrates this by comparing the band gaps of LDA (with the correlation part as parametrized by Perdew and Wang [PW92]) and the popular GGA PBE [PBE96] to experimental band

gaps. Additionally, we show the highly accurate Kohn-Sham gap of sodium chloride from Ref. [AGC⁺23] that was obtained by inversion of a QMC density. Figure 3.1 shows that LDA and GGA provide reasonable approximations to the Kohn-Sham gap [Per85], but completely miss the derivative discontinuity Δ_{xc} . This systematic failure of the traditional semilocal density functionals became known as “the band gap problem of DFT” [PL83, SS83, SS85, Per85].

We should note that the (range-separated) hybrid functional HSE06 [HSE03, HSE06, KVIS06], when appropriately evaluated, has been shown to provide much more reliable band gaps than LDA and GGA [CC10], albeit at a considerably higher computational cost, especially in solids. Therefore, the notion “band gap problem of semilocal DFT” would be more precise at this point.

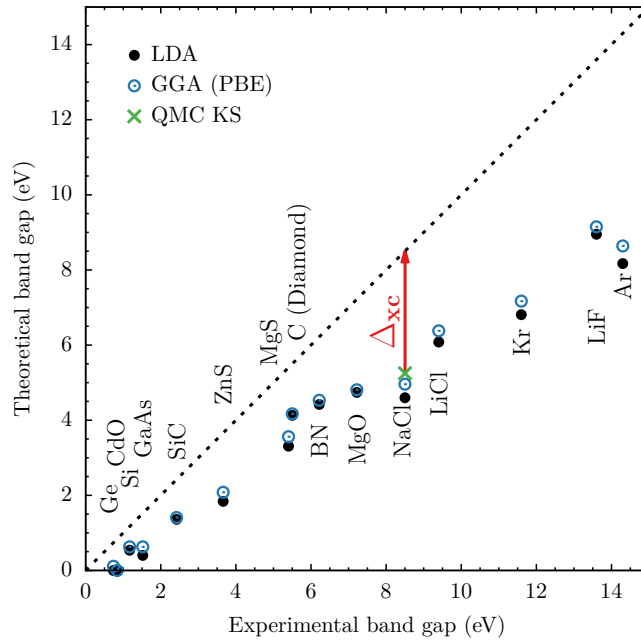


Figure 3.1: Band gaps of solids for LDA and the GGA PBE [PBE96] (calculated using the BAND code [SCM23b]) compared to experimental data (taken from [Pub1]). The dotted line illustrates agreement with the experimental values. The green cross marks the highly accurate Kohn-Sham gap of sodium chloride from Ref. [AGC⁺23]. The difference between this accurate Kohn-Sham gap and the experimental gap illustrates the derivative discontinuity Δ_{xc} .

To understand the physical origin of the band gap problem of DFT, we first need to clarify the physical meaning of the Kohn-Sham eigenvalues and how band gaps are usually calculated from Kohn-Sham DFT. Although the Kohn-Sham eigenvalues were initially introduced only as mathematical objects, at least the highest occupied eigenvalue has a precise physical interpretation [PL83]: It is minus the ionization potential [Jan78], i.e.,

$$I = -\epsilon_{HO}. \quad (3.14)$$

For the lowest unoccupied eigenvalue the Eqs. (3.10)–(3.12) then imply

$$A = -(\epsilon_{LU} + \Delta_{xc}). \quad (3.15)$$

Thus, the Kohn-Sham eigenvalue gap –even for the exact density functional– does not yield the fundamental gap $\Delta_g = I - A$, but the Kohn-Sham gap $\Delta_{KS} = \Delta_g - \Delta_x$ [SS83, PL83, GSS88]. In solids, the eigenvalue gap becomes the band gap. However, the experimental band gap corresponds to the fundamental gap, whereas the Kohn-Sham gap is only a mathematical object without direct physical meaning. Consequently, also the band gaps of solids lack Δ_{xc} when they are calculated within the Kohn-Sham scheme [SS85, Per85]. Comparison of Eqs. (3.8) and (3.9) shows that $\Delta_g = E(N+1) + E(N-1) - 2E(N)$, i.e., in finite systems, the fundamental gap can be calculated from separate Kohn-Sham calculations for the $(N-1)$ -, N -, and $(N+1)$ -particle ground states, respectively. However, this does not apply to the band gaps of solids, as solids are usually modeled using periodic boundary conditions and therefore with an infinite number of electrons.

Thus, for the calculation of band gaps in practice, we need a formalism that includes the derivative discontinuity in the eigenvalue gap. Consequently, for band gap calculations, one usually switches to a so-called generalized Kohn-Sham scheme [SGV⁺96], where the energy is no longer minimized with respect to the density, but with respect to the orbitals, and Δ_{xc} can be absorbed in the generalized Kohn-Sham eigenvalue difference. We introduce generalized Kohn-Sham schemes in more detail in the context of orbital-dependent exchange-correlation functionals in Section 4.2.2. In fact, we explain in Chapter 4 why orbital dependence is the key to incorporating the derivative discontinuity in the (generalized Kohn-Sham) eigenvalue gap and thus to more accurate band gaps. This is emphasized in [Pub1], where we demonstrate that the derivative discontinuity can be fully included in the orbital-dependent semilocal meta-GGAs. For LDA and GGA, however, switching to a generalized Kohn-Sham scheme does not help because LDA and GGA miss the derivative discontinuity anyway.

To avoid confusion, we should emphasize that there are two distinct sources of errors when calculating band gaps from DFT eigenvalue differences [PYB⁺17]. On the one hand, the exchange-correlation potential and the eigenvalue gap of the Kohn-Sham formalism do not include the derivative discontinuity. This is a characteristic of the formalism that is usually circumvented by switching to a generalized Kohn-Sham scheme. On the other hand, the chosen DFA can additionally introduce errors for the Kohn-Sham gap and/or the size of the derivative discontinuity. These errors are characteristics of the selected approximation to the exact $E_{xc}[n]$.

Delocalization error

Another noteworthy consequence of the self-interaction error and a missing derivative discontinuity is the tendency of LDA and GGA to overly delocalize electrons. This so-called delocalization error [MSCY08, CMSY08] was recently even claimed to be the “greatest outstanding challenge in DFT” [BADJ23]. Its relation to the self-interaction error and a missing derivative discontinuity

can be understood as follows [KK20]. On the one hand, due to the artificial interaction of each orbital with itself, the total energy is lowered when the orbital is smeared out, which corresponds to a more delocalized charge. This manifests itself, for example, in excessively delocalized LDA and GGA densities of the localized d and f states in transition metals [Kul15, MW16, LK19]. On the other hand, due to the missing derivative discontinuity, there is no potential barrier that stops the charge distribution from splitting into fractional contributions centered around different nuclei, thereby delocalizing the charge.

As an illustrative example for the latter, consider a combined system of two subsystems in an external electric field. As we move the subsystems apart, each subsystem must contain an integer number of electrons. But what happens if we subsequently increase the external electric field? When the subsystems are sufficiently far apart, no charge should be transferred until the strength of the external electric field exceeds the difference between the electron affinity of the acceptor and the ionization potential of the donor [Per90]. This requires a finite step in the exchange-correlation potential that counteracts the external field and prevents a fractional transfer of charge [KKP04]. This field-counteracting potential barrier is induced by the derivative discontinuity and is one central objective of study in [Pub2]. If this potential barrier is missing, such as in LDA and GGA, the total energy is minimized by delocalizing the charge distribution of one electron over both subsystems, leading to fractional electron numbers in both subsystems.

CHAPTER 4

Orbital-Dependent Semilocal Functionals

4.1 Meta-Generalized Gradient Approximations

Additionally to the more fundamental shortcomings of LDA and GGA discussed in the previous chapter, these traditional semilocal functionals are typically only accurate for either molecules or solids [PRC⁺08]. These limitations, particularly the self-correlation, were the motivation for adding further semilocal ingredients to the enhancement factor, which led to the class of meta-GGAs [Bec88, Bec96, VS98, PKZB99, TPSS03, ZT06, PRC⁺09, SRP15, TM16, DFC16, AK19, FKN⁺20]. In addition to the density and its gradient, meta-GGAs also depend on (the gradient of) the occupied orbitals via the noninteracting kinetic energy density (as obtained from Eq. (2.5) via partial integration)

$$\tau(\mathbf{r}) = \frac{1}{2} \sum_{j=1}^N |\nabla \phi_j(\mathbf{r})|^2. \quad (4.1)$$

As we explain in Sections 4.3, 5.1, and 5.3, this form of orbital dependence is the key that makes nonlocal features accessible to semilocal DFAs [EH14, AK19, Pub1, Pub2, MFH10, Pub4].

Historically, functionals that depend on the Laplacian of the density (rather than on the kinetic energy density) are also referred to as meta-GGAs. However, these differ qualitatively from kinetic energy dependent functionals, as they can not provide the same form of nonlocality, in particular no ultranonlocality at all. Therefore, throughout this thesis we neglect the dependency on the Laplacian of the density and consider only meta-GGAs of the form

$$E_{xc}^{mGGA}[n] = A_x \int n^{4/3} F_{xc}^{mGGA}[n, \nabla n, \tau] d^3r. \quad (4.2)$$

In practice, meta-GGAs are parametrized in composite variables that depend on n , ∇n , and τ and allow for a physical interpretation. These are usually the Wigner-Seitz radius $r_s = (4\pi n/3)^{-1/3}$ for the density dependence and the reduced density gradient $s = |\nabla n|/[2(3\pi^2)^{1/3}n^{4/3}]$ for the dependence on the density gradient. For the dependence on the kinetic energy density τ , $z = \tau^W/\tau$ or $\alpha = (\tau - \tau^W)/\tau^{unif}$ are often used, where $\tau^W = |\nabla n|^2/8n$ is the von Weizsäcker kinetic energy density and $\tau^{unif} = (3/10)(3\pi^2)^{2/3}n^{5/3}$ is the kinetic energy density of the uniform electron gas. To generate the spin-dependent version of Eq. (4.2), one usually applies the spin-scaling relation of exact exchange [OP79], $E_x[n_\uparrow, n_\downarrow] = \frac{1}{2}E_x[2n_\uparrow] + \frac{1}{2}E_x[2n_\downarrow]$. The exact

spin dependence of correlation is not known. It is therefore often modeled in terms of the spin-polarization $\zeta = (n_{\uparrow} - n_{\downarrow}) / (n_{\uparrow} + n_{\downarrow})$.

One major advantage of meta-GGAs over LDA and GGA is that meta-GGAs can distinguish more qualitatively different regions of space [SXR12, SXF⁺13]. In particular, the use of τ enables to detect regions of space that are dominated by a single orbital [Bec88, BE90], so-called iso-orbital regions. This is possible because τ^{W} is the iso-orbital limit of τ , i.e., $\tau = \tau^{\text{W}}$ if $n = |\varphi_i|^2$ with a single orbital φ_i . As a consequence, $z = 1$ and $\alpha = 0$ indicate regions of space dominated by a single orbital, such as the free hydrogen atom, the hydrogen molecule, or the region close to the nucleus where the 1s orbital dominates over all others. Therefore, such variables are often called iso-orbital indicators. Furthermore, for a homogeneous electron gas the gradient of the density vanishes, which implies $s = 0$ and $\tau^{\text{W}} = 0$. Thus, $z = 0$ and $\alpha = 1$, together with $s = 0$, indicate regions of homogeneous density such as in metallic bonds. Finally, α has the additional advantage over many other iso-orbital indicators that it can detect regions of large density overlap between closed shells such as the bond center of noncovalent bonds, since $\alpha \gg 1$ in such regions [SXF⁺13].

Moreover, the kinetic energy density based iso-orbital indicators enable meta-GGAs to significantly reduce the self-interaction error. This is because, on the one hand, they allow to eliminate self-correlation by making the correlation vanish in one-electron regions. On the other hand, they also make it possible to use the hydrogen atom as a model system for the iso-orbital limit of the exchange energy [TPSS03, SRP15, AK19]. The latter makes the exchange part approximately free from one-electron self-interaction for compact one-electron densities [SBW⁺19].

Their overall higher flexibility allows meta-GGAs to satisfy more properties of the exact functional simultaneously [SRP15, KLP23], which is for example realized in the SCAN meta-GGA [SRP15]. Meta-GGAs can therefore achieve higher accuracy than LDA and GGA for a variety of properties (see, e.g., Refs. [ZT06, FKN⁺20]), in particular for the geometries and energies of diversely (including weakly) bonded molecules [SRZ⁺16] and solids [IW18].

4.2 Different treatments of meta-GGAs

Besides their overall higher flexibility and accuracy, (kinetic energy dependent) meta-GGAs are conceptually different to LDA and GGA for the following reason. In contrast to these traditional semilocal DFAs that depend only on the density and its derivatives, the potential of meta-GGAs (and orbital-dependent exchange-correlation functionals in general) can not be calculated via Eq. (2.8) straightforwardly. Instead, one can either obtain the unique multiplicative Kohn-Sham potential via the optimized effective potential (OEP) method or resort to a generalized Kohn-Sham scheme. In the latter, the potential is obtained by minimizing the total energy with respect to the orbitals instead of the density. Thus, calculating the functional derivative of the exchange-correlation energy with respect to the orbitals is sufficient. The latter can be done straightforwardly also for functionals that depend on the kinetic energy density.

We briefly discuss these two approaches in the following. While generalized Kohn-Sham schemes are used in the majority of applications today, the OEP method is particularly important for conceptual reasons. For example, we exploit their subtle differences in [Pub1] to gain valuable insights into the physical origin and justification of our computational predictions.

4.2.1 The Optimized Effective Potential and the Krieger-Li-Iafrate Approximation

In this section, we briefly introduce the OEP method [SH53, TS76] and the Krieger-Li-Iafrate (KLI) approximation to the OEP [KLI92]. For a detailed derivation and comprehensive discussion of the OEP method and the KLI approximation, see Ref. [KK08]. To calculate the potential of an orbital-dependent exchange-correlation functional, we apply the chain rule to the spin-dependent version of Eq. (2.8) to obtain [GL94]

$$v_{xc,\sigma}(\mathbf{r}) = \sum_{\alpha,\beta=\uparrow,\downarrow} \sum_{i=1}^{N_\alpha} \left[\iint \frac{\delta E_{xc}[\{\varphi_{j\tau}\}]}{\delta \varphi_{i\alpha}(\mathbf{r}')} \frac{\delta \varphi_{i\alpha}(\mathbf{r}')}{\delta v_{KS,\beta}(\mathbf{r}'')} \frac{\delta v_{KS,\beta}(\mathbf{r}'')}{\delta n_\sigma(\mathbf{r})} d^3 r' d^3 r'' + c.c. \right], \quad (4.3)$$

where *c.c.* denotes the complex conjugate. Next, we identify $\delta v_{KS,\beta}(\mathbf{r}'')/\delta n_\sigma(\mathbf{r})$ with the inverse of the static non-interacting response function and evaluate the functional derivative $\delta \varphi_{i\alpha}(\mathbf{r}')/\delta v_{KS,\beta}(\mathbf{r}'')$ using first-order perturbation theory (see Ref. [KK08] for details) to obtain an integral equation for the optimized effective potential $v_{xc,\sigma}^{\text{OEP}}$,

$$\sum_{i=1}^{N_\sigma} \int \varphi_{i\sigma}^*(\mathbf{r}') [v_{xc,\sigma}^{\text{OEP}}(\mathbf{r}') - u_{xc,i\sigma}(\mathbf{r}')] G_{KS,i\sigma}(\mathbf{r}, \mathbf{r}') \varphi_{i\sigma}(\mathbf{r}) d^3 r' + c.c. = 0, \quad (4.4)$$

with orbital-specific potential operators

$$u_{xc,i\sigma}(\mathbf{r}) = \frac{1}{\varphi_{i\sigma}^*(\mathbf{r})} \frac{\delta E_{xc}[\{\varphi_{j\tau}\}]}{\delta \varphi_{i\sigma}(\mathbf{r})} \quad (4.5)$$

and the Kohn-Sham Green's function

$$G_{KS,i\sigma}(\mathbf{r}, \mathbf{r}') = \sum_{k=1, k \neq i}^{\infty} \frac{\varphi_{k\sigma}(\mathbf{r}) \varphi_{k\sigma}^*(\mathbf{r}')}{\varepsilon_{i\sigma} - \varepsilon_{k\sigma}}. \quad (4.6)$$

Solving the OEP equation (4.4) yields the unique multiplicative exchange-correlation potential $v_{xc,\sigma}^{\text{OEP}}$ associated with the orbital-dependent DFA in the Kohn-Sham formalism. However, the OEP equation is an integral equation that needs to be solved iteratively and involves the Kohn-Sham Green's function that runs over all occupied and *unoccupied* orbitals and eigenvalues. Therefore, solving the OEP equation directly is computationally extremely demanding. Consequently, approximations to the Green's function and thus to the OEP are commonly used. The most important one in the context of this thesis, and also the most popular, is the KLI approximation [KLI92].

In the KLI approximation, the eigenvalue differences in the denominator of the Green's func-

tion are approximated by a single constant for all orbitals of the same spin, i.e., $\varepsilon_{i\sigma} - \varepsilon_{k\sigma} = \Delta\varepsilon_\sigma$ for all i, k . This simplifies the Kohn-Sham Green's function to

$$G_{KS,i\sigma}(\mathbf{r}, \mathbf{r}') = \sum_{k=1, k \neq i}^{\infty} \frac{\varphi_{k\sigma}(\mathbf{r})\varphi_{k\sigma}^*(\mathbf{r}')}{\Delta\varepsilon_\sigma} = \frac{1}{\Delta\varepsilon_\sigma} [\delta(\mathbf{r} - \mathbf{r}') - \varphi_{i\sigma}(\mathbf{r})\varphi_{i\sigma}^*(\mathbf{r}')], \quad (4.7)$$

where $\delta(\mathbf{r} - \mathbf{r}')$ is the Dirac delta function. In the second step, the closure relation of the Kohn-Sham orbitals,

$$\sum_{k=1}^{\infty} \varphi_{k\sigma}(\mathbf{r}')\varphi_{k\sigma}^*(\mathbf{r}) = \delta(\mathbf{r} - \mathbf{r}'), \quad (4.8)$$

was used. Substituting this approximated Green's function into the OEP equation (4.4) and solving it for $v_{xc,\sigma}^{\text{OEP}}$ leads to the KLI equation

$$v_{xc,\sigma}^{\text{KLI}}(\mathbf{r}) = \frac{1}{2n_\sigma(\mathbf{r})} \sum_{i=1}^{N_\sigma} |\varphi_{i\sigma}(\mathbf{r})|^2 [u_{xc,i\sigma}(\mathbf{r}) + (\bar{v}_{xc,i\sigma}^{\text{KLI}} - \bar{u}_{xc,i\sigma})] + c.c., \quad (4.9)$$

where $\bar{v}_{xc,i\sigma}^{\text{KLI}}$ and $\bar{u}_{xc,i\sigma}$ denote the orbital averages

$$\bar{v}_{xc,i\sigma}^{\text{KLI}} = \int \varphi_{i\sigma}^*(\mathbf{r})v_{xc,\sigma}^{\text{KLI}}(\mathbf{r})\varphi_{i\sigma}(\mathbf{r}) d^3r, \quad \bar{u}_{xc,i\sigma} = \int \varphi_{i\sigma}^*(\mathbf{r})u_{xc,i\sigma}(\mathbf{r})\varphi_{i\sigma}(\mathbf{r}) d^3r. \quad (4.10)$$

The KLI equation (4.9) is still an integral equation because of the orbital average $\bar{v}_{xc,i\sigma}^{\text{KLI}}$ on the right-hand side. Nevertheless, solving the KLI equation is considerably less time consuming than solving the exact OEP equation. Moreover, the eigenvalues obtained within the KLI approximation are usually a good approximation to those obtained with the exact OEP method [KP03].

Both the OEP method and the KLI approximation to the OEP enable the treatment of orbital-dependent exchange-correlation functionals within the Kohn-Sham formalism. While this has several advantages, most notably a unique multiplicative potential, it has the drawback that the band gaps calculated within OEP or KLI do not correspond to the band gaps of real systems for a fundamental reason: they lack the derivative discontinuity (compare Section 3.3.3). Therefore, band gaps are usually calculated using generalized Kohn-Sham schemes [PYB⁺17, YPSP16].

4.2.2 Generalized Kohn-Sham schemes

Conceptually, a generalized Kohn-Sham scheme maps the real interacting system to a *partially interacting* model system that can be represented by a single Slater determinant [SGV⁺96] (in contrast to a noninteracting model system in the case of conventional Kohn-Sham). The basic idea of generalized Kohn-Sham schemes is that choosing a proper interacting model system that includes parts of the exchange and correlation effects leads to a smaller energy component that remains to be approximated. In practice, this translates to using a different splitting between the explicitly orbital-dependent and explicitly density-dependent parts in Eq. (2.6), i.e., using other explicitly orbital-dependent parts than the noninteracting kinetic energy.

Formally, a generalized Kohn-Sham scheme is obtained by defining an energy functional of the orbitals $S[\{\varphi_{j\sigma}\}]$ and an associated energy functional of the density $F^S[n]$ that is obtained from the Slater determinant that minimizes S and under the constraint that the orbitals yield the prescribed density n [SGV⁺96] (see also [KK08, KSRAB12]),

$$F^S[n] = \min_{\{\varphi_{j\sigma}\} \rightarrow n(\mathbf{r})} S[\{\varphi_{j\sigma}\}]. \quad (4.11)$$

The minimizing orbitals $\{\varphi_{j\sigma}\}$ play a role similar to the Kohn-Sham orbitals. Similar to Eqs. (2.2) and (2.6), the total energy can then be written as

$$E[n] = \int v_{\text{ext}}(\mathbf{r})n(\mathbf{r}) \, d^3r + F^S[n] + R^S[n] \quad (4.12)$$

with a remainder energy functional $R^S[n]$. Analogous to the Kohn-Sham equations (2.4), one obtains a set of generalized Kohn-Sham equations

$$[v_{\text{ext}}(\mathbf{r}) + O^S[\{\varphi_{j\sigma}\}] + v_{R,\sigma}(\mathbf{r})] \varphi_{i\sigma}(\mathbf{r}) = \varepsilon_{i\sigma} \varphi_{i\sigma}(\mathbf{r}) \quad (4.13)$$

with the generalized Kohn-Sham eigenvalues $\varepsilon_{i\sigma}$, the generally *nonlocal*, orbital-specific operator $O^S[\{\varphi_{j\sigma}\}]$ that depends on the choice of S (but not on v_{ext} or v_R), and a local remainder potential

$$v_{R,\sigma}(\mathbf{r}) = \frac{\delta R^S[n]}{\delta n_{\sigma}(\mathbf{r})}. \quad (4.14)$$

Importantly, the generalized Kohn-Sham equations (4.13) are as rigorous as the Kohn-Sham equations (2.4) in the sense that their solution for the orbitals retains the ground-state density of the original interacting system. The generalized Kohn-Sham system is specified by the choice for $S[\{\varphi_{j\sigma}\}]$ and in analogy to approximating $E_{\text{xc}}[n]$ in conventional Kohn-Sham, one could in principle seek for approximations to $R^S[n]$. In practice, however, orbital-dependent functionals such as meta-GGAs, self-interaction corrected functionals, and hybrid functionals are usually still based on explicit approximations to $E_{\text{xc}}[n, \{\varphi_{j\sigma}\}]$ [KK08], where we deliberately denote the orbital dependence explicitly, and not $R^S[n]$.

The conventional Kohn-Sham system is the particular generalized Kohn-Sham system in which S is the Slater-determinant expectation value of the kinetic energy operator, i.e., $S[\{\varphi_{j\sigma}\}] = T_s[\{\varphi_{j\sigma}\}]$ [SGV⁺96]. In this case, O^S is the single-particle kinetic energy operator $O^S[\{\varphi_{j\sigma}\}] = -\frac{1}{2}\nabla^2$, the remainder energy R^S is the sum of the Hartree and the exchange-correlation energy, and Eq. (4.13) reduces to the conventional Kohn-Sham equations. Consequently, compared to the conventional Kohn-Sham equations, a general S generates the additional explicitly orbital-dependent term $O^S[\{\varphi_{j\sigma}\}]\varphi_{i\sigma} + \frac{1}{2}\nabla^2\varphi_{i\sigma}$ for each orbital $\varphi_{i\sigma}$.

For an orbital-dependent exchange-correlation energy we thus have two natural choices for S . On the one hand, we can use the Slater-determinant expectation value of the kinetic energy operator and obtain the Kohn-Sham potential via the OEP method. On the other hand, we can additionally assign the orbital-dependent part of the exchange-correlation energy (eventually

plus parts of the only density-dependent part of E_{xc} or the Hartree energy to make it a functional of a single Slater determinant) to $S[\{\varphi_{j\sigma}\}]$ (or $F^S[n]$ respectively) and the (remaining) density-dependent part of E_{xc} and E_H to the remainder $R^S[n]$ [BK18]. The latter approach defines the generalized Kohn-Sham system for the particular choice of exchange-correlation functional. Reassuringly, for a DFA that depends only on the density (and its derivatives), the corresponding generalized and conventional Kohn-Sham systems coincide.

For meta-GGAs in generalized Kohn-Sham, $\delta E_{xc}/\delta\varphi_{i\sigma}$ is a one-particle operator potential. Thus, S is simply $T_s[\{\varphi_{j\sigma}\}] + E_{xc}^{mGGA}[\{\varphi_{j\sigma}\}]$, where the density and its gradient are expressed in terms of the occupied orbitals $\{\varphi_{j\sigma}\}$ via $n[\{\varphi_{j\sigma}\}] = \sum_{j,\sigma} |\varphi_{j\sigma}|^2$, while the remainder R^S is the Hartree energy [BK18, RASK23]. The corresponding meta-GGA potential

$$v_{\sigma}^{mGGA} = v_{\sigma}^{loc} + v_{\sigma}^{\tau} \quad (4.15)$$

consists of the local potential

$$v_{\sigma}^{loc} = \frac{\partial e_{xc}}{\partial n_{\sigma}} - \nabla \cdot \frac{\partial e_{xc}}{\partial(\nabla n_{\sigma})} \quad (4.16)$$

and the differential operator v_{σ}^{τ} defined by

$$v_{\sigma}^{\tau} \varphi_{i\sigma} = -\frac{1}{2} \nabla \cdot \left[\frac{\partial e_{xc}}{\partial \tau_{\sigma}} \nabla \varphi_{i\sigma} \right], \quad (4.17)$$

where $e_{xc} = A_x n^{4/3} F_{xc}^{mGGA}$ is the exchange-correlation energy density (i.e. $\int e_{xc}(\mathbf{r}) d^3r = E_{xc}$). The generalized Kohn-Sham equations for a meta-GGA thus read

$$\left[v_{\text{ext}}(\mathbf{r}) - \frac{1}{2} \nabla^2 + v_{\sigma}^{\tau}(\mathbf{r}) + v_{\sigma}^{loc}(\mathbf{r}) + v_H(\mathbf{r}) \right] \varphi_{i\sigma}(\mathbf{r}) = \varepsilon_{i\sigma} \varphi_{i\sigma}(\mathbf{r}). \quad (4.18)$$

Obviously, v_{σ}^{loc} is a local GGA-like potential, while v_{σ}^{τ} is a nonlocal orbital-dependent kinetic energy-like differential operator. Therefore, the derivative discontinuity in meta-GGAs is entirely due to v_{σ}^{τ} [YPS16, AK19]. As we discuss in [Pub1], this implies that the τ dependence of a meta-GGA makes it possible to find suitable generalized Kohn-Sham schemes in which the exchange-correlation potential includes the derivative discontinuity and the eigenvalue difference $\varepsilon_{LU} - \varepsilon_{HO}$ is a good approximation to the fundamental gap.

Conceptually, there is an important difference between conventional and generalized Kohn-Sham: unlike conventional Kohn-Sham, where there is a unique exact energy functional and potential, there are infinitely many exact generalized Kohn-Sham schemes, because for each $S[\{\varphi_{j\sigma}\}]$ and corresponding $F^S[n]$, the remainder energy functional $R^S[n] = E_{xc}^{\text{exact}}[n] - F^S[n]$ complements it to the exact exchange-correlation functional of conventional Kohn-Sham. Nevertheless, once a DFA is chosen, the generalized Kohn-Sham system is fixed, i.e., the choice of $E_{xc}[n, \{\varphi_{j\sigma}\}]$ uniquely determines the corresponding generalized Kohn-Sham equations.

Given that, in addition to losing a unique reference functional and potential, $O^S[\{\varphi_{j\sigma}\}] + \frac{1}{2} \nabla^2$ is in general an orbital-dependent operator instead of a single multiplicative potential, what is the advantage of using a generalized Kohn-Sham scheme instead of the conventional Kohn-

Sham scheme? In a nutshell, the advantage of generalized Kohn-Sham is that $O^S[\{\varphi_{j\sigma}\}] + \frac{1}{2}\nabla^2$ is additionally nonlocal and thus enables the description of (ultra)nonlocal features. Since $O^S[\{\varphi_{j\sigma}\}] + \frac{1}{2}\nabla^2$ is a nonlocal operator, it can generate the ultranonlocality associated with the derivative discontinuity, while $R^S[n]$ as an explicit functional of the density can not. Therefore, one can seek for orbital-dependent exchange-correlation approximations and thus orbital-dependent functionals S that yield a derivative discontinuity of desired size in the sense that the eigenvalue gap $\varepsilon_{LU} - \varepsilon_{HO}$ is a good approximation to the fundamental gap Δ_g [SGV⁺96, SEKB10, KSRAB12, PYB⁺17, YPSP16, AK19]. The approximation of the remainder R^S also influences the band gaps, as it changes the local potential. Compared to $O^S[\{\varphi_{j\sigma}\}]$, however, the local potential usually only has a minor influence on the eigenvalues. Consequently, choosing a suitable generalized Kohn-Sham scheme, i.e., a suitable orbital-dependent functional S , is the key that enables the prediction of reasonable band gaps of solids and HOMO-LUMO gaps of molecules from generalized Kohn-Sham eigenvalue differences.

4.3 Ultranonlocality from meta-GGAs

Current meta-GGAs with high accuracy for energetic properties of molecules and solids are still systematically wrong for properties that require a substantial ultranonlocality, such as experimental band gaps [ZT09, YPSP16]. The reason for this is that although some of these meta-GGAs include a derivative discontinuity, it is still systematically too small [YPSP16].

To achieve a derivative discontinuity of proper size, the following construction principle was found [AK19]

$$\frac{\partial F_x}{\partial \alpha} < 0. \quad (4.19)$$

The derivation of this construction principle contains one crucial approximation, namely approximating $\partial F_{xc}/\partial \alpha$ by its average in the ‘‘energetically important region’’, $\overline{\partial F_{xc}/\partial \alpha}$ [AK19, Pub1]. By doing so, one can show that

$$\Delta_x = -c\overline{\partial F_x/\partial \alpha} \quad (4.20)$$

with a constant $c > 0$. Here, Δ_x is the derivative discontinuity due to the exchange part. Thus, choosing $\partial F_x/\partial \alpha < 0$ everywhere ensures a positive exchange derivative discontinuity and the magnitude of $\partial F_x/\partial \alpha$ indicates the size of Δ_x . The same line of argumentation holds for exchange and correlation together.

Notably, the exchange part of the TASK meta-GGA [AK19] has been designed based on the construction principle (4.19). Throughout this thesis, TASK refers to the combination of TASK exchange with LDA correlation in the parametrization of Perdew and Wang [PW92], as suggested in Ref. [AK19]. In fact, TASK predicts significantly more realistic band gaps than GGAs and earlier meta-GGAs [AK19, BSH⁺20, Pub1] and also provides a substantial improvement over previous meta-GGAs for further ultranonlocal properties [HSK20, RASK23, Pub2].

However, as we show in Refs. [Pub3, Pub4], TASK systematically underestimates the binding

strength of energetic bonds, especially weak bonds. Therefore, on the one hand we have meta-GGAs like SCAN that are quite accurate for energetic bonds and reasonably accurate for weak interactions, but are systematically wrong for properties that require substantial ultranonlocality, such as band gaps. On the other hand, we have meta-GGAs like TASK that show a more realistic treatment of ultranonlocal properties, but systematically underestimate bonding energies and fail to properly bind weakly bound systems. The ultimate goal of Part II, and of this thesis, is to resolve this dilemma by constructing a best-of-both-worlds meta-GGA that combines the description of ultranonlocal properties as with TASK with the description of energetic binding as with SCAN in a single semilocal density functional.

Part II

A Guide for the Publications

CHAPTER 5

Towards combined Accuracy for Band Gaps and Energetic Bonds from meta-GGAs

Part II discusses the main findings of the papers that make up Part III in the following order. First, in Section 5.1 we show that the TASK meta-GGA predicts accurate band gaps of solids for the right reason [Pub1], i.e., by including a derivative discontinuity of proper size. Furthermore, we revisit and refine the construction principle for a sizeable derivative discontinuity given in equation (4.19) [Pub1, Pub2]. Next, in Section 5.2 we analyze the description of energetic bonds with TASK and propose a correlation functional to remove the self-correlation of TASK [Pub3]. In Section 5.3, we work out what is decisive for the description of weak interactions with meta-GGAs. In particular, we clarify the influence of the kinetic energy density dependence and deduce a construction principle for the description of short- and intermediate-range van der Waals interactions [Pub4].

To combine these findings in a new general purpose meta-GGA, we first extend the established design strategy for nonempirical meta-GGAs [Pub5, Pub4], see Section 5.4. This new design strategy requires a more flexible form of the gradient expansion [Pub5]. Therefore, we derive the general form of the gradient expansion in meta-GGAs in Section 5.5.

Finally, we bring all these insights and developments together to construct LAK [Pub5], a nonempirical meta-GGA that balances nonlocality and energetic binding and combines accuracy for band gaps, energetic bonds, and weak interactions [Pub5, Pub4]. To highlight this achievement, we present it in a separate chapter, Chapter 6.

5.1 Accurate Band Gaps for the Right Reason

We have already explained in Section 3.3.3 why the traditional semilocal DFAs, LDA and GGA, systematically underestimate the band gaps of solids: they miss the derivative discontinuity for a fundamental reason. Moreover, we discussed in Section 4.2.2 that meta-GGAs, when evaluated in a generalized Kohn-Sham scheme, can in principle include the derivative discontinuity through their orbital dependence. Finally, in Section 4.3 we noted that the TASK meta-GGA predicts fairly realistic band gaps of solids.

Notably, also GGAs with a more realistic prediction of band gaps have been constructed [AK13]. To achieve this, however, GGAs must predict artificially increased Kohn-Sham gaps, since they can not include the derivative discontinuity. Consequently, the predictions of such GGAs for many other properties deteriorate [LA16, COM14]. Therefore, it is of high interest to check whether TASK predicts the accurate band gaps for the wrong reason (i.e., mainly by increasing the Kohn-Sham gap) or for the right reason (i.e., by including the derivative discontinuity with proper size).

This is the motivation of [Pub1], where we estimate the derivative discontinuity of TASK by comparing its Kohn-Sham and generalized Kohn-Sham gaps. Figure 5.1 compares the generalized Kohn-Sham gaps of TASK with its Kohn-Sham gaps (as obtained within the KLI approximation to the OEP), the LDA gaps, and the QMC-derived Kohn-Sham gaps for silicon and sodium chloride from Ref. [AGC⁺23]. Clearly, the generalized Kohn-Sham gaps of TASK are much closer to the experimental data than the LDA gaps. Moreover, the Kohn-Sham gaps of TASK are slightly larger than the LDA gaps and close to the reliable QMC-derived Kohn-Sham gaps. Thus, TASK predicts both reliable Kohn-Sham gaps and generalized Kohn-Sham gaps close to fundamental gaps from experiments. Consequently, TASK also predicts a derivative discontinuity of proper size. This demonstrates that TASK indeed predicts the right band gaps for the right reason and thus overcomes the “band gap problem of (semilocal) DFT”.

Furthermore, in [Pub1] we revisit the construction principle for a sizeable derivative discontinuity, equation (4.19). To gain insights beyond the underlying averaging approximation, we analyze which spatial regions and corresponding parameter ranges are most important for the derivative discontinuity in differently bound solids. Based on these insights, we refine the above construction principle (4.19) in [Pub5] to

$$\frac{\partial F_x}{\partial \alpha} \begin{cases} < 0, \text{ everywhere} \\ \text{roughly constant for } 0.2 \lesssim \alpha \lesssim 1.5 \end{cases} . \quad (\text{cp1})$$

We deliberately write this construction principle for exchange-only to make it more transparent. However, the same condition applies to F_{xc} for not too small densities with $0 \leq r_s \lesssim 5$. In [Pub1], we further discuss the impact of correlation on the derivative discontinuity and find arguments for a negative correlation derivative discontinuity. As a third and final result, [Pub1] shows that TASK predicts reasonable band gaps even for metal-halide perovskites, for which the band gap is notoriously hard to predict. This demonstrates the transferability of the construction principle

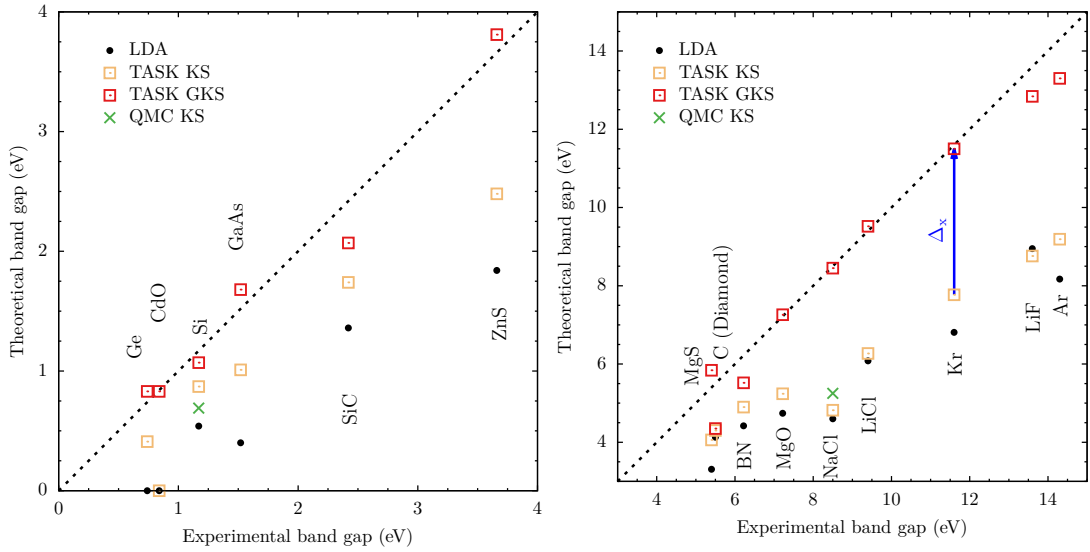


Figure 5.1: Band gaps of solids with the meta-GGA TASK [AK19] compared to LDA gaps and experimental data. Left: Small gap systems; Right: Large gap systems. The difference between the generalized Kohn-Sham (GKS) gaps and the Kohn-Sham (KS) gaps shows the exchange derivative discontinuity Δ_x , illustrated for Kr by a blue arrow. The green crosses mark the QMC-derived Kohn-Sham gaps from Ref. [AGC⁺23]. The dotted line illustrates agreement with the experimental values. Modified from [Pub1].

and its underlying approximation.

The insights from our detailed analysis of the construction principle (4.19) have also contributed to [Pub2]. There, existing meta-GGAs are analyzed with respect to the construction principle for a sizeable derivative discontinuity. As a proof-of-concept, [Pub2] shows that by using the construction principle (4.19) in an extreme way, even an exact-exchange like static response to an external electric field can be obtained from a meta-GGA. This once again demonstrates the capability of the construction principle to generate ultranonlocality.

5.2 Accurate Band Gaps and Improved Energetic Bonds

As mentioned above, the TASK meta-GGA in its original form is TASK exchange [AK19] combined with LDA correlation in the parametrization of Perdew and Wang [PW92]. Despite its success for band gaps and ultranonlocality, it was already observed in Ref. [AK19] that TASK is not particularly good for atomization energies. On the one hand, TASK exchange includes the hydrogen atom as an exact model system, which reduces the one-electron self-interaction. On the other hand, TASK still contains self-correlation through the use of LDA correlation. The latter is not only unsatisfactory from a fundamental point of view, but also contributes significantly to the strong underestimation of binding energies with the TASK meta-GGA [AK19, Pub3].

We therefore suggest in Ref. [Pub3] to combine TASK exchange with a simple corrected correlation (CC) functional that removes the self-correlation of TASK, while leaving its accuracy for band gaps unaffected. We refer to this as the TASK+CC meta-GGA. Although TASK+CC does not reach state-of-the-art meta-GGA accuracy for energetic binding, it significantly improves over the original TASK functional for atomization energies and reaction barrier heights [Pub3].

As an illustrative and simple example of density functional construction, we shortly explain the mechanism of the CC correlation. The CC correlation is based on the iso-orbital indicator z and the spin-polarization ζ (see Section 4.1 for definitions) and reads

$$E_c^{\text{CC}}[n_\uparrow, n_\downarrow] = \int n(\mathbf{r}) \varepsilon_c^{\text{CC}}(\mathbf{r}) d^3r. \quad (5.1)$$

with the CC correlation energy density per particle

$$\varepsilon_c^{\text{CC}}(\mathbf{r}) = \left(1 - z(\mathbf{r})\zeta^2(\mathbf{r})\right) \varepsilon^{\text{LDAc}}(\mathbf{r}). \quad (5.2)$$

$\varepsilon^{\text{LDAc}}(\mathbf{r})$ is the LDA correlation energy density per particle. The prefactor $(1 - z\zeta^2)$ in Eq. (5.2) vanishes if $z = 1$ and $\zeta = 1$, i.e., in one-electron regions. Thus, $\varepsilon_c^{\text{CC}} = 0$ in one-electron regions, which makes TASK+CC free from self-correlation. Both in regions of spin-unpolarized density ($\zeta = 0$) and in regions of homogeneous density ($z = 0$), the prefactor is equal to one and LDA correlation is restored. Consequently, TASK+CC is equivalent to TASK for spin-unpolarized systems, i.e., in particular for the homogeneous electron gas and for typical solids. In this way, TASK+CC restores the accuracy of TASK for the band gaps of solids.

To explore the limits of this approach, we also develop and investigate the CCaLDA correlation that reduces a systematic error of TASK+CC for systems containing hydrogen. However, this comes at the price of reintroducing self-correlation, which is why we do not consider TASK+CCaLDA a general purpose meta-GGA.

Finally, our analysis of the performance for bond lengths in Ref. [Pub3] reveals an issue for weakly bound systems, especially for systems with alkali metals. For such systems, TASK (and equivalently TASK+CC for spin-unpolarized systems) predicts a far too weak binding. The situation is even worse for van der Waals systems [Pub4]. As we show in Fig. 5.2 for the argon

dimer, TASK is even more repulsive than exact (Hartree-Fock) exchange. Unfortunately, even dispersion corrections [Gri11] are not able to reasonably compensate for such a strong repulsion.

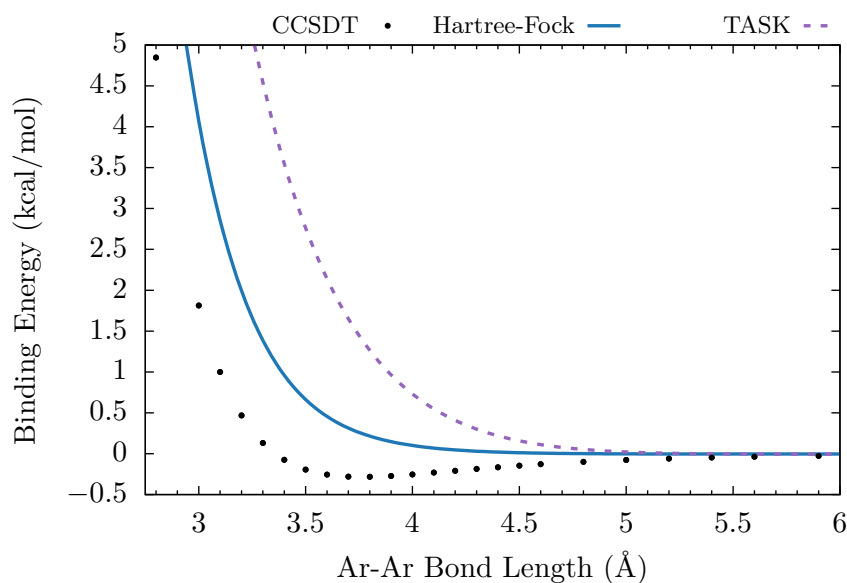


Figure 5.2: Ar₂ binding curves of TASK and exact (Hartree-Fock) exchange compared to highly accurate CCSDT reference values [JHBV09]. The DFT calculations were performed using a QZ4P basis set in the ADF code of the Amsterdam Modeling Suite [SCM23a].

Similar observations hold for other weak interactions such as hydrogen bonds [Leh23] and, to a lesser extent, ionic bonds. Unfortunately, this diminishes the otherwise useful capabilities of TASK in situations where the dynamics or geometry of weakly interacting systems is important, such as the description of charge transfer in large donor-acceptor complexes or the noncovalent adsorption of molecules on a surface, as TASK would often incorrectly predict these systems to be unstable.

5.3 Understanding van der Waals Interactions in meta-GGAs

Weak interactions in chemistry include several types of interactions, such as hydrogen bonds and van der Waals interactions. In the following, we focus on the van der Waals interactions, which include dispersion interactions in particular. Van der Waals forces originate from spontaneous dipole moments due to fluctuations in the charge density and therefore even act between neutral systems without permanent dipole moments. These spontaneous dipole moments generate an electric field that decays as $E \propto R^{-3}$ and that induces a dipole moment $d_{\text{ind}} \propto R^{-3}$ in the other system. The resulting van der Waals force corresponds to a potential $U = -C_6 R^{-6} \propto d_{\text{ind}} E$, which is the attractive long-range part of the London dispersion interactions [Lon30]. Considering quadrupole moments and three-body interactions gives rise to terms proportional to R^{-8} (quadrupole-dipole), R^{-10} (quadrupole-quadrupole), and R^{-9} (three-bodies) and so on. Consequently, the van der Waals interactions are proportional to $-C_6 R^{-6}$ in the long-range, while the higher order terms contribute in the intermediate range.

Due to the very nature of the London dispersion in charge fluctuations, they can also occur between completely non-overlapping densities. Therefore, semilocal (or even conventional hybrid) density functionals can not capture the long-range R^{-6} decay of the van der Waals interaction [AT02, RPC05, GHBB16]. Recovering this term within DFT requires to include long-range correlations between induced density fluctuations. Such a nonlocal treatment of correlation can be achieved with the random phase approximation [EF11, TTG21]. However, the use of unoccupied orbitals in the random phase approximation causes a considerable increase in computational cost, even compared to hybrid functionals. Alternatively, a DFA can be combined with an additional method for the explicit treatment of dispersion effects, such as a nonlocal density-based correlation functional [DRS⁺04, DRS⁺05, VVV10, SGD13] or an a posteriori dispersion correction [Gri04, BJ05, TS09, Gri11]. For comprehensive reviews on the explicit modeling of dispersion in electronic structure calculations, see, e.g., Refs. [GHBB16, SVVT19].

However, the exact density functional (that is unknown, but whose existence is guaranteed by the Hohenberg-Kohn theorem [HK64]) describes all electron-electron interactions exactly, including weak interactions. As we discuss in [Pub4], it is therefore desirable, both from a fundamental perspective and for practical considerations, to have the DFA itself treat dispersion interactions as well as possible, just like the exact functional would do.

Similar to the case of ultranonicity, the traditional semilocal DFAs lack the required nonlocality to describe weak interactions. However, while in the LDA this leads to an overestimation of weak interactions, typical GGAs underestimate them. In particular, both do not provide an appropriate description of the short- and intermediate-range van der Waals interactions. Once more, meta-GGAs can help to provide the required nonlocality, as first observed for the M06-L meta-GGA [ZT06, MFH10]. By virtue of their α dependence or, more generally, their kinetic energy density dependence, meta-GGAs can discriminate between covalent and dispersion interactions [MFH10, SXF⁺13]. This makes it possible for meta-GGAs to capture the short- and intermediate-range van der Waals interactions [SRZ⁺16, YKC19]. In situations where a precise description of the long-range van der Waals interactions is also important, an additional method

that only covers the long-range terms, most importantly the $-C_6R^{-6}$ term, is then sufficient [PYPS16, PBSP17].

Although several meta-GGAs provide an improved description of weak interactions [ZT06, SXF⁺13, SRP15] by recognizing different types of bonds through their kinetic energy dependence [MFH10, SXF⁺13, YKC19], the underlying mechanism is not yet well understood. In fact, an earlier study on the impact of the α dependence on the description of weakly interacting systems found unclear results [SXF⁺13]: On the one hand, the authors argue that a monotonically decreasing dependence on α would increase the binding of weakly interacting systems at the example of the MS2 meta-GGA [SHX⁺13] compared to GGAs. On the other hand, they note in the supplementary material that the meta-GGA MS1 [SHX⁺13], which falls more strongly with α than MS2 but is otherwise comparable, predicts less binding than MS2.

In [Pub4] we therefore aim to understand what is decisive for the description of weak interactions in meta-GGAs, and in particular to clarify the role of the kinetic energy density dependence. To this end, we perform a detailed analysis of the important parameter ranges, especially for the reduced density gradient s and the iso-orbital indicator α , see Fig. 2 in [Pub4]. There, we study the argon dimer as a well-established model systems for van der Waals interactions [LG93, VMG02, JWD04, TP05, RPC05, KB09, YB10, TH13]. In addition to s and α , we compare the Wigner Seitz radius r_s and the enhancement factors of the meta-GGAs SCAN, TASK, and LAK. From our analysis, we conclude that (1) $\partial F_{xc}/\partial s > 0$ increases the binding if $s \lesssim 1.2$ and decreases the binding if $s \gtrsim 1.2$, (2) $\partial F_{xc}/\partial \alpha < 0$ for $\alpha \gtrsim 0.4$ decreases the binding of weakly interacting systems, and (3) the α dependence for $\alpha \lesssim 0.4$ is of minor importance for the binding, because, except for the core region, α rarely becomes smaller than 0.4 in both the argon atom and dimer.

Our finding (1) is in line with Refs. [JBT21, JCBT24], where the authors show that in GGAs local maxima in the s dependence of the enhancement factor near $s = 1.2$ (with the precise value depending on the system of study) are decisive for the description of weakly interacting systems. Moreover, finding (1) is consistent with Ref. [YKC19], where the authors point out the importance of inflection points in the s dependence of the enhancement factor for the description of weakly interacting systems. Furthermore, finding (2) aligns with the observation noted in the supplementary material of Ref. [SXF⁺13]. In fact, our analysis can also explain the stronger binding of MS2 for weakly interacting systems compared to GGAs as a consequence of its strongly reduced increase in s for $s \gtrsim 1.2$ combined with a comparably small dependence on α , compare Fig. 2 in Ref. [SHX⁺13].

However, our conclusions differ from earlier findings for GGAs [LG93, ZPY97, MLL09, KB09, Coo10, PBJ21], where the large-gradient behavior of exchange has been found to be decisive for the description of weakly interacting systems. This originates in a fundamental difference between GGAs and meta-GGAs. Because the gradient expansion in GGAs fixes the s dependence for small s , different GGAs are merely different for small and medium values of s . Consequently, their behavior for large s , although a comparatively small contribution to the total energy, can become decisive for weak interactions. In meta-GGAs, the gradient expansion offers much more flexibility (as we discuss in Section 5.5) and the s dependence in meta-GGAs

can differ already for small values of s . Therefore, the details of finding (1) become important and dominate over the large-gradient contributions.

Moreover, our findings (1) and (2) explain why TASK predicts such a strong repulsion for weakly bound systems. On the one hand, finding (2) implies that the construction principle for proper ultranonicity of TASK, $\partial F_x/\partial\alpha < 0$, as well as its refined version (cp1), leads to a significant repulsion in weakly bound systems. On the other hand, also the s -dependence of TASK leads to increased repulsion, as one can see by comparing finding (1) with Fig. 2(b) of [Pub4]. In order to obtain an appropriately ultranonic meta-GGA that satisfies (cp1) and at the same time reasonably predicts weak interactions, we thus need a construction principle that increases the binding strength of van der Waals systems.

Fortunately, our analysis enables us to deduce the following construction principle for a proper description of the short- and intermediate-range van der Waals interactions in ultranonic meta-GGAs [Pub5, Pub4]

$$\left. \frac{\partial F_{xc}}{\partial s} \right|_{\alpha=1} \begin{cases} > 0 \text{ for } 0.5 \lesssim s \lesssim 1.2 \\ < 0 \text{ for } s \gtrsim 1.2 \end{cases} . \quad (\text{cp2})$$

Both construction principles, (cp1) and (cp2), are realized in the Lebeda-Aschebrock-Kümmel (LAK) meta-GGA [Pub5]. In Fig. 5.3, we show the binding curves of PBE, SCAN, M06-L, TASK, and LAK for the argon dimer and the krypton dimer, well-established model systems for studying van der Waals interactions [LG93, VMG02, TP05, RPC05, GÁ07, KB09, JBSD09, TH13, Goe15]. For comparison, we also show highly accurate CCSDT reference data [JHBV09, JHBV16]. The remarkable accuracy of LAK in this paradigm situation of weak interactions demonstrates the capability of the construction principle (cp2) in capturing the nonlocality associated with the short- and intermediate-range van der Waals interactions [Pub4].

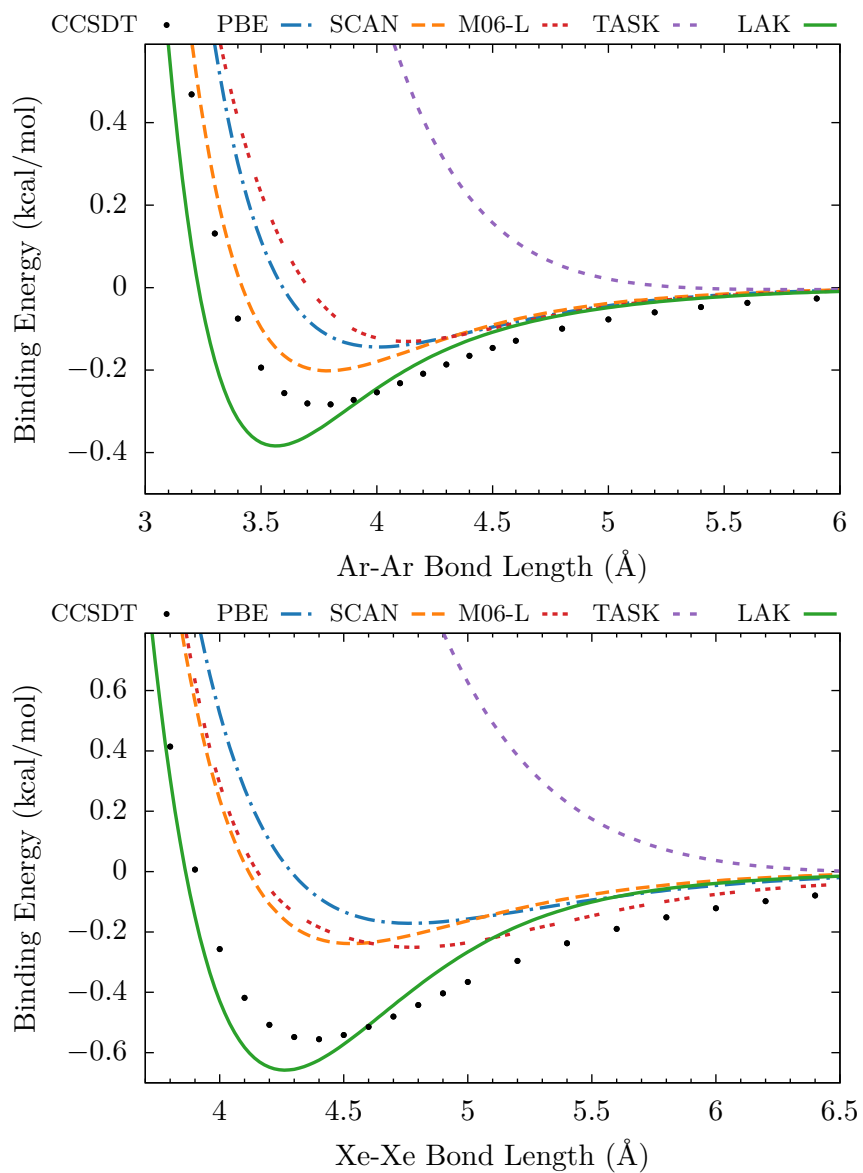


Figure 5.3: Ar₂ and Xe₂ binding curves of LAK compared to selected semilocal DFAs and highly accurate CCSDT reference values [JHBV09, HJB17]. Taken from [Pub4].

5.4 Enhancement Factor Engineering: Density Functionals based on Insights from Mathematics, Physics, and Chemistry

This section largely follows a corresponding section of [Pub4]. Following our goal of combining proper ultranonlocality with the capability to describe short- and intermediate-range van der Waals interactions in a single meta-GGA, we extend the successful design strategy for nonempirical density functionals (e.g. Refs. [PBE96, PRC⁺09, SRP15, AK19, FKN⁺20, FKN⁺22, KLP23]) of combining exact constraints with exactness for model systems, so-called appropriate norms, by the two construction principles (cp1) and (cp2). In the following, we explain the idea behind this strategy of designing exchange-correlation functionals.

A semilocal exchange-correlation functional, and thus the approximation to all electron-electron interactions, is completely defined by its enhancement factor. On the one hand, the exact constraints and model systems restrict the enhancement factor through inequalities, scaling relations, and exact limits [KLP23]. On the other hand, the degree of nonlocality of a density functional depends to a large extent on the details of its enhancement factor in between these limits. However, the exact constraints and model systems provide only limited information on how the enhancement factor should be modeled in this intermediate range. Therefore, the construction principles guide the enhancement factor in the intermediate range to ensure proper nonlocality. In our case, these are the ultranonlocality associated with the derivative discontinuity (cp1) and the short- and intermediate-range van der Waals interactions (cp2).

Importantly, we consider the *graph* of the enhancement factor the decisive property that should be obtained in a nonempirical fashion. Recall that the graph of a function f is the set of ordered pairs (x, y) , where $f(x) = y$. For example, the graph of F_x is the set $\{(s, \alpha), F_x(s, \alpha) \mid (s, \alpha) \in [0, \infty)^2\}$. The graph defines the enhancement factor and thus the density functional uniquely. Experience has shown that a lot of information about the performance of a functional can be obtained just from the graph [Pub2]. Furthermore, all exact constraints, appropriate norms, and construction principles also apply to the graph. In addition, we aim for a smooth enhancement factor, a condition found to be important for more accurate densities and the numerical stability of density functional approximations [MBS⁺17a, Kep17, MBS⁺17b]. Given these conditions, it is then up to us to find a suitable representation of the graph in terms of functions. While Occam's razor advises us to find the simplest possible representation of the graph, it remains a mathematical problem to find functions that can generate this graph.

Following the argumentation above, the construction principles thus guide the graph of the enhancement factor in a range in which the graph was not previously determined by physical reasons. In other words, the construction principles are additional conditions that tailor the choice of mathematical functions that satisfy the exact constraints and appropriate norms, based on chemical and physical insights. Because we design our functional via conditions on the graph of its enhancement factor, we call this design strategy "enhancement factor engineering".

The motivation for the design strategy of enhancement factor engineering emerges from the following considerations. From a mathematical point of view, we desire the enhancement factor

to satisfy as many analytical conditions as possible that we know about from the exact exchange-correlation functional. This is achieved by adhering to the exact constraints. From a physical point of view, we additionally want the enhancement factor to be correct for certain model systems, such as the homogeneous electron gas. These are the appropriate norms. Finally, from a chemical point of view, we wish to include existing chemical intuition into the enhancement factor. From the authors' point of view, taking into account existing knowledge about electronic structure or chemical intuition does not mean fitting parameters to large databases, but rather incorporating known facts about the electronic structure of certain types of systems into the design of the graph of the enhancement factor. This leads to the construction principles. In this sense, the strategy of enhancement factor engineering combines the insights from mathematics, physics, and chemistry.

5.5 The General Form of the Gradient Expansion for Meta-GGAs

The gradient expansion for slowly varying densities is an important exact constraint and the cornerstone of many nonempirical density functionals [PBE96, PKZB99, TPSS03, PRC⁺08, PRC⁺09, SRP15, TM16, AK19, FKN⁺20]. Furthermore, it is the origin and justification of the terms GGA and meta-GGA. For slowly varying densities, the gradient corrections to the exchange-correlation energy of the homogeneous electron gas are known to second order. Traditionally, the gradient expansion is written in terms of the reduced density gradient and reads [GR76, PK03, ED11]

$$E_{xc}^{\text{GE2}}[n] = A_x \int n^{4/3} C_s(r_s) \mu s^2 d^3 r, \quad (5.3)$$

where $\mu = 10/81$ is the gradient expansion coefficient of the exchange energy. The density dependence of C_s is known numerically from the random phase approximation [MB68, GR76, HL86, RG86] and has been parametrized by Rasolt and Geldart [RG86]. Unfortunately, the gradient expansion in the form of Eq. (5.3) is not compatible with the construction principle (cp1), because Eq. (5.3) implicitly assumes $\partial F_{xc}/\partial \alpha = 0$ for $s = 0$ and $\alpha = 1$ [SRP15]. However, this just is a remnant of the fact that Eq. (5.3) became popular for GGAs, which are not suitable for including ultranlocal features in the potential anyway. We show in the following that Eq. (5.3) is only one particular form of the gradient expansion in which the dependence on the kinetic energy density is suppressed. For meta-GGAs that depend on the kinetic energy density, reformulations of Eq. (5.3) that explicitly take into account a dependence on the kinetic energy density naturally appear more suitable.

As we demonstrate in [Pub5], the kinetic energy density dependence in meta-GGAs provides an additional degree of freedom in the gradient expansion. The origin of this additional freedom lies in the fact that not only the gradient of the density ∇n , but also the kinetic energy density τ contributes to the gradient expansion. The expansion of τ to second order in ∇n reads [BJC76, PSHP86]

$$\tau = \tau^{\text{unif}} (1 + (5/27)s^2 + (20/9)q) + \mathcal{O}(\nabla^4), \quad (5.4)$$

where $q = \nabla^2 n / [4(3\pi)^{2/3} n^{5/3}]$ is the reduced Laplacian of the density and τ^{unif} was defined in Section 4.1. For the iso-orbital indicator α this implies the gradient expansion

$$\alpha = 1 - (40/27)s^2 + (20/9)q + \mathcal{O}(\nabla^4). \quad (5.5)$$

Consequently, meta-GGAs can satisfy the gradient expansion with contributions from both s and τ or α , respectively. To obtain the general form of the gradient expansion in meta-GGAs, we rewrite Eq. (5.3) as

$$E_{xc}^{\text{GE2}}[n] = A_x \int n^{4/3} [C_{\mu_s}(r_s) \mu_s s^2 + C_{\mu_\alpha}(r_s) \mu_\alpha (\alpha - 1)] d^3 r, \quad (5.6)$$

where we assume without loss of generality $C_{\mu_s}(0) = C_{\mu_\alpha}(0) = C_s(0)$ (otherwise rescale μ_s and

μ_α). In [Pub5], we additionally assumed $C_{\mu_s} = C_{\mu_\alpha}$. This choice was made for the sake of clarity in the presentation and because in the context of [Pub5], the more general form would have led to essentially identical coefficients C_{μ_s} and C_{μ_α} anyway. Nevertheless, we stick to the more general form here and only restrict it if necessary.

To recover the correct gradient expansion in the energy, we demand that the right-hand sides of Eqs. (5.3) and (5.6) are equivalent, that is

$$\int n^{4/3} [C_{\mu_s}(r_s)\mu_s s^2 + C_{\mu_\alpha}(r_s)\mu_\alpha(\alpha - 1)] d^3r = \int n^{4/3} C_s(r_s)\mu s^2 d^3r. \quad (5.7)$$

To relate the density-dependence of the coefficients C_{μ_s} and C_{μ_α} to that of C_s , we transform the term in $\alpha - 1$ to terms in s^2 via (5.5) and integration by parts (considering only terms up to second order in ∇n and assuming that the density falls off fast enough, as is the case in physically meaningful systems),

$$\begin{aligned} & \int n^{4/3} [C_{\mu_s}(r_s)\mu_s s^2 + C_{\mu_\alpha}(r_s)\mu_\alpha(\alpha - 1)] d^3r \\ & \stackrel{(5.5)}{=} \int n^{4/3} [C_{\mu_s}(r_s)\mu_s s^2 + C_{\mu_\alpha}(r_s)\mu_\alpha (-40/27s^2 + 20/9q)] d^3r \\ & \stackrel{p.I.}{=} \int n^{4/3} \left[C_{\mu_s}(r_s)\mu_s + \frac{20}{27} [r_s C'_{\mu_\alpha}(r_s) - C_{\mu_\alpha}(r_s)] \mu_\alpha \right] s^2 d^3r. \end{aligned} \quad (5.8)$$

Thus, the general form of the gradient expansion yields the same energy as the common one, if

$$\mu C_s(r_s) = \mu_s C_{\mu_s}(r_s) + 6\mu\mu_\alpha [r_s C'_{\mu_\alpha}(r_s) - C_{\mu_\alpha}(r_s)]. \quad (5.9)$$

This differential equation finally connects C_{μ_s} and C_{μ_α} to C_s . Since $C_{\mu_s}(0) = C_{\mu_\alpha}(0) = C_s(0)$, the high-density, i.e., $r_s \rightarrow 0$, limit of Eq. (5.9) yields $\mu = \mu_s - 6\mu\mu_\alpha$. Consequently, μ_s is uniquely determined by μ_α via

$$\mu_s = (1 + 6\mu_\alpha)\mu. \quad (5.10)$$

Thus, we can eliminate μ_s in Eq. (5.9) to obtain

$$C_s(r_s) = C_{\mu_s}(r_s) + 6\mu_\alpha (r_s C'_{\mu_\alpha}(r_s) + C_{\mu_s} - C_{\mu_\alpha}(r_s)). \quad (5.11)$$

This shows that by choosing $\mu_\alpha = 0$, we get back to the common gradient expansion using only s . However, this differential equation does not determine C_{μ_s} and C_{μ_α} uniquely for a given μ_α . Therefore, in [Pub5] we additionally assume $C_{\mu_s} = C_{\mu_\alpha}$, which yields

$$C_s(r_s) = C_{\mu_\alpha}(r_s) + 6\mu_\alpha (r_s C'_{\mu_\alpha}(r_s)). \quad (5.12)$$

For $\mu_\alpha \neq 0$ this differential equation uniquely determines C_{μ_α} in terms of C_s and μ_α , as we discuss in detail in the Supplemental Material of [Pub5]. This completes the derivation of the general gradient expansion in s and α .

In summary, this yields the gradient expansion

$$E_{xc}^{GE2}[n] = A_x \int n^{4/3} [(1 + 6\mu_\alpha)\mu C_{\mu_\alpha}(r_s)s^2 + \mu_\alpha C_{\mu_\alpha}(r_s)(\alpha - 1)] d^3r, \quad (5.13)$$

where μ_α is a parameter that controls the balancing of the contributions from s and α to the gradient expansion and C_{μ_α} is uniquely determined by C_s . In particular, for $s = 0$ and $\alpha = 1$, we have $\partial F_{xc}/\partial \alpha = \mu_\alpha$, i.e., μ_α controls the size of the derivative that enters (the exchange-correlation version of) the construction principle for ultranonlocality (cp1). Consequently, μ_α allows to adjust the amount of ultranonlocality in a meta-GGA. Additionally, choosing a proper value for μ_α allows to satisfy both the gradient expansion and the construction principle (cp1) [Pub5].

The gradient expansion of the exchange energy alone is known to fourth order [SvB96]. Using similar arguments, the gradient expansion of the exchange energy can also be partitioned into contributions from s and α , which is a central pillar in the construction of TASK [AK19].

From a fundamental perspective, the partial integration from $(\alpha - 1)$ or q to s^2 means that the energy remains the same, but the energy density and thus the potential changes. In this way, we can on the one hand achieve similar accuracy for energetic binding as meta-GGAs based on the traditional form of the gradient expansion, which requires accurate total energies. On the other hand, we can simultaneously increase the ultranonlocality of the functional, which is, at fixed particle number, a property of the potential. Additionally, the balanced treatment of the gradient expansion leads to a smoother enhancement factor and thus increases the numerical stability [MBS⁺17a, Kep17, MBS⁺17b]. Figure 5.4 illustrates in a simplified way how using the balanced gradient expansion in LAK, the first meta-GGA intentionally based on the gradient expansion of the form (5.13) with $\mu_\alpha \neq 0$, makes it possible to achieve accurate predictions for both energetic binding and band gaps.

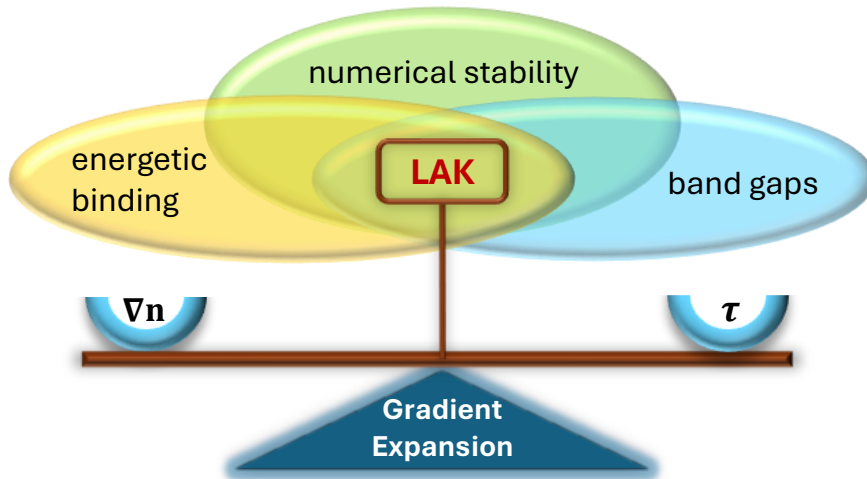


Figure 5.4: Illustration of how the balanced treatment of the gradient expansion in LAK allows to balance the “seesaw of the gradient expansion” between energetic binding, ultranonlocality (e.g. band gaps), and numerical stability.

CHAPTER 6

A new meta-GGA that combines Accuracy for Band Gaps and Energetic Bonds

Combining all the insights obtained in the previous sections, we have constructed the nonempirical meta-GGA LAK. To this end, we have combined all 17 exact constraints that a meta-GGA can satisfy [SRP15], 4 model systems (including the hydrogen atom to reduce one-electron self-interaction), the two construction principles discussed in Sections 5.1 and 5.3, and the balanced treatment of the gradient expansion. As a result, LAK is free from self-correlation, reduces the (one-electron) self-interaction, achieves an appropriate ultranonlocality, and captures the short- and intermediate-range van der Waals interactions. We will not repeat all the details of the construction and definition of LAK, but refer to [Pub5]. In the following, we focus instead on the predictions of LAK for band gaps, energetic binding, and weak interactions.

Figure 6.1 summarizes the performance of LAK for atomization energies, bond lengths, lattice constants of solids, band gaps of semiconductors, and weak interactions in a very compact form. There, we compare LAK to the two nonempirical density functionals whose design philosophy we have followed most closely, the GGA PBE [PBE96], and the meta-GGA SCAN [SRP15]. Moreover, we compare to the meta-GGA M06-L [ZT06], for which it was first observed that meta-GGAs can capture van der Waals interactions [MFH10], and to the (range-separated) hybrid functional HSE06 [KVIS06, HSE03, HSE06] that is known to yield fairly realistic band gaps [CC10] and therefore often used for band gap predictions with DFT. However, being a hybrid functional, HSE06 is significantly more computationally costly than the semilocal functionals, especially for periodic systems.

The left-hand side of Fig. 6.1 shows that LAK is an overall improvement over PBE and M06-L. In comparison to SCAN and HSE06, LAK improves or is on par for all observables except for the lattice constants of solids. On the one hand, lattice constants are important, because starting with a wrong geometry often causes errors in other observables. On the other hand, it is instructive to compare the errors relative to the reference values, as on the right-hand side of Fig. 6.1. There, we see that the relative error in the lattice constants is smaller than 3 % for all considered functionals, i.e., all functionals predict reasonable lattice constants. Overall, Fig. 6.1 underlines the universality of LAK, since only LAK achieves relative errors of 10 % or below for *all* considered properties, including band gaps and weak interactions, for which some of the other functionals exhibit significant errors.

Remarkably, LAK is furthermore the best pure semilocal density functional, i.e., density func-

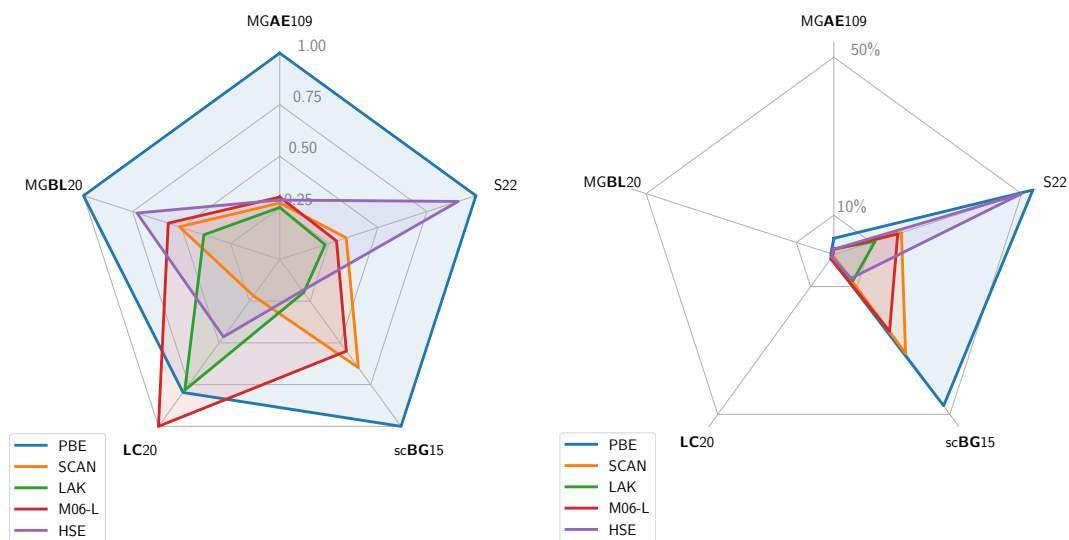


Figure 6.1: Overall performance of selected density functionals for Main-Group Atomization energies (MGAE109) [PT11], Main-Group Bond Lengths (MGBL20) [PT14], Lattice Constants (LC20) [SMC⁺11], semi-conductor Band Gaps (scBG15) [Pub5], and weak interactions (S22) [JŠČH06, MBS11]. Left: mean absolute deviation relative to the worst performing functional for each category. Right: mean absolute relative deviation from the reference values. Taken from [Pub4].

tional without additional correction, on GMTKN55 [Pub4]. GMTKN55 is a large database, often used to benchmark density functionals for General Main-group Thermochemistry, Kinetics, and Noncovalent (i.e. weak) interactions [GHB⁺17] and consists of 5 subcategories: basic properties and reaction energies of small molecules, reaction energies for large systems and isomerization reactions, barrier heights, and inter- and intramolecular noncovalent interactions (NCIs). To make the errors for the different properties and system sizes contained in GMTKN55 comparable, they are typically measured by the weighted total mean absolute deviation WTMAD-2 [GHB⁺17]. In Fig. 6.2, we compare LAK with PBE and the previously best-performing pure semilocal density functional on GMTKN55, the meta-GGA r2SCAN [FKN⁺20], a revised version of SCAN. LAK and r2SCAN both improve significantly over PBE, highlighting the overall improvement of meta-GGAs over GGAs [SRZ⁺16]. Among the meta-GGAs, LAK improves over r2SCAN for GMTKN55 as a whole and all its subcategories except for the basic properties, for which LAK and r2SCAN are on par. This demonstrates LAK's ability to accurately predict both covalent and noncovalent interactions. We attribute this improved accuracy of LAK compared to r2SCAN to the more balanced treatment of the gradient expansion and LAK's more pronounced nonlocality.

LAK reaches an accuracy that is comparable even to the best dispersion-corrected semilocal density functionals for GMTKN55 [Pub4]. The only dispersion-corrected semilocal method that shows a significant improvement over LAK for GMTKN55 is B97M-V [MHG15], which we attribute to the fact that B97M-V is constructed semi-empirically based on parts of the GMTKN55 database and the combined approach B97M-V to design the density functional together with a dispersion correction [Pub4].

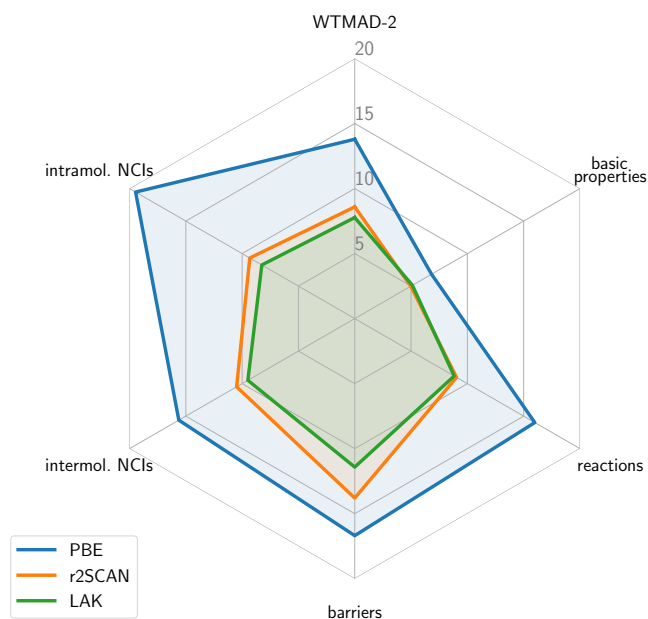


Figure 6.2: Weighted mean absolute deviation WTMAD-2 in kcal/mol for the GMTKN55 database and its subcategories for selected nonempirical semilocal density functionals: the GGA PBE [PBE96], the previously best-performing meta-GGA r2SCAN [FKN⁺20], and the newly developed meta-GGA LAK. Taken from [Pub4]

A particularly interesting subset of the GMTKN55 database is the MB16-43 set of decomposition energies of artificial molecules [KG09], because any chemical intuition was deliberately avoided in its creation. This “mindless” design makes it a good indicator of the transferability of a density functional to novel chemistry [GCDV24]. Table 6.1 compares LAK with the nonempirical GGA PBE, the empirical meta-GGA M06-L, and the nonempirical meta-GGA SCAN. This allows drawing several conclusions. First, the significantly better performance of the nonempirical functionals demonstrates the higher transferability of nonempirical density functionals compared to empirical ones [HS17, EHN⁺21, GHEM21]. Second, the improvement of SCAN and LAK over PBE emphasizes the progress in nonempirical DFAs from GGA to meta-GGA. [SRZ⁺16, IW18]. Third, and most importantly in the context of this work, the

Table 6.1: Mean absolute error of PBE, M06-L, SCAN, and LAK for the MB16-43 set of decomposition energies of artificial molecules [KG09] in kcal/mol. All values taken from [Pub4].

PBE GGA nonempirical	M06-L meta-GGA empirical	SCAN meta-GGA nonempirical	LAK meta-GGA nonempirical
23.3	64.1	15.7	16.4

similar accuracy of SCAN and LAK shows that no transferability is lost when the construction principles for proper nonlocality are included into the design strategy for nonempirical density functionals. In particular, we can thus expect that the transferability of LAK is on a similar level as the demonstrated transferability of SCAN [SRZ⁺16, FKN⁺20].

Summary

The aim of this thesis is to improve computer simulations for predicting the electronic structure of real materials by improving the underlying theoretical description. Because we aim for a computationally efficient method, we resorted to the class of semilocal density functionals within DFT. We identified a correct prediction of the electronic structure and the chemical stability, band gaps and electronic bonds, including weak bonds, to be crucial for the computational method. The combination of the (ultra)nonlocality required for accurate prediction of band gaps and weak interactions on the one hand and affordable computational cost on the other hand is provided by the class of orbital-dependent meta-GGAs [AK19, Pub1, MFH10, Pub2, Pub4].

Subsequently, we investigated what is decisive in meta-GGAs to achieve accuracy for band gaps in the first step [Pub1], band gaps *and* energetic bonds in the second step [Pub3], and third for weakly interacting systems [Pub4]. From this, we deduced two construction principles for proper nonlocality, (cp1) and (cp2) [Pub4, Pub5]. By extending the design strategy for nonempirical density functionals, leading to the design strategy of enhancement factor engineering [Pub4, Pub5], and revisiting the gradient expansion for slowly varying densities, enabling a more balanced treatment [Pub5], we were finally able to combine our insights and construct the nonempirical meta-GGA LAK [Pub5] that achieves state-of-the-art accuracy for band gaps and energetic bonds, including weak bonds, at very affordable computational cost [Pub4, Pub5]. This combination makes LAK a very promising functional for advanced materials modeling, e.g., in the field of energy materials, for large biological complexes, interfaces, and surfaces.

We expect our new strategy of enhancement factor engineering and the partitioning of the gradient expansion to inspire the future construction of DFAs and are excited to see what discoveries and material predictions the LAK functional will make possible.

Bibliography

- [Pub1] T. Lebeda, T. Aschebrock, J. Sun, L. Leppert and S. Kümmel, *Right band gaps for the right reason at low computational cost with a meta-GGA*, [Phys. Rev. Mater.](#) **7**, 093803 (2023).
- [Pub2] T. Aschebrock, T. Lebeda, M. Brütting, R. Richter, I. Schelter and S. Kümmel, *Exact exchange-like electric response from a meta-generalized gradient approximation: A semilocal realization of ultranonlocality*, [J. Chem. Phys.](#) **159**, 234107 (2023).
- [Pub3] T. Lebeda, T. Aschebrock and S. Kümmel, *First steps towards achieving both ultranonlocality and a reliable description of electronic binding in a meta-generalized gradient approximation*, [Phys. Rev. Res.](#) **4**, 023061 (2022).
- [Pub4] T. Lebeda and S. Kümmel, *A meta-Generalized Gradient Approximation that describes weak interactions in addition to bond energies and band gaps*, (submitted to Phys. Rev. B) .
- [Pub5] T. Lebeda, T. Aschebrock and S. Kümmel, *Balancing the contributions to the gradient expansion: Accurate binding and band gaps with a nonempirical Meta-GGA*, [Phys. Rev. Lett.](#) **133**, 136402 (2024).
- [AGC⁺23] A. Aouina, M. Gatti, S. Chen, S. Zhang and L. Reining, *Accurate Kohn-Sham auxiliary system from the ground state density of solids*, [Phys. Rev. B](#) **107**, 195123 (2023).
- [AK13] R. Armiento and S. Kümmel, *Orbital Localization, Charge Transfer, and Band Gaps in Semilocal Density-Functional Theory*, [Phys. Rev. Lett.](#) **111**, 036402 (2013).
- [AK19] T. Aschebrock and S. Kümmel, *Ultranonlocality and accurate band gaps from a meta-generalized gradient approximation*, [Phys. Rev. Res.](#) **1**, 033082 (2019).
- [AT02] M. J. Allen and D. J. Tozer, *Eigenvalues, integer discontinuities and NMR shielding constants in Kohn-Sham theory*, [Mol. Phys.](#) **100**, 433 (2002).
- [BADJ23] K. R. Bryenton, A. A. Adeleke, S. G. Dale and E. R. Johnson, *Delocalization error: The greatest outstanding challenge in density-functional theory*, [Wiley Interdiscip. Rev. Comput. Mol. Sci.](#) **13**, e1631 (2023).
- [BE90] A. D. Becke and K. E. Edgecombe, *A simple measure of electron localization in atomic and molecular systems*, [J. Chem. Phys.](#) **92**, 5397–5403 (1990).

- [Bec86] A. D. Becke, *Density functional calculations of molecular bond energies*, *J. Chem. Phys.* **84**, 4524–4529 (1986).
- [Bec88] A. D. Becke, *Correlation energy of an inhomogeneous electron gas: A coordinate-space model*, *J. Chem. Phys.* **88**, 1053–1062 (1988).
- [Bec93a] A. D. Becke, *A new mixing of Hartree–Fock and local density-functional theories*, *J. Chem. Phys.* **98**, 1372–1377 (1993).
- [Bec93b] A. D. Becke, *Density-functional thermochemistry. III. The role of exact exchange*, *J. Chem. Phys.* **98**, 5648–5652 (1993).
- [Bec96] A. D. Becke, *Density-functional thermochemistry. IV. A new dynamical correlation functional and implications for exact-exchange mixing*, *J. Chem. Phys.* **104**, 1040–1046 (1996).
- [BJ05] A. D. Becke and E. R. Johnson, *A density-functional model of the dispersion interaction*, *J. Chem. Phys.* **123**, 154101 (2005).
- [BJC76] M. Brack, B. Jennings and Y. Chu, *On the extended Thomas–Fermi approximation to the kinetic energy density*, *Phys. Lett. B* **65**, 1–4 (1976).
- [BK18] R. Baer and L. Kronik, *Time-dependent generalized Kohn–Sham theory*, *Eur. Phys. J. B* **91**, 1–9 (2018).
- [BO24] M. Born and R. Oppenheimer, *Zur Quantentheorie der Molekeln*, *Ann. Phys.* **379**, 1–31 (1924).
- [BSH⁺20] P. Borlido, J. Schmidt, A. Huran, F. Tran, M. Marques and S. Botti, *Exchange-correlation functionals for band gaps of solids: Benchmark, reparametrization and machine learning*, *npj Comput. Mater.* **6**, 96 (2020).
- [CA80] D. M. Ceperley and B. J. Alder, *Ground state of the electron gas by a stochastic method*, *Phys. Rev. Lett.* **45**, 566 (1980).
- [CC10] M. K. Y. Chan and G. Ceder, *Efficient band gap prediction for solids*, *Phys. Rev. Lett.* **105**, 196403 (2010).
- [CMDN20] K. Chayambuka, G. Mulder, D. L. Danilov and P. H. L. Notten, *From Li-ion batteries toward Na-ion chemistries: challenges and opportunities*, *Adv. Energy Mater.* **10**, 2001310 (2020).
- [CMSY08] A. J. Cohen, P. Mori-Sánchez and W. Yang, *Insights into current limitations of density functional theory*, *Science* **321**, 792–794 (2008).
- [CMSY12] A. J. Cohen, P. Mori-Sánchez and W. Yang, *Challenges for density functional theory*, *Chem. Rev.* **112**, 289–320 (2012).

- [COM14] T. F. T. Cerqueira, M. J. T. Oliveira and M. A. L. Marques, *Benchmarking the AK13 exchange functional: ionization potentials and electron affinities*, *J. Chem. Theory Comput.* **10**, 5625–5629 (2014).
- [Coo10] V. R. Cooper, *Van der Waals density functional: An appropriate exchange functional*, *Phys. Rev. B* **81**, 161104 (2010).
- [Cre01] D. Cremer, *Density functional theory: coverage of dynamic and non-dynamic electron correlation effects*, *Mol. Phys.* **99**, 1899–1940 (2001).
- [DFC16] F. Della Sala, E. Fabiano and L. A. Constantin, *Kinetic-energy-density dependent semilocal exchange-correlation functionals*, *Int. J. Quantum Chem.* **116**, 1641–1694 (2016).
- [DG90] R. M. Dreizler and E. K. U. Gross, *Density Functional Theory*, Springer, Berlin, Heidelberg, 1st edition, 1990.
- [DRS⁺04] M. Dion, H. Rydberg, E. Schröder, D. C. Langreth and B. I. Lundqvist, *Van der Waals density functional for general geometries*, *Phys. Rev. Lett.* **92**, 246401 (2004).
- [DRS⁺05] M. Dion, H. Rydberg, E. Schröder, D. C. Langreth and B. I. Lundqvist, *Erratum: Van der Waals density functional for general geometries*, *Phys. Rev. Lett.* **95**, 109902 (2005).
- [DV21] A. K. Datye and M. Votsmeier, *Opportunities and challenges in the development of advanced materials for emission control catalysts*, *Nat. Mater.* **20**, 1049–1059 (2021).
- [ED11] E. Engel and R. M. Dreizler, *Density Functional Theory*, Theoretical and Mathematical Physics, Springer, Berlin, Heidelberg, 1st edition, 2011.
- [EF11] H. Eshuis and F. Furche, *A parameter-free density functional that works for noncovalent interactions*, *J. Phys. Chem. Lett.* **2**, 983–989 (2011).
- [EH14] F. G. Eich and M. Hellgren, *Derivative discontinuity and exchange-correlation potential of meta-GGAs in density-functional theory*, *J. Chem. Phys.* **141**, 224107 (2014).
- [EHN⁺21] S. Ehlert, U. Huniar, J. Ning, J. W. Furness, J. Sun, A. D. Kaplan, J. P. Perdew and J. G. Brandenburg, *r2SCAN-D4: Dispersion corrected meta-generalized gradient approximation for general chemical applications*, *J. Chem. Phys.* **154**, 061101 (2021).
- [ESL⁺22] A. Y. S. Eng, C. B. Soni, Y. Lum, E. Khoo, Z. Yao, S. K. Vineeth, V. Kumar, J. Lu, C. S. Johnson, C. Wolverton and Z. W. Seh, *Theory-guided experimental design in battery materials research*, *Sci. Adv.* **8**, eabm2422 (2022).

- [FKN⁺20] J. W. Furness, A. D. Kaplan, J. Ning, J. P. Perdew and J. Sun, *Accurate and numerically efficient r2SCAN meta-generalized gradient approximation*, *J. Phys. Chem. Lett.* **11**, 8208–8215 (2020).
- [FKN⁺22] J. W. Furness, A. D. Kaplan, J. Ning, J. P. Perdew and J. Sun, *Construction of meta-GGA functionals through restoration of exact constraint adherence to regularized SCAN functionals*, *J. Chem. Phys.* **156**, 034109 (2022).
- [GÁ07] I. C. Gerber and J. G. Ángyán, *London dispersion forces by range-separated hybrid density functional with second order perturbational corrections: The case of rare gas complexes*, *J. Chem. Phys.* **126**, 044103 (2007).
- [GCDV24] T. Gould, B. Chan, S. G. Dale and S. Vuckovic, *Identifying and embedding transferability in data-driven representations of chemical space*, *Chem. Sci.* **15**, 11122–11133 (2024).
- [GHB⁺17] L. Goerigk, A. Hansen, C. Bauer, S. Ehrlich, A. Najibi and S. Grimme, *A look at the density functional theory zoo with the advanced GMTKN55 database for general main group thermochemistry, kinetics and noncovalent interactions*, *Phys. Chem. Chem. Phys.* **19**, 32184–32215 (2017).
- [GHBB16] S. Grimme, A. Hansen, J. G. Brandenburg and C. Bannwarth, *Dispersion-corrected mean-field electronic structure methods*, *Chem. Rev.* **116**, 5105–5154 (2016).
- [GHEM21] S. Grimme, A. Hansen, S. Ehlert and J.-M. Mewes, *r2SCAN-3c: A “Swiss army knife” composite electronic-structure method*, *J. Chem. Phys.* **154**, 064103 (2021).
- [GL94] A. Görling and M. Levy, *Exact Kohn-Sham scheme based on perturbation theory*, *Phys. Rev. A* **50**, 196 (1994).
- [GMR06a] M. Grüning, A. Marini and A. Rubio, *Effect of spatial nonlocality on the density functional band gap*, *Phys. Rev. B* **74**, 161103(R) (2006).
- [GMR06b] M. Grüning, A. Marini and A. Rubio, *Density functionals from many-body perturbation theory: The band gap for semiconductors and insulators*, *J. Chem. Phys.* **124**, 154108 (2006).
- [Goe15] L. Goerigk, *Treating London-dispersion effects with the latest Minnesota density functionals: problems and possible solutions*, *J. Phys. Chem. Lett.* **6**, 3891–3896 (2015).
- [GR76] D. J. W. Geldart and M. Rasolt, *Exchange and correlation energy of an inhomogeneous electron gas at metallic densities*, *Phys. Rev. B* **13**, 1477 (1976).
- [Gri04] S. Grimme, *Accurate description of van der Waals complexes by density functional theory including empirical corrections*, *J. Comp. Chem.* **25**, 1463–1473 (2004).

- [Gri11] S. Grimme, *Density functional theory with London dispersion corrections*, [Wiley Interdiscip. Rev. Comput. Mol. Sci.](#) **1**, 211–228 (2011).
- [GSB97] O. Gritsenko, P. Schipper and E. Baerends, *Exchange and correlation energy in density functional theory. Comparison of accurate DFT quantities with traditional Hartree-Fock based ones and generalized gradient approximations for the molecules Li_2 , N_2 , F_2 .*, [J. Chem. Phys.](#) **107**, 5007 (1997).
- [GSS86] R. Godby, M. Schlüter and L. Sham, *Accurate exchange-correlation potential for silicon and its discontinuity on addition of an electron*, [Phys. Rev. Lett.](#) **56**, 2415 (1986).
- [GSS88] R. W. Godby, M. Schlüter and L. Sham, *Self-energy operators and exchange-correlation potentials in semiconductors*, [Phys. Rev. B](#) **37**, 10159 (1988).
- [HC01] N. Handy and A. J. Cohen, *Left-right correlation energy*, [Mol. Phys.](#) **99**, 403 (2001).
- [HJB17] R. Hellmann, B. Jäger and E. Bich, *State-of-the-art ab initio potential energy curve for the xenon atom pair and related spectroscopic and thermophysical properties*, [J. Chem. Phys.](#) **147**, 034304 (2017).
- [HK64] P. Hohenberg and W. Kohn, *Inhomogeneous electron gas*, [Phys. Rev.](#) **136**, B864 (1964).
- [HL86] C. D. Hu and D. C. Langreth, *Beyond the random-phase approximation in nonlocal-density-functional theory*, [Phys. Rev. B](#) **33**, 943 (1986).
- [HL19] Y.-S. Hu and Y. Lu, *2019 Nobel prize for the Li-ion batteries and new opportunities and challenges in Na-ion batteries*, [ACS Energy Lett.](#) **4**, 2689–2690 (2019).
- [HS17] S. Hammes-Schiffer, *A conundrum for density functional theory*, [Science](#) **355**, 28–29 (2017).
- [HSE03] J. Heyd, G. E. Scuseria and M. Ernzerhof, *Hybrid functionals based on a screened Coulomb potential*, [J. Chem. Phys.](#) **118**, 8207 (2003).
- [HSE06] J. Heyd, G. E. Scuseria and M. Ernzerhof, *Erratum: Hybrid functionals based on a screened Coulomb potential*, [J. Chem. Phys.](#) **124**, 219906 (2006).
- [HSK20] F. Hofmann, I. Schelter and S. Kümmel, *Molecular excitations from meta-generalized gradient approximations in the Kohn–Sham scheme*, [J. Chem. Phys.](#) **153**, 114106–1–114106–11 (2020).
- [HYB⁺20] M. Hirscher, V. A. Yartys, M. Baricco, J. B. von Colbe, D. Blanchard, R. C. Bowman Jr., D. P. Broom, C. E. Buckley, F. Chang, P. Chen et al., *Materials for*

- hydrogen-based energy storage—past, recent progress and future outlook, *J. Alloys Compd.* **827**, 153548 (2020).
- [ipc23] IPCC, 2023: Sections, in *Climate Change 2023: Synthesis Report. Contribution of Working Groups I, II and III to the Sixth Assessment Report of the Intergovernmental Panel on Climate Change*, edited by Core Writing Team, H. Lee and J. Romero, pp. 35–115, Geneva, Switzerland, 2023, IPCC.
- [IW18] E. B. Isaacs and C. Wolverton, *Performance of the strongly constrained and appropriately normed density functional for solid-state materials*, *Phys. Rev. Mater.* **2**, 063801 (2018).
- [Jan78] J. F. Janak, *Proof that $\frac{\partial E}{\partial n_i} = \epsilon$ in density-functional theory*, *Phys. Rev. B* **18**, 7165 (1978).
- [JBSD09] E. R. Johnson, A. D. Becke, C. D. Sherrill and G. A. DiLabio, *Oscillations in meta-generalized-gradient approximation potential energy surfaces for dispersion-bound complexes*, *J. Chem. Phys.* **131**, 034111 (2009).
- [JBT21] T. Jenkins, K. Berland and T. Thonhauser, *Reduced-gradient analysis of van der Waals complexes*, *Electron. Struct.* **3**, 034009 (2021).
- [JCBT24] T. Jenkins, D. Chakraborty, K. Berland and T. Thonhauser, *Reduced-gradient analysis of molecular adsorption on graphene with nonlocal density functionals*, *Phys. Rev. B* **109**, 035427 (2024).
- [JHBV09] B. Jäger, R. Hellmann, E. Bich and E. Vogel, *Ab initio pair potential energy curve for the argon atom pair and thermophysical properties of the dilute argon gas. I. Argon–argon interatomic potential and rovibrational spectra*, *Mol. Phys.* **107**, 2181–2188 (2009).
- [JHBV16] B. Jäger, R. Hellmann, E. Bich and E. Vogel, *State-of-the-art ab initio potential energy curve for the krypton atom pair and thermophysical properties of dilute krypton gas*, *J. Chem. Phys.* **144**, 114304 (2016).
- [JŠČH06] P. Jurečka, J. Šponer, J. Černý and P. Hobza, *Benchmark database of accurate (MP2 and CCSD(T) complete basis set limit) interaction energies of small model complexes, DNA base pairs, and amino acid pairs*, *Phys. Chem. Chem. Phys.* **8**, 1985–1993 (2006).
- [JWD04] E. R. Johnson, R. A. Wolkow and G. A. DiLabio, *Application of 25 density functionals to dispersion-bound homomolecular dimers*, *Chem. Phys. Lett.* **394**, 334–338 (2004).
- [KB09] F. O. Kannemann and A. D. Becke, *Van der Waals interactions in density-functional theory: Rare-gas diatomics*, *J. Chem. Theory Comput.* **5**, 719–727 (2009).

- [KBM23] P. Kovács, P. Blaha and G. K. H. Madsen, *Origin of the success of mGGAs for bandgaps*, *J. Chem. Phys.* **159**, 244118 (2023).
- [Kep17] K. P. Kepp, *Comment on "Density functional theory is straying from the path toward the exact functional"*, *Science* **356**, 496 (2017).
- [KG09] M. Korth and S. Grimme, *"Mindless" DFT benchmarking*, *J. Chem. Theory Comput.* **5**, 993–1003 (2009).
- [KK08] S. Kümmel and L. Kronik, *Orbital-dependent density functionals: Theory and applications*, *Rev. Mod. Phys.* **80**, 3–60 (2008).
- [KK20] L. Kronik and S. Kümmel, *Piecewise linearity, freedom from self-interaction, and a Coulomb asymptotic potential: three related yet inequivalent properties of the exact density functional*, *Phys. Chem. Chem. Phys.* **22**, 16467–16481 (2020).
- [KKP04] S. Kümmel, L. Kronik and J. P. Perdew, *Electrical Response of Molecular Chains from Density Functional Theory*, *Phys. Rev. Lett.* **93**, 213002 (2004).
- [KLI92] J. B. Krieger, Y. Li and G. J. Iafrate, *Construction and application of an accurate local spin-polarized Kohn-Sham potential with integer discontinuity: Exchange-only theory*, *Phys. Rev. A* **45**, 101–126 (1992).
- [KLJ⁺20] J. Y. Kim, J.-W. Lee, H. S. Jung, H. Shin and N.-G. Park, *High-efficiency perovskite solar cells*, *Chem. Rev.* **120**, 7867–7918 (2020).
- [KLP23] A. D. Kaplan, M. Levy and J. P. Perdew, *The predictive power of exact constraints and appropriate norms in density functional theory*, *Annu. Rev. Phys. Chem.* **74**, 193–218 (2023).
- [Koh99] W. Kohn, *Nobel Lecture: Electronic structure of matter—wave functions and density functionals*, *Rev. Mod. Phys.* **71**, 1253 (1999).
- [KP03] S. Kümmel and J. P. Perdew, *Simple Iterative Construction of the Optimized Effective Potential for Orbital Functionals, Including Exact Exchange*, *Phys. Rev. Lett.* **90**, 043004 (2003).
- [KS65] W. Kohn and L. J. Sham, *Self-consistent equations including exchange and correlation effects*, *Phys. Rev.* **140**, A1133 (1965).
- [KSRAB12] L. Kronik, T. Stein, S. Refaely-Abramson and R. Baer, *Excitation Gaps of Finite-Sized Systems from Optimally Tuned Range-Separated Hybrid Functionals*, *J. Chem. Theory Comput.* **8**, 1515 (2012).
- [Kul15] H. J. Kulik, *Perspective: Treating electron over-delocalization with the DFT+U method*, *J. Chem. Phys.* **142**, 240901 (2015).

- [KVIS06] A. V. Krukau, O. A. Vydrov, A. F. Izmaylov and G. E. Scuseria, *Influence of the exchange screening parameter on the performance of screened hybrid functionals*, *J. Chem. Phys.* **125**, 224106 (2006).
- [LA16] A. Lindmaa and R. Armiento, *Energetics of the AK13 semilocal Kohn-Sham exchange energy functional*, *Phys. Rev. B* **94**, 155143 (2016).
- [LCdJ⁺21] S. G. Louie, Y.-H. Chan, F. H. da Jornada, Z. Li and D. Y. Qiu, *Discovering and understanding materials through computation*, *Nat. Mater.* **20**, 728–735 (2021).
- [Leh23] S. Lehtola, *private communication*, (2023).
- [Lev79] M. Levy, *Universal variational functionals of electron densities, first-order density matrices, and natural spin-orbitals and solution of the v -representability problem*, *PNAS* **76**, 6062–6065 (1979).
- [Lev91] M. Levy, *Density-functional exchange correlation through coordinate scaling in adiabatic connection and correlation hole*, *Phys. Rev. A* **43**, 4637–4646 (1991).
- [LG93] D. J. Lacks and R. G. Gordon, *Pair interactions of rare-gas atoms as a test of exchange-energy-density functionals in regions of large density gradients*, *Phys. Rev. A* **47**, 4681 (1993).
- [LK19] F. Liu and H. J. Kulik, *Impact of approximate DFT density delocalization error on potential energy surfaces in transition metal chemistry*, *J. Chem. Theory Comput.* **16**, 264–277 (2019).
- [Lon30] F. London, *Zur theorie und systematik der molekularkräfte*, *Zeitschrift für Physik* **63**, 245–279 (1930).
- [LSOM24] S. Lehtola, C. Steigemann, M. J. T. Oliveira and M. A. L. Marques, *Libxc 7.0.0*, 2024.
- [MB68] S.-K. Ma and K. A. Brueckner, *Correlation energy of an electron gas with a slowly varying high density*, *Phys. Rev.* **165**, 18 (1968).
- [MBS11] M. S. Marshall, L. A. Burns and C. D. Sherrill, *Basis set convergence of the coupled-cluster correction, $\delta_{MP2}^{CCSD(T)}$: Best practices for benchmarking non-covalent interactions and the attendant revision of the S22, NBC10, HBC6, and HSG databases*, *J. Chem. Phys.* **135**, 194102 (2011).
- [MBS⁺17a] M. G. Medvedev, I. S. Bushmarinov, J. Sun, J. P. Perdew and K. A. Lyssenko, *Density functional theory is straying from the path toward the exact functional*, *Science* **355**, 49 (2017).

- [MBS⁺17b] M. G. Medvedev, I. S. Bushmarinov, J. Sun, J. P. Perdew and K. A. Lyssenko, *Response to Comment on "Density functional theory is straying from the path toward the exact functional"*, *Science* **356**, 496 (2017).
- [MCH02] K. Molawi, A. J. Cohen and N. C. Handy, *Left–right and dynamic correlation*, *Int. J. Quantum Chem.* **89**, 86–93 (2002).
- [MFH10] G. K. H. Madsen, L. Ferrighi and B. Hammer, *Treatment of layered structures using a semilocal meta-GGA density functional*, *J. Phys. Chem. Lett.* **1**, 515–519 (2010).
- [MHG15] N. Mardirossian and M. Head-Gordon, *Mapping the genome of meta-generalized gradient approximation density functionals: The search for B97M-V*, *J. Chem. Phys.* **142**, 074111 (2015).
- [MK05] M. Mundt and S. Kümmel, *Derivative discontinuities in time-dependent density-functional theory*, *Phys. Rev. Lett.* **95**, 203004 (2005).
- [MLL09] É. D. Murray, K. Lee and D. C. Langreth, *Investigation of exchange energy density functional accuracy for interacting molecules*, *J. Chem. Theory Comput.* **5**, 2754–2762 (2009).
- [MNH96] D. K. W. Mok, R. Neumann and N. C. Handy, *Dynamical and nondynamical correlation*, *J. Phys. Chem.* **100**, 6225–6230 (1996).
- [MSCY06] P. Mori-Sánchez, A. J. Cohen and W. Yang, *Many-electron self-interaction error in approximate density functionals*, *J. Chem. Phys.* **125**, 201102 (2006).
- [MSCY08] P. Mori-Sánchez, A. J. Cohen and W. Yang, *Localization and Delocalization Errors in Density Functional Theory and Implications for Band-Gap Prediction*, *Phys. Rev. Lett.* **100**, 146401 (2008).
- [MW16] A. E. Mattsson and J. M. Wills, *Density functional theory for d- and f-electron materials and compounds*, *Int. J. Quantum Chem.* **116**, 834–846 (2016).
- [NNH96] R. Neumann, R. H. Nobes and N. Handy, *Exchange functionals and potentials*, *Mol. Phys.* **87**, 1–36 (1996).
- [NYBA18] P. K. Nayak, L. Yang, W. Brehm and P. Adelhelm, *From lithium-ion to sodium-ion batteries: advantages, challenges, and surprises*, *Angew. Chem., Int. Ed.* **57**, 102–120 (2018).
- [OP79] G. L. Oliver and J. P. Perdew, *Spin-density gradient expansion for the kinetic energy*, *Phys. Rev. A* **20**, 397–403 (1979).
- [PA82] G. S. Painter and F. W. Averill, *Bonding in the first-row diatomic molecules within the local spin-density approximation*, *Phys. Rev. B* **26**, 1781 (1982).

- [PBE96] J. P. Perdew, K. Burke and M. Ernzerhof, *Generalized Gradient Approximation Made Simple*, *Phys. Rev. Lett.* **77**, 3865–3868 (1996).
- [PBJ21] A. J. A. Price, K. R. Bryenton and E. R. Johnson, *Requirements for an accurate dispersion-corrected density functional*, *J. Chem. Phys.* **154**, 230902 (2021).
- [PBSP17] A. Patra, J. E. Bates, J. Sun and J. P. Perdew, *Properties of real metallic surfaces: Effects of density functional semilocality and van der Waals nonlocality*, *PNAS* **114**, E9188–E9196 (2017).
- [Per79] J. P. Perdew, *Orbital functional for exchange and correlation: self-interaction correction to the local density approximation*, *Chem. Phys. Lett.* **64**, 127–130 (1979).
- [Per85] J. P. Perdew, *Density functional theory and the band gap problem*, *Int. J. Quantum Chem.* **28**, 497–523 (1985).
- [Per90] J. P. Perdew, *Size-Consistency, Self-Interaction Correction, and Derivative Discontinuity in Density Functional Theory*, *Adv. Quant. Chem.* **21**, 113 (1990).
- [PK03] J. P. Perdew and S. Kurth, *Density Functionals for Non-relativistic Coulomb systems in the New Century*, in *A Primer in Density Functional Theory*, edited by C. Fiolhais, F. Nogueira and A. M. Marques, volume 620 of *Lecture Notes in Physics*, pp. 1–55, Springer, Berlin, Heidelberg, 2003.
- [PKZB99] J. P. Perdew, S. Kurth, A. Zupan and P. Blaha, *Accurate Density Functional with Correct Formal Properties: A Step Beyond the Generalized Gradient Approximation*, *Phys. Rev. Lett.* **82**, 2544–2547 (1999).
- [PL83] J. P. Perdew and M. Levy, *Physical Content of the Exact Kohn-Sham Orbital Energies: Band Gaps and Derivative Discontinuities*, *Phys. Rev. Lett.* **51**, 1884 (1983).
- [PPLB82] J. P. Perdew, R. G. Parr, M. Levy and J. L. Balduz Jr., *Density-Functional Theory for Fractional Particle Number: Derivative Discontinuities of the Energy*, *Phys. Rev. Lett.* **49**, 1691 (1982).
- [PRC⁺08] J. P. Perdew, A. Ruzsinszky, G. I. Csonka, O. A. Vydrov, G. E. Scuseria, L. A. Constantin, X. Zhou and K. Burke, *Restoring the density-gradient expansion for exchange in solids and surfaces*, *Phys. Rev. Lett.* **100**, 136406 (2008).
- [PRC⁺09] J. P. Perdew, A. Ruzsinszky, G. I. Csonka, L. A. Constantin and J. Sun, *Workhorse Semilocal Density Functional for Condensed Matter Physics and Quantum Chemistry*, *Phys. Rev. Lett.* **103**, 026403 (2009).

- [PRSP15] J. P. Perdew, A. Ruzsinszky, J. Sun and M. R. Pederson, Paradox of self-interaction correction: How can anything so right be so wrong?, volume 64 of *Advances In Atomic, Molecular, and Optical Physics*, pp. 1–14, Academic Press, 2015.
- [PSHP86] J. P. Perdew, V. Sahni, M. K. Harbola and R. K. Pathak, *Fourth-order gradient expansion of the fermion kinetic energy: Extra terms for nonanalytic densities*, *Phys. Rev. B* **34**, 686–691 (1986).
- [PSTS08] J. P. Perdew, V. N. Staroverov, J. Tao and G. E. Scuseria, *Density functional with full exact exchange, balanced nonlocality of correlation, and constraint satisfaction*, *Phys. Rev. A* **78**, 052513–1–052513–13 (2008).
- [PT11] R. Peverati and D. G. Truhlar, *Communication: A global hybrid generalized gradient approximation to the exchange-correlation functional that satisfies the second-order density-gradient constraint and has broad applicability in chemistry*, *J. Chem. Phys.* **135**, 191102 (2011).
- [PT14] R. Peverati and D. G. Truhlar, *Quest for a universal density functional: the accuracy of density functionals across a broad spectrum of databases in chemistry and physics*, *Philos. Trans. R. Soc. A* **372**, 20120476 (2014).
- [PW92] J. P. Perdew and Y. Wang, *Accurate and simple analytic representation of the electron-gas correlation energy*, *Phys. Rev. B* **45**, 13244–13249 (1992).
- [PY86] J. P. Perdew and W. Yue, *Accurate and simple density functional for the electronic exchange energy: Generalized gradient approximation*, *Phys. Rev. B* **33**, 8800 (1986).
- [PYB⁺17] J. P. Perdew, W. Yang, K. Burke, Z. Yang, E. K. U. Gross, M. Scheffler, G. E. Scuseria, T. M. Henderson, I. Y. Zhang, A. Ruzsinszky, H. Peng, J. Sun, E. Trushin and A. Görling, *Understanding band gaps of solids in generalized Kohn–Sham theory*, *PNAS* **114**, 2801–2806 (2017).
- [PYPS16] H. Peng, Z.-H. Yang, J. P. Perdew and J. Sun, *Versatile van der Waals density functional based on a meta-generalized gradient approximation*, *Phys. Rev. X* **6**, 041005 (2016).
- [PZ81] J. P. Perdew and A. Zunger, *Self-interaction correction to density-functional approximations for many-electron systems*, *Phys. Rev. B* **23**, 5048 (1981).
- [RASK23] R. Richter, T. Aschebrock, I. Schelter and S. Kümmel, *Meta-generalized gradient approximations in time dependent generalized Kohn–Sham theory: Importance of the current density correction*, *J. Chem. Phys.* **159**, 124117 (2023).
- [RG86] M. Rasolt and D. J. W. Geldart, *Exchange and correlation energy in a nonuniform fermion fluid*, *Phys. Rev. B* **34**, 1325 (1986).

- [RPC05] A. Ruzsinszky, J. P. Perdew and G. I. Csonka, *Binding energy curves from nonempirical density functionals II. van der Waals bonds in rare-gas and alkaline-earth diatomics*, *J. Phys. Chem. A* **109**, 11015–11021 (2005).
- [RPC⁺06] A. Ruzsinszky, J. P. Perdew, G. I. Csonka, O. A. Vydrov and G. E. Scuseria, *Spurious fractional charge on dissociated atoms: Pervasive and resilient self-interaction error of common density functionals*, *J. Chem. Phys.* **125**, 194112 (2006).
- [RPC⁺07] A. Ruzsinszky, J. P. Perdew, G. I. Csonka, O. A. Vydrov and G. E. Scuseria, *Density functionals that are one- and two-are not always many-electron self-interaction-free, as shown for H_2^+ , He_2^+ , LiH^+ , and Ne_2^+* , *J. Chem. Phys.* **126**, 104102 (2007).
- [RZ22] J. Roberts and E. Zurek, *Computational materials discovery*, *J. Chem. Phys.* **156**, 210401 (2022).
- [SBW⁺19] C. Shahi, P. Bhattarai, K. Wagle, B. Santra, S. Schwalbe, T. Hahn, J. Kortus, K. A. Jackson, J. E. Peralta, K. Trepte, S. Lehtola, N. K. Nepal, H. Myneni, B. Neupane, S. Adhikari, A. Ruzsinszky, Y. Yamamoto, T. Baruah, R. R. Zope and J. P. Perdew, *Stretched or noded orbital densities and self-interaction correction in density functional theory*, *J. Chem. Phys.* **150**, 174102 (2019).
- [Sch26] E. Schrödinger, *An undulatory theory of the mechanics of atoms and molecules*, *Phys. Rev.* **28**, 1049 (1926).
- [SCM23a] SCM, Theoretical Chemistry, Vrije Universiteit, Amsterdam, The Netherlands, *ADF 2023.104*, 2023.
- [SCM23b] SCM, Theoretical Chemistry, Vrije Universiteit, Amsterdam, The Netherlands, *BAND 2023.104*, 2023.
- [SCM24a] SCM, Theoretical Chemistry, Vrije Universiteit, Amsterdam, The Netherlands, *ADF 2024*, 2024.
- [SCM24b] SCM, Theoretical Chemistry, Vrije Universiteit, Amsterdam, The Netherlands, *BAND 2024*, 2024.
- [SCM25] SCM, Theoretical Chemistry, Vrije Universiteit, Amsterdam, The Netherlands, *Amsterdam Modeling Suite 2025*, 2025.
- [SD21] Y. Sun and S. Dai, *High-entropy materials for catalysis: A new frontier*, *Sci. Adv.* **7**, eabg1600 (2021).
- [SEKB10] T. Stein, H. Eisenberg, L. Kronik and R. Baer, *Fundamental gaps in finite systems from eigenvalues of a generalized Kohn-Sham method*, *Phys. Rev. Lett.* **105**, 266802 (2010).

- [SGDG13] R. Sabatini, T. Gorni and S. De Gironcoli, *Nonlocal van der Waals density functional made simple and efficient*, *Phys. Rev. B* **87**, 041108 (2013).
- [SGV⁺96] A. Seidl, A. Görling, P. Vogl, J. A. Majewski and M. Levy, *Generalized Kohn-Sham schemes and the band-gap problem*, *Phys. Rev. B* **53**, 3764 (1996).
- [SH53] R. T. Sharp and G. K. Horton, *A variational approach to the unipotential many-electron problem*, *Phys. Rev.* **90**, 317 (1953).
- [SHX⁺13] J. Sun, R. Haunschild, B. Xiao, I. W. Bulik, G. E. Scuseria and J. P. Perdew, *Semilocal and hybrid meta-generalized gradient approximations based on the understanding of the kinetic-energy-density dependence*, *J. Chem. Phys.* **138**, 044113 (2013).
- [SK16] T. Schmidt and S. Kümmel, *One-and many-electron self-interaction error in local and global hybrid functionals*, *Phys. Rev. B* **93**, 165120 (2016).
- [SMC⁺11] J. Sun, M. Marsman, G. I. Csonka, A. Ruzsinszky, P. Hao, Y.-S. Kim, G. Kresse and J. P. Perdew, *Self-consistent meta-generalized gradient approximation within the projector-augmented-wave method*, *Phys. Rev. B* **84**, 035117 (2011).
- [SRP15] J. Sun, A. Ruzsinszky and J. P. Perdew, *Strongly Constrained and Appropriately Normed Semilocal Density Functional*, *Phys. Rev. Lett.* **115**, 036402 (2015).
- [SRZ⁺16] J. Sun, R. C. Remsing, Y. Zhang, Z. Sun, A. Ruzsinszky, H. Peng, Z. Yang, A. Paul, U. Waghmare, X. Wu et al., *Accurate first-principles structures and energies of diversely bonded systems from an efficient density functional*, *Nat. Chem.* **8**, 831–836 (2016).
- [SS83] L. J. Sham and M. Schlüter, *Density-functional theory of the energy gap*, *Phys. Rev. Lett.* **51**, 1888 (1983).
- [SS85] L. J. Sham and M. Schlüter, *Density-functional theory of the band gap*, *Phys. Rev. B* **32**, 3883 (1985).
- [SvB96] P. S. Svendsen and U. von Barth, *Gradient expansion of the exchange energy from second-order density response theory*, *Phys. Rev. B* **54**, 17402–17413 (1996).
- [SVVT19] M. Stöhr, T. Van Voorhis and A. Tkatchenko, *Theory and practice of modeling van der Waals interactions in electronic-structure calculations*, *Chem. Soc. Rev.* **48**, 4118–4154 (2019).
- [SXF⁺13] J. Sun, B. Xiao, Y. Fang, R. Haunschild, P. Hao, A. Ruzsinszky, G. I. Csonka, G. E. Scuseria and J. P. Perdew, *Density Functionals that Recognize Covalent, Metallic, and Weak Bonds*, *Phys. Rev. Lett.* **111**, 106401 (2013).

- [SXR12] J. Sun, B. Xiao and A. Ruzsinszky, *Communication: Effect of the orbital-overlap dependence in the meta generalized gradient approximation*, *J. Chem. Phys.* **137**, 051101 (2012).
- [TH13] F. Tran and J. Hutter, *Nonlocal van der Waals functionals: The case of rare-gas dimers and solids*, *J. Chem. Phys.* **138**, 204103 (2013).
- [TM16] J. Tao and Y. Mo, *Accurate Semilocal Density Functional for Condensed-Matter Physics and Quantum Chemistry*, *Phys. Rev. Lett.* **117**, 073001 (2016).
- [TP05] J. Tao and J. P. Perdew, *Test of a nonempirical density functional: Short-range part of the van der Waals interaction in rare-gas dimers*, *J. Chem. Phys.* **122**, 114102 (2005).
- [TPSS03] J. Tao, J. P. Perdew, V. N. Staroverov and G. E. Scuseria, *Climbing the Density Functional Ladder: Nonempirical Meta-Generalized Gradient Approximation Designed for Molecules and Solids*, *Phys. Rev. Lett.* **91**, 146401 (2003).
- [TS76] J. D. Talman and W. F. Shadwick, *Optimized effective atomic central potential*, *Phys. Rev. A* **14**, 36 (1976).
- [TS09] A. Tkatchenko and M. Scheffler, *Accurate molecular Van der Waals interactions from ground-state electron density and free-atom reference data*, *Phys. Rev. Lett.* **102**, 073005 (2009).
- [TTG21] E. Trushin, A. Thierbach and A. Görling, *Toward chemical accuracy at low computational cost: Density-functional theory with σ -functionals for the correlation energy*, *J. Chem. Phys.* **154**, 014104 (2021).
- [Val80] S. M. Valone, *Consequences of extending 1-matrix energy functionals from pure-state representable to all ensemble representable 1 matrices*, *J. Chem. Phys.* **73**, 1344–1349 (1980).
- [VAS24] VASP Software GmbH, Vienna, Austria, VASP 6.5.0, 2024.
- [VMG02] T. Van Mourik and R. J. Gdanitz, *A critical note on density functional theory studies on rare-gas dimers*, *J. Chem. Phys.* **116**, 9620–9623 (2002).
- [VS98] T. Van Voorhis and G. E. Scuseria, *A novel form for the exchange-correlation energy functional*, *J. Chem. Phys.* **109**, 400–410 (1998).
- [VS04] O. A. Vydrov and G. E. Scuseria, *Effect of the Perdew–Zunger self-interaction correction on the thermochemical performance of approximate density functionals*, *J. Chem. Phys.* **121**, 8187–8193 (2004).
- [VVV10] O. A. Vydrov and T. Van Voorhis, *Nonlocal van der Waals density functional: The simpler the better*, *J. Chem. Phys.* **133**, 244103 (2010).

- [VWN80] S. H. Vosko, L. Wilk and M. Nusair, *Accurate spin-dependent electron liquid correlation energies for local spin density calculations: a critical analysis*, *Can. J. Phys.* **58**, 1200 – 1211 (1980).
- [YB10] K. E. Yousaf and E. N. Brothers, *Applications of screened hybrid density functionals with empirical dispersion corrections to rare gas dimers and solids*, *J. Chem. Theory Comput.* **6**, 864–872 (2010).
- [YCMS12] W. Yang, A. J. Cohen and P. Mori-Sanchez, *Derivative discontinuity, bandgap and lowest unoccupied molecular orbital in density functional theory*, *J. Chem. Phys.* **136**, 204111 (2012).
- [YKC19] J. H. Yang, D. A. Kitchaev and G. Ceder, *Rationalizing accurate structure prediction in the meta-GGA SCAN functional*, *Phys. Rev. B* **100**, 035132 (2019).
- [YPSP16] Z. H. Yang, H. Peng, J. Sun and J. P. Perdew, *More realistic band gaps from meta-generalized gradient approximations: Only in a generalized Kohn-Sham scheme*, *Phys. Rev. B* **93**, 205205 (2016).
- [ZHL⁺18] Q. Zhang, F. Hao, J. Li, Y. Zhou, Y. Wei and H. Lin, *Perovskite solar cells: must lead be replaced—and can it be done?*, *Sci. Technol. Adv. Mater.* **19**, 425–442 (2018).
- [ZPY97] Y. Zhang, W. Pan and W. Yang, *Describing van der Waals Interaction in diatomic molecules with generalized gradient approximations: The role of the exchange functional*, *J. Chem. Phys.* **107**, 7921–7925 (1997).
- [ZT06] Y. Zhao and D. G. Truhlar, *A new local density functional for main-group thermochemistry, transition metal bonding, thermochemical kinetics, and noncovalent interactions*, *J. Chem. Phys.* **125**, 194101 (2006).
- [ZT09] Y. Zhao and D. G. Truhlar, *Calculation of semiconductor band gaps with the M06-L density functional*, *J. Chem. Phys.* **130**, 074103 (2009).

List of Publications

- Pub. 1** *Right band gaps for the right reason at low computational cost with a meta-GGA,*
Timo Lebeda, Thilo Aschebrock, Jianwei Sun, Linn Leppert, and
Stephan Kümmel,
[Physical Review Materials](#) **7**, 093803 (2023)
- Pub. 2** *Exact exchange-like electric response from a meta-generalized gradient approximation: A semilocal realization of ultranonlocality,*
Thilo Aschebrock, Timo Lebeda, Moritz Brütting, Rian Richter, Ingo Schelter,
and Stephan Kümmel,
[Journal of Chemical Physics](#) **159**, 234107 (2023).
- Pub. 3** *First steps towards achieving both ultranonlocality and a reliable description of electronic binding in a meta-generalized gradient approximation,*
Timo Lebeda, Thilo Aschebrock, and Stephan Kümmel,
[Physical Review Research](#) **4**, 023061 (2022).
- Pub. 4** *A meta-Generalized Gradient Approximation that describes weak interactions in addition to bond energies and band gaps,*
Timo Lebeda and Stephan Kümmel,
submitted on December 10, 2024.
- Pub. 5** *Balancing the Contributions to the Gradient Expansion: Accurate Binding and Band Gaps with a Nonempirical Meta-GGA,*
Timo Lebeda, Thilo Aschebrock, and Stephan Kümmel,
[Physical Review Letters](#) **133**, 136402 (2024).

Part III

Publications

Publication 1

Publ. 1

Right band gaps for the right reason at low computational cost with a meta-GGA

Physical Review Materials 7, 093803 (2023)

**Timo Lebeda,^{1,2} Thilo Aschebrock,¹ Jianwei Sun,² Linn Leppert,³ and
Stephan Kümmel¹**

¹Theoretical Physics IV, University of Bayreuth, 95440 Bayreuth, Germany

²Department of Physics and Engineering Physics, Tulane University, New Orleans, Louisiana 70118, USA



³MESA+ Institute for Nanotechnology, University of Twente, 7500 AE Enschede, The Netherlands

Author contributions

All authors together conceptualized the work. T.L. performed the calculations reported in Secs. III, IV, and V and wrote the required routines. T.A. performed the calculations reported in Sec. VI and wrote the required routines. T.L. and S.K. wrote the manuscript, and all authors discussed the final version.

Publ.1

Right band gaps for the right reason at low computational cost with a meta-GGA

Timo Lebeda ^{1,2} Thilo Aschebrock,¹ Jianwei Sun,² Linn Leppert,³ and Stephan Kümmel ^{1,*}

¹Theoretical Physics IV, University of Bayreuth, 95440 Bayreuth, Germany

²Department of Physics and Engineering Physics, Tulane University, New Orleans, Louisiana 70118, USA

³MESA+ Institute for Nanotechnology, University of Twente, 7500 AE Enschede, The Netherlands



(Received 4 February 2023; revised 15 June 2023; accepted 22 August 2023; published 19 September 2023)

In density functional theory, traditional explicit density functionals such as the local density approximation and generalized gradient approximations cannot accurately predict the band gap of solids for a fundamental reason: They lack the exchange-correlation derivative discontinuity. By comparing Kohn-Sham and generalized Kohn-Sham calculations, we here show that the nonempirical meta-generalized-gradient-approximation (meta-GGA) TASK from Aschebrock and Kümmel [*Phys. Rev. Res.* **1**, 033082 (2019)] predicts the right gaps for the right reason, i.e., as a combination of a proper Kohn-Sham gap and a substantial derivative discontinuity contribution. For many materials from small-gap semiconductors to large-gap insulators, the proper band gap is thus obtained. We further study a group of metal-halide perovskites for which the band gap is notoriously hard to predict. For these materials, TASK yields band gaps very similar to the nonlocal screened hybrid Heyd-Scuseria-Ernzerhof functional, yet at a fraction of the hybrid functional's computational cost. We discuss the influence of correlation functionals, and open questions in the comparison of calculated band gaps with experimental ones.

DOI: [10.1103/PhysRevMaterials.7.093803](https://doi.org/10.1103/PhysRevMaterials.7.093803)

I. INTRODUCTION

The discovery of new materials is key for many applications [1] such as the next generation of solar modules [2–4], catalysts with improved efficiency [5], or batteries for energy storage [6,7]. For the computational screening of new materials, numerically efficient methods are required that predict material properties with sufficient accuracy [7–9]. Density functional theory (DFT) is very popular for such electronic structure calculations due to its balance between useful accuracy and reasonable computational cost. An example for an ongoing materials discovery quest is the search for nontoxic, earth-abundant, and stable semiconductors that can serve as light-converting materials in a wide range of applications. Metal-halide perovskites are a broad family of materials with outstanding chemical and electronic diversity that have received a lot of attention because of their versatile and highly tunable material properties [10–13]. The quintessential metal-halide perovskite, methylammonium (MA) lead iodide ($\text{CH}_3\text{NH}_3\text{PbI}_3$), e.g., has been used in solar cells with certified power conversion efficiencies exceeding 26% [14]. Since the family of metal-halide perovskites comprises thousands of stable materials [15,16], material-selection procedures have to be based on suitable criteria. The band gap is one of the most important properties for high-throughput material discovery and should be slightly larger than 1 eV for single-junction solar cells as a consequence of the detailed-balance limit [17]. Predicting the band gaps of perovskites with a reasonable reliability, yet at the same time low computational cost such that

many materials can be computationally screened, is therefore an important task.

The (fundamental) band gap E_g of a system with N electrons is defined by

$$E_g = I(N) - A(N), \quad (1)$$

where $I(N)$ is the ionization potential and $A(N)$ is the electron affinity of the N -electron system, respectively. In a DFT calculation within the Kohn-Sham scheme, the band gap splits [18,19] into the Kohn-Sham gap Δ_{KS} and the exchange-correlation (xc) derivative discontinuity Δ_{xc} ,

$$E_g = I(N) - A(N) = \Delta_{\text{KS}} + \Delta_{\text{xc}}. \quad (2)$$

The Kohn-Sham gap

$$\Delta_{\text{KS}} = \varepsilon_{\text{LU}}^{\text{KS}} - \varepsilon_{\text{HO}}^{\text{KS}} \quad (3)$$

stems from the orbital-dependent kinetic energy [20] and is the difference between the lowest unoccupied (LU) and the highest occupied (HO) one-electron energy. For occupation numbers that respect the Aufbau principle, it is always non-negative [21].

The xc derivative discontinuity on the other hand vanishes for density functional approximations that explicitly depend only on the density, or quantities directly derived from it, e.g., its spatial derivatives [18,22–26]. Therefore the local density approximation (LDA) [27] and generalized gradient approximations (GGAs) [28,29] severely underestimate the band gaps of semiconductors and insulators. The comparison with Green's-function-based quasiparticle calculations has led to the estimate that the xc derivative discontinuity often is responsible for 30–50% or more of the band gap [30,31], and recent reconstructions of the exact Kohn-Sham system

*stephan.kuettel@uni-bayreuth.de

for solids have confirmed the substantial contribution that Δ_{xc} makes to the gap [32].

Within the Kohn-Sham scheme, Δ_{KS} would not generally correspond to the fundamental gap even for the unknown exact xc functional [22,30,32–35]. However, for orbital-dependent functionals, the generalized Kohn-Sham formalism offers an attractive alternative [36]. In generalized Kohn-Sham theory the potential is no longer multiplicative. Depending on the xc approximation used, it leads to a set of orbital-dependent differential (meta-GGA) or integral (exact exchange) operators. This allows one to strive for xc approximations where the eigenvalue gap of the generalized partially interacting reference system equals the fundamental gap, i.e., for which

$$\Delta_{gKS} = \varepsilon_{LU}^{gKS} - \varepsilon_{HO}^{gKS} = E_g. \quad (4)$$

This is exploited, for example, in the range-separated hybrid Heyd-Scuseria-Ernzerhof functional (HSE) [37,38], where the short-range–long-range splitting parameter is used to empirically find a good generalized Kohn-Sham system. A more sophisticated choice of the generalized Kohn-Sham system is made in the optimally tuned range-separated hybrids [39,40], where a system-dependent parameter is fixed by enforcing the ionization potential (IP) theorem [41] for the N and $N + 1$ electron systems as closely as possible. This tuning amounts to choosing the generalized Kohn-Sham system which minimizes Δ_{xc} [40,42,43] and aims for $\Delta_{gKS} = E_g$.

Comparison of Eqs. (2) and (4) shows that for a given xc functional, the difference between the generalized Kohn-Sham gap and the Kohn-Sham gap equals the xc derivative discontinuity,

$$\Delta_{xc} = \Delta_{gKS} - \Delta_{KS}. \quad (5)$$

Note that Eq. (5) only holds under the assumption that the orbitals do not change when switching from the Kohn-Sham to a generalized Kohn-Sham formalism. The latter is at least true in perturbation theory to first order [44].

In the past, local multiplicative potentials were constructed yielding a Kohn-Sham gap that closely approximates the fundamental gap [45,46]. These constructions, however, lead to other problems, e.g., divergences [47,48], too narrow bands [49], the lack of an energy functional and therefore, e.g., no prediction of bond lengths [45], a rather poor description of energetic binding [50], and numerical issues [51]. In the light of Eq. (2), one might interpret these issues as reflections of intrinsic inconsistencies that result when trying to map the effects of the nonlocal Δ_{xc} into a local potential.

Meta-generalized-gradient-approximations (meta-GGAs) [52–61] that depend on the kinetic energy density τ , and thus on the occupied Kohn-Sham orbitals, can have a nonvanishing xc derivative discontinuity [61–63], because the orbitals are implicit, nonlocal functionals of the density. Thus meta-GGAs in principle can improve band-gap prediction when evaluated in a generalized Kohn-Sham scheme [63,64]. In practice, however, the derivative discontinuity of many meta-GGAs is relatively small [62,63,65], so that the band gaps are not quantitatively accurate.

Therefore, so far functionals used for band-gap prediction typically include exact exchange [38,39,66,67] and thus come at a computational expense much larger than an LDA

or GGA calculation. As a consequence, they have rarely been used for computationally demanding applications such as extensive materials screening. Because meta-GGAs have semilocal computational costs, they are the natural choice for large-scale calculations, provided they achieve the desired accuracy. Therefore understanding the nature of the xc derivative discontinuity in meta-GGAs and how it relates to the prediction of band gaps is a topic of substantial current interest [61,63,68–70].

In this paper, we show that the TASK meta-GGA from Aschbrock and Kümmel [61] yields the right band gaps for the right reason, namely by incorporating a substantial contribution from the derivative discontinuity on top of a Kohn-Sham gap with a magnitude similar to exact Kohn-Sham gaps.

II. GENERATING A SIZABLE DERIVATIVE DISCONTINUITY IN META-GGAS

The meta-GGAs that we study here [71] depend on the electron density n , its gradient ∇n , and the (positive) noninteracting kinetic energy density

$$\tau = \frac{\hbar^2}{2m} \sum_{\sigma} \sum_{i=1}^{N_{\sigma}} |\nabla \varphi_{i\sigma}|^2. \quad (6)$$

In the single-orbital limit, the kinetic energy density tends to the von Weizsäcker kinetic energy density

$$\tau_W = \frac{\hbar^2}{8m} \frac{|\nabla n|^2}{n}, \quad (7)$$

while in the uniform-density limit it becomes

$$\tau_{\text{unif}} = \frac{3\hbar^2}{10m} (3\pi^2)^{2/3} n^{5/3} =: A_s n^{5/3}. \quad (8)$$

The exchange energy is typically parametrized in dimensionless quantities that have a physical interpretation in certain limits. Here, we consider the reduced density gradient

$$s^2 = \frac{1}{4(3\pi^2)^{2/3}} \frac{|\nabla n|^2}{n^{8/3}}, \quad (9)$$

which can be used to detect noncovalent interactions [72], and the iso-orbital indicator

$$\alpha = \frac{\tau - \tau_W}{\tau_{\text{unif}}}, \quad (10)$$

which tends to zero in the iso-orbital limit, to one in the uniform-density limit, and to infinity in regions dominated by density overlap between closed shells [73]. Thus the meta-GGA exchange energy of a spin-unpolarized system reads

$$\begin{aligned} E_x^{\text{mGGA}} &= \int e_x^{\text{mGGA}}(n, \nabla n, \tau) d^3r \\ &= A_x \int n^{4/3} F_x^{\text{mGGA}}(s^2, \alpha) d^3r \end{aligned} \quad (11)$$

with the (exchange) enhancement factor $F_x^{\text{mGGA}}(s^2, \alpha)$ and $A_x = -(3e^2/4)(3/\pi)^{1/3}$. To obtain the exchange energy of a spin-polarized system, the exact spin scaling relation [74] can be applied to Eq. (11). The correlation energy is often defined via the (correlation) energy density per particle ε_c . For a direct comparison between exchange and correlation,

the enhancement factor of correlation over LDA exchange is defined as

$$E_c^{\text{mGGA}} = \int n e_c^{\text{mGGA}}(n, \nabla n, \tau) d^3 r$$

$$=: A_x \int n^{\frac{4}{3}} F_c^{\text{mGGA}}(r_s, s^2, \alpha) d^3 r, \quad (12)$$

where the correlation enhancement factor, in addition to the dependence on s and α , depends on the Seitz radius $r_s = (4\pi n/3)^{-1/3}$. Typically, it also depends on a quantity for modeling the spin dependence, e.g., the spin polarization $\zeta = (n_\uparrow - n_\downarrow)/(n_\uparrow + n_\downarrow)$, but we have suppressed the spin dependence here for ease of notation.

It is well established that the xc derivative discontinuity is an important feature of the exact functional [18–20,75]. It was already discussed 40 years ago in the context of the straight line condition of Perdew, Parr, Levy, and Balduz [20], which states that the total energy as a function of the (fractional) particle number consists of straight lines between integer particle numbers. At integer particle numbers, however, the total energy has a kink, corresponding to a jump in its derivative. This derivative discontinuity with respect to the particle number equals the fundamental band gap of a solid,

$$E_g = \left. \frac{\partial E}{\partial N} \right|_+ - \left. \frac{\partial E}{\partial N} \right|_-, \quad (13)$$

where $|_-$ and $|_+$ denote derivatives evaluated on the electron-deficient and electron-rich side of the integer particle number. On the right-hand side, all energy contributions that are continuous in the density do not contribute. Thus

$$E_g = \underbrace{\left(\left. \frac{\delta T_s[n]}{\delta n(\mathbf{r})} \right|_+ - \left. \frac{\delta T_s[n]}{\delta n(\mathbf{r})} \right|_- \right)}_{\Delta_{\text{KS}}} + \underbrace{\left(\left. \frac{\delta E_{\text{xc}}[n]}{\delta n(\mathbf{r})} \right|_+ - \left. \frac{\delta E_{\text{xc}}[n]}{\delta n(\mathbf{r})} \right|_- \right)}_{\Delta_{\text{xc}}}, \quad (14)$$

where the discontinuity originating in the noninteracting kinetic energy equals the Kohn-Sham gap of Eq. (3), and the second term is the derivative discontinuity of the exchange-correlation energy. In a meta-GGA, the latter is due to the orbital dependence of E_{xc} . Consequently, the xc derivative discontinuity of a meta-GGA reads

$$\Delta_{\text{xc}}^{\text{mGGA}} = \int \frac{\partial e_{\text{xc}}}{\partial \tau}(\mathbf{r}') \left[\left. \frac{\delta \tau(\mathbf{r}')}{\delta n(\mathbf{r})} \right|_+ - \left. \frac{\delta \tau(\mathbf{r}')}{\delta n(\mathbf{r})} \right|_- \right] d^3 r'. \quad (15)$$

To obtain further insight, one can simplify this expression by approximating the first term by its average over an “energetically important region,”

$$\frac{\partial e_{\text{xc}}}{\partial \tau} \approx \overline{\frac{\partial e_{\text{xc}}}{\partial \tau}}. \quad (16)$$

This derivation has been used in the construction of the TASK functional for exchange [61], and here we underpin it with additional considerations. The “energetically important region” denotes the spatial region in which the dominant contributions to the above integral emerge. The accuracy of this approximation may vary from system to system and especially between solids and molecules. Still, it provides useful insights into how an xc derivative discontinuity of desired sign and size can be generated.

The approximation of Eq. (16) allows one to pull the approximated term in front of the integral. Since the noninteracting kinetic energy density τ integrates to the usual noninteracting kinetic energy functional T_s , this leads to

$$\Delta_{\text{xc}}^{\text{mGGA}} \approx \overline{\frac{\partial e_{\text{xc}}}{\partial \tau}} \Delta_{\text{KS}}. \quad (17)$$

This implies that the xc derivative discontinuity of a meta-GGA is approximately proportional to the Kohn-Sham gap—if the approximation of Eq. (16) is justified. When one goes beyond this approximation, then there is the possibility for a nonvanishing xc discontinuity despite a vanishing Kohn-Sham gap. We discuss such a case (CdO) below. Within the approximation, the sign as well as the size of the xc derivative discontinuity can be controlled via the proportionality factor $\overline{\partial e_{\text{xc}}/\partial \tau}$, since the Kohn-Sham gap is non-negative.

It has been conjectured that the total xc derivative discontinuity as well as that of exchange must be positive in electronic systems. These conclusions have been based on, e.g., the numerical evidence that typical semilocal functionals (LDA and GGAs) systematically underestimate band gaps of solids [32] and explicit calculations of Δ_x and Δ_{xc} [76–80], as well as the observation that the ground-state energy as a function of particle number is concave upwards for systems with repulsive interactions. Because the exchange contribution to the xc derivative discontinuity, Δ_x , is typically much larger than that from correlation, we first consider exchange. A detailed discussion of the contribution from correlation follows in Sec. V.

To obtain a positive exchange derivative discontinuity, the proportionality condition equation (17) implies that one has to construct the meta-GGA exchange energy such that

$$\frac{\partial e_x}{\partial \tau} > 0 \quad (18)$$

in the energetically important region. Moreover, the magnitude of $\partial e_x/\partial \tau$, together with the Kohn-Sham gap, determines the size of Δ_x . For a parametrization of the exchange enhancement factor F_x in s and α the condition of Eq. (18) is equivalent to the condition [61]

$$\frac{\partial F_x}{\partial \alpha} < 0. \quad (19)$$

Thus there is a construction principle for the meta-GGA enhancement factor by which one can control the sign as well as the size of the exchange (x) or exchange-correlation (xc) derivative discontinuity.

III. RIGHT BAND GAPS FOR THE RIGHT REASON

In the following, we show that this construction principle indeed leads to the proper prediction of band gaps. In the context of this discussion, it is helpful to have in mind some general aspects of band-gap calculations. First, one must be aware that the calculated gaps depend on the lattice parameters and on numerical choices such as the size of the basis set, whether a pseudopotential is used or not, and possibly the details of the employed pseudopotential. Second, relativistic effects can influence the band structure of some materials noticeably. Third, the xc approximation influences the band

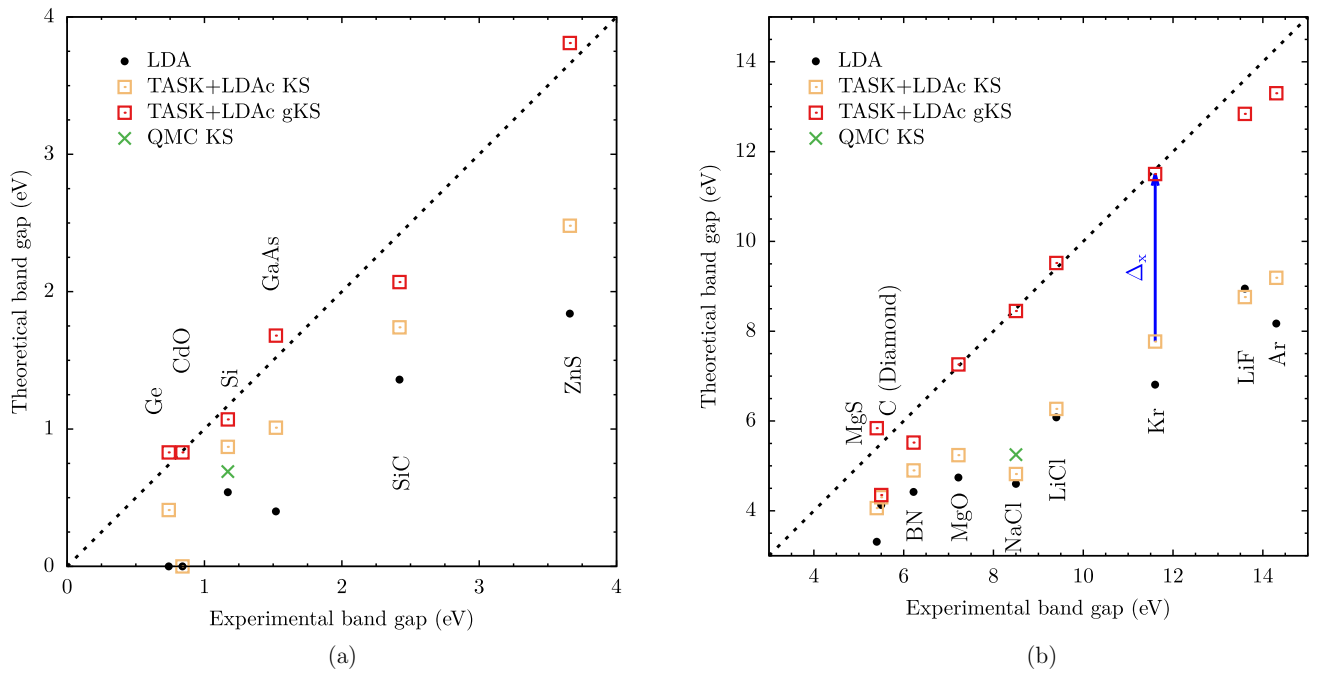


FIG. 1. Calculated vs experimental band gaps of (a) small-gap systems and (b) large-gap systems. The difference between the generalized Kohn-Sham (gKS) gaps and the Kohn-Sham (KS) gaps shows the exchange derivative discontinuity, illustrated for Kr by a blue arrow. Experimental bond lengths and experimental band gaps have been chosen as in Ref. [61] for all systems except NaCl. The bond length and reference value of NaCl are taken from Ref. [32] to allow for comparison with the QMC data. The green crosses mark the QMC-derived Kohn-Sham gaps of Si (0.69 eV) and NaCl (5.25 eV) from Ref. [32]. The dotted line illustrates exact agreement with the reference values.

structure via the single-particle gap and possibly the derivative discontinuity. Fourth and finally, for orbital-dependent xc approximations, it can make an important difference whether one is using the Kohn-Sham or the generalized Kohn-Sham scheme. In the Supplemental Material [81] we discuss these different aspects and show, e.g., in Tables SII and SIII, results for different density functionals and different levels of taking into account relativistic effects. In this paper, our focus is on the above-discussed meta-GGA construction principle.

The TASK meta-GGA for exchange [61] adheres to this principle and combines it with the fulfillment of nonempirical exact constraints. A correlation functional to go along with TASK is the iso-orbital corrected correlation (CC) [82]. It is based on the local spin density approximation (LSDA) in the parametrization of Perdew and Wang [83]. For systems without spin polarization, such as the solids in the test set studied below, the CC is identical to the LSDA correlation. In the following, we just write “TASK” to refer to TASK exchange with LSDA correlation to simplify the notation.

The decisive step for disentangling the single-particle contribution and the derivative discontinuity contribution to the band gap is to compare the gaps obtained within the Kohn-Sham scheme with those obtained from the generalized Kohn-Sham scheme; cf. Eq. (5) [84]. This logic has already been followed in Ref. [63]. Additionally, we compare the Kohn-Sham gaps of TASK with those of the LDA and with very recent quasixact Kohn-Sham gaps obtained by inversion of highly accurate quantum Monte Carlo (QMC) ground-state densities [32].

We have performed all calculations using the BAND code [85–91] of the Amsterdam Modeling Suite. To this end, we

have implemented an optimized effective potential (OEP) routine for TASK, using the Krieger-Li-Iafrate (KLI) approximation [92]. The Supplemental Material [81] lists the numerical details. It has previously been reported that the OEP routine for meta-GGAs in BAND needs an extremely fine (radial) Becke grid [63]. Our calculations with the TASK functional did not need this fine grid; cf. Sec. VI and the Supplemental Material [81]. Our experience that TASK [with both LDA correlation (LDAc) and CC] is numerically stable and efficient is in line with several very recent numerical stability analyses [93–95], which conclude that the numerical stability of TASK is on par with that of the Perdew-Burke-Ernzerhof functional (PBE) [96].

Figure 1 shows the computed band gaps compared with the experimental reference values for small-gap [i.e., smaller than 4 eV; Fig. 1(a)] and large-gap [i.e., larger than 4 eV; Fig. 1(b)] systems. On the one hand, the figure confirms the previous finding [61] that TASK evaluated in the generalized Kohn-Sham scheme predicts band gaps reliably for a large variety of systems. Especially for large-gap systems, which are very challenging for many other methods [69], TASK predicts the band gap quite accurately. The same trend has very recently been observed in a comprehensive study on the impact of the exchange enhancement factor on band gaps [70].

An important insight going beyond Ref. [61], on the other hand, emerges when looking at the Kohn-Sham gaps of TASK. The figures show that these Kohn-Sham gaps are close to or slightly larger than the gaps from LDA. Comparison of the Kohn-Sham and the generalized Kohn-Sham gaps thus demonstrates that the accurate prediction of the band gaps with TASK is *not* obtained by incorrectly open-

ing large Kohn-Sham gaps. Instead, TASK correctly includes a substantial contribution from the derivative discontinuity, which here stems from the TASK exchange. The difference between the generalized Kohn-Sham gap and the Kohn-Sham gaps indicates the derivative discontinuity, as highlighted for the example of Kr by the blue arrow in Fig. 1. One sees that here, $\Delta_x \approx 3.7$ eV, i.e., the discontinuity is responsible for about a third of the gap.

For most small-gap semiconductors, the fact that TASK achieves larger gaps than LDA can be attributed to two effects: First, the Kohn-Sham gaps are larger than those of the LDA, closing about half of the difference with respect to experiment. The remaining difference is then closed by the derivative discontinuity contribution that is included in the generalized Kohn-Sham eigenvalue gap. The situation is different for the large-gap systems. There, the relative increase of the TASK Kohn-Sham gaps over the LDA gaps is much smaller. This trend is in line with the accurate QMC-derived Kohn-Sham gaps from Ref. [32]: Also for the quasixact Kohn-Sham gaps, the relative increase compared with the LDA gaps is larger for the small-gap system Si than for the large-gap system NaCl. Furthermore, also in terms of the absolute magnitude, the QMC-derived gaps support the meta-GGA results, as similar Kohn-Sham gaps are found in both approaches. The meta-GGA generalized Kohn-Sham gaps, on the other hand, are much larger and close to the experimental band gaps.

These results thus demonstrate that the meta-GGA predicts the right band gaps for the right reason: TASK does not require that the Kohn-Sham gap be spuriously opened up to match the experiment, but instead yields a Kohn-Sham gap that is somewhat larger than the LDA gap yet still of similar magnitude. It combines the Kohn-Sham gap with a substantial contribution from the derivative discontinuity to reach a band gap close to the experimental one. The high accuracy of the meta-GGA generalized Kohn-Sham gaps attests the usefulness of the construction principle of Eq. (19).

As a side remark, and in view of Sec. VI, we note that we also compared the band gaps obtained with TASK with the ones obtained with the HSE functional. The corresponding data are shown in Table SIV of the Supplemental Material. It shows that (with the exception of diamond, see below), TASK and HSE yield similar results for systems with gaps of up to ~ 5 eV, whereas TASK yields larger gaps than HSE for systems with larger band gaps, in agreement with experiment.

IV. ENERGETICALLY IMPORTANT REGIONS IN DIFFERENT TYPES OF SYSTEMS

The trends described in the previous section hold for the large majority of systems. However, it is worthwhile to discuss the concept of averaging over the “energetically important region” [cf. Eq. (16)] in greater detail, because there are two interesting exceptions in our set of data. The first one is diamond, where we observe a rather large deviation of the TASK generalized Kohn-Sham gap from the experimental band gap. TASK enhances the Kohn-Sham gap of diamond only marginally compared with LDA, and the derivative discontinuity is insignificant. At least as remarkable is CdO. There, the Kohn-Sham gap of TASK vanishes like that of

LDA, but the generalized Kohn-Sham gap is nevertheless in very good agreement with the experimental data.

These effects must have their origin in the electronic structure. In order to understand what is special about these two systems, we analyze their electronic structure in comparison to other materials. For this comparison we chose as one reference Ge, because its band gap is of very similar magnitude to the one of CdO and its lattice structure is similar to the one of diamond. As a second reference we chose NaCl, as its lattice structure is similar to the one of CdO and the QMC reference value is available. In the Supplemental Material we also discuss Si as a third natural reference system.

Figure 2 shows the electronic structure parameters r_s , s , and α , which enter the meta-GGA as the input, as well as the enhancement factor of TASK and (minus) its derivative with respect to α for Ge and C (diamond), and NaCl and CdO in Figs. 2(a) and 2(b), respectively. The input parameters are taken from a self-consistent TASK calculation in BAND. From these, we calculate F_{xc}^{TASK} and $-\partial F_{xc}^{\text{TASK}}/\partial\alpha$ and finally plot all quantities along a path in the unit cell as indicated in the caption.

First, we compare Ge and diamond. Both systems are covalently bonded and have a diamond cubic lattice, so one might expect that they are similarly well described. However, Fig. 1 shows that for Ge the derivative discontinuity Δ_{xc} is responsible for about half of the experimental gap, while it nearly vanishes for diamond. It is not obvious where this difference comes from; therefore we take a closer look at the electronic structure. Figure 2(a) shows that in both systems, $\partial F_{xc}^{\text{TASK}}/\partial\alpha$ has a similar magnitude everywhere except for the core region and the bonding region, where we define the bonding region as the central region between the nuclei with the shortest core-core distance, as denoted in Fig. 2. The core region, however, is unlikely to contribute significantly to Δ_{xc} . In the bonding region the magnitude of $\partial F_{xc}^{\text{TASK}}/\partial\alpha$ is approximately a factor of 2 larger for Ge than for diamond, as seen in the insets in Fig. 2(a). This is a relevant observation in view of Eq. (19): A more negative $\partial F_{xc}^{\text{TASK}}/\partial\alpha$ leads to a larger derivative discontinuity. Therefore we conclude that the bonding region is very important for these strongly bound systems, i.e., the bonding region makes a large part of the energetically important region in the sense of Eqs. (15) and (16). The reason for the different values of $\partial F_{xc}^{\text{TASK}}/\partial\alpha$ is the different values of α in the bonding region. In the bonding region of diamond, α takes rather small values down to $\alpha \approx 0.2$, while in Ge, as well as in NaCl and CdO, α is larger than 0.4 everywhere (except for the core region). However, for $\alpha \approx 0.2$, TASK has much less α -derivative than for larger values of α ; cf. Fig. 3. Furthermore, in diamond the density in the bonding region is larger, i.e., r_s is smaller than for Ge, and this also reduces the derivative discontinuity because $\partial e_{xc}/\partial\tau \propto n^{-1/3} \partial F_{xc}/\partial\alpha \propto r_s \partial F_{xc}/\partial\alpha$. Thus, in the case of diamond, the chosen parametrization of the TASK functional does not sufficiently pick up the energetically important region.

Next, let us compare Ge and CdO. Ge and CdO have a similar experimental band gap, and TASK predicts similar generalized Kohn-Sham gaps for both. However, TASK predicts a vanishing Kohn-Sham gap for CdO, while for Ge the predicted Kohn-Sham gap is of the magnitude that one

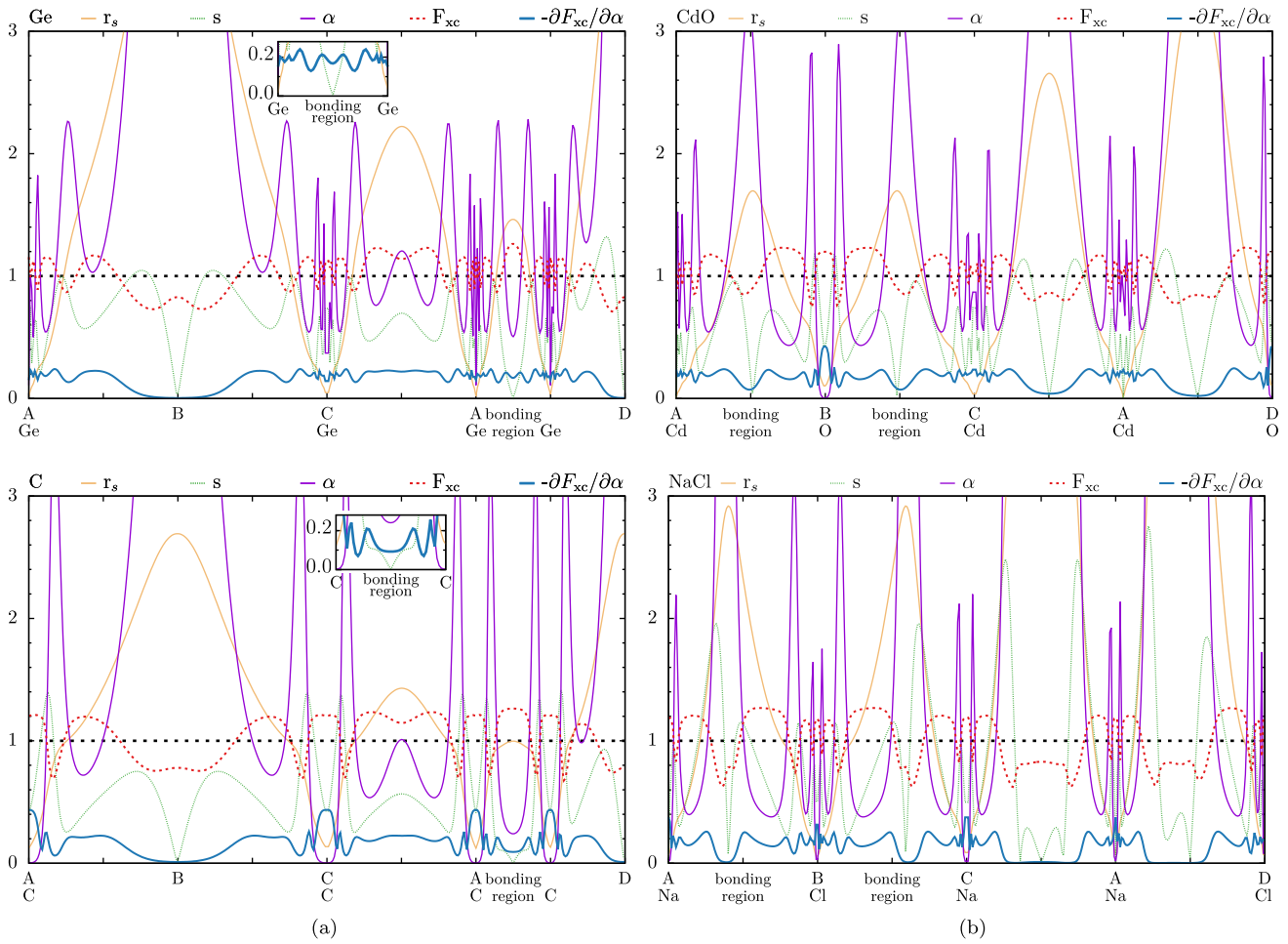


FIG. 2. The values of the Seitz radius r_s , the reduced density gradient s , and the iso-orbital indicator α along a path in the unit cell. (a) Ge and C in the diamond cubic structure. (b) NaCl and CdO in the rock-salt cubic structure. All values are calculated self-consistently with TASK in BAND [91]. Based on these values, the TASK enhancement factor F_{xc} and its derivative with respect to α , $\partial F_{xc}/\partial\alpha$, are calculated. The path is defined as $A \rightarrow B \rightarrow C \rightarrow A \rightarrow D$, where $A = (0, 0, 0)$, $B = (0, 0, \frac{1}{2})$, $C = (0, \frac{1}{2}, \frac{1}{2})$, and $D = (\frac{1}{2}, \frac{1}{2}, \frac{1}{2})$ (fractional coordinates with respect to lattice vectors). Along the path, the positions of the nuclei and the bonding region are indicated. The insets for Ge and C show a zoomed version of the bonding region. Note that the plots show the negative of $\partial F_{xc}/\partial\alpha$.

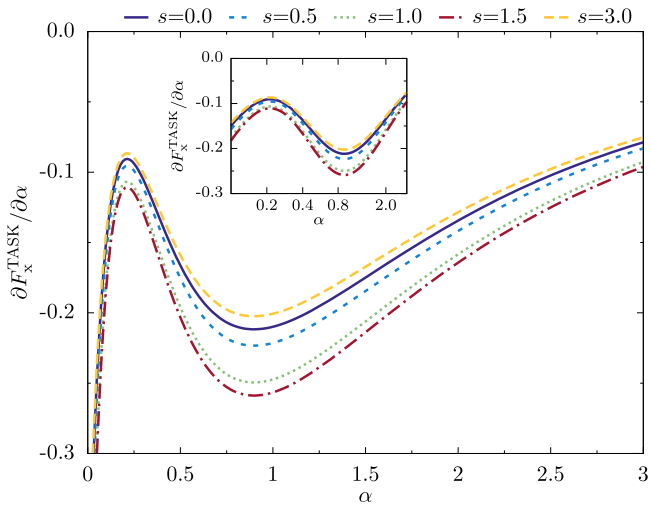


FIG. 3. Derivative of the TASK (exchange) enhancement factor F_x^{TASK} with respect to α as a function of α for different values of s . The inset has a logarithmic x axis.

expects for such semiconductors [30,32,34]. Figure 2 reveals the obvious substantial differences between Ge and CdO as a consequence of their different crystal structures. While Ge is in the diamond cubic structure, CdO is in the rock-salt cubic structure, like NaCl. This reflects their different bonding types: Ge and diamond are covalently bound, while CdO and NaCl are ionic crystals. Therefore a Kohn-Sham gap close to the (vanishing) LDA Kohn-Sham gap for CdO—and consequently, a larger contribution from the derivative discontinuity—is in line with the discussion in the previous section: There, we already observed that the difference between the Kohn-Sham gaps of LDA and TASK is different for ionic crystals and covalently bound crystals.

For the ionic crystals NaCl and CdO, it is not as clear as for the covalently bound systems what the energetically important region is. While the size of the Kohn-Sham gap of TASK in NaCl corresponds to about two-thirds of the size of the experimental gap, which is the right order of magnitude as confirmed by the QMC-derived Kohn-Sham gap, TASK predicts a vanishing Kohn-Sham gap for CdO. Still, the gen-

eralized Kohn-Sham gap of TASK matches the experimental value quite accurately in both systems. From Fig. 2, we observe that in a large part of the bonding region, $\partial F_{xc}^{\text{TASK}}/\partial\alpha$ nearly vanishes in NaCl and is small in CdO. This suggests that in the ionic crystals the bonding region is not as important for the gap as it is in the covalently bound semiconductors. Instead, the inner valence region, and possibly the core-valence region, become more important. (Here we define the inner valence region in the following way: Starting from the point where the reduced density gradient s has a minimum between two nuclei, go in the direction of one of the neighboring nuclei towards the highest maximum of s . The inner valence region starts at this maximum and reaches to the next minimum of s in the direction of the nearest nucleus.) The dependence of F_{xc} on r_s , s , and α , i.e., many input quantities, hinders a detailed analysis. However, the overall more negative $\partial F_{xc}^{\text{TASK}}/\partial\alpha$ in CdO compared with NaCl can explain a larger relative contribution from the derivative discontinuity in CdO. To gain further insight, it would be of great interest to know the exact Kohn-Sham gap of CdO and see whether it indeed vanishes. QMC calculations in the spirit of Ref. [32] for CdO would therefore be of great interest.

Finally, we summarize the influence of the different bonding types on the energetically important region. In Fig. 2, we observe that for the covalently bound systems, α has a local minimum at the bond center, while in the ionic crystals α has a local maximum at the bond center. Therefore different regions of α are energetically important for the different types of bonds. On the one hand, in Ge and C the bonding region and thus values of α between 0.2 and 1 are very important. On the other hand, in NaCl and CdO the inner valence and the core-valence regions and thus values of α between 0.4 and 2 appear to be energetically most important. Figure 3 shows that the magnitude of $\partial F_{xc}^{\text{TASK}}/\partial\alpha$ is particularly high for α between 0.4 and 2. This underlines the importance of the construction principle, Eq. (19), and explains why TASK yields reliable band gaps for many systems.

V. THE IMPACT OF CORRELATION

While there is a lot of evidence that the total xc derivative discontinuity as well as the one of pure exact exchange should be positive, there are several hints that the contribution from correlation should typically be negative: Exact exchange typically yields a derivative discontinuity that is too large [34,77], which implies that the correlation part of the exact functional must have a negative contribution to Δ_{xc} . For the correlation that corresponds to the dynamical (random phase approximation) screening in the *GW* approximation, this has also been confirmed explicitly [34].

In the context of meta-GGAs, we have a further argument supporting this point of view based on the enhancement factor for fully spin-polarized systems. As shown above, the derivative discontinuity can be linked to the derivative of the enhancement factor with respect to α via Eq. (19). In the one-electron case ($\alpha = 0$), the exact correlation must vanish identically to make the correlation free from self-interaction. Since the correlation energy of the exact functional is nonpositive, we have [97] $\varepsilon_c(\alpha = 0) \geq \varepsilon_c(\alpha)$, and thus $F_c(\alpha = 0) \leq F_c(\alpha)$ for all values of α and of the remaining parameters. In

particular, the correlation energy density of the homogeneous electron gas is negative everywhere, and thus $F_c(n, \nabla n = 0, \alpha = 0) < F_c(n, \nabla n = 0, \alpha = 1)$ for all values of the density n . Consequently, the average of $\partial F_c/\partial\alpha$ for α between 0 and 1 must be positive. Because $0 < \alpha < 1$ typically makes a large part of the energetically important region, the analog of Eq. (19) for correlation indicates $\Delta_c < 0$.

These considerations indicate which trends are to be expected for exact exchange and exact correlation. In the construction of approximate functionals, however, one additionally has to take into account that semilocal exchange functionals do not model exact exchange, but effectively cover exchange and nondynamical correlation [75,98–103]. Therefore the relative contributions of meta-GGA exchange and meta-GGA correlation to the total derivative discontinuity may differ depending on the specific functional construction strategy, and only their sum, i.e., the total Δ_{xc} , is of decisive relevance. This is in line with the long-known experience that semilocal approximations for exchange (x) and correlation (c) must match and are therefore best designed together. The correlation functionals of popular meta-GGAs such as Strongly Constrained and Appropriately Normed (SCAN) [60], r2SCAN [104], and M06-L [56] have a noticeable negative contribution to the derivative discontinuity. They are therefore expected to reduce band gaps (cf. the Supplemental Material [81], where this is explicitly confirmed for SCAN). The results shown in Fig. 1 indicate that TASK exchange, which has been constructed differently from previous meta-GGAs by following the philosophy of Eq. (18), needs a different kind of correlation functional. The CC–meta-GGA correlation [82] takes this into account: While having a nonpositive derivative discontinuity in general, it preserves the high quality of the band gaps for the systems in the test set.

VI. BAND GAPS OF METAL-HALIDE PEROVSKITES

The test set studied in Sec. III provides a reasonable benchmark as it spans a broad range of materials with band gaps from large to small. While the focus of Sec. III is on the comparison of the gaps from generalized Kohn-Sham and Kohn-Sham theory, it is reassuring to know that the high quality of the generalized Kohn-Sham gaps from the TASK functional has been confirmed also for other, yet larger test sets [69]. However, from a materials science perspective, the question of how reliably DFT can predict the gaps of very complex materials is also highly relevant. For many such materials, definite reference values have not been established yet, excluding them from typical test sets. Furthermore, for some materials, predicting the band gap correctly is challenging in general, i.e., not only for DFT, but also for other many-body methods. A paradigmatic example is the material family of metal-halide perovskites, which pose a serious challenge even for Green’s-function-based many-body perturbation theory in the *GW* approximation [105–108]. The *GW* approach is currently considered to be the “gold standard” for the prediction of band gaps of solids [109], but it requires material-dependent, sufficiently accurate DFT starting points [108,110] or computationally demanding (partial) self-consistency and the incorporation of vertex corrections for halide perovskites [107,111]. While the considerations

TABLE I. Kohn-Sham (for PBE) and generalized Kohn-Sham (for HSE and TASK) band gaps (in eV) calculated with the different programs VASP [113,114] and BAND [115]. The VASP values are taken from Ref. [108]; other values are from this work. See main text for details.

System	PBE	PBE	HSE	TASK	HSE
	VASP	BAND	VASP	BAND	BAND
MAPbI ₃	0.21	0.09	0.82	0.81	
MAPbBr ₃	0.55	0.41	1.30	1.38	
CsSnBr ₃	0.06	0.01	0.63	0.73	
(MA) ₂ BiTiBr ₆	0.60	0.44	1.00	1.25	
Cs ₂ TlAgBr ₆	-0.66	-0.57	0.20	-0.05	0.08
Cs ₂ TlAgCl ₆	0.00	0.00	1.09	0.75	1.07
Cs ₂ BiAgBr ₆	1.09	1.05	1.95	1.86	
Cs ₂ InAgCl ₆	1.16	1.18	2.61	2.49	2.49
Cs ₂ SnBr ₆	1.10	1.10	2.14	2.07	
Cs ₂ Au ₂ I ₆	0.70	0.71	1.16	0.91	

presented in the literature [56,63,69,112] and in this paper suggest that a meta-GGA such as the TASK functional is an attractive option for predicting band gaps, the question arises whether it can also predict the band gaps of metal-halide perovskites with quantitative accuracy.

The HSE screened hybrid functional [37,38] is one of the most reliable common functionals for the purposes of band-gap prediction [69]. A reasonable description of the band gaps of semiconductors has been part of its construction strategy, and HSE generalized Kohn-Sham gaps often give reasonable estimates of the true fundamental gaps. A major drawback is, however, that the Fock-like integrals that are required in an HSE calculation are computationally demanding, and especially so in plane-wave calculations, limiting the possibilities of rapid materials screening. A computationally efficient meta-GGA giving band gaps similar to the HSE functional would thus be an attractive alternative. Therefore we examine in the following whether the TASK meta-GGA can fulfill this promise by comparing TASK band gaps with HSE band gaps. Table I summarizes results for ten different metal-halide perovskites. These systems span a broad range of gaps from below 1 eV to over 2.5 eV, and a broad range of chemical complexity from single perovskites with chemical formula ABX_3 to the quaternary double perovskites with formula $A_2BB'X_6$, where A is a monovalent cation such as Cs^+ or $CH_3NH_3^+$ (MA), B and B' are metal cations, and X is a halide anion. In all cases we used experimental structures with the structural details reported in Ref. [108]. In the compounds in which $A = MA$, we replaced MA with Cs in our calculations to avoid spurious symmetry breaking induced by the dipole moment of the MA molecule in the primitive cubic unit cell [116,117]. This choice, as well as other technical choices, e.g., regarding pseudopotentials, basis sets, the \mathbf{k} grid, and other convergence criteria, influence the calculated numbers. We report these parameters and resulting estimates of the technical accuracy of the calculations in the Supplemental Material [81].

We use the all-electron code BAND for the TASK calculations. In this way we avoid any inconsistency that would result from the fact that self-consistent pseudopotentials are not yet

available for the TASK functional. On the other hand, we cannot use BAND for all HSE calculations, because in BAND, HSE via the LIBXC interface [118] is only available for calculations without spin-orbit coupling (SOC) or with scalar-relativistic SOC. Full SOC, however, plays an important role in some of the materials in Table I. Therefore, for the HSE band gaps, we rely on the Vienna *ab initio* simulation package (VASP) values reported in Ref. [108] (with self-consistent SOC) for most of the halide perovskites and double-check only the ones for which SOC plays a negligible role ($Cs_2TlAgBr_6$, $Cs_2TlAgCl_6$, and $Cs_2InAgCl_6$) with HSE in BAND. The TASK calculations with BAND use the zeroth-order regular approximation (ZORA) [89] for including SOC for all materials except the abovementioned three exceptions, for which we performed scalar-relativistic calculations.

To give an impression of the possible consequences of the technical differences between VASP and BAND, we report in the first column of Table I the PBE band gaps calculated with VASP using plane waves and projector-augmented wave pseudopotentials, and in the second column we report the PBE gaps from our calculations using BAND with an all-electron localized basis set. This comparison shows that differences of ~ 0.15 eV can result just due to technical differences between the VASP calculations from Ref. [108] and the BAND calculations from this work.

With this in mind, we now compare the HSE band gaps in the third column of Table I with the TASK band gaps in the fourth column. For most systems, the values are rather close, and differences are within the ~ 0.15 eV range that we already observed in the PBE comparison. However, for $MA_2BiTiBr_6$, the TASK gap is larger by 0.25 eV, and for $Cs_2TlAgBr_6$, $Cs_2Au_2I_6$, and $Cs_2TlAgCl_6$, the HSE gap is larger by 0.25, 0.25, and 0.34 eV, respectively. We therefore take a closer look at these special cases before drawing general conclusions. Among these outliers, $Cs_2TlAgBr_6$ appears particularly noteworthy, because with TASK the gap is close to zero but negative, whereas with HSE we find a gap close to zero but positive. We look into this case in more detail in order to check whether this reflects a qualitative difference between the two xc approximations, or just sensitivity to the computational details. To this end, we repeated the HSE calculation for $Cs_2TlAgBr_6$ using BAND. This is possible because SOC plays a minor role here, as discussed above. The corresponding number is shown in the fifth column of Table I. With BAND, the HSE gap of $Cs_2TlAgBr_6$ is 0.12 eV smaller than with VASP. As a further test we also calculated the band gap of $Cs_2TlAgBr_6$ using the TASK functional in QUANTUM ESPRESSO (QE) [122,123], i.e., another plane-wave code. In QE, the TASK gap of $Cs_2TlAgBr_6$ is 0.04 eV, i.e., small but positive. Both results show that technical differences play a major role for the sign of the band gap in this system, and we conclude that $Cs_2TlAgBr_6$ does not reveal a qualitative difference between HSE and TASK; however, the gap is so close to zero in either case that technical differences can be decisive for whether the gap is slightly positive or slightly negative.

For the sake of completeness we also calculated the band gaps of the other two materials for which full SOC does not play a role with HSE in BAND. The corresponding numbers in the fifth column of Table I show that TASK and

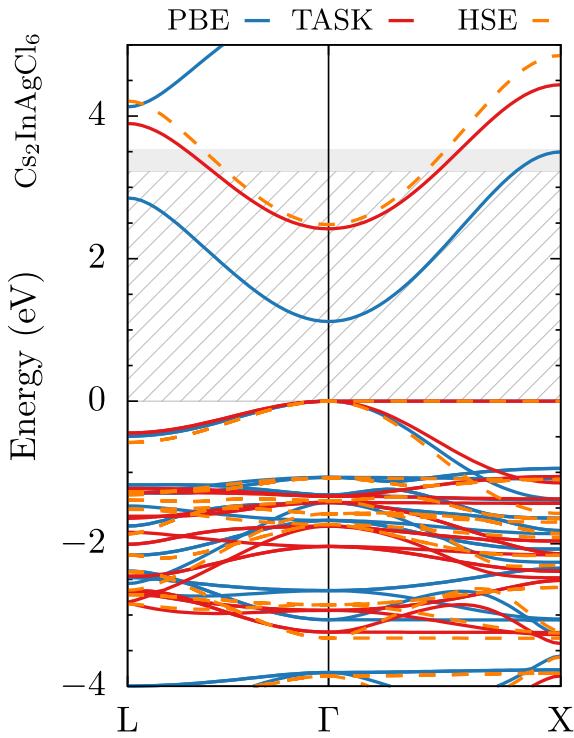


FIG. 4. PBE, HSE, and TASK band structures as calculated with BAND for $\text{Cs}_2\text{InAgCl}_6$. Not only the gaps, but also the band structures are rather similar for HSE and TASK. The hatched and shaded regions indicate experimental values for the band gap, with the hatched region indicating the gap, and the shaded region indicating the range from different experiments [119–121].

HSE yield identical gaps for $\text{Cs}_2\text{InAgCl}_6$ with BAND, and for $\text{Cs}_2\text{TlAgCl}_6$ the difference between HSE and TASK is slightly reduced when the functionals are compared within BAND. As

a further check, we compared not only the gaps, but also the band structures. Figure 4 shows the comparison for the exemplary case of $\text{Cs}_2\text{InAgCl}_6$. The band structures obtained with TASK and HSE are very similar, with slight differences in the dispersion of the conduction band at the L and X points.

In summary, we therefore conclude that the band gaps obtained from HSE and TASK are not identical, but close to each other. Both functionals seem to capture the band structure physics of complex metal-halide perovskite materials in a similar way. This finding suggests that instead of basing band structure estimates on the nonlocal, screened hybrid functional HSE, one may as well use the meta-GGA TASK for these purposes. Our findings also suggest that the TASK functional may be an attractive starting point for a subsequent GW calculation.

The reason for why this is an attractive option from a computational perspective is summarized in Table II. It shows the computational time required for an HSE and a TASK calculation for each of the three metal-halide perovskites for which SOC plays a minor role and which therefore can reasonably be compared within BAND. The most relevant column is the last one. It reports the time relative to a PBE calculation with the same computational settings for a complete calculation with the given xc functional. By reporting these relative values, Table II provides an impression of the computational expense independent of the specific hardware that we used. For the sake of transparency and completeness, we further report the hardware and absolute timings. The numbers reveal that a calculation using TASK takes about three times as long as the PBE calculation, whereas an HSE calculation can take more than a factor of 90 longer than the PBE calculation. Using TASK instead of HSE typically saves a factor of about 25 in computational time. As a relevant side note we point out that calculations with TASK do not require a finer numerical grid than the PBE calculations. Many program packages have default settings that use an extra fine radial grid (“grid

TABLE II. Computational time required for a self-consistent field (SCF) calculation with PBE, TASK, and HSE with BAND including the sampling of the band structure. The last column reports the compute time of HSE and TASK relative to a PBE calculation. For completeness, the prior columns report absolute numbers obtained on a compute node with two CPUs of type Intel Xeon E5-2630 v4 at 2.20 GHz (Broadwell) with 2×32 GB RAM (in total 20 physical cores, hyperthreading enabled) using a $4 \times 4 \times 4$ k grid, without a frozen core, normal numerical quality, and disabled symmetry and including scalar relativistic effects in the ZORA. Note that the TASK calculations do *not* require the grid boost, which many programs switch on as a default for meta-GGAs. DZ and TZP denote double-zeta and triple-zeta polarized basis sets, respectively.

System	xc	Basis	Grid boost	CPU time (s)		CPU time relative to PBE (s)	
				SCF step	Total	SCF step	Total
$\text{Cs}_2\text{TlAgCl}_6$	PBE	TZP	✗	45	1021	1.00	1.00
$\text{Cs}_2\text{TlAgCl}_6$	TASK	TZP	✗	140	2969	3.11	2.88
$\text{Cs}_2\text{TlAgCl}_6$	TASK	TZP	✓	324	6890	7.20	6.75
$\text{Cs}_2\text{TlAgCl}_6$	HSE	TZP	✗	4560	78699	106.05	77.09
$\text{Cs}_2\text{TlAgBr}_6$	PBE	DZ	✗	25	561	1.00	1.00
$\text{Cs}_2\text{TlAgBr}_6$	TASK	DZ	✗	106	2170	4.24	3.87
$\text{Cs}_2\text{TlAgBr}_6$	TASK	DZ	✓	258	5153	10.32	9.18
$\text{Cs}_2\text{TlAgBr}_6$	HSE	DZ	✗	2867	53006	114.68	94.47
$\text{Cs}_2\text{InAgCl}_6$	PBE	DZ	✗	13	453	1.00	1.00
$\text{Cs}_2\text{InAgCl}_6$	TASK	DZ	✗	56	1268	4.31	2.80
$\text{Cs}_2\text{InAgCl}_6$	TASK	DZ	✓	141	2913	10.85	6.43
$\text{Cs}_2\text{InAgCl}_6$	HSE	DZ	✗	1320	23518	101.54	51.91

boost”) in meta-GGA calculations, because meta-GGAs such as SCAN and M06-L require a fine grid due to their numerical sensitivity. TASK calculations, however, converge well to the proper values on the regular grid. Therefore the grid boost, which typically more than doubles computational times, can be disabled.

We thus arrive at the final important finding of this paper: The TASK meta-GGA functional that only requires semilocal orbital input predicts band gaps similar to the ones from the fully nonlocal screened hybrid HSE, but at much lower computational cost—in the cases that we studied typically lower by a factor of 25.

Finally, we briefly comment on the comparison with experimental band gaps, which is particularly challenging for complex materials such as the metal-halide perovskites for which the range of experimentally reported band gaps can be substantial. While the focus of our paper is not on the comparison with experiment, it is worth noting that for some systems, e.g., $\text{Cs}_2\text{BiAgBr}_6$, the gaps calculated with HSE and TASK are close to the measured gaps, while for others the difference can be as large as ~ 0.8 eV, e.g., for MAPbI_3 and $\text{Cs}_2\text{InAgCl}_6$; cf. Fig. 4. These differences are generally in line with observations from molecular-dynamics simulations showing that anharmonic structural fluctuations at elevated temperatures can lead to a significant renormalization of the band gap [107,124,125], reported to be as large as 0.7 eV for some halide perovskites [107]. Furthermore, exciton binding energies of some metal-halide perovskites are of the order of several hundred meV [126], and orbital symmetries can lead to parity-forbidden transitions [127,128]. This further complicates the comparison with experimentally measured band gaps, which are typically extracted from optical absorption measurements. A detailed, benchmarklike comparison of theory and experiment is therefore challenging for the broad family of metal-halide perovskites. Nevertheless, in itself and as a starting point for subsequent *GW* calculations, it is a promising finding for computational materials science that the TASK meta-GGA allows for a qualitatively reasonable prediction of the gap similar to HSE at much reduced computational cost.

VII. SUMMARY AND CONCLUSIONS

In summary, we have shown why and how meta-GGAs can predict the right band gaps of solids for the right reason by generating a sizable derivative discontinuity. This demonstrates that meta-GGAs can provide accurate band gaps

at semilocal computational cost without suffering from the shortcomings that other semilocal methods have. By comparing calculations within the Kohn-Sham scheme and the generalized Kohn-Sham scheme for the TASK functional, we have demonstrated how the construction principle $\partial e_{xc}/\partial \tau > 0$, which corresponds to $\partial F_{xc}/\partial \alpha < 0$, is crucial for the derivative discontinuity and thus the nonlocality of a meta-GGA. We further argued that the contribution that correlation makes to the derivative discontinuity should generally be negative, and that the relative magnitude of the contributions from exchange and correlation for semilocal functionals may depend on the specific construction principles that are used. In addition to a test set of well-studied solids for which TASK yields band gaps close to the experimentally measured ones, we have also investigated a set of ten metal-halide perovskites for which the band gaps are notoriously difficult to predict. We have shown that for these systems, the band gaps found with TASK are close to the band gaps that one finds with HSE; yet the computational cost of the TASK calculation is lower by a factor of about 25. The combination of reasonable accuracy and numerical efficiency thus makes the TASK meta-GGA a natural choice for computationally efficient first-principles band-gap screening.

All authors together conceptualized the work. T.L. performed the calculations reported in Secs. III, IV, and V and wrote the required routines. T.A. performed the calculations reported in Sec. VI and wrote the required routines. T.L. and S.K. wrote the manuscript, and all authors discussed the final version.

ACKNOWLEDGMENTS

S.K. and T.L. appreciate financial support from the Deutsche Forschungsgemeinschaft, DFG Project No. KU 1410/4-1, and from the Bavarian State Ministry of Science, Research, and the Arts for the Collaborative Research Network “Solar Technologies go Hybrid.” L.L. acknowledges funding from the Dutch Research Council (NWO) under Grant No. OCENW.M20.337. S.K. and T.L. are further grateful for support from the Elite Study Program “Biological Physics” of the Elite Network of Bavaria, and T.L. acknowledges discussions with Pier Philippesen on generating data for plots with BAND. J.S. acknowledges the support of the U.S. DOE, Office of Science, Basic Energy Sciences Grant No. DE-SC0019350.

-
- [1] G. Ceder, Opportunities and challenges for first-principles materials design and applications to Li battery materials, *MRS Bull.* **35**, 693 (2010).
 - [2] I. E. Castelli, T. Olsen, S. Datta, D. D. Landis, S. Dahl, K. S. Thygesen, and K. W. Jacobsen, Computational screening of perovskite metal oxides for optimal solar light capture, *Energy Environ. Sci.* **5**, 5814 (2012).
 - [3] J. Kang, X. Zhang, and S.-H. Wei, Advances and challenges in DFT-based energy materials design, *Chin. Phys. B* **31**, 107105 (2022).
 - [4] X. Ye, A. Liu, L. Gao, C. Zhang, L. Yan, S. Wen, and T. Ma, Computational screening of Cs based vacancy-ordered double perovskites for solar cell and photocatalysis applications, *EcoMat* **5**, e12295 (2023).
 - [5] Q. Wu, M. Pan, S. Zhang, D. Sun, Y. Yang, D. Chen, D. A. Weitz, and X. Gao, Research progress in high-throughput screening of CO_2 reduction catalysts, *Energies* **15**, 6666 (2022).
 - [6] Q. He, B. Yu, Z. Li, and Y. Zhao, Density functional theory for battery materials, *Energy Environ. Mater.* **2**, 264 (2019).
 - [7] L. Kahle, A. Marcolongo, and N. Marzari, High-throughput computational screening for solid-state Li-ion conductors, *Energy Environ. Sci.* **13**, 928 (2020).

- [8] A. Jain, S. P. Ong, G. Hautier, W. Chen, W. D. Richards, S. Dacek, S. Cholia, D. Gunter, D. Skinner, G. Ceder, and K. A. Persson, Commentary: The Materials Project: A materials genome approach to accelerating materials innovation, *APL Mater.* **1**, 011002 (2013).
- [9] Y. Kang, Y. Youn, S. Han, J. Park, and C.-S. Oh, Computational screening of indirect-gap semiconductors for potential photovoltaic absorbers, *Chem. Mater.* **31**, 4072 (2019).
- [10] C. C. Stoumpos, D. H. Cao, D. J. Clark, J. Young, J. M. Rondinelli, J. I. Jang, J. T. Hupp, and M. G. Kanatzidis, Ruddlesden-Popper hybrid lead iodide perovskite 2D homologous semiconductors, *Chem. Mater.* **28**, 2852 (2016).
- [11] B. Saparov and D. B. Mitzi, Organic-inorganic perovskites: Structural versatility for functional materials design, *Chem. Rev.* **116**, 4558 (2016).
- [12] M. D. Smith, E. J. Crace, A. Jaffe, and H. I. Karunadasa, The diversity of layered halide perovskites, *Annu. Rev. Mater. Res.* **48**, 111 (2018).
- [13] N. R. Wolf, B. A. Connor, A. H. Slavney, and H. I. Karunadasa, Doubling the stakes: The promise of halide double perovskites, *Angew. Chem. Int. Ed.* **60**, 16264 (2021).
- [14] National Renewable Energy Laboratory, Best research-cell efficiencies, <https://www.nrel.gov/pv/assets/images/efficiency-chart.png>.
- [15] F. A. Faber, A. Lindmaa, O. A. von Lilienfeld, and R. Armiento, Machine Learning Energies of 2 Million Elpasolite (ABC_2D_6) Crystals, *Phys. Rev. Lett.* **117**, 135502 (2016).
- [16] M. R. Filip and F. Giustino, The geometric blueprint of perovskites, *Proc. Natl. Acad. Sci. USA* **115**, 5397 (2018).
- [17] W. Shockley and H. J. Queisser, Detailed balance limit of efficiency of p - n junction solar cells, *J. Appl. Phys.* **32**, 510 (1961).
- [18] J. P. Perdew and M. Levy, Physical Content of the Exact Kohn-Sham Orbital Energies: Band Gaps and Derivative Discontinuities, *Phys. Rev. Lett.* **51**, 1884 (1983).
- [19] L. J. Sham and M. Schlüter, Density-Functional Theory of the Energy Gap, *Phys. Rev. Lett.* **51**, 1888 (1983).
- [20] J. P. Perdew, R. G. Parr, M. Levy, and J. L. Balduz, Jr., Density-Functional Theory for Fractional Particle Number: Derivative Discontinuities of the Energy, *Phys. Rev. Lett.* **49**, 1691 (1982).
- [21] With periodic boundary conditions, one can distinguish between a direct and an indirect one-electron gap, and for a chosen band occupation, the indirect gap can be negative.
- [22] J. P. Perdew, Density functional theory and the band gap problem, *Int. J. Quantum Chem.* **28**, 497 (1985).
- [23] A. J. Cohen, P. Mori-Sánchez, and W. Yang, Fractional charge perspective on the band gap in density-functional theory, *Phys. Rev. B* **77**, 115123 (2008).
- [24] P. Mori-Sánchez, A. J. Cohen, and W. Yang, Localization and Delocalization Errors in Density Functional Theory and Implications for Band-Gap Prediction, *Phys. Rev. Lett.* **100**, 146401 (2008).
- [25] P. Mori-Sánchez, A. J. Cohen, and W. Yang, Discontinuous Nature of the Exchange-Correlation Functional in Strongly Correlated Systems, *Phys. Rev. Lett.* **102**, 066403 (2009).
- [26] W. Yang, A. J. Cohen, and P. Mori-Sánchez, Derivative discontinuity, bandgap and lowest unoccupied molecular orbital in density functional theory, *J. Chem. Phys.* **136**, 204111 (2012).
- [27] W. Kohn and L. J. Sham, Self-consistent equations including exchange and correlation effects, *Phys. Rev.* **140**, A1133 (1965).
- [28] A. D. Becke, Density-functional exchange-energy approximation with correct asymptotic behavior, *Phys. Rev. A* **38**, 3098 (1988).
- [29] J. P. Perdew, K. Burke, and M. Ernzerhof, Generalized Gradient Approximation Made Simple, *Phys. Rev. Lett.* **77**, 3865 (1996).
- [30] R. W. Godby, M. Schlüter, and L. J. Sham, Self-energy operators and exchange-correlation potentials in semiconductors, *Phys. Rev. B* **37**, 10159 (1988).
- [31] G. Onida, L. Reining, and A. Rubio, Electronic excitations: Density-functional versus many-body Green's-function approaches, *Rev. Mod. Phys.* **74**, 601 (2002).
- [32] A. Aouina, M. Gatti, S. Chen, S. Zhang, and L. Reining, Accurate Kohn-Sham auxiliary system from the ground state density of solids, *Phys. Rev. B* **107**, 195123 (2023).
- [33] R. W. Godby, M. Schlüter, and L. J. Sham, Accurate Exchange-Correlation Potential for Silicon and Its Discontinuity on Addition of an Electron, *Phys. Rev. Lett.* **56**, 2415 (1986).
- [34] M. Grüning, A. Marini, and A. Rubio, Density functionals from many-body perturbation theory: The band gap for semiconductors and insulators, *J. Chem. Phys.* **124**, 154108 (2006).
- [35] M. Grüning, A. Marini, and A. Rubio, Effect of spatial non-locality on the density functional band gap, *Phys. Rev. B* **74**, 161103(R) (2006).
- [36] A. Seidl, A. Görling, P. Vogl, J. A. Majewski, and M. Levy, Generalized Kohn-Sham schemes and the band-gap problem, *Phys. Rev. B* **53**, 3764 (1996).
- [37] J. Heyd, G. E. Scuseria, and M. Ernzerhof, Hybrid functionals based on a screened Coulomb potential, *J. Chem. Phys.* **118**, 8207 (2003); **124**, 219906(E) (2006).
- [38] A. V. Krukau, O. A. Vydrov, A. F. Izmaylov, and G. E. Scuseria, Influence of the exchange screening parameter on the performance of screened hybrid functionals, *J. Chem. Phys.* **125**, 224106 (2006).
- [39] L. Kronik, T. Stein, S. Refaely-Abramson, and R. Baer, Excitation gaps of finite-sized systems from optimally tuned range-separated hybrid functionals, *J. Chem. Theory Comput.* **8**, 1515 (2012).
- [40] L. Kronik and S. Kümmel, Dielectric screening meets optimally tuned density functionals, *Adv. Mater.* **30**, 1706560 (2018).
- [41] J. F. Janak, Proof that $\frac{\partial E}{\partial n_i} = \epsilon$ in density-functional theory, *Phys. Rev. B*, **18**, 7165 (1978).
- [42] T. Stein, J. Autschbach, N. Govind, L. Kronik, and R. Baer, Curvature and frontier orbital energies in density functional theory, *J. Phys. Chem. Lett.* **3**, 3740 (2012).
- [43] D. Wing, J. B. Haberb, M. R. Filipd, S. E. Gantb, J. B. Neaton, G. Ohadaand, and L. Kronik, Band gaps of crystalline solids from Wannier-localization-based optimal tuning of a screened range-separated hybrid functional, *Proc. Natl. Acad. Sci. USA* **118**, e2104556118 (2021).
- [44] S. Kümmel and J. P. Perdew, Optimized effective potential made simple: Orbital functionals, orbital shifts, and the exact Kohn-Sham exchange potential, *Phys. Rev. B* **68**, 035103 (2003).

- [45] F. Tran and P. Blaha, Accurate Band Gaps of Semiconductors and Insulators with a Semilocal Exchange-Correlation Potential, *Phys. Rev. Lett.* **102**, 226401 (2009).
- [46] R. Armiento and S. Kümmel, Orbital Localization, Charge Transfer, and Band Gaps in Semilocal Density-Functional Theory, *Phys. Rev. Lett.* **111**, 036402 (2013).
- [47] T. Aschebrock, R. Armiento, and S. Kümmel, Orbital nodal surfaces: Topological challenges for density functionals, *Phys. Rev. B* **95**, 245118 (2017).
- [48] T. Aschebrock, R. Armiento, and S. Kümmel, Challenges for semilocal density functionals with asymptotically nonvanishing potentials, *Phys. Rev. B* **96**, 075140 (2017).
- [49] D. Waroquiers, A. Lherbier, A. Miglio, M. Stankovski, S. Poncé, M. J. T. Oliveira, M. Giantomassi, G.-M. Rignanese, and X. Gonze, Band widths and gaps from the Tran-Blaha functional: Comparison with many-body perturbation theory, *Phys. Rev. B* **87**, 075121 (2013).
- [50] A. Lindmaa and R. Armiento, Energetics of the AK13 semilocal Kohn-Sham exchange energy functional, *Phys. Rev. B* **94**, 155143 (2016).
- [51] J. Camargo-Martínez and R. Baquero, Performance of the modified Becke-Johnson potential for semiconductors, *Phys. Rev. B* **86**, 195106 (2012).
- [52] A. D. Becke, Density-functional thermochemistry. IV. A new dynamical correlation functional and implications for exact-exchange mixing, *J. Chem. Phys.* **104**, 1040 (1996).
- [53] T. Van Voorhis and G. E. Scuseria, A novel form for the exchange-correlation energy functional, *J. Chem. Phys.* **109**, 400 (1998).
- [54] A. D. Boese and N. C. Handy, New exchange-correlation density functionals: The role of the kinetic-energy density, *J. Chem. Phys.* **116**, 9559 (2002).
- [55] J. Tao, J. P. Perdew, V. N. Staroverov, and G. E. Scuseria, Climbing the Density Functional Ladder: Nonempirical Meta-Generalized Gradient Approximation Designed for Molecules and Solids, *Phys. Rev. Lett.* **91**, 146401 (2003).
- [56] Y. Zhao and D. G. Truhlar, A new local density functional for main-group thermochemistry, transition metal bonding, thermochemical kinetics, and noncovalent interactions, *J. Chem. Phys.* **125**, 194101 (2006).
- [57] J. Sun, B. Xiao, and A. Ruzsinszky, Communication: Effect of the orbital-overlap dependence in the meta generalized gradient approximation, *J. Chem. Phys.* **137**, 051101 (2012).
- [58] R. Peverati and D. G. Truhlar, An improved and broadly accurate local approximation to the exchange–correlation density functional: The MN12-L functional for electronic structure calculations in chemistry and physics, *Phys. Chem. Chem. Phys.* **14**, 13171 (2012).
- [59] J. Sun, R. Haunschild, B. Xiao, I. W. Bulik, G. E. Scuseria, and J. P. Perdew, Semilocal and hybrid meta-generalized gradient approximations based on the understanding of the kinetic-energy-density dependence, *J. Chem. Phys.* **138**, 044113 (2013).
- [60] J. Sun, A. Ruzsinszky, and J. P. Perdew, Strongly Constrained and Appropriately Normed Semilocal Density Functional, *Phys. Rev. Lett.* **115**, 036402 (2015).
- [61] T. Aschebrock and S. Kümmel, Ultranonlocality and accurate band gaps from a meta-generalized gradient approximation, *Phys. Rev. Res.* **1**, 033082 (2019).
- [62] F. G. Eich and M. Hellgren, Derivative discontinuity and exchange-correlation potential of meta-GGAs in density-functional theory, *J. Chem. Phys.* **141**, 224107 (2014).
- [63] Z. H. Yang, H. Peng, J. Sun, and J. P. Perdew, More realistic band gaps from meta-generalized gradient approximations: Only in a generalized Kohn-Sham scheme, *Phys. Rev. B* **93**, 205205 (2016).
- [64] J. P. Perdew, W. Yang, K. Burke, Z. Yang, E. K. U. Gross, M. Scheffler, G. E. Scuseria, T. M. Henderson, I. Y. Zhang, A. Ruzsinszky, H. Peng, J. Sun, E. Trushin, and A. Görling, Understanding band gaps of solids in generalized Kohn–Sham theory, *Proc. Natl. Acad. Sci. USA* **114**, 2801 (2017).
- [65] V. U. Nazarov and G. Vignale, Optics of Semiconductors from Meta-Generalized-Gradient-Approximation-Based Time-Dependent Density-Functional Theory, *Phys. Rev. Lett.* **107**, 216402 (2011).
- [66] J. Heyd, J. E. Peralta, G. E. Scuseria, and R. L. Martin, Energy band gaps and lattice parameters evaluated with the Heyd-Scuseria-Ernzerhof screened hybrid functional, *J. Chem. Phys.* **123**, 174101 (2005).
- [67] M. K. Y. Chan and G. Ceder, Efficient Band Gap Prediction for Solids, *Phys. Rev. Lett.* **105**, 196403 (2010).
- [68] B. Patra, S. Jana, L. A. Constantin, and P. Samal, Relevance of the Pauli kinetic energy density for semilocal functionals, *Phys. Rev. B* **100**, 155140 (2019).
- [69] P. Borlido, J. Schmidt, A. Huran, F. Tran, M. Marques, and S. Botti, Exchange-correlation functionals for band gaps of solids: Benchmark, reparametrization and machine learning, *npj Comput. Mater.* **6**, 96 (2020).
- [70] P. Kovács, F. Tran, P. Blaha, and G. K. Madsen, What is the optimal mGGA exchange functional for solids? *J. Chem. Phys.* **157**, 094110 (2022).
- [71] In the literature, functionals that depend on the Laplacian of the density are also labeled meta-GGAs. In this paper, however, we consider functionals that must depend on the kinetic energy density and may depend on the Laplacian of the density, since the nonlocality in meta-GGAs is fully due to their orbital dependence.
- [72] E. R. Johnson, S. Keinan, P. Mori-Sánchez, J. Contreras-García, A. J. Cohen, and W. Yang, Revealing noncovalent interactions, *J. Am. Chem. Soc.* **132**, 6498 (2010).
- [73] J. Sun, B. Xiao, Y. Fang, R. Haunschild, P. Hao, A. Ruzsinszky, G. I. Csonka, G. E. Scuseria, and J. P. Perdew, Density Functionals that Recognize Covalent, Metallic, and Weak Bonds, *Phys. Rev. Lett.* **111**, 106401 (2013).
- [74] G. L. Oliver and J. P. Perdew, Spin-density gradient expansion for the kinetic energy, *Phys. Rev. A* **20**, 397 (1979).
- [75] S. Kümmel and L. Kronik, Orbital-dependent density functionals: Theory and applications, *Rev. Mod. Phys.* **80**, 3 (2008).
- [76] G. K.-L. Chan, A fresh look at ensembles: Derivative discontinuities in density functional theory, *J. Chem. Phys.* **110**, 4710 (1999).
- [77] M. Städele, M. Moukara, J. A. Majewski, P. Vogl, and A. Görling, Exact exchange Kohn-Sham formalism applied to semiconductors, *Phys. Rev. B* **59**, 10031 (1999).
- [78] M. J. Allen and D. J. Tozer, Eigenvalues, integer discontinuities and NMR shielding constants in Kohn-Sham theory, *Mol. Phys.* **100**, 433 (2002).

- [79] M. Mundt and S. Kümmel, Derivative Discontinuities in Time-Dependent Density-Functional Theory, *Phys. Rev. Lett.* **95**, 203004 (2005).
- [80] M. Lein and S. Kümmel, Exact Time-Dependent Exchange-Correlation Potentials for Strong-Field Electron Dynamics, *Phys. Rev. Lett.* **94**, 143003 (2005).
- [81] See Supplemental Material at <http://link.aps.org/supplemental/10.1103/PhysRevMaterials.7.093803> for details on the numerical parameters used and detailed data.
- [82] T. Lebeda, T. Aschebrock, and S. Kümmel, First steps towards achieving both ultranonlocality and a reliable description of electronic binding in a meta-generalized gradient approximation, *Phys. Rev. Res.* **4**, 023061 (2022).
- [83] J. P. Perdew and Y. Wang, Accurate and simple analytic representation of the electron-gas correlation energy, *Phys. Rev. B* **45**, 13244 (1992).
- [84] Alternatively, one could calculate Δ_x directly in the OEP formalism [75,77,92], but the generalized Kohn-Sham calculation is technically more straightforward.
- [85] G. te Velde and E. J. Baerends, Precise density-functional method for periodic structures, *Phys. Rev. B* **44**, 7888 (1991).
- [86] G. Wiesenekker and E. J. Baerends, Quadratic integration over the three-dimensional Brillouin zone, *J. Phys.: Condens. Matter* **3**, 6721 (1991).
- [87] M. Franchini, P. H. T. Philipsen, and L. Visscher, The Becke fuzzy cells integration scheme in the Amsterdam density functional program suite, *J. Comput. Chem.* **34**, 1819 (2013).
- [88] M. Franchini, P. H. T. Philipsen, E. van Lenthe, and L. Visscher, Accurate Coulomb potentials for periodic and molecular systems through density fitting, *J. Chem. Theory Comput.* **10**, 1994 (2014).
- [89] E. van Lenthe, E.-J. Baerends, and J. G. Snijders, Relativistic regular two-component Hamiltonians, *J. Chem. Phys.* **99**, 4597 (1993).
- [90] E. Van Lenthe and E. J. Baerends, Optimized Slater-type basis sets for the elements 1–118, *J. Comput. Chem.* **24**, 1142 (2003).
- [91] SCM, Theoretical Chemistry, Vrije Universiteit, BAND 2022.1, <https://www.scm.com/>; note that a modified version is used in this paper.
- [92] J. B. Krieger, Y. Li, and G. J. Iafrate, Construction and application of an accurate local spin-polarized Kohn-Sham potential with integer discontinuity: Exchange-only theory, *Phys. Rev. A* **45**, 101 (1992).
- [93] S. Lehtola and M. A. Marques, Many recent density functionals are numerically ill-behaved, *J. Chem. Phys.* **157**, 174114 (2022).
- [94] S. Lehtola, Meta-GGA density functional calculations on atoms with spherically symmetric densities in the finite element formalism, *J. Chem. Theory Comput.* **19**, 2502 (2023).
- [95] S. Lehtola, Atomic electronic structure calculations with Hermite interpolating polynomials, *J. Phys. Chem. A* **127**, 4180 (2023).
- [96] In Ref. [93], the numerical problems of other meta-GGAs are attributed to the use of the iso-orbital indicator α . However, α is also used in TASK. Therefore the numerical stability of TASK suggests that numerically stable density functional approximations can be constructed using α .
- [97] Strictly speaking, this only implies $E_c \leq 0$. In practical approximations, however, typically $\varepsilon_c \leq 0$ also holds.
- [98] A. D. Becke, Density-functional thermochemistry. III. The role of exact exchange, *J. Chem. Phys.* **98**, 5648 (1993).
- [99] R. Neumann, R. H. Nobes, and N. Handy, Exchange functionals and potentials, *Mol. Phys.* **87**, 1 (1996).
- [100] D. K. W. Mok, R. Neumann, and N. C. Handy, Dynamical and nondynamical correlation, *J. Phys. Chem.* **100**, 6225 (1996).
- [101] K. Burke, J. P. Perdew, and M. Ernzerhof, Why the generalized gradient approximation works and how to go beyond it.
- [102] O. Gritsenko, P. Schipper, and E. Baerends, Exchange and correlation energy in density functional theory: Comparison of accurate DFT quantities with traditional Hartree-Fock based ones and generalized gradient approximations for the molecules Li_2 , N_2 , F_2 , *J. Chem. Phys.* **107**, 5007 (1997).
- [103] D. Cremer, Density functional theory: coverage of dynamic and non-dynamic electron correlation effects, *Mol. Phys.* **99**, 1899 (2001).
- [104] J. W. Furness, A. D. Kaplan, J. Ning, J. P. Perdew, and J. Sun, Accurate and numerically efficient $r^2\text{SCAN}$ meta-generalized gradient approximation, *J. Phys. Chem. Lett.* **11**, 8208 (2020).
- [105] M. R. Filip and F. Giustino, *GW* quasiparticle band gap of the hybrid organic-inorganic perovskite $\text{CH}_3\text{NH}_3\text{PbI}_3$: Effect of spin-orbit interaction, semicore electrons, and self-consistency, *Phys. Rev. B* **90**, 245145 (2014).
- [106] P. Scherpelz, M. Govoni, I. Hamada, and G. Galli, Implementation and validation of fully relativistic *GW* calculations: Spin-orbit coupling in molecules, nanocrystals, and solids, *J. Chem. Theory Comput.* **12**, 3523 (2016).
- [107] J. Wiktor, U. Rothlisberger, and A. Pasquarello, Predictive determination of band gaps of inorganic halide perovskites, *J. Phys. Chem. Lett.* **8**, 5507 (2017).
- [108] L. Leppert, T. Rangel, and J. B. Neaton, Towards predictive band gaps for halide perovskites: Lessons from one-shot and eigenvalue self-consistent *GW*, *Phys. Rev. Mater.* **3**, 103803 (2019).
- [109] D. Golze, M. Dvorak, and P. Rinke, The *GW* compendium: A practical guide to theoretical photoemission spectroscopy, *Front. Chem.* **7**, 377 (2019).
- [110] S. E. Gant, J. B. Haber, M. R. Filip, F. Sagredo, D. Wing, G. Ohad, L. Kronik, and J. B. Neaton, Optimally tuned starting point for single-shot *GW* calculations of solids, *Phys. Rev. Mater.* **6**, 053802 (2022).
- [111] F. Brivio, K. T. Butler, A. Walsh, and M. van Schilfgaarde, Relativistic quasiparticle self-consistent electronic structure of hybrid halide perovskite photovoltaic absorbers, *Phys. Rev. B* **89**, 155204 (2014).
- [112] B. Patra, S. Jana, L. A. Constantin, and P. Samal, Efficient band gap prediction of semiconductors and insulators from a semilocal exchange-correlation functional, *Phys. Rev. B* **100**, 045147 (2019).
- [113] G. Kresse and J. Hafner, Norm-conserving and ultrasoft pseudopotentials for first-row and transition elements, *J. Phys.: Condens. Matter* **6**, 8245 (1994).
- [114] G. Kresse and J. Furthmüller, Efficient iterative schemes for *ab initio* total-energy calculations using a plane-wave basis set, *Phys. Rev. B* **54**, 11169 (1996).
- [115] SCM, Theoretical Chemistry, Vrije Universiteit, BAND 2017, <https://www.scm.com/>.

- [116] L. Leppert, S. E. Reyes-Lillo, and J. B. Neaton, Electric field and strain induced Rashba effect in hybrid halide perovskites, *J. Phys. Chem. Lett.* **7**, 3683 (2016).
- [117] K. Frohna, T. Deshpande, J. Harter, W. Peng, B. A. Barker, J. B. Neaton, S. G. Louie, O. M. Bakr, D. Hsieh, and M. Bernardi, Inversion symmetry and bulk Rashba effect in methylammonium lead iodide perovskite single crystals, *Nat. Commun.* **9**, 1829 (2018).
- [118] S. Lehtola, C. Steigemann, M. J. Oliveira, and M. A. Marques, Recent developments in LIBXC—A comprehensive library of functionals for density functional theory, *SoftwareX* **7**, 1 (2018).
- [119] G. Volonakis, A. A. Haghighirad, R. L. Milot, W. H. Sio, M. R. Filip, B. Wenger, M. B. Johnston, L. M. Herz, H. J. Snaith, and F. Giustino, Cs₂InAgCl₆: A new lead-free halide double perovskite with direct band gap, *J. Phys. Chem. Lett.* **8**, 772 (2017).
- [120] J. Zhou, Z. Xia, M. S. Molokeev, X. Zhang, D. Peng, and Q. Liu, Composition design, optical gap and stability investigations of lead-free halide double perovskite Cs₂AgInCl₆, *J. Mater. Chem. A* **5**, 15031 (2017).
- [121] T. T. Tran, J. R. Panella, J. R. Chamorro, J. R. Morey, and T. M. McQueen, Designing indirect–direct bandgap transitions in double perovskites, *Mater. Horiz.* **4**, 688 (2017).
- [122] P. Giannozzi, S. Baroni, N. Bonini, M. Calandra, R. Car, C. Cavazzoni, D. Ceresoli, G. L. Chiarotti, M. Cococcioni, I. Dabo, A. D. Corso, S. Fabris, G. Fratesi, S. de Gironcoli, R. Gebauer, U. Gerstmann, C. Gougoussis, A. Kokalj, M. Lazzeri, L. Martin-Samos *et al.*, QUANTUM ESPRESSO: A modular and open-source software project for quantum simulations of materials, *J. Phys.: Condens. Matter* **21**, 395502 (2009).
- [123] P. Giannozzi, Jr., O. Andreussi, T. Brumme, O. Bunau, M. B. Nardelli, M. Calandra, R. Car, C. Cavazzoni, D. Ceresoli, M. Cococcioni, N. Colonna, I. Carnimeo, A. D. Corso, S. de Gironcoli, P. Delugas, R. A. DiStasio, Jr., A. Ferretti, A. Floris, G. Fratesi, G. Fugallo *et al.*, Advanced capabilities for materials modelling with quantum espresso, *J. Phys.: Condens. Matter* **29**, 465901 (2017).
- [124] X. G. Zhao, Z. Wang, O. I. Malyi, and A. Zunger, Effect of static local distortions vs dynamic motions on the stability and band gaps of cubic oxide and halide perovskites, *Mater. Today* **49**, 107 (2021).
- [125] S. A. Seidl, X. Zhu, G. Reuveni, S. Aharon, C. Gehrman, S. Caicedo-Dávila, O. Yaffe, and D. A. Egger, Anharmonic fluctuations govern the band gap of halide perovskites, *Phys. Rev. Mater.* **7**, L092401 (2023).
- [126] R. I. Biega, M. R. Filip, L. Leppert, and J. B. Neaton, Chemically localized resonant excitons in silver-pnictogen halide double perovskites, *J. Phys. Chem. Lett.* **12**, 2057 (2021).
- [127] A. H. Slavney, B. A. Connor, L. Leppert, and H. I. Karunadasa, A pencil-and-paper method for elucidating halide double perovskite band structures, *Chem. Sci.* **10**, 11041 (2019).
- [128] W. Meng, X. Wang, Z. Xiao, J. Wang, D. B. Mitzi, and Y. Yan, Parity-forbidden transitions and their impacts on the optical absorption properties of lead-free metal halide perovskites and double perovskites, *J. Phys. Chem. Lett.* **8**, 2999 (2017).

Supplementary material for “Right band gaps for the right reason at low computational cost with a meta-GGA”

Timo Lebeda,^{1,2} Thilo Aschebrock,¹ Jianwei Sun,² Linn Leppert,³ and Stephan Kümmel^{1,*}

¹*Theoretical Physics IV, University of Bayreuth, 95440 Bayreuth, Germany*

²*Department of Physics and Engineering Physics,*

Tulane University, New Orleans, Louisiana 70118, USA

³*MESA+ Institute for Nanotechnology, University of Twente, 7500 AE Enschede, The Netherlands*

I. COMPUTATIONAL DETAILS REGARDING SECTIONS III – V OF THE MAIN PAPER

In this Section we list the numerical settings that we used to calculate the band gaps in the Kohn-Sham (KS) and the generalized Kohn-Sham (gKS) approach. We used the code BAND [1–7] for all calculations. For the KS calculations, we relied on the Krieger-Li-Iafrate (KLI) approximation [8] to the Optimized Effective Potential (OEP) and a frozen core, just as done in previous work [9]. Our numerical settings are listed in Table I.

TABLE I. Numerical settings used in the KS and gKS calculations in BAND. Default is used for all calculations except for SCAN in the Kohn-Sham scheme (OEP in the KLI approximation). For Ar and Kr, we used a different basis set and a different value for MGGAOEPWaitIter than for the other systems, see text.

key	default	SCAN OEP
NumericalQuality	Good	Good
KSpace		
Type	Regular	Regular
Quality	Good	Good
BeckeGrid		
RadialGridBoost	3.0	1.0
Quality	Good	-
UserRadMulFactor	-	20
UserCoreL	-	11
UserInter1L	-	13
UserInter2L	-	21
UserExterL	-	31
UserExterLBoost	-	35
XC		
MGGAOEPMaxIter	-	10000
MGGAOEPConvergence	-	1.0d-10
MGGAOEPMaxAbortIter	-	100
MGGAOEPMaxErrorIncrease	-	100
MGGAOEPWaitIter	- 10 7	10 7
Basis		
Type	TZ2P QZ4P	TZ2P QZ4P
Relativity		
Level	Scalar	Scalar
BandStructure		
Enabled	True	True
Automatic	False	False
DeltaK	0.02	0.02

Previous work reported that for SCAN, the KLI routine in BAND needs an extremely fine (radial) Becke grid [9]. We observe the same in our calculations with the SCAN functional, but TASK exchange with SCAN correlation (TASKx+SCANc) and even more TASK (with LDA or CC correlation) are much easier to converge than SCAN.

* stephan.kuettel@uni-bayreuth.de; <http://tp4.uni-bayreuth.de/en>

TABLE II. Band gaps in eV. The calculations were performed in BAND [7] with fixed experimental bond lengths. Experimental bond lengths and experimental band gaps are chosen as in Ref. [13] for all systems except NaCl. The bond length and reference value of NaCl are taken from Ref. [14] to allow for comparison with the QMC data. We used the numerical settings reported in Table I.

System	LDA	PBE	M06-L gKS	SCAN		TASK _x +SCAN _c		TASK		Expt.
				gKS	KS	gKS	KS	gKS	KS	
Ar	8.17	8.64	10.36	9.52	8.53	12.35	8.64	13.30	9.19	14.3
BN	4.42	4.53	4.93	5.04	4.74	4.55	4.23	5.52	4.90	6.22
C	4.13	4.17	4.68	4.58	4.27	3.61	3.83	4.35	4.30	5.48
CdO	0.00	0.00	0.00	0.01	0.00	0.20	0.00	0.83	0.00	0.84
GaAs	0.40	0.63	1.11	0.86	0.58	1.22	0.88	1.68	1.01	1.52
Ge	0.00	0.11	0.48	0.18	0.00	0.40	0.32	0.83	0.41	0.74
Kr	6.81	7.17	8.34	8.02	7.14	10.69	7.35	11.50	7.77	11.6
LiCl	6.08	6.38	7.18	7.31	6.38	8.29	5.70	9.52	6.27	9.4
LiF	8.95	9.15	9.41	10.09	9.12	11.71	8.09	12.84	8.76	13.6
MgO	4.74	4.81	5.05	5.66	4.83	6.25	4.67	7.26	5.24	7.22
MgS	3.31	3.56	4.26	4.24	3.54	4.84	3.51	5.84	4.06	5.4
NaCl	4.60	4.96	5.85	5.74	5.08	7.35	4.31	8.45	4.82	8.5
Si	0.54	0.63	1.04	0.89	0.71	0.36	0.45	1.07	0.87	1.17
SiC	1.36	1.41	1.65	1.74	1.60	1.28	1.17	2.07	1.74	2.42
ZnS	1.84	2.08	2.86	2.62	2.10	3.08	2.10	3.81	2.48	3.66
MSE	-2.4	-2.3	-1.7	-1.7	-2.2	-1.1	-2.5	-0.2	-2.0	
MAE	2.4	2.3	1.7	1.7	2.2	1.1	2.5	0.3	2.0	
RMSE	3.0	2.7	2.1	2.1	2.7	1.2	3.0	0.5	2.6	
rel. MAE	50	45	30	35	45	28	46	7	36	%

While TASK_x+SCAN_c still needs a very fine radial grid (RadialGridBoost 3.0), TASK by itself is already converged with BeckeGrid Quality Good and a RadialGridBoost of 1, cf. Table IV.

Our implementation of the KLI routine for TASK is similar to that of SCAN [9]. However, our numerical settings differ from those used in [9] in two points: First, we use the QZ4P basis set [6] for Ar and Kr, since the results are different from those obtained using the TZ2P basis set if a frozen core is used. In particular, with QZ4P the all-electron results and the frozen core results coincide with the all-electron TZ2P results, compare Tables IV and II, while they differ from the frozen core results with TZ2P, both in the KS and gKS calculations. It should be noted that one can not use the QZ4P basis set for all systems because it is too diffuse and therefore leads to (almost) linear dependency for most systems. Second, we improve the numerical stability and computation time of the KS calculations by first running some self-consistent gKS cycles before switching to the KS scheme. We use 10 gKS cycles for all systems except Ar, Kr, and NaCl, because these three systems are already converged after 10 gKS cycles. Thus, we use 7 gKS cycles for Ar, Kr, and NaCl. The difference that one obtains in the band gaps when using some initial gKS cycles or not is less than 0.01 eV.

To generate the data shown in Figure 2 in the main text, we use TASK with the numerical settings shown in Table I, but we perform all-electron calculations, i.e., core none.

II. DETAILED RESULTS FOR THE BAND GAPS OF THE MATERIALS FROM THE TEST SET USED IN SECTION III OF THE MAIN PAPER

Table II lists the values of the band gaps discussed in Section III of the main text, and additional values for the PBE [10], M06-L [11], SCAN [12], and TASK_x+SCAN_c functionals.

Additionally, we study the effect of relativistic corrections in Table III. There, we compare for PBE, SCAN, and TASK the band gaps obtained without relativistic corrections (None), with scalar relativistic corrections in the ZORA approximation (Scalar) and with Spin-Orbit coupling (SOC) in the ZORA approximation. In line with earlier observations [9], we conclude that scalar relativistic effects are important and have to be included. The computationally much more expensive spin-orbit coupling on the other hand is negligible for most systems and its effect is not larger than 0.1 eV for the semiconductors Ge and GaAs and 0.2 eV for the large gap insulator Kr. Moreover, its effect is very similar for all three functionals studied in Table III. Therefore, we include scalar relativistic effects in the ZORA

approximation in the Sections III – V of the main paper, as denoted in Table I.

TABLE III. Generalized Kohn-Sham band gaps in eV. The calculations were performed in BAND [7] with fixed experimental bond lengths. Experimental bond lengths and experimental band gaps are the same as in Table II. The numerical parameters are taken from Table I, except for the explicitly specified level of relativity. Note that in contrast to Table I, all-electron calculations were performed here.

System	PBE			SCAN			TASK			Expt.
	None	Scalar	SOC	None	Scalar	SOC	None	Scalar	SOC	
Ar	8.71	8.65	8.58	9.60	9.53	9.47	13.36	13.28	13.22	14.3
BN	4.54	4.53	4.52	5.02	5.01	5.00	5.51	5.50	5.49	6.22
C	4.18	4.17	4.17	4.57	4.56	4.56	4.34	4.33	4.33	5.48
CdO	0.28	0.00	0.00	0.78	0.00	0.00	1.77	0.89	0.87	0.84
GaAs	1.21	0.55	0.44	1.56	0.83	0.73	2.36	1.72	1.61	1.52
Ge	0.54	0.06	0.00	0.73	0.24	0.14	1.25	0.86	0.76	0.74
Kr	7.35	7.17	6.95	8.21	8.02	7.80	11.68	11.45	11.23	11.6
LiCl	6.46	6.37	6.33	7.41	7.32	7.28	9.65	9.55	9.51	9.4
LiF	9.21	9.17	9.15	10.21	10.17	10.15	12.97	12.93	12.91	13.6
MgO	4.84	4.78	4.77	5.75	5.69	5.68	7.39	7.33	7.32	7.22
MgS	3.63	3.55	3.52	4.33	4.25	4.22	5.76	5.74	5.72	5.4
NaCl	5.04	4.97	4.92	5.83	5.76	5.72	8.66	8.57	8.53	8.5
Si	0.62	0.61	0.59	0.86	0.85	0.83	1.05	1.04	1.02	1.17
SiC	1.41	1.41	1.41	1.73	1.73	1.72	2.05	2.05	2.04	2.42
ZnS	2.38	2.10	2.08	2.93	2.63	2.61	4.20	3.84	3.82	3.66
MSE	-2.1	-2.3	-2.3	-1.5	-1.7	-1.7	-0.0	-0.2	-0.2	
MAE	2.1	2.3	2.3	1.5	1.7	1.7	0.5	0.4	0.4	
RMSE	2.7	2.7	2.8	2.0	2.1	2.2	0.6	0.5	0.5	
rel. MAE	36	46	48	20	35	36	22	8	7	%

To allow for a direct comparison with HSE results, we additionally report all-electron results with TASK in Table IV. There, we show that first, the choice RadialGridBoost 1.0, i.e., no grid boost, is sufficient with TASK, second, that the calculations are converged with respect to the basis set, and third, that we obtain the same generalized Kohn-Sham gaps with TASK in an all-electron calculation and with a frozen core.

Because Si is a well-studied material and is often used as a reference system, we supplement the discussion of Figure 2 in the main text with a comparison of Si and diamond in Figure 1. Overall, α (and s) take similar values in Si and diamond. Therefore, on first sight one may think that the analysis given in the main text that explains the underestimation of the band gap in diamond should also apply to Si. However, in diamond the fraction of the bonding region, and therefore the region of small α , is larger than in Si. Additionally, the density in the bonding region is larger in diamond, i.e., r_s is larger in the bonding region of Si. As $\partial e_{xc}/\partial\tau \propto r_s \partial F_{xc}/\partial\alpha$, both of these effects increase the gap in Si compared to the one in diamond.

We further note that in comparison to Ge, in Si the contribution from the Kohn-Sham gap to the band gap is larger. This is in line with the QMC data for Si and the fact that the LDA gap vanishes for Ge, whereas the Kohn-Sham gap is about half of the experimental gap for Si.

TABLE IV. Generalized Kohn-Sham band gaps in eV. The calculations were performed in BAND [7] with fixed experimental bond lengths. Experimental bond lengths and experimental band gaps are the same as in Table II. The numerical parameters are taken from Table I, except for the explicitly specified basis set and the RadialGridBoost (RGB), which is set to 1.0, since this is sufficient with TASK. Note that for comparison with HSE, all-electron calculations were performed here, i.e., core none, which is the reason for the differences between TASK TZ2P in this table and in Table II.

System	TASK				HSE	
	RGB 3.0, TZ2P	RGB 1.0, TZ2P	TZP	DZ	TZ2P	DZ
Ar	13.28	13.28	14.41	21.79	10.31	20.54
BN	5.50	5.50	5.51	6.29	5.91	6.57
C	4.33	4.33	4.35	4.79	5.37	5.75
CdO	0.89	0.89	0.88	0.80	0.86	0.77
GaAs	1.72	1.72	1.71	1.40	not conv.	1.10
Ge	0.86	0.86	0.88	0.53	0.74	0.44
Kr	11.45	11.45	12.20	18.17	8.55	16.36
LiCl	9.56	9.55	9.55	9.35	7.71	7.66
LiF	12.93	12.93	12.92	12.67	not conv.	11.29
MgO	7.33	7.33	7.31	7.09	6.53	6.31
MgS	5.74	5.74	5.87	5.76	4.58	4.44
NaCl	8.57	8.57	8.57	8.40	not conv.	6.23
Si	1.04	1.04	1.06	1.53	1.17	1.48
SiC	2.05	2.05	2.06	2.91	2.36	3.04
ZnS	3.84	3.84	3.84	3.75	3.23	3.24
MSE	-0.2	-0.2	-0.1	0.9		0.2
MAE	0.4	0.4	0.3	1.2		1.5
RMSE	0.5	0.5	0.5	2.6		2.3
rel. MAE	8	8	8	16		22

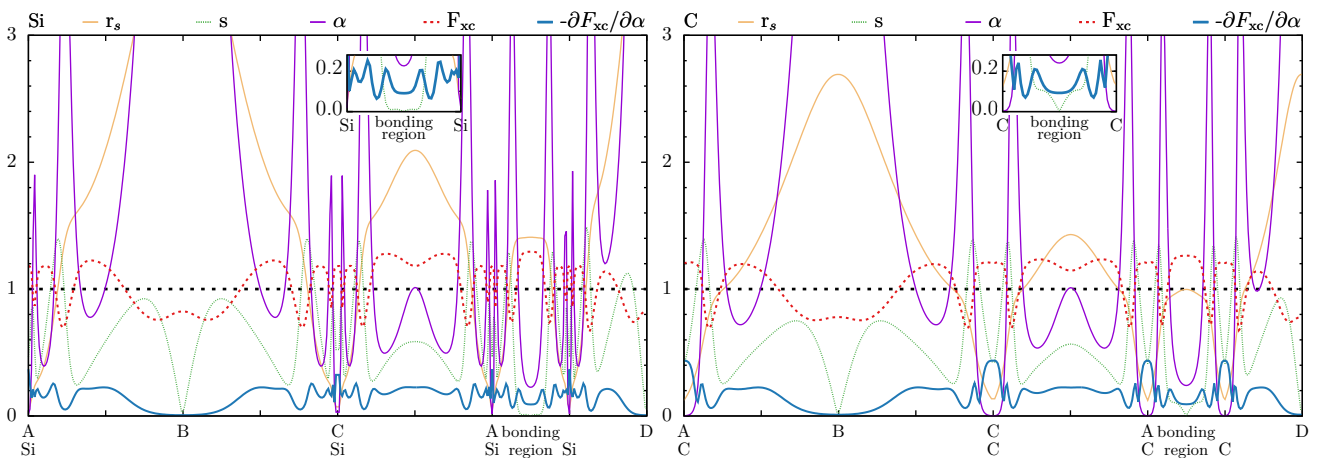


FIG. 1. The values of the Wigner-Seitz radius r_s , the reduced density gradient s , and the iso-orbital indicator α along a path in the unit cell. All values are calculated self-consistently using TASK in BAND [7]. Based on these values, the TASK+LDAc enhancement factor F_{xc} and its derivative with respect to α , $\partial F_{xc}/\partial\alpha$, are calculated. Note that the negative of $\partial F_{xc}/\partial\alpha$ is shown. The path is defined as $A \rightarrow B \rightarrow C \rightarrow A \rightarrow D$, where $A = (0, 0, 0)$, $B = (0, 0, \frac{1}{2})$, $C = (0, \frac{1}{2}, \frac{1}{2})$, and $D = (\frac{1}{2}, \frac{1}{2}, \frac{1}{2})$. Along the path, the positions of the nuclei and the bonding region are indicated.

III. COMPUTATIONAL DETAILS RELATED TO THE METAL-HALIDE PEROVSKITE CALCULATIONS IN SECTION VI OF THE MAIN PAPER

The upper lines of Table V show for the example of $\text{Cs}_2\text{BiAgBr}_6$ how the computational parameters in BAND influence the band gap that one obtains with PBE. Taking into account spin-orbit coupling (SOC) is mandatory. The differences between the TZ2P basis and a small core on the one hand, and the QZ4P basis with no core on the other,

are however negligible. Also the differences between a $4 \times 4 \times 4$ \mathbf{k} -grid and a $5 \times 5 \times 5$ \mathbf{k} -grid are negligible for the purposes of this paper. Therefore, a $4 \times 4 \times 4$ \mathbf{k} -grid with a small core and the TZ2P basis was used for the TASK calculations, as shown in the last line. We also performed convergence tests with respect to the \mathbf{k} -grid and core for CsPbBr₂ with TASK. These confirmed that with the above mentioned settings, the band gap is converged within ca. 0.01 eV.

TABLE V. Band gap of Cs₂BiAgBr₆ as obtained with the listed computational parameters in BAND for PBE exchange and correlation and for TASK exchange with LDA correlation.

xc	\mathbf{k} -grid	Basis	Numerical Quality	Core	SOC (ZORA)	Band Gap (eV)
PBE	$4 \times 4 \times 4$	TZ2P	Good	Small	SOC	1.050
PBE	$4 \times 4 \times 4$	TZ2P	Good	Small	Scalar	1.269
PBE	$4 \times 4 \times 4$	TZ2P	Good	Small	w/o	0.876
PBE	$4 \times 4 \times 4$	TZ2P	Good	None	SOC	1.049
PBE	$4 \times 4 \times 4$	QZ4P	Good	None	SOC	1.052
PBE	$5 \times 5 \times 5$	TZ2P	Good	None	SOC	1.063
TASK	$4 \times 4 \times 4$	TZ2P	Good	Small	SOC	1.857

For the HSE calculations in BAND the numerical situation is more involved. As mentioned in the main text, HSE is only available via LibXC [15] in BAND for calculations without SOC or with scalar relativistic SOC. Therefore, we had to restrict the HSE calculations with BAND to Cs₂TlAgBr₆, Cs₂TlAgCl₆, and Cs₂InAgCl₆. However, when we tried to use in the HSE calculations the same numerical parameters that we used for PBE and TASK, the HSE calculations did not converge. For being able to converge the calculations, we had to use somewhat less strict numerical settings, as shown in Table VI.

TABLE VI. Numerical settings used for the HSE calculations with BAND. SC indicates a lower (BASIC) soft confinement radius of the basis functions.

System	\mathbf{k} -grid	Basis	Numerical Quality	Core	Band Gap (eV)
Cs ₂ TlAgCl ₆	$4 \times 4 \times 4$	DZ	Normal	None	1.061
Cs ₂ TlAgCl ₆	$4 \times 4 \times 4$	TZP	Normal	None	1.070
Cs ₂ TlAgBr ₆	$4 \times 4 \times 4$	DZ (SC)	Normal	None	0.128
Cs ₂ TlAgBr ₆	$4 \times 4 \times 4$	DZ	Normal	None	0.117
Cs ₂ TlAgBr ₆	$4 \times 4 \times 4$	TZP (SC)	Normal	None	0.084
Cs ₂ InAgCl ₆	$4 \times 4 \times 4$	DZ	Normal	None	2.478
Cs ₂ InAgCl ₆	$4 \times 4 \times 4$	TZP	Normal	None	2.490

In QUANTUM ESPRESSO (QE) we could use the TASK functional only via LibXC (version 5.0.0) for systems without SOC, as a noncollinear implementation of meta-GGAs is not available and SOC calculations require noncollinearity in QE. This, however, is sufficient to check the special case of Cs₂TlAgBr₆ discussed in the main text. Fully-relativistic optimized norm-conserving Vanderbilt PBE pseudopotentials (ONCVSP) were obtained from <http://www.pseudo-dojo.org/> and used for all QE calculations. We used a cutoff energy of 120 Ryd., a $10 \times 10 \times 10$ \mathbf{k} -grid, and a convergence threshold of 1×10^{-6} Ryd. for the TASK (+LDA correlation) calculation with QE. As discussed in the main text, this calculation leads to a slightly positive band gap of 0.04 eV, in contrast to the slightly negative gap of -0.05 eV obtained with BAND.

-
- [1] G. te Velde and E. J. Baerends, Precise density-functional method for periodic structures, *Phys. Rev. B* **44**, 7888 (1991).
 - [2] G. Wiesenekker and E. J. Baerends, Quadratic integration over the three-dimensional brillouin zone, *J. Phys. Condens. Matter* **3**, 6721 (1991).
 - [3] M. Franchini, P. H. T. Philipsen, and L. Visscher, The becke fuzzy cells integration scheme in the amsterdam density functional program suite, *J. Comput. Chem.* **34**, 1819 (2013).
 - [4] M. Franchini, P. H. T. Philipsen, E. van Lenthe, and L. Visscher, Accurate coulomb potentials for periodic and molecular systems through density fitting, *J. Chem. Theory Comput.* **10**, 1994 (2014).
 - [5] E. v. Lenthe, E.-J. Baerends, and J. G. Snijders, Relativistic regular two-component Hamiltonians, *J. Chem. Phys.* **99**, 4597 (1993).
 - [6] E. Van Lenthe and E. J. Baerends, Optimized slater-type basis sets for the elements 1–118, *J. Comput. Chem.* **24**, 1142 (2003).

- [7] SCM, Theoretical Chemistry, Vrije Universiteit, Amsterdam, The Netherlands, *BAND 2022.1 (a modified version is used)*.
- [8] J. B. Krieger, Y. Li, and G. J. Iafrate, Construction and application of an accurate local spin-polarized kohn-sham potential with integer discontinuity: Exchange-only theory, *Phys. Rev. A* **45**, 101 (1992).
- [9] Z. H. Yang, H. Peng, J. Sun, and J. P. Perdew, More realistic band gaps from meta-generalized gradient approximations: Only in a generalized kohn-sham scheme, *Phys. Rev. B* **93**, 205205 (2016).
- [10] J. P. Perdew, K. Burke, and M. Ernzerhof, Generalized gradient approximation made simple, *Phys. Rev. Lett.* **77**, 3865 (1996).
- [11] Y. Zhao and D. G. Truhlar, A new local density functional for main-group thermochemistry, transition metal bonding, thermochemical kinetics, and noncovalent interactions, *J. Chem. Phys.* **125**, 194101 (2006).
- [12] J. Sun, A. Ruzsinszky, and J. P. Perdew, Strongly constrained and appropriately normed semilocal density functional, *Phys. Rev. Lett.* **115**, 036402 (2015).
- [13] T. Aschebrock and S. Kümmel, Ultranonlocality and accurate band gaps from a meta-generalized gradient approximation, *Phys. Rev. Res.* **1**, 033082 (2019).
- [14] A. Aouina, M. Gatti, S. Chen, S. Zhang, and L. Reining, Accurate kohn-sham auxiliary system from the ground state density of solids, *Phys. Rev. B* **107**, 195123 (2023).
- [15] S. Lehtola, C. Steigemann, M. J. Oliveira, and M. A. Marques, Recent developments in libxc — a comprehensive library of functionals for density functional theory, *SoftwareX* **7**, 1 (2018).

Publication 2

Exact exchange-like electric response from a meta-generalized gradient approximation: A semilocal realization of ultranonlocality

Journal of Chemical Physics **159**, 234107 (2023)

Thilo Aschebrock, **Timo Lebeda**, Moritz Brütting, Rian Richter, Ingo Schelter, and
Stephan Kümmel

Theoretical Physics IV, University of Bayreuth, 95440 Bayreuth, Germany

Publ. 2

Author contributions

T.A. wrote the routines for the EEL functional, did all the calculations, prepared first versions of most figures, developed the functional construction, and contributed to the text. T.L., M.B., and R.R. participated in discussions about functional construction. I.S. helped with the numerical implementation. S.K. conceptualized the work, prepared final versions of the figures, and wrote the manuscript. All authors discussed the results and read and discussed the manuscript.

Publ.2

Exact exchange-like electric response from a meta-generalized gradient approximation: A semilocal realization of ultranonlocality

Cite as: J. Chem. Phys. 159, 234107 (2023); doi: 10.1063/5.0173776

Submitted: 24 August 2023 • Accepted: 24 November 2023 •

Published Online: 15 December 2023



View Online



Export Citation



CrossMark

Thilo Aschebrock,  Timo Lebeda,  Moritz Brütting,  Rian Richter,  Ingo Schelter,  and Stephan Kümmel^{a)} 

AFFILIATIONS

Theoretical Physics IV, University of Bayreuth, 95440 Bayreuth, Germany

Note: This paper is part of the JCP Festschrift for John Perdew.

^{a)} Author to whom correspondence should be addressed: stephan.kuemmel@uni-bayreuth.de.

URL: <http://tp4.uni-bayreuth.de/en>

ABSTRACT

We review the concept of ultranonlocality in density functional theory and the relation between ultranonlocality, the derivative discontinuity of the exchange energy, and the static electric response in extended molecular systems. We present the construction of a new meta-generalized gradient approximation for exchange that captures the ultranonlocal response to a static electric field in very close correspondence to exact exchange, yet at a fraction of its computational cost. This functional, in particular, also captures the dependence of the response on the system size. The static electric polarizabilities of hydrogen chains and oligo-acetylene molecules calculated with this meta-GGA are quantitatively close to the ones obtained with exact exchange. The chances and challenges associated with the construction of meta-GGAs that are intended to combine a substantial derivative discontinuity and ultranonlocality with an accurate description of electronic binding are discussed.

© 2023 Author(s). All article content, except where otherwise noted, is licensed under a Creative Commons Attribution (CC BY) license (<http://creativecommons.org/licenses/by/4.0/>). <https://doi.org/10.1063/5.0173776>

I. LOCALITY, NONLOCALITY, AND ULTRANONLOCALITY IN DFT

Density functional theory (DFT) is a very successful approach to the electronic structure problem.^{1–4} This success rests on the highly non-trivial fact that the intricate quantum many-body effects of exchange and correlation (xc) can be captured with an accuracy that is good enough for many practical applications with relatively “simple” functionals of the density, such as the local density approximation (LDA) and generalized gradient approximations (GGAs). Such semilocal xc approximations provide an unrivaled computational efficiency. The constraint-guided construction strategy that has been advocated by Perdew, to whom this special issue is dedicated, has led to some of the most widely used semilocal functionals.^{5–7}

However, there are well-known classes of problems where LDA and typical GGAs fail even qualitatively. One of them is the electrical response of extended systems and long-range charge-transfer.

The challenges, both conceptual and practical, that DFT can face in describing the electrical response of infinite periodic systems have been discussed from different perspectives in the past.^{8–17} Here, we focus on extended but finite systems. In these, the long-range charge-transfer problem manifests itself in both ground-state^{18,19} and time-dependent^{20,21} DFT. Our focus here is on ground-state DFT, and in this ground-state theory, the hallmark charge-transfer problem is the huge overestimation of the static electric longitudinal dipole polarizability of extended molecular systems that is observed with LDA and GGAs. The failure can be traced back^{19,22} to a well-known qualitative difference between the response of the exact exchange potential and the one of LDA and GGAs: the exact exchange response potential counteracts the externally applied dipole field, while the one of LDA and GGAs works with it. This feature of exact exchange has been termed “ultranonlocality.”^{19,22,23} Hydrogen chains and polyacetylene serve as the prime examples for studying this ultranonlocality and the ground-state charge-transfer problem,^{18,19,22,24–42} and they also set the stage for the present work.

Since the terms local, semilocal, nonlocal, and ultranlocal have been used in somewhat different contexts in the past, we first clarify in which sense we use these terms in the present work.

One context in which these terms are used in ground-state DFT is the definition of the xc energy

$$E_{xc}[n] = \int e_{xc}[n](\mathbf{r}) d^3r \quad (1)$$

in terms of an xc energy density $e_{xc}[n](\mathbf{r})$. An approximation to $e_{xc}(\mathbf{r})$ is called nonlocal when evaluating it at the point \mathbf{r} requires information from far-distant points \mathbf{r}' , e.g., via an integration over all space. The hallmark example of nonlocality is the exact exchange energy density

$$e_x^{\text{ex}}(\mathbf{r}) = -\frac{e^2}{2} \sum_{\sigma=\uparrow,\downarrow} \sum_{i,j=1}^{N_\sigma} \int \frac{\varphi_{i\sigma}^*(\mathbf{r})\varphi_{j\sigma}^*(\mathbf{r}')\varphi_{j\sigma}(\mathbf{r})\varphi_{i\sigma}(\mathbf{r}')}{|\mathbf{r}-\mathbf{r}'|} d^3r'. \quad (2)$$

An approximation is local or semilocal in terms of Eq. (1) when the xc energy density can be evaluated based on quantities that are already available in a usual calculation, such as the density and the orbitals, and these quantities need to be evaluated only at \mathbf{r} or an infinitesimal neighborhood of \mathbf{r} , respectively, to find $e_{xc}(\mathbf{r})$.

When the terms semilocal and nonlocal are used in this sense, they are also often associated with computational expense, in the sense that semilocal functionals are usually cheaper to evaluate than nonlocal ones. The term ultranlocal, however, is difficult to define based on Eq. (1). For defining and understanding ultranlocality, it is helpful to look at the terms local, semilocal, and nonlocal from a second, different perspective and think in terms of the xc potential $v_{xc}(\mathbf{r})$.

In this second perspective, the term “locality” refers to how the xc potential v_{xc} at a given point \mathbf{r} depends on the density $n(\mathbf{r})$. That is, in a local approximation, it suffices to know the density n at \mathbf{r} to compute $v_{xc}(\mathbf{r})$ at this point \mathbf{r} . In a semilocal approximation, it suffices to know n and ∇n at the given point \mathbf{r} to calculate $v_{xc}(\mathbf{r})$. Although calculating $\nabla n(\mathbf{r})$ requires information about the density beyond just \mathbf{r} and is, therefore, not a strictly local procedure, the required additional information is restricted to an infinitesimally small neighborhood around \mathbf{r} , i.e., semilocal. An approximation is called “nonlocal” when $v_{xc}(\mathbf{r})$ depends continuously on the value of the density in regions of space that are far from the point \mathbf{r} .⁴³ The Hartree potential is a typical example of a potential that is nonlocal in this sense.

Ultralocality is different from this usual nonlocality. We call a potential ultranlocal when $v_{xc}(\mathbf{r})$ non-vanishingly depends on the density at points \mathbf{r}' that can be infinitely distant from \mathbf{r} , or when an infinitesimally small change of the density can lead to a finite change of the potential. The finite “jumps” of the Kohn–Sham xc potential that are associated with the derivative discontinuity^{44,45} are a paradigm example of ultranlocality. The field-counteracting terms mentioned in the second paragraph can be understood in terms of such potential steps induced by the derivative discontinuity.^{26,34} As the external field moves charge to a molecular unit, the potential “jumps up” on this unit and, thus, counteracts the polarizing field.

One should be aware that the three different contexts—energy density, computational cost, and xc potential—in which the terms

local, semilocal, etc., are used, result in the fact that the classification of a functional can be non-obvious. We elucidate what we mean by this sentence with the help of two examples. The first is the Average Density Self-Interaction Correction (ADSIC) functional,⁴⁶ which can be interpreted as a global average over the well-known orbital specific Perdew–Zunger SIC.⁴⁷ In terms of the first definition via the energy density, ADSIC is nonlocal, as it features a Hartree-type integral in the xc approximation. In terms of computational cost, however, ADSIC is classified as local as it is hardly more expensive than the LDA. Furthermore, the ADSIC functional does not show⁴⁸ the field-counteracting terms that are the hallmark of (ultra)nonlocality.

The second example is meta-GGAs. They are semilocal in terms of energy density and computational cost. However, their potential can show ultranlocality, as demonstrated in Ref. 49. There is, however, an open question with respect to the degree of ultranlocality that can be reached with a meta-GGA. While Ref. 49 demonstrated that a meta-GGA can show ultranlocality and can thus also improve the static electric response of extended molecular systems, the degree of ultranlocality did not match the one of exact exchange. Furthermore, the electrical response, while being much improved compared to usual semilocal functionals, did not fully capture the features that exact exchange shows, for example, with respect to the dependence of the response on the system size. This raises the question whether a meta-GGA can really reach the same degree of ultranlocality as exact exchange or whether the electrical response that exact exchange yields incorporates features that decisively depend on the nonlocal Fock integrals and, thus, cannot be reproduced by a meta-GGA.

This is the question that this paper addresses. In Sec. II, we review existing meta-GGAs in view of a criterion that allows one to estimate the degree of ultranlocality that one can expect from a meta-GGA. In Sec. III, we present a new meta-GGA that we construct non-empirically by focusing on constraints that guarantee important properties of the potential $v_x(\mathbf{r})$ and ultranlocality. We demonstrate in Sec. IV that this meta-GGA reproduces the static electric response in close and quantitative similarity to exact exchange, despite using only quantities that can be evaluated at semilocal computational cost. The calculations also show that the functional can be evaluated without numerical problems. In the concluding Sec. V, we put these results into perspective with other requirements that xc approximations are typically expected to fulfill and discuss possible future developments.

II. ULTRANLOCALITY IN META-GGAS

By convention, semilocal functionals are often not given in the form of Eq. (1) but use a factorization with an enhancement factor F_x that indicates how strongly the functional differs from the LDA. We here focus on meta-GGAs for exchange that are written in the form

$$E_x^{\text{mGGA}}[n] = A_x \int n^{4/3} F_x(s, \alpha) d^3r, \quad (3)$$

where $A_x = -(3e^2/4)(3/\pi)^{1/3}$, and the enhancement factor $F_x(s, \alpha)$ is parameterized in terms of the dimensionless variables $s = |\nabla n|/(2(3\pi^2)^{1/3}n^{4/3})$ and $\alpha = (\tau - \tau^W)/\tau^{\text{unif}}$. Here,

$n = \sum_{\sigma=\uparrow,\downarrow} \sum_{j=1}^{N_{\sigma}} |\varphi_{j\sigma}|^2$ is the density, and the kinetic energy density τ ,

$$\tau(\mathbf{r}) = \frac{\hbar^2}{2m} \sum_{\sigma=\uparrow,\downarrow} \sum_{j=1}^{N_{\sigma}} |\nabla \varphi_{j\sigma}(\mathbf{r})|^2, \quad (4)$$

is evaluated using the Kohn–Sham or generalized Kohn–Sham orbitals $\varphi_{i\sigma}$, depending on which framework of DFT one is working in. The von Weizsäcker kinetic energy density is $\tau^W = \hbar^2 |\nabla n|^2 / (8mn)$, and $\tau^{\text{unif}} = A_s n^{5/3}$ with $A_s = (3\hbar^2/10m)(3\pi^2)^{2/3}$ is the kinetic energy density of the homogeneous electron gas. e and m are the elementary charge and the electron mass, respectively. The parameterization of the enhancement factor in s and α is used in many meta-GGAs⁵⁰ (although other variables are used with success as well⁵¹). In our experience, s and α are well suited for modeling xc approximations in which representing limiting cases, such as the homogenous electron gas limit ($\alpha \rightarrow 1$) or iso-orbital limit ($\alpha \rightarrow 0$), is part of the construction strategy.

In the following, we focus the formal discussion mostly on the derivative discontinuity and not on other manifestations of ultranonlocality, such as the field-counteracting terms. We can do so because, as explained in previous studies,^{20,26,49,52} a substantial derivative discontinuity will automatically translate into an improved description of the observables for which ultranonlocality is of interest, such as static charge-transfer properties and field-counteracting terms. Since exchange contributes dominant parts to the ultranlocal response,^{19,24} as confirmed by the exact correlation contribution to the response in hydrogen chains,³⁹ we further focus on exchange functionals.

The exchange derivative discontinuity for a system with N electrons is defined by

$$\Delta_x = v_x(\mathbf{r})|_+ - v_x(\mathbf{r})|_- = \frac{\delta E_x[n]}{\delta n(\mathbf{r})} \Big|_+ - \frac{\delta E_x[n]}{\delta n(\mathbf{r})} \Big|_-, \quad (5)$$

where $|_+$ and $|_-$ denote evaluation of the functional derivative at $N + \epsilon$ and $N - \epsilon$, with $\epsilon \rightarrow 0$, respectively. As the functional derivative of a meta-GGA is given by

$$\frac{\delta E_x^{\text{mGGA}}[n]}{\delta n(\mathbf{r})} = \frac{\partial e_x}{\partial n}(\mathbf{r}) - \nabla \cdot \left[\frac{\partial e_x}{\partial \nabla n}(\mathbf{r}) \right] + \int \frac{\partial e_x}{\partial \tau}(\mathbf{r}') \frac{\delta \tau(\mathbf{r}')}{\delta n(\mathbf{r})} d^3 r', \quad (6)$$

the derivative discontinuity of a meta-GGA is given by

$$\Delta_x^{\text{mGGA}} = \int \frac{\partial e_x}{\partial \tau}(\mathbf{r}') \left[\frac{\delta \tau(\mathbf{r}')}{\delta n(\mathbf{r})} \Big|_+ - \frac{\delta \tau(\mathbf{r}')}{\delta n(\mathbf{r})} \Big|_- \right] d^3 r'. \quad (7)$$

From this exact expression, one can derive an approximate one that allows one to easily develop a feeling for the expected nonlocality of a given meta-GGA by simple visual inspection of the enhancement factor. The key thought is the “system averaging approximation” that replaces $\partial e_x / \partial \tau$ in the integrand of Eq. (7) by its average over the integration region. This allows us to pull this average $\overline{\partial e_x / \partial \tau}$ out of the integral. Interchanging the integration and the functional

derivative, one can then integrate τ and obtain the approximate relation

$$\Delta_x^{\text{mGGA}} \approx \overline{\frac{\partial e_x}{\partial \tau}} \left[\frac{\delta T_s[n]}{\delta n(\mathbf{r})} \Big|_+ - \frac{\delta T_s[n]}{\delta n(\mathbf{r})} \Big|_- \right]. \quad (8)$$

The second factor on the right is just the Kohn–Sham eigenvalue gap⁵³ Δ_s , and thus, one obtains $\Delta_x^{\text{mGGA}} \approx (\overline{\partial e_x / \partial \tau}) \Delta_s$ in the system averaging approximation. Since $\Delta_s > 0$, this equation shows that a meta-GGA that fulfills

$$\overline{\frac{\partial e_x}{\partial \tau}} > 0 \quad (9)$$

will yield a positive exchange derivative discontinuity, as it should. Thus, Eq. (9) can be used as a guideline in meta-GGA constructions that aim at functionals that yield a pronounced derivative discontinuity Δ_x and related features, such as ultranonlocality.

For practical purposes, one prefers meta-GGAs that are parameterized in s and α ; cf. Eq. (3). One can translate the condition of Eq. (9) to these variables by using the chain rule in combination with Eq. (3) and the definition of α . This shows⁴⁹ that a positive Δ_x^{mGGA} is guaranteed when

$$\partial F_x / \partial \alpha < 0. \quad (10)$$

The system averaging approximation is a non-trivial step, and its consequences have recently been discussed in detail in the context of band-gap prediction.⁵⁴ However, based on it, Eqs. (9) and (10) allow us to gain *a priori* intuition for how much derivative discontinuity and (ultra)nonlocality to expect from a meta-GGA in a very simple way, namely by inspecting plots of the enhancement factor.

Figure 1 shows plots of the exchange enhancement factor $F_x(s, \alpha)$ as a function of α for different values of s for some paradigm meta-GGAs that we selected from the large number of meta-GGAs that are available in the literature. The left and middle panels in the top row show plots of the PKZB (Perdew, Kurth, Zupan, and Blaha⁵⁵) and TPSS (Tao, Perdew, Staroverov, and Scuseria⁶) meta-GGAs, respectively. Evidently, their enhancement factors hardly show any slope, and the enhancement factor of PKZB for small values of s even slightly increases as a function of α . This observation, together with Eqs. (9) and (10), explains the earlier reported findings that, e.g., TPSS does not show non-locality,⁵¹ PKZB and TPSS show only a minute derivative discontinuity,⁵² and yield band gaps similar to usual GGAs.⁶² Many other meta-GGAs, e.g., the ones from Refs. 63–68, show similarly small derivatives $\partial F_x / \partial \alpha$, and one thus expects similarly little ultranonlocality from them.

The rightmost panel in the first row depicts the enhancement factor of the local τ approximation.⁵⁶ This non-empirical meta-GGA shows a very pronounced dependence of the enhancement factor on α , and one can, therefore, expect pronounced effects of ultranonlocality. However, all the curves for different values of s are monotonically increasing. Thus, Eq. (10) indicates that the local τ approximation⁵⁶ will lead to a negative exchange derivative discontinuity, contrary to the sign that one finds in exact exchange. Based on general arguments,⁵⁴ one expects that correlation will also contribute a negative sign to the derivative discontinuity. Therefore, the local τ approximation will yield an overall negative xc derivative

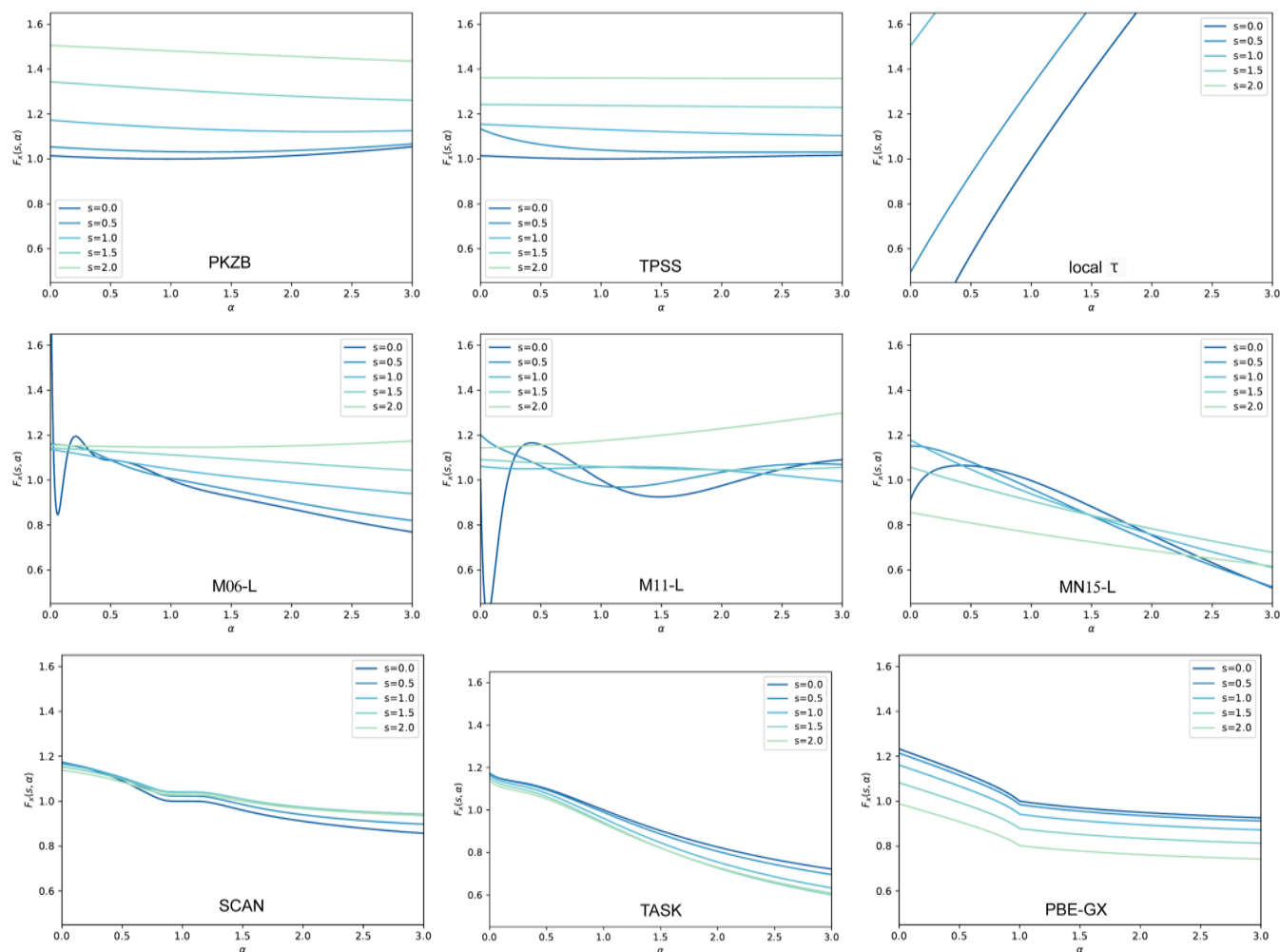


FIG. 1. Plots of the enhancement factor $F_x(s, \alpha)$ as a function of α for different values of s for the meta-GGAs (from left top to bottom right): PKZB,⁵⁵ TPSS,⁸ local τ ,⁵⁶ M06-L,⁵⁷ M11-L,⁵⁸ MN15-L,⁵⁹ SCAN,⁷ TASK,⁴⁹ and PBE-GX.⁶⁰ A negative slope in these plots leads to a positive exchange derivative discontinuity. For the local- τ approximation, not all the curves for the different values of s fall within the plotted range.

discontinuity—which calls this approximation into question in view of the expectation of a positive derivative discontinuity.⁶⁹

The second row of panels depicts the enhancement factors of the M06-L,⁵⁷ M11-L,⁵⁸ and MN15-L⁵⁹ meta-GGAs for exchange. Fitting parameters to large databases is part of the construction strategy of these functionals, and this leads to substantial variations in the enhancement factors. Consequently, because there is no universal trend in the slope of F_x , it is difficult to deduce general statements about the magnitude and the sign of the derivative discontinuity for M06-L and M11-L based on Eq. (10) and the plots of the enhancement factor: For some ranges of α , the slope is negative while it is positive for others, and for values of $s \gtrsim 2$, the enhancement factor increases with increasing α , i.e., shows a trend similar to the local τ approximation. The same is true for the revM06-L functional,⁷⁰ which is not shown in Fig. 1. Thus, the strength of the derivative discontinuity and ultranlocal effects with these functionals can

be very different for different systems, depending on which values of s and α are realized and which range of the enhancement factor is thus probed. The MN15-L functional, on the other hand, shows a more uniform enhancement factor. For most values of s , F_x decreases with increasing α , which translates into the proper sign for the exchange discontinuity according to Eq. (10). This general trend is, however, violated for $s = 0$ for values of $\alpha \lesssim 0.5$, and therefore, some uncertainty about the strength of the exchange discontinuity in this functional remains.

The bottom line of panels in Fig. 1 finally shows three examples of functionals for which one can be sure to find a non-negative exchange discontinuity and at least some degree of ultranlocality: The enhancement factors of the meta-GGAs SCAN,⁷ TASK,⁴⁹ and PBE-GX⁶⁰ decrease with increasing α for all values of s . SCAN shows more slope than, e.g., TPSS, and consequently, SCAN improves band gaps more than TPSS due to a larger contribution from the deriva-

tive discontinuity.^{71–73} There are several other functionals,^{74–78} not shown in Fig. 1 for the sake of space, whose enhancement factors show a similar or somewhat less negative derivative in α than SCAN. These functionals can, therefore, be expected to also show some degree of ultranonlocality, although not much. A larger degree of ultranonlocality can be expected from the TASK functional, which, while satisfying the same set of exact constraints as SCAN, has a more pronounced negative slope. Consequently, band gaps predicted with TASK reach a yet higher and remarkable accuracy^{49,62} due to a substantial contribution⁵⁴ from the exchange discontinuity. In terms of the slope of the enhancement factor, cf. the bottom right panel in Fig. 1, one would expect that the PBE-GX functional shows a derivative discontinuity and ultranonlocality of a strength between SCAN and TASK. However, checking this in practice for systems of practically relevant complexity seems presently impossible, as the PBE-GX functional is numerically very ill-behaved.⁷⁹

The degree of ultranonlocality and the magnitude and sign of the derivative discontinuity that one expects from a meta-GGA can thus, in many cases, simply be estimated by analyzing the slope of the enhancement factor as a function of α . (We note in passing that this slope also determines the importance of the gauge-invariance restoring current-density correction when meta-GGAs are used in time-dependent DFT.^{80,81}) To the best of our knowledge, among the presently existing meta-GGAs, the TASK functional is the one that shows the most pronounced effects of ultranonlocality.^{82,99} This, however, leads to the question that was mentioned toward the end of the introduction. In Ref. 49, the practical manifestation of ultranonlocality was tested for the TASK functional by using it to calculate the static electric polarizabilities of hydrogen chains, i.e., one of the paradigm test systems for the static charge-transfer problem.^{18,19,22,24,26,27,29–38,40,41} While TASK significantly improves the calculated polarizabilities compared to other semilocal functionals, it does not fully match exact exchange in terms of the strength of the field-counteracting terms. In particular, for the longer chains, the differences between TASK and exact exchange became noticeable. Thus, the question arises whether a meta-GGA can really capture the same degree of ultranonlocality as exact exchange or whether there is a fundamental limitation of the meta-GGA concept, e.g., resulting from the lack of exchange-like integrals, to yield full, exact-exchange-like ultranonlocality.

III. THE EXACT-EXCHANGE LIKE RESPONSE (EEL) META-GGA

In the following, we demonstrate that one can construct a meta-GGA based solely on semilocal-cost functional ingredients that indeed yields an ultranonlocal static electric response in quantitative agreement with the exact exchange for hydrogen chains and in close similarity for real oligomers. The guidelines in our construction are the hydrogen atom as the paradigm localized one-electron system and the homogeneous electron gas as the paradigm extended many-electron system.

Our construction starts at the iso-orbital limit. In this limit, $\alpha \equiv 0$, the exchange enhancement factor effectively depends only on s and can, therefore, be represented by a GGA-type enhancement factor,

$$F_x(s, \alpha = 0) = G(s^2). \quad (11)$$

The SCAN⁷ and TASK⁴⁹ meta-GGAs choose

$$G_{\text{SCAN}}(x) = h_x^0 \left[1 - \exp(-c_0 x^{-1/4}) \right] \quad (12)$$

in order to obey the strongly tightened bound⁸³ for two-electron densities,

$$F_x(s, \alpha = 0) \leq 1.174 = h_x^0, \quad (13)$$

and to enforce the correct nonuniform coordinate scaling of the exchange energy per particle to the true two-dimensional limit.^{84,85} With the choice⁷ $c_0 = 4.9479$, SCAN and TASK obtain the exact hydrogen atom energy via spin scaling. Thus, for hydrogenic systems, the ansatz indirectly also minimizes the one-electron self-interaction energy. As our aim is to obtain a physical potential that is similar to the one of exact exchange, we want to avoid the divergences that GGA-type potentials typically show at a nucleus. Therefore, we generalize $G_{\text{SCAN}}(x)$ of Eq. (12) to

$$G(x; x_0) = h_x^0 \left\{ 1 - \exp \left[-c(x - x_0)^{-1/4} \right] \Theta(x - x_0) \right\}, \quad (14)$$

where $\Theta(x)$ is the Heaviside step function. Here, $x_0 \geq 0$ is an additional parameter that ensures $G(x; x_0) = h_x^0$ for $x \leq x_0$. We choose $x_0 = s_0^2$ with $s_0 = (6\pi)^{-1/3}$ being the minimal value of s realized in a doubly occupied, 1s-orbital like exponential density. This eliminates the spurious divergence in the exchange potential at the nucleus due to $\nabla^2 n$ contributions.^{6,86} With the choice $c = 4.759279$, we ensure that the exact hydrogen atom energy is obtained again. This one-orbital limit enhancement factor is referred to as $G(x)$ in the following.

We now generalize the one-orbital limit $G(x)$ to a general meta-GGA enhancement factor $F_x(s, \alpha)$ by making use of the observation that in the one-orbital limit, the reduced kinetic energy density $t = \tau/\tau^{\text{unif}}$ is proportional to s^2 , i.e., more precisely $t \rightarrow \frac{5}{3}s^2$, because $\tau \rightarrow \tau^{\text{W}}$.⁸⁷ Furthermore, we make use of the general relation $3t/5 = s^2 + 3\alpha/5$, which follows from the definition of α . Combining these steps, one can define a general enhancement factor by the linear combination

$$F_x(s, \alpha; k) = k \left[G(s^2 + 3\alpha/5) - G(s^2) \right] + G(s^2). \quad (15)$$

The idea of this linear combination is to define a family of enhancement factors as a function of the parameter k that all share the same one-orbital limit, i.e., respect the hydrogen atom limiting case, yet differ in their dependence on α . Furthermore, the strength of the α -dependence is directly controlled by the parameter k . As $G(x)$ is a monotonically decreasing function, restricting k to positive values, i.e., $k > 0$, ensures that

$$\partial F_x / \partial \alpha < 0. \quad (16)$$

Thus, the correct sign of the exchange derivative discontinuity, i.e., $\Delta_x > 0$, is guaranteed for all enhancement factors of the type of Eq. (15).

In the following, we are interested in $k > 1$ to obtain an appreciable magnitude of the derivative discontinuity and associated ultranonlocal properties. Since $\alpha \geq 0$, the monotonicity of G implies that the enhancement factors of Eq. (15) for $k > 1$ are bounded from both below and above,

$$(-k + 1)h_x^0 \leq F_x(s, \alpha; k) \leq F_x(s, \alpha = 0; k) \leq h_x^0. \quad (17)$$

While the upper bound is reasonable as it imposes the conjectured strongly tightened bound,⁸³

$$F_x(s, \alpha) \leq F_x(s, \alpha = 0) \leq h_x^0, \quad (18)$$

the lower bound does not ensure the positivity of F_x and, thus, cannot guarantee the negativity of the exchange energy for any density. In practice, a negative F_x can arise from Eq. (15) for $k > 1$ when s is small and α is very large because then the negative second term can dominate over the positive first and third terms. This problem, however, can be avoided by a change of variables. We replace α with the monotonically increasing expression

$$\tilde{\alpha}(\alpha; \alpha_0) = \alpha_0 \tanh(\alpha/\alpha_0). \quad (19)$$

This maintains the behavior for small values of α , i.e., $\tilde{\alpha} \sim \alpha$ for $\alpha \rightarrow 0$, while realizing an upper bound α_0 , i.e., $\lim_{\alpha \rightarrow \infty} \tilde{\alpha} = \alpha_0$.

The thus introduced parameter α_0 has to be chosen large enough to guarantee that Eq. (19) provides a non-constant mapping from α to $\tilde{\alpha}$ for the physically significant range of α -values, i.e., preserves the physically relevant behavior of α , and small enough to guarantee the positivity of F_x . We found that the choice of $\alpha_0 = 3$ respects both conditions.⁸⁸ Therefore, we arrive at the final expression

$$F_x(s, \alpha; k, \alpha_0) = k[G(s^2 + 3\tilde{\alpha}(\alpha; \alpha_0)/5) - G(s^2)] + G(s^2). \quad (20)$$

The remaining parameter k is determined by enforcing the homogeneous electron gas limit, i.e.,

$$F_x(s = 0, \alpha = 1) = 1. \quad (21)$$

Imposing this limit yields

$$k(\alpha_0) = (1 - h_x^0) / [G(3\alpha_0 \tanh(\alpha_0^{-1})/5) - h_x^0] \quad (22)$$

with $k \approx 51.5558$ for $\alpha_0 = 3$. This concludes the construction of the exact-exchange-like response (EEL) functional, i.e., E_x^{EEL} is given by Eq. (3) with the F_x of Eq. (20) and the just mentioned values for the parameters k and α_0 .

Figure 2 shows a plot of this F_x^{EEL} as a function of α for different values of s , in analogy to the plots shown in Fig. 1. However, note that the scale of the vertical axis has been extended in Fig. 2 due to the EEL functional's stronger dependence on α .

IV. STATIC ELECTRIC RESPONSE OF EXTENDED MOLECULAR SYSTEMS

This functional construction did not address covalent binding, and therefore, it should not be expected that it leads to a “general purpose” functional that would, for example, reliably describe electron bonds of different kinds. However, by constructing Eq. (20) such that it respects the hydrogen atom, the homogeneous electron gas, and the principle of a large derivative discontinuity, we aimed at a functional that is reasonable for $1s$ -orbital densities, for delocalized electrons, and yields sizeable field-counteracting terms. As a consequence, Eq. (20) should be well capable of describing the static electric response of systems such as hydrogen chains or conjugated polymers, whose electronic structure shows both atomic-like and delocalized features and in which field-counteracting terms

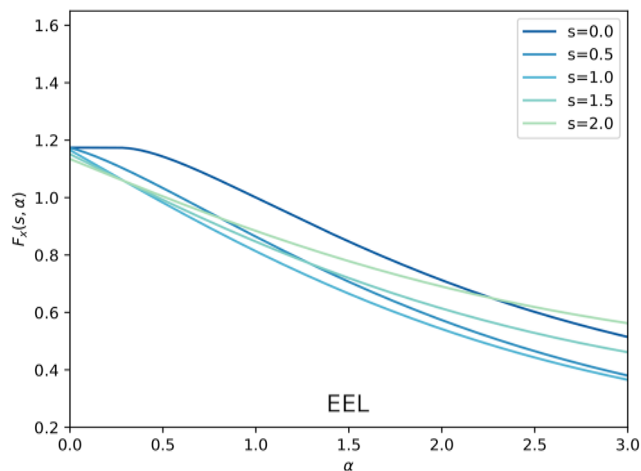


FIG. 2. Plots of the enhancement factor $F_x^{\text{EEL}}(s, \alpha)$ from Eq. (20) as a function of α for different values of s .

are decisive for obtaining reasonable values for the electric polarizability. As previously explained, we thus want to clarify whether a meta-GGA that only uses semilocal ingredients can achieve an ultranlocal response of the same magnitude as the fully non-local exact exchange.

Hydrogen chains with alternating bond lengths of 2 and 3 a_0 are, as mentioned above, a well-established reference system for checking the ability of many-body methods to describe the electrical response of and static charge-transfer in extended systems. In fact, among the different molecular chains that have been studied in the context of ultranlocality in DFT, hydrogen chains have even been identified as a particularly challenging test.²³ Table I lists the results from our calculations of the longitudinal static electric dipole polarizability of hydrogen chains of increasing length. We here do not compare to many other previously published meta-GGAs, because such a comparison has been done in earlier work⁴⁹ and it showed—confirming earlier findings^{52,61}—that traditional meta-GGAs do not show much ultranlocality and, therefore, lead to a substantial overestimation of the polarizabilities of extended, chain-like systems. Our focus is, therefore, on meta-GGAs that have been constructed to yield a substantial derivative discontinuity and, thus, field-counteracting terms, i.e., the PoC and TASK functionals from Ref. 49 and the EEL functional from this work. We compare these functionals to exact exchange (EXX) as the reference, and we also show results from the exchange LDA as the paradigm local approximation.

The rightmost column of Table I shows the exact exchange results, which are the reference numbers for our present purposes. The leftmost column shows the results from the local exchange, and these highlight the well-known problem of the local approximation: The polarizability is systematically overestimated, and the deviation has a pronounced size dependence: Errors increase significantly with increasing system size and reach almost 60% for H_{40} . TASK, which is constructed to fulfill the gradient expansion and many other exact constraints, i.e., follows universal design criteria for overall accuracy,⁸⁹ considerably improves over the LDA and yields much more

TABLE I. Static electric longitudinal dipole polarizabilities in a_0^3 for the hydrogen chains H_{2N} for different exchange energy functionals. DFT calculations were performed self-consistently with the potentials of all orbital-dependent functionals evaluated in the Krieger–Li–Iafrate (KL) approximation.⁴⁴

H_{2N}	xLDA	TASK	PoC	EEL	EXX
H_2	13.2	12.1	12.1	12.0	12.0
H_4	39.6	34.7	31.9	33.7	33.2
H_6	76.4	64.5	55.5	60.9	60.3
H_8	120.6	98.7	81.0	91.9	90.9
H_{10}	169.6	135.5	107.4	123.7	123.4
H_{12}	221.8	173.7	134.3	158.0	156.9
H_{14}	275.9	212.9	161.4	190.8	191.1
H_{16}	331.2	252.5	188.6	226.4	225.5
H_{18}	387.3	292.4	215.9	259.4	260.3
H_{20}	444.0	332.6	243.3	295.8	295.1
H_{24}	558.1	413.2	298.1	365.4	365.0
H_{28}	672.9	494.1	353.1	435.3	435.1
H_{32}	788.1	575.2	408.1	505.2	505.3
H_{36}	903.6	656.4	463.2	575.3	575.6
H_{40}	1019.2	737.6	518.4	645.3	646.0

realistic polarizabilities than other meta-GGAs.⁴⁹ However, for large chain lengths, the deviation goes up to 14%, i.e., the difference with respect to exact exchange becomes noticeable. The PoC functional, which was presented in Ref. 49 as a very simple proof-of-concept with a focus on only the derivative discontinuity, shows deviations of up to 19% but of the opposite sign, i.e., it yields polarizabilities that are significantly too low. The EEL functional finally yields polarizabilities in very close agreement with exact exchange.

The trends in these results become yet clearer when one visualizes the data by plotting the relative polarizability with respect to exact exchange as a function of system size, as shown in Fig. 3. This shows that the smallest systems are reasonably well described by all exchange approximations, except for LDA, which shows a 10% deviation already for H_2 . However, the dependence on the system size is very different for the different functionals. LDA deviations increase significantly with system size and have not yet saturated at H_{40} , the largest hydrogen system in our study. This size dependence is a hallmark sign of missing the required ultranonicity.^{19,23} TASK also shows an increasing deviation, but the deviation saturates at about 15% already around H_{24} . The simple PoC functional shows both a larger deviation with the opposite sign and a slower convergence of the deviation. The EEL functional, finally, stays very close to the exact exchange values for all system sizes, i.e., yields an almost ideal horizontal line at 1.00. This demonstrates that a meta-GGA can capture ultranonicity in hydrogen chains in very close, quantitative agreement with exact exchange, despite being constructed from semilocal functional ingredients and without using non-local Fock exchange integrals.

This is a truly encouraging result. However, the hydrogen atom was one of the guinea pigs in the construction of the EEL functional and one may, therefore, argue that it is to some extent “natural” that the EEL functional describes hydrogen chains well. Checking whether the EEL functional yields a reasonable response for other extended systems is, therefore, a relevant second test. Polyacetylene,

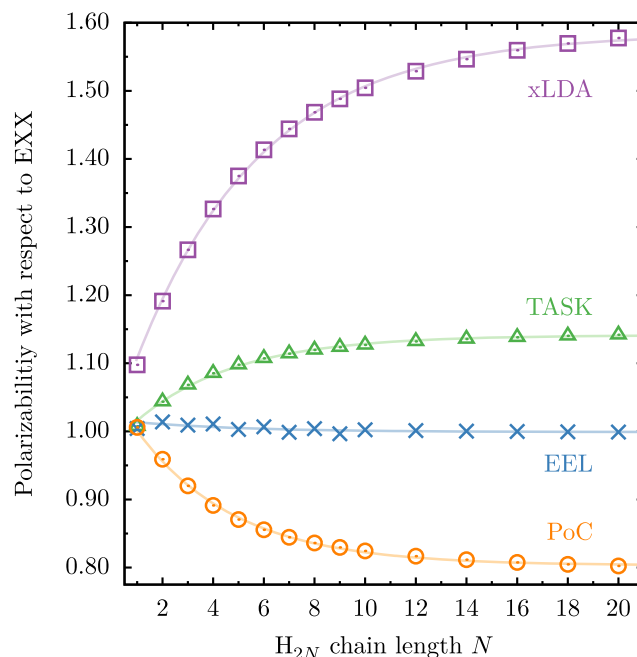


FIG. 3. Static electric longitudinal dipole polarizability from density functional exchange approximations divided by the polarizability obtained with exact exchange for different meta-GGAs and LDA as labeled in the figure. The discrete symbols denote the calculated data, while the continuous lines are fits that just serve as a guide to the eye.

or more precisely, $C_{2N}H_{2N+2}$ oligomers of increasing length, provide for a second established and challenging test of response properties. Figure 4 clarifies the geometry that we based our calculations on and which we chose as in earlier studies^{18,36} for ease of comparison of the results. Table II shows the longitudinal static electric dipole polarizabilities that one obtains for such acetylene oligomers. It is interesting to note that here, all functionals, including the PoC, yield larger polarizabilities than exact exchange. In order to clarify the trends, we again plot the polarizability with respect to the one from exact exchange as a function of the system size. Figure 5 reveals that the situation for polyacetylene differs from the one for the hydrogen chains in several respects. First, the trend with the system size is less uniform for all functionals, even the LDA. As a consequence, one cannot safely determine a saturation value for the deviation of any of the functionals, and we thus also refrain from showing fits. The data points themselves, however, still reveal the trends clearly enough. The LDA again shows the largest deviations, up to ~35%, and also the steepest slope in the relative deviation. The PoC functional shows relatively large deviations for the small oligomers but has a negative slope in the relative deviation, i.e., the relative deviation decreases for the larger systems. For most systems, PoC yields deviations of about 20%. The deviation of the TASK functional increases with increasing system size, but at a lesser rate than LDA, and the deviations are between 9% and 19%. The best results are again obtained with the EEL functional: for most systems, the deviations are around 5% and the largest deviation is about 10%. It is also interesting to observe that for smaller oligomers, there seems

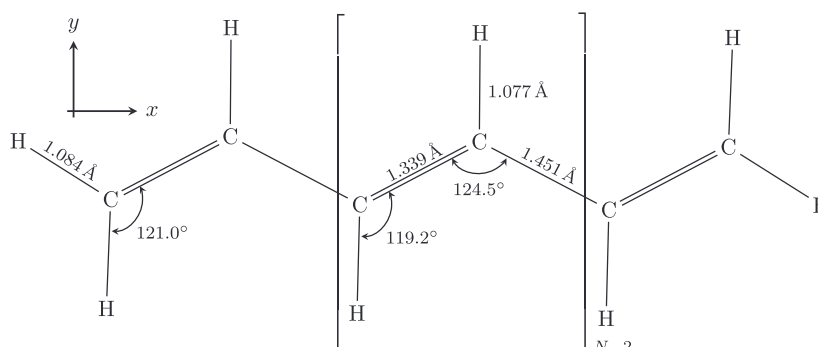


FIG. 4. Sketch of the geometry^{18,36} that the polyacetylene calculations are based on; see the main text for discussion.

TABLE II. Static electric longitudinal dipole polarizabilities in a_0^3 for the $C_{2N}H_{2N+2}$ oligomers of polyacetylene for different exchange energy functionals. DFT calculations were performed self-consistently with the potentials of all orbital-dependent functionals evaluated in the KLI approximation.⁴⁴

$C_{2N}H_{2N+2}$	xLDA	TASK	PoC	EEL	EXX
C_4H_6	91	85	95	81	77
C_6H_8	179	167	189	160	153
C_8H_{10}	301	280	307	265	254
$C_{10}H_{12}$	460	426	467	406	385
$C_{12}H_{14}$	656	606	658	566	539
$C_{14}H_{16}$	889	819	860	765	721
$C_{16}H_{18}$	1158	1056	1103	990	917
$C_{20}H_{22}$	1798	1621	1645	1509	1367
$C_{24}H_{26}$	2564	2312	2282	2111	1970
$C_{28}H_{30}$	3439	3071	2977	2824	2570

to be very little variation in the deviation with the system size, which indicates that the EEL functional captures the size dependence of the response in great similarity to exact exchange. For large oligomers, there seems to be some increase in the deviation, although the situation is not uniform as $C_{24}H_{26}$ shows a relatively small deviation of 7%.

These findings might appear somewhat unsystematic at first sight, but they can be understood when one analyzes the response potential in the way suggested by Ref. 19, i.e., by plotting the difference between the response potential with an external applied dipole field and without. This analysis is shown for the largest system in our study, $C_{28}H_{30}$, in Fig. 6. The full black line shows the exact exchange response, and the dashed line shows the constant potential of the polarizing dipole field. One clearly sees the field-counteracting effect of exact exchange: The response potential has an overall slope opposite to the slope of the external polarizing field. It is well known^{19,24,26} that functionals such as LDA and GGAs miss this field-counteracting term completely and, therefore, their polarizabilities are too large. Figure 6 also shows the response obtained from the three meta-GGAs, and this leads to an explanation of the above discussed findings.

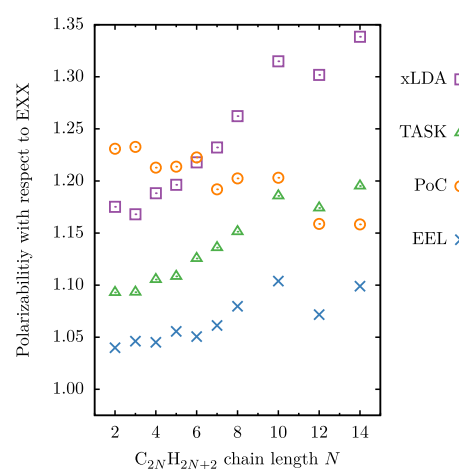


FIG. 5. Longitudinal polarizabilities for the $C_{2N}H_{2N+2}$ oligomers of polyacetylene for different exchange energy functionals relative to the polarizability found with EXX.

The first striking observation is that the PoC functional is more strongly field-counteracting than the exact exchange itself, as seen by the higher value of response potential on the far left and the lower value on the far right. However, along the chain, the PoC potential shows much more pronounced up- and down-spikes than exact exchange. To connect these observations to the above reported findings, one has to keep in mind that the response of an extended molecular system is strongly influenced by two different effects: On the one hand, the field-counteracting terms are important, and their relative importance increases with increasing system size. On the other hand, the shape of the potential itself, i.e., the wells and barriers that the Kohn-Sham potential features between the different segments of the molecular chain, also have a pronounced influence. If these wells and barriers are not of the correct height, then an externally applied field can shift electron density along the molecular backbone too easily or too hard, and this, too, leads to errors in the polarizability. This second effect, however, does not depend strongly on the system size, as the potential structure is similar in every repeat unit of the polymer. The pronounced spikes that one

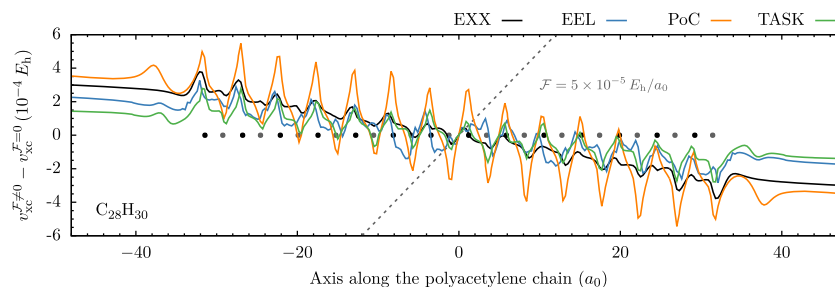


FIG. 6. Full lines: plots of the difference of the response potentials with and without an externally applied field¹⁹ for the molecule $C_{28}H_{30}$ for exact exchange as the reference and the meta-GGAs EEL, PoC, and TASK, as labeled. The dashed line indicates the potential associated with the polarizing uniform electric field. See the text for discussion.

sees in Fig. 6 in the response potential of the PoC functional show that the potential structure differs pronouncedly from the one of exact exchange. Thus, the PoC functional gives a wrong response, yet the deviation decreases for larger systems because for the latter, the relative importance of the field-counteracting terms increases, and these are overestimated by PoC. The decrease in the relative deviation that is observed for PoC in Fig. 5 is thus a consequence of a lucky error cancellation of the two different effects for intermediate oligomer lengths. For systems longer than the ones that we study here, one thus expects from the PoC functional an underestimation of the relative polarizability in analogy to the trend that was observed for the hydrogen chains.

Looking at the potential structure of the TASK functional in Fig. 6 shows that it is much more similar to the exact exchange than the one of PoC. The field counteracting term, however, is underestimated: One clearly sees that there is a field-counteracting effect, i.e., the existence of the ultranonlocality effect is confirmed also for polyacetylene. The counteracting slope, however, is somewhat too small. This explains why TASK overestimates the polarizabilities of polyacetylene.

Finally, looking at the plot for the EEL functional shows that its response potential structure is also quite similar to exact exchange. Furthermore, it shows a significant field-counteracting term. The slope does not fully reach the one of exact exchange, but it is more pronounced than the one found with TASK and can thus keep the relative errors below 10% for all system sizes. These observations are in line with Table II and Fig. 5: They explain the relative accuracy of the different meta-GGAs and, more importantly, demonstrate that while the quantitative accuracy of the EEL functional is smaller for the polarizability of polyacetylene than for the one of hydrogen chains, the pronounced increase in the deviation with the system size is strongly reduced. This confirms that meta-GGAs can indeed capture the ultranonlocal response in great similarity to exact exchange.

V. CONCLUSION

The above results demonstrate that ultranonlocality of the Kohn–Sham exchange potential can be reached with meta-GGAs. This finding has the potential for a significant impact: Meta-GGAs offer the hope that material research in which a proper description of the derivative discontinuity and field-counteracting terms is decisive, e.g., because band gaps or long-range charge transfer and

the electric response play an important role, can be done based on meta-GGAs. Up until now, such studies have usually had to resort to the different variants of hybrid functionals. Hybrids increase the computational cost enormously. This often limits studies to small, simplified models and prevents calculations that correspond to experimental reality. The much lower computational cost of meta-GGAs⁵⁴ can enable calculations on larger scales, both in space and in time, and can thus bring first-principles simulations closer to material research reality.

Whether meta-GGAs can live up to this promise will, however, depend on further serious research efforts. Our construction of the EEL functional, which took into account just two paradigm systems, the hydrogen atom and the homogenous electron gas, and one construction principle, the negative slope of F_x in α , showed that a reasonable accuracy was obtained for polyacetylene, while extremely accurate results were obtained for the hydrogen chain response. The accuracy for the hydrogen chains is plausible in view of the hydrogen atom being taken into account in the functional construction. Following this logic, it seems reasonable to assume that a generally accurate functional needs to be constructed by taking into account more of the physics of, for example, covalent binding, which is important in molecules and solids. Thus, the challenge is to construct more general functionals that yield a sizeable derivative discontinuity and ultranonlocal response while at the same time yielding accurate binding energies.

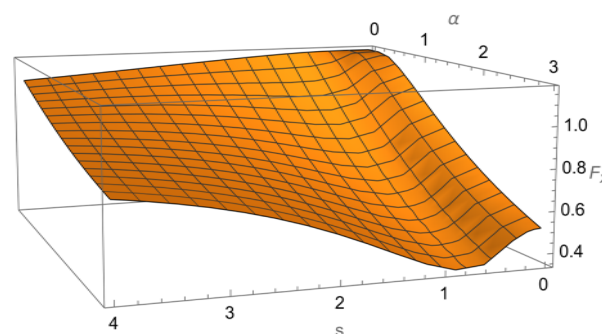


FIG. 7. Visualization of $F_x^{\text{EEL}}(s, \alpha)$ as a three-dimensional contour. One can thus see that Eq. (10) is fulfilled at all points in (s, α) -space.

There is hope that this will be possible because, so far, we have taken Eq. (10) literally: Functionals such as TASK and EEL fulfill this condition for all values of s and α , as visualized for the EEL functional in Fig. 7. This is sufficient for guaranteeing a positive derivative discontinuity. However, while Eq. (10) is a sufficient condition, it is not a necessary one. Equation (9) shows that violating Eq. (10) for some regions of s and α is acceptable as long as Eq. (9) is fulfilled for the energetically important region. The yet more general Eq. (7) widens the perspective further: Depending on which values of s and α are probed by a given system's electronic structure, the integral of Eq. (7) can be positive even if the integrand locally takes on negative values in some regions of space. Thus, there is flexibility in constructing functionals with a pronounced ultranlocality that has not yet been systematically explored in functionals such as TASK and EEL.

These ideas are in line with Ref. 90, which argues that enforcing conditions locally to guarantee satisfaction of global bounds is typically excessive. Some guidance on which values of s are relevant for, for example, atomization energies or transition state barrier heights, is available from earlier studies.^{91,92} For α , and yet more for the combination of the variables, the situation is more complex. However, some steps to identify decisive parameter regions have recently been taken, e.g., by demonstrating the importance of the semicore region for bond lengths in solids,⁹³ by analyzing which combinations of n , s , and α are important for determining the band gaps of solids,⁵⁴ and by studying which part of the vast parameter space is probed by the densities of real Coulomb systems and the constraints that are relevant there.⁹⁰ It is also clear that exploiting the freedom to locally deviate from Eq. (10) on the one hand, while, on the other hand, respecting the requirement of a negative derivative of F_x in α in a way that overall guarantees a positive derivative discontinuity, might require new ways of thinking about functional construction. In this light, it is reassuring to observe that promising new construction principles for meta-GGAs keep emerging.^{94–97}

Based on the demonstration that meta-GGAs, without doubt, can reach ultranlocality, which has been given in this paper, there is thus hope that semi-local functionals can shed off some of their traditional qualitative shortcomings while retaining their computational efficiency. However, one must also be aware that meta-GGAs do not feature conventional nonlocality as in the Hartree-term. This puts some limits on what can be reached within the meta-GGA form. It seems unlikely, for example, that a meta-GGA will generally be able to meet the straight-line condition for the energy as a function of particle number.^{69,98} Furthermore, while meta-GGAs can easily be made self-correlation-free for one-electron densities by using iso-orbital indicators, the missing nonlocality prevents them from being generally free from one-electron self-interaction. The static charge transfer that we studied here is not too sensitive to these limitations. However, the limitations are more strongly seen in recent time-dependent DFT calculations based on meta-GGAs.⁸¹ While incorporating the derivative discontinuity does improve charge-transfer excitations to some extent, quantitative accuracy would require further improvements in the potential, e.g., to yield more strongly bound eigenvalues and the proper long-range asymptotics. It might, therefore, be a promising route for future functional development to combine the ultranlocality that meta-GGAs naturally incorporate with the nonlocality that a one-electron

self-interaction correction, e.g., of the Perdew–Zunger type,⁴⁷ can bring.

ACKNOWLEDGMENTS

We gratefully acknowledge the financial support from the Deutsche Forschungsgemeinschaft, DFG Project Grant No. KU 1410/4-1, from the Elite Study Program “Biological Physics” of the Elite Network of Bavaria, and from the Bavarian State Ministry of Science, Research, and the Arts for the Collaborative Research Network “Solar Technologies go Hybrid.” M.B. acknowledges the support from the “Studienstiftung des Deutschen Volkes.”

AUTHOR DECLARATIONS

Conflict of Interest

The authors have no conflicts to disclose.

Author Contributions

T.A. wrote the routines for the EEL functional, did all the calculations, prepared first versions of most figures, developed the functional construction, and contributed to the text. T.L., M.B., and R.R. participated in discussions about functional construction. I.S. helped with the numerical implementation. S.K. conceptualized the work, prepared final versions of the figures, and wrote the manuscript. All authors discussed the results and read and discussed the manuscript.

Thilo Aschebrock: Conceptualization (supporting); Formal analysis (lead); Investigation (equal); Methodology (equal); Software (lead); Validation (lead); Visualization (lead); Writing – original draft (supporting); Writing – review & editing (equal). **Timo Lebeda:** Investigation (supporting); Writing – review & editing (supporting). **Moritz Brütting:** Investigation (supporting); Writing – review & editing (supporting). **Rian Richter:** Investigation (supporting); Writing – review & editing (supporting). **Ingo Schelter:** Software (supporting); Supervision (supporting); Writing – review & editing (supporting). **Stephan Kümmel:** Conceptualization (lead); Funding acquisition (lead); Investigation (equal); Project administration (lead); Resources (lead); Supervision (lead); Visualization (supporting); Writing – original draft (lead).

DATA AVAILABILITY

The data that support the findings of this study are available from the corresponding author upon reasonable request.

REFERENCES

- 1 J. P. Perdew and S. Kurth, “Density functionals for non-relativistic Coulomb systems in the new century,” in *A Primer in Density Functional Theory, Lecture Notes in Physics* (Springer Verlag Berlin Heidelberg, New York, 2003), Vol. 620, pp. 1–55.
- 2 K. Burke, “Perspective on density functional theory,” *J. Chem. Phys.* **136**, 150901 (2012).

- ³N. Mardirossian and M. Head-Gordon, "Thirty years of density functional theory in computational chemistry: An overview and extensive assessment of 200 density functionals," *Mol. Phys.* **115**, 2315–2372 (2017).
- ⁴A. M. Teale, T. Helgaker, A. Savin, C. Adamo, B. Aradi, A. V. Arbuznikov, P. W. Ayers, E. J. Baerends, V. Barone, P. Calaminici, E. Cancès, E. A. Carter, P. K. Chattaraj, H. Chermette, I. Ciofini, T. D. Crawford, F. De Proft, J. F. Dobson, C. Draxl, T. Frauenheim, E. Fromager, P. Fuentealba, L. Gagliardi, G. Galli, J. Gao, P. Geerlings, N. Gidopoulos, P. M. W. Gill, P. Gori-Giorgi, A. Görling, T. Gould, S. Grimme, O. Gritsenko, H. J. A. Jensen, E. R. Johnson, R. O. Jones, M. Kaupp, A. M. Köster, L. Kronik, A. I. Krylov, S. Kvaal, A. Laestadius, M. Levy, M. Lewin, S. Liu, P.-F. Loos, N. T. Maitra, F. Neese, J. P. Perdew, K. Pernal, P. Pernot, P. Piecuch, E. Rebolini, L. Reining, P. Romaniello, A. Ruzsinszky, D. R. Salahub, M. Scheffler, P. Schwerdtfeger, V. N. Staroverov, J. Sun, E. Tellgren, D. J. Tozer, S. B. Trickey, C. A. Ullrich, A. Vela, G. Vignale, T. A. Wesolowski, X. Xu, and W. Yang, "DFT exchange: Sharing perspectives on the workhorse of quantum chemistry and materials science," *Phys. Chem. Chem. Phys.* **24**, 28700–28781 (2022).
- ⁵J. P. Perdew, K. Burke, and M. Ernzerhof, "Generalized gradient approximation made simple," *Phys. Rev. Lett.* **77**, 3865–3868 (1996).
- ⁶J. Tao, J. P. Perdew, V. N. Staroverov, and G. E. Scuseria, "Climbing the density functional ladder: Nonempirical meta-generalized gradient approximation designed for molecules and solids," *Phys. Rev. Lett.* **91**, 146401 (2003).
- ⁷J. Sun, A. Ruzsinszky, and J. P. Perdew, "Strongly constrained and appropriately normed semilocal density functional," *Phys. Rev. Lett.* **115**, 036402 (2015).
- ⁸X. Gonze, P. Ghosez, and R. W. Godby, "Density-polarization functional theory of the response of a periodic insulating solid to an electric field," *Phys. Rev. Lett.* **74**, 4035–4038 (1995).
- ⁹R. Resta, "Density-polarization-functional theory and long-range correlation in dielectrics," *Phys. Rev. Lett.* **77**, 2265–2267 (1996).
- ¹⁰R. M. Martin and G. Ortiz, "Comment on 'density-polarization-functional theory and long-range correlation in dielectrics,'" *Phys. Rev. Lett.* **78**, 2028 (1997).
- ¹¹R. M. Martin and G. Ortiz, "Functional theory of extended Coulomb systems," *Phys. Rev. B* **56**, 1124–1140 (1997).
- ¹²X. Gonze, P. Ghosez, and R. W. Godby, "Polarization dependence of the exchange energy," *Phys. Rev. Lett.* **78**, 2029 (1997).
- ¹³X. Gonze, P. Ghosez, and R. W. Godby, "Density-functional theory of polar insulators," *Phys. Rev. Lett.* **78**, 294–297 (1997).
- ¹⁴P. Ghosez, X. Gonze, and R. W. Godby, "Long-wavelength behavior of the exchange-correlation kernel in the Kohn-Sham theory of periodic systems," *Phys. Rev. B* **56**, 12811 (1997).
- ¹⁵R. Resta, "Resta replies," *Phys. Rev. Lett.* **78**, 2030 (1997).
- ¹⁶D. Vanderbilt, "Nonlocality of Kohn-Sham exchange-correlation fields in dielectrics," *Phys. Rev. Lett.* **79**, 3966–3969 (1997).
- ¹⁷G. Ortiz, I. Souza, and R. M. Martin, "Exchange-correlation hole in polarized insulators: Implications for the microscopic functional theory of dielectrics," *Phys. Rev. Lett.* **80**, 353–356 (1998).
- ¹⁸B. Champagne, E. A. Perpète, S. J. A. van Gisbergen, E.-J. Baerends, J. G. Snijders, C. Soubra-Ghaoui, K. A. Robins, and B. Kirtman, "Assessment of conventional density functional schemes for computing the polarizabilities and hyperpolarizabilities of conjugated oligomers: An *ab initio* investigation of polyacetylene chains," *J. Chem. Phys.* **109**, 10489 (1998).
- ¹⁹S. J. A. van Gisbergen, P. R. T. Schipper, O. V. Gritsenko, E. J. Baerends, J. G. Snijders, B. Champagne, and B. Kirtman, "Electric field dependence of the exchange-correlation potential in molecular chains," *Phys. Rev. Lett.* **83**, 694 (1999).
- ²⁰D. Tozer, "Relationship between long-range charge-transfer excitation energy error and integer discontinuity in Kohn-Sham theory," *J. Chem. Phys.* **119**, 12697–12699 (2003).
- ²¹A. Dreuw and M. Head-Gordon, "Failure of time-dependent density functional theory for long-range charge-transfer excited States: The zincbacteriochlorin–bacteriochlorin and bacteriochlorophyll–spheroidene complexes," *J. Am. Chem. Soc.* **126**, 4007 (2004).
- ²²M. Grüning, O. V. Gritsenko, and E. J. Baerends, "Exchange potential from the common energy denominator approximation for the Kohn-Sham Green's function: Application to (hyper)polarizabilities of molecular chains," *J. Chem. Phys.* **116**, 6435 (2002).
- ²³M. van Faassen, P. L. de Boeij, R. van Leeuwen, J. A. Berger, and J. G. Snijders, "Ultranonlocality in time-dependent current-density-functional theory: Application to conjugated polymers," *Phys. Rev. Lett.* **88**, 186401 (2002).
- ²⁴P. Mori-Sánchez, Q. Wu, and W. Yang, "Accurate polymer polarizabilities with exact exchange density-functional theory," *J. Chem. Phys.* **119**, 11001–11004 (2003).
- ²⁵S. Kümmel, "Damped gradient iteration and multigrid relaxation: Tools for electronic structure calculations using orbital density-functionals," *J. Comput. Phys.* **201**, 333–343 (2004).
- ²⁶S. Kümmel, L. Kronik, and J. P. Perdew, "Electrical response of molecular chains from density functional theory," *Phys. Rev. Lett.* **93**, 213002 (2004).
- ²⁷P. Umari, A. J. Williamson, G. Galli, and N. Marzari, "Dielectric response of periodic systems from quantum Monte Carlo calculations," *Phys. Rev. Lett.* **95**, 207602 (2005).
- ²⁸S. Kümmel and L. Kronik, "Hyperpolarizabilities of molecular chains: A real-space approach," *Comput. Mater. Sci.* **35**, 321–326 (2006).
- ²⁹H. Sekino, Y. Maeda, M. Kamiya, and K. Hirao, "Polarizability and second hyperpolarizability evaluation of long molecules by the density functional theory with long-range correction," *J. Chem. Phys.* **126**, 014107 (2007).
- ³⁰N. Maitra and M. van Faassen, "Improved exchange-correlation potential for polarizability and dissociation in density functional theory," *J. Chem. Phys.* **126**, 191106 (2007).
- ³¹R. Armiento, S. Kümmel, and T. Körzdörfer, "Electrical response of molecular chains in density functional theory: Ultranonlocal response from a semilocal functional," *Phys. Rev. B* **77**, 165106 (2008).
- ³²C. D. Pemmaraju, S. Sanvito, and K. Burke, "Polarizability of molecular chains: A self-interaction correction approach," *Phys. Rev. B* **77**, 121204 (2008).
- ³³A. Ruzsinszky, J. P. Perdew, G. I. Csonka, G. E. Scuseria, and O. A. Vydrov, "Understanding and correcting the self-interaction error in the electrical response of hydrogen chains," *Phys. Rev. A* **77**, 060502 (2008).
- ³⁴A. Ruzsinszky, J. P. Perdew, and G. I. Csonka, "Simple charge-transfer model to explain the electrical response of hydrogen chains," *Phys. Rev. A* **78**, 022513 (2008).
- ³⁵T. Körzdörfer, M. Mundt, and S. Kümmel, "Electrical response of molecular systems: The power of self-interaction corrected Kohn-Sham theory," *Phys. Rev. Lett.* **100**, 133004 (2008).
- ³⁶A. Karolewski, R. Armiento, and S. Kümmel, "Polarizabilities of polyacetylene from a field-counteracting semilocal functional," *J. Chem. Theory Comput.* **5**, 712–718 (2009).
- ³⁷B. Champagne and B. Kirtman, "Polarizabilities and second hyperpolarizabilities of hydrogen chains using the spin-component-scaled Møller–Plesset second-order method," *Int. J. Quantum Chem.* **109**, 3103 (2009).
- ³⁸A. Heßelmann, "Polarisabilities of long conjugated chain molecules with density functional response methods: The role of coupled and uncoupled response," *J. Chem. Phys.* **142**, 164102 (2015).
- ³⁹A. Kaiser and S. Kümmel, "Revealing the field-counteracting term in the exact Kohn-Sham correlation potential," *Phys. Rev. A* **98**, 052505 (2018).
- ⁴⁰Y. Mei, N. Yang, and W. Yang, "Describing polymer polarizability with localized orbital scaling correction in density functional theory," *J. Chem. Phys.* **154**, 054302 (2021).
- ⁴¹S. Akter, J. A. Vargas, K. Sharkas, J. E. Peralta, K. A. Jackson, T. Baruah, and R. R. Zope, "How well do self-interaction corrections repair the overestimation of static polarizabilities in density functional calculations?," *Phys. Chem. Chem. Phys.* **23**, 18678–18685 (2021).
- ⁴²M. Hellgren and L. Baguet, "Strengths and limitations of the adiabatic exact-exchange kernel for total energy calculations," *J. Chem. Phys.* **158**, 184107 (2023).
- ⁴³To avoid confusion, one should realize that the term "nonlocal" is also used in other contexts of DFT with other meanings, e.g., in order to denote a non-multiplicative potential, or referring to the temporal dependence in time-dependent DFT.
- ⁴⁴J. B. Krieger, Y. Li, and G. J. Iafrate, "Construction and application of an accurate local spin-polarized Kohn-Sham potential with integer discontinuity: Exchange-only theory," *Phys. Rev. A* **45**, 101–126 (1992).
- ⁴⁵M. Lein and S. Kümmel, "Exact time-dependent exchange-correlation potentials for strong-field electron dynamics," *Phys. Rev. Lett.* **94**, 143003 (2005).

- ⁴⁶C. Legrand, E. Suraud, and P.-G. Reinhard, "Comparison of self-interaction-corrections for metal clusters," *J. Phys. B: At. Mol. Opt. Phys.* **35**, 1115–1128 (2002).
- ⁴⁷J. P. Perdew and A. Zunger, "Self-interaction correction to density-functional approximations for many-electron systems," *Phys. Rev. B* **23**, 5048–5079 (1981).
- ⁴⁸J. Kehrler, R. Richter, J. M. Foerster, I. Schelter, and S. Kümmel, "Self-interaction correction, electrostatic, and structural influences on time-dependent density functional theory excitations of bacteriochlorophylls from the light-harvesting complex 2," *J. Chem. Phys.* **153**, 144114 (2020).
- ⁴⁹T. Aschebrock and S. Kümmel, "Ultranonlocality and accurate band gaps from a meta-generalized gradient approximation," *Phys. Rev. Res.* **1**, 033082 (2019).
- ⁵⁰F. Della Sala, E. Fabiano, and L. A. Constantin, "Kinetic-energy-density dependent semilocal exchange-correlation functionals," *Int. J. Quantum Chem.* **116**, 1641–1694 (2016).
- ⁵¹A. D. Becke, "Simulation of delocalized exchange by local density functionals," *J. Chem. Phys.* **112**, 4020–4026 (2000).
- ⁵²F. G. Eich and M. Hellgren, "Derivative discontinuity and exchange-correlation potential of meta-GGAs in density-functional theory," *J. Chem. Phys.* **141**, 224107 (2014).
- ⁵³R. M. Dreizler and E. K. U. Gross, *Density Functional Theory: An Approach to the Quantum Many-Body Problem* (Springer, Berlin, 1990).
- ⁵⁴T. Lebeda, T. Aschebrock, J. Sun, L. Leppert, and S. Kümmel, "Right band gaps for the right reason at low computational cost with a meta-GGA," *Phys. Rev. Mater.* **7**, 093803 (2023).
- ⁵⁵J. P. Perdew, S. Kurth, A. Zupan, and P. Blaha, *Phys. Rev. Lett.* **82**, 2544 (1999).
- ⁵⁶M. Ernzerhof and G. E. Scuseria, "Kinetic energy density dependent approximations to the exchange energy," *J. Chem. Phys.* **111**, 911–915 (1999).
- ⁵⁷Y. Zhao and D. G. Truhlar, "A new local density functional for main-group thermochemistry, transition metal bonding, thermochemical kinetics, and noncovalent interactions," *J. Chem. Phys.* **125**, 194101 (2006).
- ⁵⁸R. Peverati and D. G. Truhlar, "M11-L: A local density functional that provides improved accuracy for electronic structure calculations in chemistry and physics," *J. Phys. Chem. Lett.* **3**, 117–124 (2012).
- ⁵⁹H. S. Yu, X. He, and D. G. Truhlar, "MN15-L: A new local exchange-correlation functional for Kohn–Sham density functional theory with broad accuracy for atoms, molecules, and solids," *J. Chem. Theory Comput.* **12**, 1280–1293 (2016).
- ⁶⁰P.-F. Loos, "Exchange functionals based on finite uniform electron gases," *J. Chem. Phys.* **146**, 114108 (2017).
- ⁶¹V. U. Nazarov and G. Vignale, "Optics of semiconductors from meta-generalized-gradient-approximation-based time-dependent density-functional theory," *Phys. Rev. Lett.* **107**, 216402 (2011).
- ⁶²P. Borlido, J. Schmidt, A. Huran, F. Tran, M. Marques, and S. Botti, "Exchange-correlation functionals for band gaps of solids: Benchmark, reparametrization and machine learning," *npj Comput. Mater.* **6**, 96 (2020).
- ⁶³A. D. Boese and N. C. Handy, "New exchange-correlation density functionals: The role of the kinetic-energy density," *J. Chem. Phys.* **116**, 9559–9569 (2002).
- ⁶⁴J. M. del Campo, J. L. Gázquez, S. Trickey, and A. Vela, "A new meta-GGA exchange functional based on an improved constraint-based gga," *Chem. Phys. Lett.* **543**, 179–183 (2012).
- ⁶⁵J. Tao and Y. Mo, "Accurate semilocal density functional for condensed-matter physics and quantum chemistry," *Phys. Rev. Lett.* **117**, 073001 (2016).
- ⁶⁶L. A. Constantin, E. Fabiano, J. M. Pitarke, and F. Della Sala, "Semilocal density functional theory with correct surface asymptotics," *Phys. Rev. B* **93**, 115127 (2016).
- ⁶⁷L. A. Constantin, E. Fabiano, and F. Della Sala, "Meta-GGA exchange-correlation functional with a balanced treatment of nonlocality," *J. Chem. Theory Comput.* **9**, 2256–2263 (2013).
- ⁶⁸J. P. Perdew, A. Ruzsinszky, G. I. Csonka, L. A. Constantin, and J. Sun, "Workhorse semilocal density functional for condensed matter physics and quantum chemistry," *Phys. Rev. Lett.* **103**, 026403 (2009).
- ⁶⁹J. P. Perdew, R. G. Parr, M. Levy, and J. L. Balduz, Jr., "Density-functional theory for fractional particle number: Derivative discontinuities of the energy," *Phys. Rev. Lett.* **49**, 1691–1694 (1982).
- ⁷⁰Y. Wang, X. Jin, H. S. Yu, D. G. Truhlar, and X. He, "Revised M06-L functional for improved accuracy on chemical reaction barrier heights, noncovalent interactions, and solid-state physics," *Proc. Natl. Acad. Sci. U. S. A.* **114**, 8487–8492 (2017).
- ⁷¹Z. Yang, H. Peng, J. Sun, and J. P. Perdew, "More realistic band gaps from meta-generalized gradient approximations: Only in a generalized Kohn–Sham scheme," *Phys. Rev. B* **93**, 205205 (2016).
- ⁷²J. P. Perdew, W. Yang, K. Burke, Z. Yang, E. K. U. Gross, M. Scheffler, G. E. Scuseria, T. M. Henderson, I. Y. Zhang, A. Ruzsinszky, H. Peng, J. Sun, E. Trushin, and A. Görling, "Understanding band gaps of solids in generalized Kohn–Sham theory," *Proc. Natl. Acad. Sci. U. S. A.* **114**, 2801–2806 (2017).
- ⁷³W. Yang, A. J. Cohen, and P. Mori-Sanchez, "Derivative discontinuity, bandgap and lowest unoccupied molecular orbital in density functional theory," *J. Chem. Phys.* **136**, 204111 (2012).
- ⁷⁴T. Van Voorhis and G. E. Scuseria, "A novel form for the exchange-correlation energy functional," *J. Chem. Phys.* **109**, 400–410 (1998).
- ⁷⁵J. Sun, B. Xiao, and A. Ruzsinszky, "Communication: Effect of the orbital-overlap dependence in the meta generalized gradient approximation," *J. Chem. Phys.* **137**, 051101 (2012).
- ⁷⁶J. Sun, R. Haunschild, B. Xiao, I. W. Bulik, G. E. Scuseria, and J. P. Perdew, "Semilocal and hybrid meta-generalized gradient approximations based on the understanding of the kinetic-energy-density dependence," *J. Chem. Phys.* **138**, 044113 (2013).
- ⁷⁷J. Sun, J. P. Perdew, and A. Ruzsinszky, "Semilocal density functional obeying a strongly tightened bound for exchange," *Proc. Natl. Acad. Sci. U. S. A.* **112**, 685–689 (2015).
- ⁷⁸J. Wellendorff, K. T. Lundgaard, K. W. Jacobsen, and T. Bligaard, "mBEEF: An accurate semi-local Bayesian error estimation density functional," *J. Chem. Phys.* **140**, 144107 (2014).
- ⁷⁹S. Lehtola and M. A. Marques, "Many recent density functionals are numerically ill-behaved," *J. Chem. Phys.* **157**, 174114 (2022).
- ⁸⁰R. Grotjahn, F. Furche, and M. Kaupp, "Importance of imposing gauge invariance in time-dependent density functional theory calculations with meta-generalized gradient approximations," *J. Chem. Phys.* **157**, 111102 (2022).
- ⁸¹R. Richter, T. Aschebrock, I. Schelter, and S. Kümmel, "Meta-generalized gradient approximations in time dependent generalized Kohn–Sham theory: Importance of the current density correction," *J. Chem. Phys.* **159**, 124117 (2023).
- ⁸²We note that the B97M-V functional,⁹⁹ in which exchange and correlation have been designed together and which, therefore, falls out of our present discussion that focuses on exchange only, also shows a continuous non-positive slope of appreciable magnitude.
- ⁸³J. P. Perdew, A. Ruzsinszky, J. Sun, and K. Burke, "Gedanken densities and exact constraints in density functional theory," *J. Chem. Phys.* **140**, 18A533 (2014).
- ⁸⁴M. Levy, "Density-functional exchange correlation through coordinate scaling in adiabatic connection and correlation hole," *Phys. Rev. A* **43**, 4637–4646 (1991).
- ⁸⁵L. Pollack and J. P. Perdew, "Evaluating density functional performance for the quasi-two-dimensional electron gas," *J. Phys.: Condens. Matter* **12**, 1239–1252 (2000).
- ⁸⁶J. P. Perdew, J. Tao, V. N. Staroverov, and G. E. Scuseria, "Meta-generalized gradient approximation: Explanation of a realistic nonempirical density functional," *J. Chem. Phys.* **120**, 6898 (2004).
- ⁸⁷The equivalence of t and $\frac{5}{3}s^2$ for any single-orbital system does not only hold for the energy but also for the Kohn–Sham potential, as the corresponding Kohn–Sham potential of the meta-GGA reduces to the GGA potential associated with the energy functional one obtains by replacing t with $\frac{5}{3}s^2$. In the generalized Kohn–Sham scheme, the equivalence is only guaranteed for the occupied orbitals.
- ⁸⁸We checked that the results of Sec. IV are not very sensitive to the precise value of α_0 as long as the two conditions are met; for example, almost identical results are obtained with $\alpha_0 = 2$.
- ⁸⁹T. Lebeda, T. Aschebrock, and S. Kümmel, "First steps towards achieving both ultranonlocality and a reliable description of electronic binding in a meta-generalized gradient approximation," *Phys. Rev. Res.* **4**, 023061 (2022).

- ⁹⁰R. Pederson and K. Burke, “The difference between molecules and materials: Reassessing the role of exact conditions in density functional theory,” [arXiv:2303.01766](#) (2023).
- ⁹¹A. Zupan, K. Burke, M. Ernzerhof, and J. P. Perdew, “Distributions and averages of electron density parameters: Explaining the effects of gradient corrections,” *J. Chem. Phys.* **106**, 10184–10193 (1997).
- ⁹²J. P. Perdew, M. Ernzerhof, A. Zupan, and K. Burke, “Nonlocality of the density functional for exchange and correlation: Physical origins and chemical consequences,” *J. Chem. Phys.* **108**, 1522–1531 (1998).
- ⁹³P. Kovács, F. Tran, P. Blaha, and G. K. H. Madsen, “Comparative study of the PBE and SCAN functionals: The particular case of alkali metals,” *J. Chem. Phys.* **150**, 164119 (2019).
- ⁹⁴S. Dick and M. Fernandez-Serra, “Highly accurate and constrained density functional obtained with differentiable programming,” *Phys. Rev. B* **104**, L161109 (2021).
- ⁹⁵C. M. Horowitz, C. R. Proetto, and J. M. Pitarke, “Towards a universal exchange enhancement factor in density functional theory,” *Phys. Rev. B* **107**, 195120 (2023).
- ⁹⁶C. M. Horowitz, C. R. Proetto, and J. M. Pitarke, “Construction of a semilocal exchange density functional from a three-dimensional electron gas collapsing to two dimensions,” *Phys. Rev. B* **108**, 115119 (2023).
- ⁹⁷S. Jana, L. A. Constantin, and P. Samal, “Density functional applications of jellium with a local gap model correlation energy functional,” *J. Chem. Phys.* **159**, 114109 (2023).
- ⁹⁸P. Mori-Sánchez, A. J. Cohen, and W. Yang, “Many-electron self-interaction error in approximate density functionals,” *J. Chem. Phys.* **125**, 201102 (2006).
- ⁹⁹N. Mardirossian and M. Head-Gordon, “Mapping the genome of meta-generalized gradient approximation density functionals: The search for B97M-V,” *J. Chem. Phys.* **142**, 074111 (2015).

Publication 3

First steps towards achieving both ultranonlocality and a reliable description of electronic binding in a meta-generalized gradient approximation

Physical Review Research 4, 023061 (2022)

Timo Lebeda, Thilo Aschebrock, and Stephan Kümmel

Theoretical Physics IV, University of Bayreuth, 95440 Bayreuth, Germany




Publ. 3

Author contributions

All authors together conceptualized the research. T.L. performed the investigation and formal analysis. T.L. implemented the CC correlation in DARSEC and ADF with help from T.A.. T.L. developed and implemented the variants of the CC correlation, as well as the required routines for the setup and analysis of the test sets. All authors together discussed the results. T.L. wrote the first draft of the manuscript together with S.K. and all authors contributed to the review and editing.

Publ.3

First steps towards achieving both ultranlocality and a reliable description of electronic binding in a meta-generalized gradient approximation

Timo Lebeda , Thilo Aschebrock , and Stephan Kümmel *

Theoretical Physics IV, University of Bayreuth, 95440 Bayreuth, Germany



(Received 27 January 2022; accepted 24 March 2022; published 21 April 2022)

It has been demonstrated that a meta-generalized gradient approximation (meta-GGA) to the exchange-correlation energy of density functional theory can show a pronounced derivative discontinuity and significant ultranlocality similar to exact exchange, and can accurately predict the band gaps of many solids. We here investigate whether within the meta-GGA form these properties are compatible with a reasonable accuracy for electronic binding energies. With the help of two transparent and inexpensive correlation functional constructions we demonstrate that this is the case. We report atomization energies, show that reliable bond lengths are obtained for many systems, and find promising results for reaction barrier heights, while keeping the strong derivative discontinuity and ultranlocality, and thus accuracy for band gaps.

DOI: [10.1103/PhysRevResearch.4.023061](https://doi.org/10.1103/PhysRevResearch.4.023061)

I. INTRODUCTION

Density functional theory (DFT) is one of the most widely used many-body theories, with successes in many branches of electronic structure theory [1]. DFT comes in the mathematical structure of a single-particle theory, yet incorporates many-particle effects via the exchange-correlation (xc) energy functional E_{xc} . This allows the practitioner who is interested in electronic structure problems to choose the level of accuracy and computational cost by choosing a certain class of xc approximation. The local density approximation [2,3] (LDA) and generalized gradient approximation [4,5] (GGA) functionals are computationally efficient. Higher accuracy can typically be reached with hybrid functionals [6], where recent years have seen a lot of activity in the development of advanced forms such as local hybrid functionals [7–10], range-separated hybrid functionals [11–20], and local range-separated hybrid functionals [21–23]. Further advanced xc approximations can reach a level at which DFT rivals wavefunction-based methods in accuracy [24].

However, much of the success of DFT in applied electronic structure theory rests on its computational efficiency, and a certain dilemma has thus been limiting DFT applications for a long time: The computationally efficient LDA and GGA forms suffer from systematic shortcomings, many of which can be traced back to the very features which make these forms efficient. The sole dependence of their energy density on the electron density $n(\mathbf{r})$ and its gradient $\nabla n(\mathbf{r})$ leads to expressions for the energy and the xc potential that can efficiently be numerically evaluated, but also pre-

vents that important features of the exact xc functional are reflected in these functionals. Especially the lack of a derivative discontinuity in E_{xc} , which leads to a particle-number discontinuity in the corresponding Kohn-Sham xc potential $v_{xc}(\mathbf{r})$, has seriously detrimental consequences in many applications, e.g., the prediction of band gaps [25] and response properties [26–28]. The derivative discontinuity and the corresponding (ultra-)nonlocality can be incorporated into E_{xc} , e.g., by including exact exchange [29–31] or via self-interaction corrections [32–34]. This, however, increases the computational cost sharply compared to a plain GGA calculation. Model potentials [35–37] and especially tailored GGAs can provide some improvement [38,39], but come with their own set of problems and serious limitations [40–44].

The functional class of the meta-GGAs [45] seems ideally suited to resolve the dilemma between the need for semilocal computational efficiency on the one hand, and the need to capture (ultra-)nonlocality-physic on the other hand. Depending only on the density, its gradient, and the gradient of the orbitals, makes meta-GGAs semilocal in terms of the computational cost. However, as the orbitals are nonlocal functionals of the density, meta-GGAs, in principle, depend nonlocally on the density as well [31]. Unfortunately though, the experience in practice for a long time had been that typical meta-GGAs can improve over GGAs in the accuracy of, e.g., atomization energies [46–50], yet offer little nonlocality [51].

With the recent construction of the meta-GGA by T. Aschebrock, S. Kümmel (TASK) for exchange [52] it has been demonstrated that a meta-GGA can have a pronounced derivative discontinuity and can reproduce many of the (ultra-)nonlocal features that previously could only be reached with exact exchange. This demonstrated that (ultra-)nonlocality is not just, in principle, a feature that meta-GGAs can have, but also in practice. However, the TASK meta-GGA for exchange has so far been combined with plain LDA correlation [52] (LDAc) [53]. This was a preliminary step, taken for the simple reason that LDAc is universal and thus better suited for combining it with a new exchange functional than

*stephan.kuettel@uni-bayreuth.de; <http://tp4.uni-bayreuth.de/en>

Published by the American Physical Society under the terms of the [Creative Commons Attribution 4.0 International license](https://creativecommons.org/licenses/by/4.0/). Further distribution of this work must maintain attribution to the author(s) and the published article's title, journal citation, and DOI.

a correlation functional that has been tailored towards some other specific exchange functional. While the combination of TASK exchange with LDAc yields excellent results for the fundamental band gap of many materials in the generalized Kohn-Sham evaluation [39,52], and promising results for response properties [52,54], the atomization energies are of limited accuracy [52]. Thus, one may speculate whether the meta-GGA form is too limited to yield accurate binding energy physics and pronounced nonlocality at the same time, e.g., whether one and the same meta-GGA can yield both good atomization energies and band gaps.

In this article we take a step towards answering this question. Our focus here is not (yet) on the development of the best possible meta-GGA correlation functional to go with the TASK exchange functional, but on exploring whether having a pronounced derivative discontinuity and having good atomization energies are necessarily mutually exclusive within the meta-GGA functional form. To this end we focus on very transparent forms for a semilocal correlation functional that ensure that the excellent band gaps that are found with TASK exchange and LDAc remain intact, while atomization energies are improved. We specifically discuss the role of one-electron self-interaction, and we also report bond lengths, atomization energies, and reaction barrier heights for TASK exchange in combination with different correlation functionals. We find that it is possible to construct a functional that yields the same accurate band gaps as the combination of TASK and LDAc, while at the same time yielding greatly improved atomization energies.

II. TASK EXCHANGE WITH ISO-ORBITAL CORRECTED LDA CORRELATION

Following usual practice we write the correlation energy in terms of the electron density $n(\mathbf{r})$ and the correlation energy density per particle ε_c ,

$$E_c[n_\uparrow, n_\downarrow] = \int n(\mathbf{r})\varepsilon_c(\mathbf{r})d^3\mathbf{r}. \quad (1)$$

As explained above our aim is to check whether one can find a transparent correlation functional that yields reasonable atomization energies when combined with the TASK exchange functional, without ruining the good features of TASK exchange that result from its pronounced nonlocality. Our first step is to correct for one-electron self-correlation. This is close-lying and natural because first, TASK exchange was designed with a focus on reducing one-electron errors (by ensuring the correct energy for the hydrogen atom), second, TASK exchange mimics exact exchange, which is one-electron self-interaction free, and third, one-electron self-correlation can readily be eliminated within the meta-GGA form by using iso-orbital indicators [55]. One such indicator is

$$z(\mathbf{r}) = \frac{\tau_W(\mathbf{r})}{\tau(\mathbf{r})}, \quad (2)$$

where

$$\tau(\mathbf{r}) = \frac{\hbar^2}{2m} \sum_{\sigma=\uparrow,\downarrow} \sum_{i=1}^{N_\sigma} |\nabla\varphi_{i\sigma}(\mathbf{r})|^2 \quad (3)$$

is the noninteracting kinetic energy density that is obtained from the Kohn-Sham or generalized Kohn-Sham spin orbitals $\varphi_{i\sigma}(\mathbf{r})$, respectively, and

$$\tau_W(\mathbf{r}) = \frac{\hbar^2}{8m} \frac{|\nabla n(\mathbf{r})|^2}{8n(\mathbf{r})} \quad (4)$$

is the von Weizsäcker kinetic energy density. The latter is the single-orbital limit of τ , thus, z approaches one in regions of spatially identical orbitals. By multiplying z with the square of the spin polarization

$$\zeta(\mathbf{r}) = \frac{n_\uparrow(\mathbf{r}) - n_\downarrow(\mathbf{r})}{n_\uparrow(\mathbf{r}) + n_\downarrow(\mathbf{r})}, \quad (5)$$

one obtains the one-spin-orbital region indicator $z\zeta^2$. This can be used to define a transparent form of an LDA-based self-interaction corrected correlation (CC) functional [10] via

$$\varepsilon^{\text{CC}}(\mathbf{r}) = (1 - z(\mathbf{r})\zeta^2(\mathbf{r}))\varepsilon^{\text{LDAc}}(\mathbf{r}), \quad (6)$$

where $\varepsilon^{\text{LDAc}}$ is the correlation energy density of LDA, including its spin dependence, which we, however, do not denote explicitly for ease of notation. In our calculations we use the LDA in the parametrization of Perdew and Wang [3].

The CC correlation is a very transparent functional that does not contain any empirical parameter. Combining it with TASK exchange, denoted by TASK+CC in the following, leads to a nonempirical meta-GGA that fulfills many exact constraints. TASK exchange satisfies all exact constraints for exchange that SCAN exchange does [52,56]. Since τ_W and hence z vanish for a uniform density, the CC correlation equals the LDA correlation in the uniform-density limit and for spin-unpolarized densities. On the other hand, the CC correlation vanishes for any fully spin-polarized one-electron density because $(1 - z\zeta^2)$ vanishes in this case, resulting in no one-electron self-interaction error. Thus, TASK+CC is exact for the ground-state energy of the hydrogen atom. The same would hold for $(1 - z|\zeta|^k)$ with $k > 0$, but in our experience $k = 2$ is optimal. Both the LDA correlation energy and the CC correlation energy are nonpositive and vanish under uniform density scaling to the low-density limit, i.e., go to the correct limiting value. The combined functionals TASK+LDAc and TASK+CC are size extensive and satisfy the general Lieb-Oxford bound ($F_{xc} \leq 2.215$) [57] as tightened by Chan and Handy [58], where F_{xc} , the enhancement over local exchange, is defined by $E_{xc} = \int n\varepsilon_x^{\text{LDA}}F_{xc}d^3r$. Finally, TASK+LDAc and TASK+CC are smooth at fixed electron number, which is beneficial for numerical computations and has recently been suggested as an exact constraint that a meta-GGA can satisfy [59].

By construction, the CC correlation equals the LDA correlation in the uniform-density limit and for spin-unpolarized systems. Therefore, the sizable derivative discontinuity is guaranteed to be preserved for spin-unpolarized systems and it is guaranteed that TASK+CC yields the same good results as TASK+LDAc for the band gaps that were studied in Ref. [52].

For a first impression of the performance of TASK+CC in predicting atomization energies we use a test set of 10 diatomic molecules [63]. For those, very accurate Kohn-Sham all-electron calculations can be done on a real-space prolate spheroidal grid with the all-electron code DARSEC [64].

TABLE I. Atomization energies of diatomic molecules in kcal/ mol. The values for the established nonempirical functionals LDA [3], Perdew-Burke-Ernzerhof (PBE) [5], and the Strongly Constrained and Appropriately Normed meta-GGA (SCAN) [56] are listed for comparison. TASK+LDAc, TASK+CC, and TASK+CCaLDA are TASK exchange with PW92-LDA correlation, CC correlation, and the functional that combines CC and LDA correlation in the form of Eq. (9) (CCaLDA), respectively. The CCaLDA correlation is introduced in Sec. III. The experimental values (with zero point vibration removed) and the experimental bond lengths were taken from Ref. [60] (cf. the Supplemental Material [61] of Ref. [22] for numerical details and comments about numerical stability [52,62]).

Molec.	LDA	PBE	SCAN	TASK +LDAc	TASK +CC	TASK +CCaLDA	Expt.
H ₂	112.9	104.6	107.7	117.0	144.8	117.0	109.5
FH	162.0	142.0	138.7	139.2	158.5	144.6	141.1
LiH	60.8	53.5	55.6	58.9	79.4	64.0	58.0
Li ₂	23.8	19.9	18.1	11.6	24.8	21.8	24.7
LiF	156.3	139.0	138.1	130.2	142.2	140.7	138.3
F ₂	78.0	52.8	37.4	23.4	34.2	34.2	38.4
CO	299.2	269.1	255.2	234.6	265.9	265.9	259.5
N ₂	268.0	243.9	220.9	174.9	227.4	227.4	228.3
NO	199.4	170.9	146.5	109.3	147.3	147.3	152.5
O ₂	175.1	144.1	127.0	103.8	124.7	124.7	120.5
MSE	26.5	6.9	-2.6	-16.8	7.8	1.7	
MAE	26.7	9.7	3.9	18.5	9.9	4.3	
RMSE	32.7	12.3	4.6	24.8	14.6	4.7	

Table I compares TASK+CC with LDA, the GGA PBE [5], the meta-GGA SCAN [56], and TASK+LDAc [65]. We used the Krieger-Li-Iafrate (KLI) approximation [29] for the Kohn-Sham calculations with orbital dependent functionals, and information about numerical details, e.g., the advantages of writing the functional derivative in terms of \sqrt{n} instead of n , is given in the Supplemental Material [61]. At the bottom of the table the usual statistical measures summarize the performance of each functional, i. e., the mean absolute error (MAE), the mean signed error (MSE), and the root mean square error (RMSE), cf. the Supplemental Material [61]. The comparison shows that TASK+CC is still significantly less accurate than SCAN, but the CC correlation reduces the MAE by more than a factor of two compared to TASK+LDAc. TASK+CC is thus on a similar level of accuracy as the PBE functional for this test set. This first test therefore already demonstrates that a suitable correlation functional can signif-

icantly improve atomization energies while maintaining the pronounced ultranonicity of the TASK exchange.

A closer look at the data reveals that the error is mostly due to a systematic overestimation of the atomization energy of hydrogen-containing molecules. For molecules that do not contain hydrogen, the MAE is reduced by a further factor of two. Therefore, in the next section we explore how much can be gained by focusing on hydrogen in a specific construction called CCaLDA correlation. However, before doing so we study the main group atomization energies (MGAE109) [66] as a large benchmark test set for atomization energies. Table II summarizes the statistical measures for MGAE109. Similar to what we have already seen for the diatomic test set, TASK+CC improves significantly over TASK+LDAc. For detailed data we refer to Table S.II in the Supplemental Material [61]. These show that the performance is systematically different for different classes of molecules. TASK+CC is systematically overbinding all hydrocarbons by about 5 kcal/ mol. For inorganic molecules the situation is different and less systematic. While TASK+CC tends to underbind most of the inorganic molecules that contain elements from the second main group, it overbinds many molecules that contain heavier elements. However, TASK+CC is systematically overbinding all molecules which contain hydrogen. Therefore, one again observes that hydrogen containing systems play a special role for TASK+CC, and we thus take a closer look at them in the following. We mention in passing that in the Supplemental Material [61] we also show results for TASK exchange alone and in combination with SCAN correlation.

III. HEURISTIC FURTHER IMPROVEMENT OF ATOMIZATION ENERGIES

The systematic overestimation of the atomization energies of hydrogen-containing molecules that we observed in the previous section can be improved by changing the isoorbital limit. In the following we show that one can reduce the MAE of TASK+CC by nearly another factor of two by modifying solely this limit. To this end, we interpolate between the CC correlation and LDA correlation by a function of the isoorbital indicator α [69], which is defined by

$$\alpha(\mathbf{r}) = \frac{\tau(\mathbf{r}) - \tau_W(\mathbf{r})}{\tau_F(\mathbf{r})}, \quad (7)$$

where

$$\tau_F(\mathbf{r}) = \frac{3\hbar^2}{10m} (3\pi^2)^{\frac{2}{3}} n(\mathbf{r})^{\frac{5}{3}} \quad (8)$$

TABLE II. MGAE109 [66] main-group atomization energies per bond in kcal/ mol. The calculations were performed with the QZ4P-basis set in the Amsterdam Density Functional (ADF) program of the Amsterdam Modeling Suite (AMS) [67] using the generalized Kohn-Sham scheme.

	LDA	PBE	SCAN	TASK +LDAc	TASK +CC	TASK +CCaLDA [68]
MSE	19.5	3.8	-0.1	-12.1	6.1	-1.4
MAE	19.5	4.2	1.4	12.3	7.3	4.2
RMSE	21.7	6.0	2.2	14.4	9.2	5.2

TABLE III. MGBL20 [71] main-group bond lengths in Å. The calculations were performed with the QZ4P-basis set in AMS/ADF [67].

	LDA	PBE	SCAN	TASKx	TASK +LDAc	TASK +SCANc	TASK +CC
MGHBL9 [72] (Main-group hydrogenic bond lengths)							
MSE	0.015	0.011	0.002	0.016	0.001	0.009	0.001
MAE	0.015	0.011	0.002	0.016	0.005	0.009	0.005
RMSE	0.015	0.011	0.003	0.018	0.007	0.011	0.007
MGNHBL11 [71] (Main-group Non-hydrogenic bond lengths)							
MSE	-0.006	0.007	-0.005	0.024	0.006	0.006	0.006
MAE	0.007	0.007	0.006	0.024	0.006	0.009	0.006
RMSE	0.010	0.008	0.007	0.030	0.011	0.012	0.011

is the uniform-density limit of τ . The correlation energy density of the CCaLDA functional reads

$$\varepsilon^{\text{CCaLDA}}(\mathbf{r}) = f(\alpha(\mathbf{r}))\varepsilon^{\text{CC}}(\mathbf{r}) + [1 - f(\alpha(\mathbf{r}))]\varepsilon^{\text{LDAc}}(\mathbf{r}), \quad (9)$$

where we use the function

$$f(\alpha(\mathbf{r})) = (1 + c) \frac{\alpha(\mathbf{r})}{1 + c\alpha(\mathbf{r})} \quad (10)$$

to switch between LDA and CC correlation. The form of $f(\alpha)$ and the parameter $c = 10000$ are chosen such that only the isorbital limit ($\alpha \approx 0$) of ε^{CC} is modified. The changes in the atomization energies that result from the CCaLDA construction can be studied in Table I for the dimer test set. As intended, the atomization energies of TASK+CCaLDA match those of TASK+CC for molecules containing neither hydrogen nor lithium, while the energy of H_2 matches that of TASK+LDAc. Only the energies of the hydrogen atom and the lithium atom are changed compared to TASK+CC, where the latter effect is due to the singly occupied 2s orbital in the lithium atom, which induces a relatively large iso-orbital region. As one can see in Table II, TASK+CCaLDA also significantly improves the prediction of the atomization energies for the large MGAE109 test set and is on par with PBE. Taking into account that the TASK exchange is designed for a qualitatively correct description of ultranonlocality and the derivative discontinuity, this is an encouraging observation. It is noteworthy also from the perspective that the CCaLDA functional does not use any empirical parameters, as c has not been fitted to minimize the deviation from experimental data, but was chosen to provide the desired single-orbital limit.

Detailed data for the MGAE109 test can be found in Table S.II in the Supplemental Material [61].

For putting these results into a larger perspective we note that the LDA correlation is far from being the optimal choice for a correlation functional in the iso-orbital limit: Neither is it free from self-interaction, nor is it the best choice for optimizing the atomization energies of TASK for hydrogen-containing molecules. We are therefore convinced that the MAE could be further improved by a more sophisticated choice for the iso-orbital limit. However, we do not pursue a functional construction of the TASK+CCaLDA type any further because of a conceptual shortcoming: Compared to TASK+CC, TASK+CCaLDA gains its increased accuracy for the atomization energies of hydrogen containing systems by making a correction to the energy of the hydrogen atom, which is exact in TASK+CC, instead of the energy of the hydrogen-containing molecules, which would need the correction. The results for TASK+CCaLDA can therefore be seen in the light of Ref. [70], which discusses the limits of judging the quality of an exchange-correlation approximation based on the errors in atomization energies. Nevertheless, the TASK+CCaLDA construction has the value that it demonstrates that atomization energies at least on the level of PBE, and at the same time band gaps on the level of TASK+LDAc, are possible with a meta-GGA. Further efforts for a meta-GGA correlation functional to go along with TASK exchange will therefore be well invested. In such efforts, one will need to pay attention to the form of the orbital dependence of the correlation functional, since this dependence will in general also lead to a correlation contribution to the derivative discontinuity.

TABLE IV. DGH4 [73] bond lengths of diatomic molecules containing heavy elements, in Å. The calculations were performed with the QZ4P-basis set in AMS/ADF [67]. Relativistic effects were included in the ZORA [74] approximation (required for Ag).

Molecule	LDA	PBE	SCAN	TASKx	TASK + LDAc	TASK + SCANc	TASK + CC	Expt.
NaBr	2.471	2.518	2.503	2.678	2.638	2.623	2.638	2.502
HBr	1.430	1.431	1.417	1.432	1.413	1.420	1.413	1.414
ZnS	2.007	2.046	2.017	2.053	2.026	2.006	2.026	2.046
Ag ₂	2.485	2.571	2.520	2.605	2.564	2.519	2.564	2.530
MSE	-0.025	0.019	-0.008	0.069	0.037	0.019	0.037	
MAE	0.032	0.019	0.011	0.069	0.047	0.045	0.047	
RMSE	0.034	0.024	0.015	0.096	0.071	0.064	0.071	

TABLE V. DBH24/08 [78] barrier heights in kcal/mol. The calculations were performed with the QZ4P-basis set in AMS/ADF [67].

	LDA	PBE	SCAN	TASKx	TASK +LDAc	TASK +SCANc	TASK +CC
MSE	-13.7	-8.5	-7.2	5.8	4.1	-0.6	2.6
MAE	13.7	8.5	7.3	7.5	5.0	3.1	4.5
RMSE	17.1	10.4	8.3	9.0	6.3	4.0	6.5

IV. BOND LENGTHS AND BARRIER HEIGHTS

In the remaining part of this paper we return to investigating TASK+CC, as this functional is better justified than CCaLDA from a conceptual point of view, and also test TASK+LDAc for further observables, namely bond lengths and reaction barriers. As the functionals TASK+LDAc, TASK+CC, and TASK+CCaLDA are equivalent for spin-unpolarized systems, the bond-length tests done for TASK+LDAc also tell us the bond lengths that one obtains with the other two functionals for spin-unpolarized systems.

We show results for the bond lengths of molecules consisting of main-group atoms (MGBL20) in Table III (details are listed in Table S.III in the Supplemental Material [61]) and for bond lengths of diatomic molecules which contain heavy elements (DGH4) in Table IV. TASK+LDAc has an MAE of about 0.005 Å for the MGBL20 set of main-group bond lengths, i.e., an accuracy on the level of PBE and SCAN. For the DGH4 set which contains heavy elements, TASK+LDAc performs significantly worse. However, the error is at the level of PBE and SCAN except for the NaBr molecule. The bond length of the latter is overestimated by more than 0.1 Å. Table S.I in the Supplemental Material [61] shows that this is a general feature of TASK for systems which contain alkali metals [75]. We have analyzed the interplay of s and α in these systems and found that systems with alkali metal atoms are special because both α and s become rather large in the core-valence separation region. This finding is to some extent in line with earlier, GGA-based observations about the special role of s in alkali-metal atom containing solids [76], and systematic deviations for solids with alkali metal atoms have also been observed with the Haas, Tran, Blaha, Schwarz (HTBS) GGA [77]. The bond length analysis thus revealed an issue that will need to be addressed in future work.

Table V shows results for a test set of diverse barrier heights (DBH24). For detailed data we refer to Table S.IV in the Supplemental Material [61]. The main observation is that TASK in combination with each of the correlation functionals reaches a remarkable accuracy in comparison to LDA, PBE, and SCAN. This observation is interesting also from the perspective that it has been argued that for a good description of barrier heights, true exchange nonlocality is beneficial [56,79]. From this point of view the good results that we find here can be interpreted as a natural consequence of the ultranlocality that has been one of the main guiding principles in the construction of the TASK functional.

V. SUMMARY AND CONCLUSIONS

Traditionally, there has been a dividing gap in the world of density functional exchange-correlation approximations. They were either computationally efficient like the (semi)local LDA and GGAs, but lacked a derivative discontinuity and ultranlocality. Or they could show ultranlocality, like the self-interaction corrections [34] and various forms of hybrid functionals [18], yet at the price of a steeply increased computational cost. It has long been known that meta-GGAs, in principle, can build a bridge over this gap, because being orbital dependent they can incorporate ultranlocality, while using the density, the orbitals and their gradients only locally, their computational cost remains semilocal [31]. The TASK meta-GGA for exchange is a functional that, different from many previous meta-GGAs, shows pronounced ultranlocality. Previous work that combined it with LDA correlation demonstrated very good accuracy for the band gaps of many solids, but a limited accuracy for the atomization energies of molecules. This raised the question whether it is at all possible to achieve both, good binding energies on the one hand, and pronounced ultranlocality and accurate band gaps on the other, within the meta-GGA form. It also was an open question what kind of results would be achieved with the TASK construction for other observables such as bond lengths and reaction barrier heights. These questions were addressed in this work.

We showed that TASK exchange with LDA correlation is accurate for many bond lengths, and we identified alkali metals as difficult cases that will need further work. TASK exchange in combination with different correlation functionals is accurate for reaction barrier heights. One can interpret this as a natural consequence of the exact-exchange-like nonlocality that is guaranteed by the construction principles that were used for the TASK exchange.

We further showed that two correlation functionals of very transparent form and without empirical parameters lead to a considerably improved accuracy for atomization energies. Furthermore, TASK exchange with CC correlation is attractive from a computational perspective because the calculations converge well, in contrast to some other meta-GGAs. It is not as accurate for atomization energies as other functionals, e.g., the SCAN meta-GGA, yet its remarkable accuracy for band gaps in combination with the reasonable description of electronic binding makes it ideal for material science problems, e.g., when one wants to screen the band gap of many compounds from first principles, and thus needs computational efficiency together with qualitative nonempirical reliability. The present paper presents an important step forward by demonstrating that pronounced ultranlocality and reasonable electronic binding are not mutually exclusive and can well be achieved within the meta-GGA form. Therefore, there is hope that further improved meta-GGAs with pronounced ultranlocality can be developed in future work.

ACKNOWLEDGMENTS

We acknowledge discussions with F. Tran about the bond lengths obtained with TASK+LDAc. We appreciate financial support from the Deutsche Forschungsgemeinschaft

(KU 1410/4-1), we are grateful for support from the Elite Study Program Biological Physics of the Elite Network of Bavaria, and we appreciate support from the Bavarian Polymer Institute in terms of computing resources. The

Open Access publication has partially been funded by the Deutsche Forschungsgemeinschaft (DFG, German Research Foundation) - 491183248, and the Open Access Publishing Fund of the University of Bayreuth.

- [1] K. Burke, Perspective on density functional theory, *J. Chem. Phys.* **136**, 150901 (2012).
- [2] S. H. Vosko, L. Wilk, and M. Nusair, Accurate spin-dependent electron liquid correlation energies for local spin density calculations: A critical analysis, *Can. J. Phys.* **58**, 1200 (1980).
- [3] J. P. Perdew and Y. Wang, Accurate and simple analytic representation of the electron-gas correlation energy, *Phys. Rev. B* **45**, 13244 (1992).
- [4] A. D. Becke, Density functional calculations of molecular bond energies, *J. Chem. Phys.* **84**, 4524 (1986).
- [5] J. P. Perdew, K. Burke, and M. Ernzerhof, Generalized Gradient Approximation Made Simple, *Phys. Rev. Lett.* **77**, 3865 (1996).
- [6] A. D. Becke, Density-functional thermochemistry. III. The role of exact exchange, *J. Chem. Phys.* **98**, 5648 (1993).
- [7] J. Jaramillo, G. E. Scuseria, and M. Ernzerhof, Local hybrid functionals, *J. Chem. Phys.* **118**, 1068 (2003).
- [8] A. V. Arbuznikov, M. Kaupp, and H. Bahmann, From local hybrid functionals to “localized local hybrid” potentials: Formalism and thermochemical tests, *J. Chem. Phys.* **124**, 204102 (2006).
- [9] J. P. Perdew, V. N. Staroverov, J. Tao, and G. E. Scuseria, Density functional with full exact exchange, balanced nonlocality of correlation, and constraint satisfaction, *Phys. Rev. A* **78**, 052513 (2008).
- [10] T. Schmidt, E. Kraisler, A. Makmal, L. Kronik, and S. Kümmel, A self-interaction-free local hybrid functional: Accurate binding energies vis-à-vis accurate ionization potentials from Kohn-Sham eigenvalues, *J. Chem. Phys.* **140**, 18A510 (2014).
- [11] H. Iikura, T. Tsuneda, T. Yanai, and K. Hirao, A long-range correction scheme for generalized-gradient-approximation exchange functionals, *J. Chem. Phys.* **115**, 3540 (2001).
- [12] J. Heyd, G. E. Scuseria, and M. Ernzerhof, Hybrid functionals based on a screened Coulomb potential, *J. Chem. Phys.* **118**, 8207 (2003).
- [13] J. Heyd, G. E. Scuseria, and M. Ernzerhof, Erratum: Hybrid functionals based on a screened Coulomb potential, *J. Chem. Phys.* **124**, 219906 (2006).
- [14] T. Yanai, D. P. Tew, and N. C. Handy, A new hybrid exchange-correlation functional using the Coulomb-attenuating method (CAM-B3LYP), *Chem. Phys. Lett.* **393**, 51 (2004).
- [15] R. Baer and D. Neuhauser, Density Functional Theory with Correct Long-Range Asymptotic Behavior, *Phys. Rev. Lett.* **94**, 043002 (2005).
- [16] M. J. G. Peach, T. Helgaker, P. Salek, T. W. Keal, O. B. Lutnæs, D. J. Tozer, and N. C. Handy, Assessment of a Coulomb-attenuated exchange–correlation energy functional, *Phys. Chem. Chem. Phys.* **8**, 558 (2006).
- [17] J.-D. Chai and M. Head-Gordon, Systematic optimization of long-range corrected hybrid density functionals, *J. Chem. Phys.* **128**, 084106 (2008).
- [18] L. Kronik, T. Stein, S. Refaely-Abramson, and R. Baer, Excitation gaps of finite-sized systems from optimally tuned range-separated hybrid functionals, *J. Chem. Theory Comput.* **8**, 1515 (2012).
- [19] T. B. de Queiroz and S. Kümmel, Charge-transfer excitations in low-gap systems under the influence of solvation and conformational disorder: Exploring range-separation tuning, *J. Chem. Phys.* **141**, 084303 (2014).
- [20] A. Savin, Models and corrections: Range separation for electronic interaction – Lessons from density functional theory, *J. Chem. Phys.* **153**, 160901 (2020).
- [21] A. V. Krukau, G. E. Scuseria, J. P. Perdew, and A. Savin, Hybrid functionals with local range separation, *J. Chem. Phys.* **129**, 124103 (2008).
- [22] T. Aschebrock and S. Kümmel, Exploring local range separation: The role of spin scaling and one-electron self-interaction, *J. Chem. Phys.* **151**, 154108 (2019).
- [23] S. Klawohn and H. Bahmann, Self-consistent implementation of hybrid functionals with local range separation, *J. Chem. Theory Comput.* **16**, 953 (2020).
- [24] J. Erhard, P. Bleiziffer, and A. Görling, Power Series Approximation for the Correlation Kernel Leading to Kohn-Sham Methods Combining Accuracy, Computational Efficiency, and General Applicability, *Phys. Rev. Lett.* **117**, 143002 (2016).
- [25] J. P. Perdew and M. Levy, Physical Content of the Exact Kohn-Sham Orbital Energies: Band Gaps and Derivative Discontinuities, *Phys. Rev. Lett.* **51**, 1884 (1983).
- [26] D. Tozer, Relationship between long-range charge-transfer excitation energy error and integer discontinuity in Kohn-Sham theory, *J. Chem. Phys.* **119**, 12697 (2003).
- [27] P. Mori-Sánchez, Q. Wu, and W. Yang, Accurate polymer polarizabilities with exact exchange density-functional theory, *J. Chem. Phys.* **119**, 11001 (2003).
- [28] S. Kümmel, L. Kronik, and J. P. Perdew, Electrical Response of Molecular Chains from Density Functional Theory, *Phys. Rev. Lett.* **93**, 213002 (2004).
- [29] J. B. Krieger, Y. Li, and G. J. Iafrate, Construction and application of an accurate local spin-polarized kohn-sham potential with integer discontinuity: Exchange-only theory, *Phys. Rev. A* **45**, 101 (1992).
- [30] M. Städele, M. Moukara, J. A. Majewski, P. Vogl, and A. Görling, Exact exchange kohn-sham formalism applied to semiconductors, *Phys. Rev. B* **59**, 10031 (1999).
- [31] S. Kümmel and L. Kronik, Orbital-dependent density functionals: Theory and applications, *Rev. Mod. Phys.* **80**, 3 (2008).
- [32] J. Chen, J. B. Krieger, Y. Li, and G. J. Iafrate, Kohn-sham calculations with self-interaction-corrected local-spin-density exchange-correlation energy functional for atomic systems, *Phys. Rev. A* **54**, 3939 (1996).
- [33] C. Toher, A. Filippetti, S. Sanvito, and K. Burke, Self-Interaction Errors in Density-Functional Calculations of Electronic Transport, *Phys. Rev. Lett.* **95**, 146402 (2005).
- [34] D. Hofmann and S. Kümmel, Integer particle preference during charge transfer in Kohn-Sham theory, *Phys. Rev. B* **86**, 201109(R) (2012).

- [35] A. D. Becke and E. R. Johnson, A simple effective potential for exchange, *J. Chem. Phys.* **124**, 221101 (2006).
- [36] R. Armiento, S. Kümmel, and T. Körzdörfer, Electrical response of molecular chains in density functional theory: Ultranonlocal response from a semilocal functional, *Phys. Rev. B* **77**, 165106 (2008).
- [37] F. Tran and P. Blaha, Accurate Band Gaps of Semiconductors and Insulators with a Semilocal Exchange–Correlation Potential, *Phys. Rev. Lett.* **102**, 226401 (2009).
- [38] R. Armiento and S. Kümmel, Orbital Localization, Charge Transfer, and Band Gaps in Semilocal Density-Functional Theory, *Phys. Rev. Lett.* **111**, 036402 (2013).
- [39] P. Borlido, J. Schmidt, A. Huran, F. Tran, M. Marques, and S. Botti, Exchange-correlation functionals for band gaps of solids: Benchmark, reparametrization and machine learning, *npj Comput. Mater.* **6**, 96 (2020).
- [40] A. Karolewski, R. Armiento, and S. Kümmel, Polarizabilities of polyacetylene from a field-counteracting semilocal functional, *J. Chem. Theory Comput.* **5**, 712 (2009).
- [41] A. P. Gaiduk, S. K. Chulkov, and V. N. Staroverov, Reconstruction of density functionals from Kohn-Sham potentials by integration along density scaling paths, *J. Chem. Theory Comput.* **5**, 699 (2009).
- [42] A. Karolewski, R. Armiento, and S. Kümmel, Electronic excitations and the Becke-Johnson potential: The need for and the problem of transforming model potentials to functional derivatives, *Phys. Rev. A* **88**, 052519 (2013).
- [43] T. Aschebrock, R. Armiento, and S. Kümmel, Orbital nodal surfaces: Topological challenges for density functionals, *Phys. Rev. B* **95**, 245118 (2017).
- [44] T. Aschebrock, R. Armiento, and S. Kümmel, Challenges for semilocal density functionals with asymptotically nonvanishing potentials, *Phys. Rev. B* **96**, 075140 (2017).
- [45] F. Della Sala, E. Fabiano, and L. A. Constantin, Kinetic-energy-density dependent semilocal exchange-correlation functionals, *Int. J. Quantum Chem.* **116**, 1641 (2016).
- [46] A. D. Becke, A new inhomogeneity parameter in density-functional theory, *J. Chem. Phys.* **109**, 2092 (1998).
- [47] J. P. Perdew, S. Kurth, A. Zupan, and P. Blaha, Accurate Density Functional with Correct Formal Properties: A Step Beyond the Generalized Gradient Approximation, *Phys. Rev. Lett.* **82**, 2544 (1999).
- [48] J. Tao, J. P. Perdew, V. N. Staroverov, and G. E. Scuseria, Climbing the Density Functional Ladder: Nonempirical Meta-Generalized Gradient Approximation Designed for Molecules and Solids, *Phys. Rev. Lett.* **91**, 146401 (2003).
- [49] A. P. Bartók and J. R. Yates, Regularized scan functional, *J. Chem. Phys.* **150**, 161101 (2019).
- [50] J. W. Furness and J. Sun, Enhancing the efficiency of density functionals with an improved iso-orbital indicator, *Phys. Rev. B* **99**, 041119(R) (2019).
- [51] F. G. Eich and M. Hellgren, Derivative discontinuity and exchange-correlation potential of meta-ggas in density-functional theory, *J. Chem. Phys.* **141**, 224107 (2014).
- [52] T. Aschebrock and S. Kümmel, Ultranonlocality and accurate band gaps from a meta-generalized gradient approximation, *Phys. Rev. Research* **1**, 033082 (2019).
- [53] In the context of the development of a modification of the TASK functional [80], TASK has also been combined with SCAN [56] correlation.
- [54] F. Hofmann, I. Schelter, and S. Kümmel, Molecular excitations from meta-generalized gradient approximations in the Kohn-Sham scheme, *J. Chem. Phys.* **153**, 114106 (2020).
- [55] S. Kümmel and J. P. Perdew, Two avenues to self-interaction correction within Kohn-Sham theory: Unitary invariance is the shortcut, *Mol. Phys.* **101**, 1363 (2003).
- [56] J. Sun, A. Ruzsinszky, and J. P. Perdew, Strongly Constrained and Appropriately Normed Semilocal Density Functional, *Phys. Rev. Lett.* **115**, 036402 (2015).
- [57] E. H. Lieb and S. Oxford, Improved lower bound on the indirect coulomb energy, *Int. J. Quantum Chem.* **19**, 427 (1981).
- [58] G.-L. Chan and N. C. Handy, Optimized lieb-oxford bound for the exchange-correlation energy, *Phys. Rev. A* **59**, 3075 (1999).
- [59] J. W. Furness, A. D. Kaplan, J. Ning, J. P. Perdew, and J. Sun, Construction of meta-GGA functionals through restoration of exact constraint adherence to regularized scan functionals, *J. Chem. Phys.* **156**, 034109 (2022).
- [60] *CRC Handbook of Chemistry and Physics*, 98th ed., edited by J. Rumble, (CRC Press, Boca Raton, FL, 2017).
- [61] See Supplemental Material at <http://link.aps.org/supplemental/10.1103/PhysRevResearch.4.023061> for the definition of statistical measures, detailed data, comments on meta-GGA numerics, and comments on the OH molecule.
- [62] J. W. Furness, A. D. Kaplan, J. Ning, J. P. Perdew, and J. Sun, Accurate and numerically efficient r2scan meta-generalized gradient approximation, *J. Phys. Chem. Lett.* **11**, 8208 (2020).
- [63] Different from other work using the diatomic test set [22,52,81] we here omit the OH molecule for reasons discussed [82,83] in the Supplemental Material [61].
- [64] A. Makmal, S. Kümmel, and L. Kronik, Fully numerical all-electron solutions of the optimized effective potential equation for diatomic molecules, *J. Chem. Theory Comput.* **5**, 1731 (2009).
- [65] The values of TASK+LDAc for molecules that contain oxygen differ from those reported earlier in Ref. [52] because we found a configuration with lower energy for the oxygen atom.
- [66] R. Peverati and D. G. Truhlar, Communication: A global hybrid generalized gradient approximation to the exchange-correlation functional that satisfies the second-order density-gradient constraint and has broad applicability in chemistry, *J. Chem. Phys.* **135**, 191102 (2011).
- [67] SCM, Theoretical Chemistry, Vrije Universiteit, Amsterdam, The Netherlands, ADF 2020, G. Te Velde *et al.*, Chemistry with ADF, *J. Comput. Chem.* **22**, 931 (2001).
- [68] In ADF, it was not possible to converge the hydrogen atom self-consistently with TASK+CCaLDA. For the hydrogen atom, however, TASK+CCaLDA is equivalent to TASK+LDAc. Therefore, we use the energy of the hydrogen atom obtained with TASK+LDAc in our calculations for TASK+CCaLDA in ADF.
- [69] J. Sun, B. Xiao, Y. Fang, R. Haunschuld, P. Hao, A. Ruzsinszky, G. I. Csonka, G. E. Scuseria, and J. P. Perdew, Density Functionals that Recognize Covalent, Metallic, and Weak Bonds, *Phys. Rev. Lett.* **111**, 106401 (2013).
- [70] J. P. Perdew, J. Sun, A. Ruzsinszky, P. D. Mezei, and G. I. Csonka, Why density functionals should not be judged primarily by atomization energies, *Period. Polytech. Chem Eng.* **60**, 2 (2016).

- [71] R. Peverati and D. G. Truhlar, Quest for a universal density functional: the accuracy of density functionals across a broad spectrum of databases in chemistry and physics, *Philos. Trans. R. Soc. A* **372**, 20120476 (2014).
- [72] Y. Zhao and D. G. Truhlar, Construction of a generalized gradient approximation by restoring the density-gradient expansion and enforcing a tight Lieb-Oxford bound, *J. Chem. Phys.* **128**, 184109 (2008).
- [73] H. S. Yu, W. Zhang, P. Verma, X. He, and D. G. Truhlar, Nonseparable exchange-correlation functional for molecules, including homogeneous catalysis involving transition metals, *Phys. Chem. Chem. Phys.* **17**, 12146 (2015).
- [74] E. v. Lenthe, E.-J. Baerends, and J. G. Snijders, Relativistic regular two-component Hamiltonians, *J. Chem. Phys.* **99**, 4597 (1993).
- [75] This finding is also in line with some findings obtained with TASK for solids; F. Tran (private communication) (2021).
- [76] P. Haas, F. Tran, P. Blaha, K. Schwarz, and R. Laskowski, Insight into the performance of gga functionals for solid-state calculations, *Phys. Rev. B* **80**, 195109 (2009).
- [77] P. Haas, F. Tran, P. Blaha, and K. Schwarz, Construction of an optimal GGA functional for molecules and solids, *Phys. Rev. B* **83**, 205117 (2011).
- [78] J. Zheng, Y. Zhao, and D. G. Truhlar, The DBH24/08 database and its use to assess electronic structure model chemistries for chemical reaction barrier heights, *J. Chem. Theory Comput.* **5**, 808 (2009).
- [79] P. D. Mezei, G. I. Csonka, and M. Kállay, Simple modifications of the scan meta-generalized gradient approximation functional, *J. Chem. Theory Comput.* **14**, 2469 (2018).
- [80] B. Neupane, H. Tang, N. K. Nepal, S. Adhikari, and A. Ruzsinszky, Opening band gaps of low-dimensional materials at the meta-gga level of density functional approximations, *Phys. Rev. Materials* **5**, 063803 (2021).
- [81] M. Brütting, H. Bahmann, and S. Kümmel, Hybrid functionals with local range separation: Accurate atomization energies and reaction barrier heights, *J. Chem. Phys.* **156**, 104109 (2022).
- [82] R. D. Johnson, NIST computational chemistry comparison and benchmark database, NIST Standard Reference Database Number 101 (2020), doi: [10.18434/T47C7Z](https://doi.org/10.18434/T47C7Z).
- [83] Y. Shao, Z. Gan, E. Epifanovsky, A. T. Gilbert, M. Wormit, J. Kussmann, A. W. Lange, A. Behn, J. Deng, X. Feng, D. Ghosh, M. Goldey, P. R. Horn, L. D. Jacobson, I. Kaliman, R. Z. Khaliullin, T. Kuś, A. Landau, J. Liu, E. I. Proynov, Y. M. Rhee, R. M. Richard, M. A. Rohrdanz, R. P. Steele, E. J. Sundstrom, H. L. W. III, P. M. Zimmerman, D. Zuev, B. Albrecht, E. Alguire, B. Austin, G. J. O. Beran, Y. A. Bernard, E. Berquist, K. Brandhorst, K. B. Bravaya, S. T. Brown, D. Casanova, C.-M. Chang, Y. Chen, S. H. Chien, K. D. Closser, D. L. Crittenden, M. Diedenhofen, R. A. D. Jr., H. Do, A. D. Dutoi, R. G. Edgar, S. Fatehi, L. Fusti-Molnar, A. Ghysels, A. Golubeva-Zadorozhnaya, J. Gomes, M. W. Hanson-Heine, P. H. Harbach, A. W. Hauser, E. G. Hohenstein, Z. C. Holden, T.-C. Jagau, H. Ji, B. Kaduk, K. Khistyayev, J. Kim, J. Kim, R. A. King, P. Klunzinger, D. Kosenkov, T. Kowalczyk, C. M. Krauter, K. U. Lao, A. D. Laurent, K. V. Lawler, S. V. Levchenko, C. Y. Lin, F. Liu, E. Livshits, R. C. Lochan, A. Luenser, P. Manohar, S. F. Manzer, S.-P. Mao, N. Mardirossian, A. V. Marenich, S. A. Maurer, N. J. Mayhall, E. Neuscamman, C. M. Oana, R. Olivares-Amaya, D. P. O'Neill, J. A. Parkhill, T. M. Perrine, R. Peverati, A. Prociuk, D. R. Rehn, E. Rosta, N. J. Russ, S. M. Sharada, S. Sharma, D. W. Small, A. Sodt, T. Stein, D. Stück, Y.-C. Su, A. J. Thom, T. Tsuchimochi, V. Vanovschi, L. Vogt, O. Vydrov, T. Wang, M. A. Watson, J. Wenzel, A. White, C. F. Williams, J. Yang, S. Yeganeh, S. R. Yost, Z.-Q. You, I. Y. Zhang, X. Zhang, Y. Zhao, B. R. Brooks, G. K. Chan, D. M. Chipman, C. J. Cramer, W. A. G. III, M. S. Gordon, W. J. Hehre, A. Klamt, H. F. S. III, M. W. Schmidt, C. D. Sherrill, D. G. Truhlar, A. Warshel, X. Xu, A. Aspuru-Guzik, R. Baer, A. T. Bell, N. A. Besley, J.-D. Chai, A. Dreuw, B. D. Dunietz, T. R. Furlani, S. R. Gwaltney, C.-P. Hsu, Y. Jung, J. Kong, D. S. Lambrecht, W. Liang, C. Ochsenfeld, V. A. Rassolov, L. V. Slipchenko, J. E. Subotnik, T. V. Voorhis, J. M. Herbert, A. I. Krylov, P. M. Gill, and M. Head-Gordon, Advances in molecular quantum chemistry contained in the q-chem 4 program package, *Mol. Phys.* **113**, 184 (2015).

Supplementary material for “First Steps towards Achieving Both Ultranonlocality and a Reliable Description of Electronic Binding in a Meta-Generalized Gradient Approximation”

Timo Lebeda, Thilo Aschebrock, and Stephan Kümmel*
Theoretical Physics IV, University of Bayreuth, 95440 Bayreuth, Germany

I. STATISTICAL MEASURES

The following statistical measures are used in the tables here and in the main paper for summarizing the functionals’ performance. For a set of N calculated values of a given quantity, x_1, \dots, x_N , and a corresponding set of experimental values e_1, \dots, e_N , one obtains a general impression of a functional’s performance by the mean absolute error, $\text{MAE} = \frac{1}{N} \sum_{i=1}^N |x_i - e_i|$. Systematic deviations show up in the mean signed error, $\text{MSE} = \frac{1}{N} \sum_{i=1}^N (x_i - e_i)$. Finally, one can check whether the error is dominated by a few outliers or uniformly distributed across all systems via the root mean square error, $\text{RMSE} = \left(\frac{1}{N} \sum_{i=1}^N (x_i - e_i)^2 \right)^{1/2}$.

II. DETAILED DATA

In the following we provide the bond lengths of Na_2 and Li_2 (Table S.I), the detailed data for the MGAE109 testset of main-group atomization energies (Table S.II), the MGBL20 testset of main-group bond lengths (Table S.III), and the DBH24/08 testset of diverse barrier heights (Table S.IV).

TABLE S.I. Bond lengths of Na_2 and Li_2 in Å. The calculations were performed with the QZ4P-basis set in AMS/ADF [1]. The experimental values are taken from Ref. [2].

	Na_2	Li_2
LDA	3.003	2.708
PBE	3.090	2.729
SCAN	3.096	2.747
TASKx	3.674	3.049
TASK+LDAc	3.522	2.935
TASK+SCANc	3.498	2.963
TASK+CC	3.522	2.935
Expt.	3.079	2.673

* stephan.kuettel@uni-bayreuth.de; <http://tp4.uni-bayreuth.de/en>

TABLE S.II. Atomization energies per bond of main group molecules in kcal/mol. The calculations were performed with the QZ4P-basis set in AMS/ADF [1]. The MGAE109 set of main-group atomization energies is taken from Ref. [3].

Molecule	LDA	PBE	SCAN	TASKx	TASK+LDAc	TASK+SCANc	TASK+CC	TASK+CCaLDA[4]	Expt.
CH	92.31	84.65	81.72	46.51	72.95	66.92	97.18	83.28	84.23
CH ₂ (3B1.)	106.37	97.26	98.34	74.91	93.23	93.24	108.68	94.78	95.38
CH ₂ (1A1.)	99.35	89.44	87.65	55.14	80.91	75.50	103.36	89.46	90.73
CH ₃	113.02	103.31	104.10	74.82	97.19	95.65	114.84	100.94	102.63
CH ₄	115.55	104.98	104.90	75.53	98.66	96.89	116.83	102.93	105.11
C ₂ H ₂	153.28	138.32	133.90	96.28	122.26	123.17	142.92	133.65	135.18
C ₂ H ₄	126.42	114.27	112.52	79.50	102.64	102.64	120.60	109.48	112.74
C ₂ H ₆	113.39	102.38	101.88	71.33	93.24	92.78	110.04	98.13	101.85
HCO	166.25	147.40	140.85	98.47	125.09	127.99	145.14	138.02	139.72
H ₂ CO	144.43	128.50	124.34	86.81	112.44	112.90	132.06	122.68	124.89
CH ₃ OH	117.20	103.95	102.50	69.76	92.71	92.53	110.04	98.86	102.71
HCN	180.27	163.08	153.59	99.81	133.44	134.07	162.09	155.14	156.72
NH ₂ NH ₂	103.08	90.58	86.88	44.73	71.17	70.91	92.82	81.70	87.72
CH ₃ Cl	112.19	99.97	99.00	69.29	90.42	91.02	106.40	95.96	99.11
CH ₃ SH	107.25	95.65	94.98	64.94	86.84	87.02	103.90	92.81	94.90
C ₃ H ₄ (pro.)	133.58	120.16	117.38	82.58	105.79	107.06	123.60	114.33	117.51
C ₄ H ₄ O	129.39	114.51	111.24	75.12	96.26	99.87	111.59	105.38	110.48
C ₄ H ₄ S	124.57	110.72	107.81	73.27	94.01	97.97	109.19	103.03	107.07
C ₄ H ₅ N	124.95	111.05	107.76	70.34	92.31	95.50	108.73	101.78	107.19
C ₄ H ₆ (tra.)	127.79	114.91	112.72	78.24	100.50	101.88	117.37	108.10	112.53
C ₄ H ₆ (yne.)	126.85	113.95	111.71	77.80	100.09	101.48	116.96	107.69	111.61
C ₅ H ₅ N	130.89	116.77	113.22	74.73	96.86	100.17	113.34	107.03	112.56
CCH	154.60	138.48	132.86	95.32	117.88	122.17	137.84	130.90	132.66
CH ₂ OH	119.29	105.35	103.59	69.58	92.27	93.17	109.29	98.78	102.52
CH ₃ CN	141.07	127.07	122.63	82.04	107.77	108.95	128.21	119.87	123.20
CH ₃ NH ₂	110.11	98.46	96.75	61.38	85.22	84.74	104.04	92.46	97.05
CH ₃ NO ₂	123.83	106.81	101.07	59.08	83.81	86.97	102.64	95.58	100.30
CHCl ₃	106.09	89.71	86.77	55.91	73.07	79.51	84.65	81.15	86.45
CHF ₃	139.61	119.37	114.97	83.56	102.35	106.89	114.16	110.69	114.68
CH ₂ CH	126.73	114.44	112.61	79.23	101.45	102.48	118.90	108.48	111.52
HCOOCH ₃	131.57	115.76	112.91	76.09	99.06	100.86	115.87	107.83	112.27
HCOOH	149.24	130.41	125.75	86.19	111.22	113.89	129.43	122.31	125.38
C ₂ H ₅	112.82	101.97	101.71	70.87	92.32	92.33	108.76	97.17	100.65
C ₄ H ₆ (bic.)	103.11	91.96	90.10	60.77	79.43	81.77	93.23	85.65	89.78
C ₄ H ₆ (cyc.)	114.42	102.39	100.40	68.17	88.51	90.53	103.69	95.35	100.20
HCOCOH	150.37	132.45	126.99	86.36	110.78	113.71	128.76	123.07	126.80
CH ₃ CHO	129.69	115.66	113.12	78.34	101.34	102.39	118.63	109.31	112.91
C ₂ H ₄ O	126.07	111.60	109.04	72.90	96.22	98.15	113.51	104.19	108.52
C ₂ H ₅ O	114.30	101.45	100.30	66.72	88.28	89.02	104.47	94.49	99.86
CH ₃ OCH ₃	113.92	101.18	100.06	67.16	89.04	89.24	105.49	95.02	99.81
CH ₃ CH ₂ OH	115.42	102.64	101.42	68.82	90.77	91.20	107.22	96.75	101.35
C ₃ H ₄ (all.)	134.11	120.64	117.71	82.65	105.85	107.33	123.66	114.40	117.25
C ₃ H ₄ (cyc.)	112.07	100.23	97.51	66.62	86.83	88.93	102.10	94.16	97.57
CH ₃ COOH	134.13	118.17	115.23	78.83	101.89	104.05	118.71	110.67	114.81
CH ₃ COCH ₃	124.47	111.05	109.12	75.16	97.30	98.54	113.81	104.51	108.72
C ₃ H ₆	107.56	96.46	95.14	65.28	85.25	86.45	100.22	90.95	94.85
CH ₃ CHCH ₂	121.26	109.17	107.71	74.96	97.06	97.66	113.89	103.47	107.61
C ₃ H ₈	112.77	101.48	100.88	69.74	91.17	91.28	107.42	96.29	100.71
C ₂ H ₅ OCH ₃	113.51	100.98	99.94	67.19	88.65	89.19	104.69	94.55	99.60
C ₄ H ₁₀ (iso.)	112.57	101.06	100.44	68.88	90.06	90.52	106.01	95.32	100.26
C ₄ H ₁₀ (anti.)	112.44	101.00	100.34	68.88	90.06	90.48	106.01	95.32	100.13
C ₄ H ₈ (cyc.)	108.64	97.26	96.11	65.06	85.14	86.46	100.11	90.84	95.78
C ₄ H ₈ (iso.)	118.95	106.83	105.56	72.82	94.45	95.35	110.78	100.67	105.36
C ₅ H ₈ (spi.)	105.27	93.96	92.28	62.35	81.41	83.53	95.46	87.51	91.77
C ₆ H ₆	131.07	117.41	114.69	79.13	100.33	103.44	115.83	108.88	114.01
CH ₃ CO	135.33	120.65	117.43	81.35	104.27	106.31	121.42	113.01	116.40
CH ₃ CHCH ₃	112.84	101.57	101.02	69.62	90.74	91.30	106.76	95.95	100.11
C ₄ H ₉ (t.)	112.86	101.36	100.70	68.97	89.92	90.77	105.71	95.29	99.98
CH ₂ CO	156.77	139.45	134.35	95.28	120.53	123.35	139.52	132.48	133.18

Continued on next page.

Molecule	LDA	PBE	SCAN	TASKx	TASK+LDAc	TASK+SCANc	TASK+CC	TASK+CCaLDA[4]	Expt.
CN	219.10	197.06	177.00	101.71	139.92	147.14	178.85	178.86	181.36
CO	298.58	268.50	253.92	196.05	234.09	238.05	265.13	264.80	259.74
N ₂	266.97	243.11	218.72	116.76	172.70	173.32	225.33	225.32	228.48
NO	197.70	171.60	150.51	70.06	112.20	118.62	148.85	148.51	152.75
O ₂	174.46	143.06	127.02	75.51	103.87	115.19	124.22	123.55	120.83
F ₂	78.00	52.67	36.89	7.38	22.57	29.21	33.39	33.39	39.03
CO ₂	236.25	207.77	196.17	144.97	176.79	183.31	199.29	198.96	195.08
Si ₂	94.07	79.60	75.70	47.01	69.42	74.93	90.82	90.83	76.38
P ₂	143.05	121.28	111.68	51.92	97.06	98.74	142.91	142.91	117.59
S ₂	134.94	114.87	108.85	73.54	97.69	109.10	115.52	115.86	104.25
Cl ₂	86.55	65.43	58.07	31.85	47.16	57.12	57.40	57.31	59.75
SiO	224.71	196.62	187.66	138.74	175.58	175.87	204.44	204.10	193.06
SC	201.80	179.55	167.18	121.42	154.39	160.69	184.09	184.27	171.76
SO	167.42	140.95	131.82	85.37	112.64	122.45	130.66	130.49	126.48
ClO	105.35	81.30	69.61	25.03	47.28	57.46	63.15	62.76	65.45
ClF	96.91	72.12	61.27	31.61	48.06	56.02	58.59	58.54	62.79
SO ₂	167.96	140.10	130.36	81.59	111.18	119.27	131.44	131.19	130.31
AlCl ₃	116.15	101.92	104.24	87.58	102.83	104.41	110.45	110.41	104.21
AlF ₃	161.04	142.59	141.15	123.47	141.89	141.06	149.81	149.81	143.65
BCl ₃	128.95	111.67	110.75	84.31	99.36	105.67	107.20	107.15	108.48
BF ₃	182.57	160.22	156.75	129.83	147.61	150.85	155.75	155.75	156.99
C ₂ Cl ₄	119.29	100.11	95.33	59.85	77.08	86.72	88.01	87.98	93.96
C ₂ F ₄	148.76	125.82	119.02	83.15	101.79	109.12	112.95	112.96	118.21
CCl ₄	101.97	83.24	79.35	47.46	62.67	72.33	72.06	72.02	79.05
CF ₃ CN	157.72	135.88	128.03	85.79	107.91	114.24	123.25	123.26	128.23
CF ₄	149.36	125.34	119.81	88.09	105.55	112.67	115.23	115.23	119.48
ClF ₃	77.17	55.02	46.29	17.24	30.63	39.74	37.75	37.73	42.44
NF ₃	103.88	81.18	70.04	29.41	48.89	56.83	63.07	63.07	68.56
PF ₃	147.59	124.85	120.45	88.03	108.73	112.24	121.78	121.78	121.67
SiCl ₄	112.59	96.30	97.31	74.14	89.90	94.66	98.74	98.69	97.18
SiF ₄	164.18	143.00	141.83	118.53	137.23	138.48	146.37	146.37	144.07
NH	95.31	88.50	84.92	38.91	67.59	64.29	93.41	79.50	83.10
NH ₂	103.90	94.33	92.27	49.21	77.48	74.89	101.76	87.85	91.30
NH ₃	112.39	100.65	98.20	59.89	87.35	85.42	110.03	96.13	99.34
OH	124.03	109.88	108.68	69.13	97.38	95.15	119.74	105.50	107.22
H ₂ O	133.17	117.13	114.59	81.52	108.73	107.57	129.61	115.54	116.49
HF	162.01	142.01	136.94	112.60	139.24	139.07	158.56	144.65	141.63
SiH ₂ (1A1.)	83.29	73.92	74.64	49.49	73.87	67.65	95.22	81.32	76.11
SiH ₂ (3B1.)	73.79	65.85	69.25	53.41	69.72	67.48	84.96	71.06	65.74
SiH ₃	82.42	74.15	76.86	55.70	76.05	71.98	92.97	79.07	76.00
SiH ₄	86.93	78.38	80.87	58.04	79.82	74.84	97.44	83.54	81.24
PH ₂	86.79	77.20	78.27	47.17	72.34	68.94	94.91	81.00	76.60
PH ₃	89.85	79.68	80.50	50.72	75.49	72.07	97.03	83.13	80.76
H ₂ S	103.17	91.05	91.07	63.79	88.01	86.63	108.22	94.40	91.95
HCl	122.20	106.43	105.64	82.46	106.33	106.13	125.35	111.40	107.50
NH ₂ NH ₂	103.08	90.58	86.88	44.73	71.17	70.91	92.82	81.70	87.72
H ₂ O ₂	111.62	93.95	88.98	51.40	75.90	77.20	94.47	84.98	89.68
Si ₂ H ₆	82.92	74.31	76.56	53.61	73.95	70.37	90.12	78.21	76.56
HOCl	106.37	87.62	82.13	47.14	69.52	73.08	86.00	78.86	83.12
H ₂	113.05	104.62	107.65	85.25	116.98	107.65	144.79	116.98	109.49
SH	99.56	87.99	88.60	59.42	84.03	82.45	105.29	91.56	87.00
MSE	19.51	3.79	-0.10	-35.61	-12.05	-10.09	6.11	-1.39	
MAE	19.51	4.23	1.36	35.61	12.26	10.22	7.33	4.21	
RMSE	21.73	5.99	2.16	37.80	14.39	12.30	9.25	5.17	

TABLE S.III. MGBL20 [5] main-group bond lengths in Å. The calculations were performed with the QZ4P-basis set in AMS/ADF [1].

Molecule	LDA	PBE	SCAN	TASKx	TASK+LDAc	TASK+SCANc	TASK+CC	Expt.
MGHBL9 [6] (Main-Group Hydrogenic Bond Lengths)								
H ₂	0.765	0.750	0.741	0.744	0.729	0.741	0.729	0.741
CH ₄	1.096	1.095	1.087	1.107	1.090	1.097	1.090	1.086
NH ₃	1.021	1.021	1.012	1.027	1.011	1.018	1.011	1.012
H ₂ O	0.970	0.969	0.960	0.968	0.955	0.961	0.955	0.957
HF	0.932	0.930	0.920	0.924	0.913	0.919	0.913	0.917
C ₂ H ₂	1.074	1.070	1.062	1.080	1.065	1.074	1.065	1.063
HCN (C–H)	1.079	1.075	1.066	1.085	1.070	1.079	1.070	1.065
H ₂ CO (C–H)	1.121	1.117	1.107	1.135	1.117	1.126	1.117	1.102
OH	0.985	0.983	0.974	0.986	0.972	0.978	0.971	0.970
MSE	0.015	0.011	0.002	0.016	0.001	0.009	0.001	
MAE	0.015	0.011	0.002	0.016	0.005	0.009	0.005	
RMSE	0.015	0.011	0.003	0.018	0.007	0.011	0.007	
MGNHBL11 [5] (Main-Group Non-Hydrogenic Bond Lengths)								
CO	1.127	1.135	1.125	1.145	1.134	1.139	1.134	1.128
N ₂	1.095	1.102	1.092	1.108	1.098	1.102	1.098	1.098
F ₂	1.385	1.414	1.399	1.432	1.411	1.395	1.411	1.412
C ₂ H ₂ (C–C)	1.201	1.207	1.196	1.219	1.205	1.212	1.205	1.203
HCN (C–N)	1.150	1.158	1.147	1.167	1.155	1.161	1.155	1.153
H ₂ CO (C–O)	1.198	1.208	1.197	1.216	1.204	1.207	1.204	1.203
CO ₂	1.162	1.171	1.158	1.179	1.166	1.171	1.166	1.160
N ₂ O (N–N)	1.129	1.137	1.125	1.144	1.131	1.137	1.131	1.128
N ₂ O (N–O)	1.176	1.189	1.180	1.198	1.184	1.183	1.184	1.184
Cl ₂	1.980	2.005	1.997	2.049	2.015	1.989	2.015	1.988
MgS	2.127	2.152	2.130	2.204	2.166	2.170	2.166	2.143
MSE	-0.006	0.007	-0.005	0.024	0.006	0.006	0.006	
MAE	0.007	0.007	0.006	0.024	0.006	0.009	0.006	
RMSE	0.010	0.008	0.007	0.030	0.011	0.012	0.011	

TABLE S.IV. DBH24/08 [7] barrier heights in kcal/mol. The calculations were performed with the QZ4P-basis set in AMS/ADF [1].

Reaction	LDA	PBE	SCAN	TASKx	TASK+LDAc	TASK+SCANc	TASK+CC	Expt.
OH + CH ₄ → CH ₃ + H ₂ O	-16.77	-5.24	-1.36	16.54	11.98	5.07	9.02	6.50
reverse	2.43	9.13	11.83	32.77	28.99	24.44	25.68	19.60
H + OH → O + H ₂	-1.88	3.72	3.28	13.48	5.92	5.06	0.66	10.70
reverse	-12.85	-1.54	2.15	29.92	25.82	17.04	25.81	13.10
H + H ₂ S → H ₂ + HS	-6.77	-1.13	-2.68	12.43	6.66	2.38	1.14	3.50
reverse	-0.49	9.38	11.43	29.52	31.65	19.23	34.79	17.30
H + N ₂ O → OH + N ₂	2.71	10.11	9.55	32.55	25.88	20.94	19.14	17.13
reverse	32.69	53.07	65.18	92.48	91.31	70.67	92.97	82.27
H + ClH → HCl + H	2.05	9.58	9.18	31.46	22.90	16.45	18.39	18.00
reverse	2.05	9.58	9.18	31.46	22.90	16.45	18.39	18.00
CH ₃ + FCl → CH ₃ F + Cl	-10.69	-5.69	-3.77	12.32	9.53	8.95	6.75	6.75
reverse	35.55	41.23	45.46	57.53	57.69	52.96	55.73	59.16
Cl ⁻ ...CH ₃ Cl → ClCH ₃ ...Cl ⁻	6.74	7.09	6.99	11.92	12.80	13.22	12.80	13.41
reverse	6.74	7.09	6.99	11.92	12.80	13.22	12.80	13.41
F ⁻ ...CH ₃ Cl → ClCH ₃ ...F ⁻	-1.29	-1.07	-1.94	0.60	1.52	2.24	1.52	3.44
reverse	21.51	21.43	24.91	31.72	31.34	29.10	31.34	29.42
OH ⁻ + CH ₃ F → CH ₃ OH + F ⁻	-14.85	-11.39	-10.86	7.03	5.42	3.65	5.42	-2.44
reverse	3.92	6.70	7.26	23.39	24.45	22.82	24.45	17.66
H + N ₂ → HN ₂	-2.24	5.21	4.20	25.55	16.73	11.75	10.33	14.36
reverse	9.29	8.99	9.68	3.51	9.37	7.14	12.84	10.61
H + C ₂ H ₄ → CH ₃ CH ₂	-5.46	-0.15	-4.50	10.87	8.21	2.55	3.56	1.72
reverse	39.36	40.31	43.16	38.58	48.92	43.31	53.11	41.75
HCN → HNC	44.91	45.65	46.38	45.53	47.72	43.90	47.72	48.07
reverse	30.89	30.79	32.50	32.06	33.71	30.52	33.71	32.82
MSE	-13.70	-8.47	-7.17	5.79	4.08	-0.55	2.58	
MAE	13.70	8.47	7.29	7.54	5.00	3.08	4.52	
RMSE	17.07	10.37	8.25	9.01	6.30	4.01	6.51	

III. META-GGA NUMERICS

Numerical observations for meta-GGAs

Some Meta-GGAs have been observed to be numerically difficult [8, 9]. Most of these numerical problems arise in the outer region of a system, and they are quite sensitive to the actual implementation of the functional derivative of the (x/c)-energy with respect to the Kohn-Sham orbitals,

$$\frac{\delta E_{x/c}}{\delta \varphi_{i\sigma}}, \quad (\text{S.1})$$

used in the calculation of the KLI and generalized Kohn-Sham potential, respectively. Therefore, the potential in such cases is typically set to zero at spatial points at which the density is lower than a functional- and algorithm-dependent threshold. We do not need such a cut-off in the CC correlation in our calculations with TASK+CC. However, we find that it is strongly beneficial to write terms that appear in the functional derivative of Eq. S.1, i.e., in the potential, in terms of \sqrt{n} instead of n wherever possible. This can be done using the relations

$$\nabla n = 2\sqrt{n}\nabla n^{1/2} \quad \text{and} \quad \nabla^2 n = 2\sqrt{n}\nabla^2 n^{1/2} + \frac{|\nabla n|^2}{2n}. \quad (\text{S.2})$$

One example is the von Weizsäcker kinetic energy density, which can be rewritten from Eq. (4) to $\tau_W(\mathbf{r}) = \frac{\hbar^2}{2m} \left| \nabla n^{1/2}(\mathbf{r}) \right|^2$. In this way, numerical instabilities that can arise from division by the electron density at outer grid points, at which the density is extremely small, are avoided. Replacing n by \sqrt{n} can make the difference between convergence and non-convergence for certain systems in the diatomic testset with DARSEC for TASK+CC. A similar observation has previously been made in the context of local hybrid functionals [10].

The CCaLDA correlation is numerically more demanding due to its almost step-like interpolation. To converge the calculation of the lithium atom with TASK+CCaLDA in DARSEC, we need to implement a spin-dependent density cut-off, i.e., we set the potential with corresponding spin to zero whenever the density with corresponding spin becomes smaller than a given threshold. Otherwise, the unoccupied spin-channel in the 2s-orbital causes numerical problems. However, this is not sufficient in ADF. We assume that this is the case because in ADF the above mentioned replacement of n by \sqrt{n} is not implemented. The same holds for the calculation of the hydrogen atom with TASK+CCaLDA in ADF. In ADF, α does not exactly vanish in the calculation of the hydrogen atom due to numerical issues (in contrast to the corresponding calculation in DARSEC). Similar numerical problems in regions of small α have been described for the SCAN meta-GGA [8].

Replacing z by terms in α or β

We have investigated whether the numerical stability can be improved by replacing z by a term in the iso-orbital indicators α or

$$\beta(\mathbf{r}) = \frac{\tau(\mathbf{r}) - \tau_W(\mathbf{r})}{\tau(\mathbf{r}) + \tau_F(\mathbf{r})}. \quad (\text{S.3})$$

While α can take values in $[0, \infty[$, β is restricted to the interval $[0, 1[$ and therefore has been suggested to be suitable for improving numerical stability by avoiding large numbers [11]. Moreover, β is reported to reduce the sharp oscillations in the derivatives with respect to n_σ , ∇n_σ , and τ_σ , which lead to numerical difficulties in other α -based meta-GGAs [11]. In the iso-orbital limit one finds $\tau_W = \tau$ and thus $z = 1$, $\alpha = 0$, and $\beta = 0$. For the uniform density limit, one has $\tau_W = 0$ and $\tau = \tau_F$, which implies $z = 0$, $\alpha = 1$, and $\beta = \frac{1}{2}$.

Thus, to restore the correct behavior of the CC correlation in the iso-orbital limit and in the uniform density limit, z can be replaced by an iso-orbital indicator designed in terms of, e.g., $1 - \alpha$ or $1 - 2\beta$.

All tested combinations of TASK exchange with correlation functionals that mimic the CC correlation using terms of α or β give worse atomization energies than TASK combined with the original CC correlation. Additionally, their numerical stability in self-consistent calculations is not improved. While TASK combined with correlation functionals of β appears to be of similar numerical stability as TASK+CC, the functionals designed with α are numerically much less stable. Thus, the choice of the iso-orbital indicator is important for the accuracy and the numerical stability of the corresponding functional.

Comment on OH not being axially symmetric

The diatomic test set that we use here differs from the one used in some other works [12–14] as we chose to omit the OH molecule. The reason is that the DARSEC code requires axial symmetry, but the hydroxyl radical density as obtained in an PBE calculation with QChem 5.2[15] deviates slightly from axial symmetry. To see this, we compare the density of the OH molecule in a plane perpendicular to the bond axis (z-axis), which is shifted from the center of the bond by twice the Bohr radius towards the oxygen atom, with that of the O₂ molecule in Figure S.1. While the density of the O₂ molecule remains unchanged under rotation of 90° around the bond axis, the density of the OH molecule does not. The density of the OH molecule however remains unchanged under rotation of 180° around the bond axis.

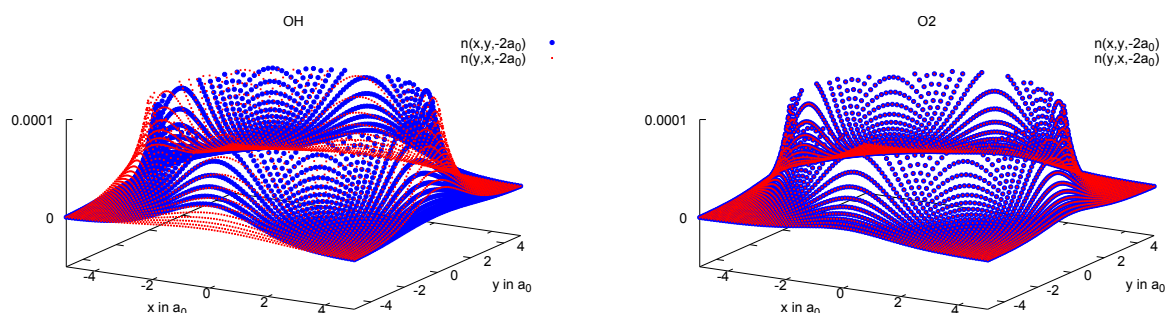


FIG. S.1. Total density in a plane perpendicular to the bond axis. Both calculations were performed in QChem 5.2[15] with PBE and the 6-311G++(3df,3dp) basis set. Left: OH molecule. Right: O₂ molecule.

-
- [1] SCM, Theoretical Chemistry, Vrije Universiteit, Amsterdam, The Netherlands, *ADF 2020*.
- [2] R. D. Johnson, Nist computational chemistry comparison and benchmark database, *NIST Standard Reference Database Number 101 (2020)*.
- [3] R. Peverati and D. G. Truhlar, Communication: A global hybrid generalized gradient approximation to the exchange-correlation functional that satisfies the second-order density-gradient constraint and has broad applicability in chemistry, *J. Chem. Phys.* **135**, 191102 (2011).
- [4] In ADF, it was not possible to converge the hydrogen atom self-consistently with TASK+CCaLDA. For the hydrogen atom, however, TASK+CCaLDA is equivalent to TASK+LDAc. Therefore, we use the energy of the hydrogen atom obtained with TASK+LDAc in our calculations for TASK+CCaLDA in ADF.
- [5] R. Peverati and D. G. Truhlar, Quest for a universal density functional: the accuracy of density functionals across a broad spectrum of databases in chemistry and physics, *Philos. Trans. R. Soc. A* **372**, 20120476 (2014).
- [6] Y. Zhao and D. G. Truhlar, Construction of a generalized gradient approximation by restoring the density-gradient expansion and enforcing a tight Lieb–Oxford bound, *J. Chem Phys.* **128**, 184109 (2008).
- [7] J. Zheng, Y. Zhao, and D. G. Truhlar, The DBH24/08 Database and Its Use to Assess Electronic Structure Model Chemistries for Chemical Reaction Barrier Heights, *J. Chem. Theory Comput.* **5**, 808 (2009).
- [8] A. P. Bartók and J. R. Yates, Regularized scan functional, *J. Chem. Phys.* **150**, 161101 (2019).
- [9] J. W. Furness, A. D. Kaplan, J. Ning, J. P. Perdew, and J. Sun, Accurate and numerically efficient r2scan meta-generalized gradient approximation, *J. Chem. Phys. Lett.* **11**, 8208 (2020).
- [10] T. Schmidt, E. Kraisler, A. Makmal, L. Kronik, and S. Kümmel, A self-interaction-free local hybrid functional: Accurate binding energies vis-à-vis accurate ionization potentials from kohn-sham eigenvalues, *J. Chem. Phys.* **140**, 18A510 (2014).
- [11] J. W. Furness and J. Sun, Enhancing the efficiency of density functionals with an improved iso-orbital indicator, *Phys. Rev. B* **99**, 041119(R) (2019).
- [12] T. Aschebrock and S. Kümmel, Ultranonlocality and accurate band gaps from a meta-generalized gradient approximation, *Phys. Rev. Research* **1**, 033082 (2019).
- [13] T. Aschebrock and S. Kümmel, Exploring local range separation: The role of spin scaling and one-electron self-interaction, *J. Chem. Phys.* **151**, 154108 (2019).
- [14] M. Brütting, H. Bahmann, and S. Kümmel, Hybrid functionals with local range separation: Accurate atomization energies and reaction barrier heights, *J. Chem. Phys.* **156**, 104109 (2022).

- [15] Y. Shao, Z. Gan, E. Epifanovsky, A. T. Gilbert, M. Wormit, J. Kussmann, A. W. Lange, A. Behn, J. Deng, X. Feng, D. Ghosh, M. Goldey, P. R. Horn, L. D. Jacobson, I. Kaliman, R. Z. Khaliullin, T. Kuś, A. Landau, J. Liu, E. I. Proynov, Y. M. Rhee, R. M. Richard, M. A. Rohrdanz, R. P. Steele, E. J. Sundstrom, H. L. W. III, P. M. Zimmerman, D. Zuev, B. Albrecht, E. Alguire, B. Austin, G. J. O. Beran, Y. A. Bernard, E. Berquist, K. Brandhorst, K. B. Bravaya, S. T. Brown, D. Casanova, C.-M. Chang, Y. Chen, S. H. Chien, K. D. Closser, D. L. Crittenden, M. Diedenhofen, R. A. D. Jr., H. Do, A. D. Dutoi, R. G. Edgar, S. Fatehi, L. Fusti-Molnar, A. Ghysels, A. Golubeva-Zadorozhnaya, J. Gomes, M. W. Hanson-Heine, P. H. Harbach, A. W. Hauser, E. G. Hohenstein, Z. C. Holden, T.-C. Jagau, H. Ji, B. Kaduk, K. Khistyayev, J. Kim, J. Kim, R. A. King, P. Klunzinger, D. Kosenkov, T. Kowalczyk, C. M. Krauter, K. U. Lao, A. D. Laurent, K. V. Lawler, S. V. Levchenko, C. Y. Lin, F. Liu, E. Livshits, R. C. Lochan, A. Luenser, P. Manohar, S. F. Manzer, S.-P. Mao, N. Mardirossian, A. V. Marenich, S. A. Maurer, N. J. Mayhall, E. Neuscamman, C. M. Oana, R. Olivares-Amaya, D. P. O'Neill, J. A. Parkhill, T. M. Perrine, R. Peverati, A. Prociuk, D. R. Rehn, E. Rosta, N. J. Russ, S. M. Sharada, S. Sharma, D. W. Small, A. Sodt, T. Stein, D. Stück, Y.-C. Su, A. J. Thom, T. Tsuchimochi, V. Vanovschi, L. Vogt, O. Vydrov, T. Wang, M. A. Watson, J. Wenzel, A. White, C. F. Williams, J. Yang, S. Yeganeh, S. R. Yost, Z.-Q. You, I. Y. Zhang, X. Zhang, Y. Zhao, B. R. Brooks, G. K. Chan, D. M. Chipman, C. J. Cramer, W. A. G. III, M. S. Gordon, W. J. Hehre, A. Klamt, H. F. S. III, M. W. Schmidt, C. D. Sherrill, D. G. Truhlar, A. Warshel, X. Xu, A. Aspuru-Guzik, R. Baer, A. T. Bell, N. A. Besley, J.-D. Chai, A. Dreuw, B. D. Dunietz, T. R. Furlani, S. R. Gwaltney, C.-P. Hsu, Y. Jung, J. Kong, D. S. Lambrecht, W. Liang, C. Ochsenfeld, V. A. Rassolov, L. V. Slipchenko, J. E. Subotnik, T. V. Voorhis, J. M. Herbert, A. I. Krylov, P. M. Gill, and M. Head-Gordon, *Advances in molecular quantum chemistry contained in the q-chem 4 program package*, *Molecular Physics* **113**, 184 (2015).

Publication 4

A meta-Generalized Gradient Approximation that describes weak interactions in addition to bond energies and band gaps

submitted on December 10, 2024

Timo Lebeda and Stephan Kümmel

Theoretical Physics IV, University of Bayreuth, 95440 Bayreuth, Germany

Publ. 4

Author contributions

TL and SK conceptualized the work. TL performed the research, wrote the required routines, ran the calculations, and analyzed the results. TL wrote the first draft of the manuscript. TL and SK worked out the final manuscript.

Publ.4

A meta-Generalized Gradient Approximation that describes weak interactions in addition to bond energies and band gaps

Timo Lebeda* and Stephan Kümmel†

Theoretical Physics IV, University of Bayreuth, 95440 Bayreuth, Germany

We show that the recently proposed Lebeda-Aschebrock-Kümmel (LAK) meta-generalized gradient approximation, the accuracy of which was previously established for atomization energies, bond lengths, and band gaps, also captures weak interactions near equilibrium without a dispersion correction. We discuss how this is achieved. Furthermore, we show that among the semilocal cost pure functionals, LAK is the one that reaches the highest accuracy for the large GMTKN55 database for general thermochemistry and kinetics. Next, we explain the design strategy of enhancement factor engineering. Its key idea is to complement exact constraints with construction principles. Finally, we discuss areas of research in which the use of LAK may offer advantages over existing functionals.

I. INTRODUCTION

For modeling real materials, weak interactions are of considerable importance. In the realm of soft materials, e.g., biological systems, at interfaces, and surfaces, the accurate description of both covalent binding and weak interactions is essential [1]. As such systems typically also comprise a large number of atoms, computational efficiency becomes a critical aspect.

Its attractive balance between computational accuracy and computational cost made density functional theory (DFT) the workhorse of electronic structure theory. Regarding weak interactions, however, there is a long-standing debate whether ground-state exchange-correlation approximations can and should capture weak interactions [1–15]. In principle, the situation is clear: The exact exchange-correlation functional correctly describes all electron-electron interactions, and thus also weak interactions. However, early and common approximations to the exact functional, such as the local density approximation (LDA), the generalized gradient approximation (GGA), and exact (Hartree-Fock) exchange poorly describe weak interactions. Therefore, these methods are typically combined with additional methods for the explicit treatment of dispersion effects, such as nonlocal density-based functionals [16–18] or a posteriori dispersion corrections [19–23]. An alternative are fully nonlocal functionals, e.g., based on the random phase approximation [24, 25]. While conceptually satisfying, they usually come at a steeply increased computational cost.

In this paper we focus on the computationally most efficient exchange-correlation approximations, i.e., the class of semilocal density functionals. The capability of meta-generalized gradient approximations (meta-GGAs) to describe noncovalent interactions [26] has been attributed to their ability to discriminate between covalent and dispersion interactions through their kinetic energy dependence [27]. Thus, in contrast to the LDA and

GGA, the description of dispersion interactions in meta-GGAs can be based on systematic concepts, as meta-GGAs can describe both covalent and dispersive interactions by "seeing" and responding adequately to the different bonding types [27, 28]. This allows for an accurate description of short- and intermediate-range van der Waals interactions [13, 29]. Of course, semilocal density functionals can not capture the long-range $-C_6/R^6$ decay of the van der Waals attraction that exists even for non-overlapping electron densities [23, 30, 31]. In case an accurate description of noncovalent interactions far from equilibrium is important, meta-GGAs that include short- and intermediate-range van der Waals interactions can still benefit from a long-range dispersion correction [12], as is well-known from the many successes of dispersion-corrected DFT.

While some authors argue that a proper density functional approximation should not contain *any* dispersion interaction and dispersion should only be captured by a dispersion correction [9, 14], many of the frequently and successfully used density functionals today either capture the short- and intermediate-range part of the dispersion interaction [13, 29] and are corrected for the long-range part if necessary [12, 32], or the density functional is directly designed together with its dispersion correction [33–35]. However, from a fundamental perspective, as well as for practical computations, it is desirable to have the density functional itself treat dispersion interactions as well as possible, just like the exact functional would do.

Here, we show that the recent nonempirical Lebeda-Aschebrock-Kümmel (LAK) meta-GGA [36] captures noncovalent interactions near equilibrium remarkably well. In this article we rationalize this property of the functional by working out what is decisive for the description of weak interactions in meta-GGAs. Furthermore, we assess LAK on the large GMTKN55 database for thermochemistry, kinetics, and noncovalent interactions [37]. The results show that LAK is the best pure, semilocal cost density functional on GMTKN55, where pure means without an additional dispersion correction. This demonstrates that LAK manages to describe both covalent and noncovalent interactions with good accuracy

* timo.lebeda@uni-bayreuth.de

† stephan.kuemmel@uni-bayreuth.de

from pure DFT. Finally, we discuss the general performance of LAK and outline areas where we consider LAK a possible improvement upon existing functionals.

II. LAK FOR NONCOVALENT BINDING

We start by directly assessing the LAK functional for a paradigm situation of weak interaction, the binding energy curves of rare gas dimers. Figure 1 shows that LAK captures the van der Waals attraction of rare gas dimers near the equilibrium bond length quite reasonably, and in particularly so for the often challenging heavier atoms. In Figure 1, we compare the binding curves of Ne_2 , Ar_2 , Kr_2 , and Xe_2 for the GGA PBE [38] and the meta-GGAs SCAN [39], M06-L [26], TASK [40], and LAK [36] with highly accurate CCSDT reference data [41–44]. Rare gas dimers are well-established model systems for van der Waals interactions [6–8, 10, 31, 45–53] because, firstly, dispersion interactions are the only source of attraction between rare gas atoms and, secondly, highly accurate reference data is available for these systems. We compare LAK with PBE, SCAN, and TASK exchange plus LDA correlation (in the parametrization of Perdew and Wang [54]) because they all share the same nonempirical construction philosophy. Additionally, we compare to M06-L [26], because it was the first semilocal density functional for which the capture of noncovalent interactions was systematically explained [27].

All DFT results in this section are obtained from self-consistent all-electron calculations in ADF [55, 56] using the QZ4P basis set, the setting “excellent” numerical accuracy and a radial grid boost of 3. These extremely fine numerical settings are required to avoid oscillations in the M06-L binding curves [50], and we adopt them for all functionals. However, we should point out that the numerical properties of meta-GGAs depend very much on the details of the construction, and while some meta-GGA are numerically cumbersome, others are as benevolent as GGAs [36, 40, 57, 58].

Figure 1 summarizes the well-known behavior of PBE, M06-L, and SCAN: PBE, while still rather accurate for the Ne_2 binding curve, increasingly underestimates the binding with increasing atomic mass. M06-L predicts similar binding curves as PBE for Ar_2 and Kr_2 , but its binding strength relative to PBE increases with the atomic mass. SCAN improves over PBE and M06-L for all systems except Ne_2 , predicting a larger binding energy near equilibrium and much more accurate equilibrium bond lengths. However, while SCAN is reasonably accurate for the argon dimer, it increasingly underestimates the binding energy with increasing atomic mass, similar to PBE. This might be due to the use of the compressed argon dimer as one of the “appropriate norms” in the construction of SCAN.

LAK and TASK, whose exchange enhancement factors look formally similar to each other and share the same realization of the gradient expansion of exchange, pre-

dict decisively different binding curves: LAK, on the one hand, predicts reasonable binding curves and is remarkably accurate even for the xenon dimer. TASK, on the other hand, predicts no binding at all (or only minimal binding at about twice the CCSDT bond length) and is even more repulsive than exact exchange. This broad spectrum of predictions for weakly bound systems illustrates the delicate sensitivity of the description of weak interactions on details of the meta-GGA construction.

III. RATIONALIZING NONCOVALENT INTERACTIONS IN META-GGAS

In the following we take a look at how meta-GGAs acquire their sensitivity to noncovalent interactions. Nonempirical meta-GGAs often use the iso-orbital indicator

$$\alpha = \frac{\tau - \tau^W}{\tau^{\text{unif}}} \quad (1)$$

with the kinetic energy density $\tau = \frac{1}{2} \sum_{j=1}^N |\nabla \varphi_j|^2$, its uniform electron gas limit $\tau^{\text{unif}} = (3/10)(3\pi^2)^{2/3} n^{5/3}$, and its iso-orbital limit $\tau^W = |\nabla n|^2 / (8n)$. Here, $\{\phi_j\}$ denote the (generalized) Kohn-Sham orbitals, $n = \sum_{j=1}^N |\phi_j|^2$ is the electron density, and we use atomic units throughout. Since we only consider spin-unpolarized systems in this section, we suppress spin indices in the notation.

Using α as the kinetic energy dependent variable has the advantage that it can discriminate between iso-orbital regions ($\alpha = 0$), uniform densities ($\alpha = 1$), and regions of density overlap between closed shells ($\alpha \gg 1$) [28]. Consequently, covalent bonds have small α at the middle of the bond, whereas dispersive bonds have large α .

Besides n and α , the exchange energy of a meta-GGA depends on the reduced density gradient $s = |\nabla n| / [2(3\pi^2)^{1/3} n^{4/3}]$ in the form

$$E_x[n] = A_x \int n^{4/3} F_x(s, \alpha) d^3r, \quad (2)$$

where the exchange enhancement factor F_x is the local enhancement of the exchange energy density over the exchange energy density of a uniform electron gas, $e_x^{\text{unif}} = A_x n^{4/3}$ with $A_x = -(3/4)(3/\pi)^{1/3}$. Consequently, regions of $F_x > 1$ correspond to a locally enhanced exchange energy density and are energetically favored, whereas regions of $F_x < 1$ correspond to a lower local exchange energy density and are energetically suppressed. Similarly, the enhancement factor of exchange and correlation together, F_{xc} , is defined by

$$E_{xc}[n] = A_x \int n^{4/3} F_{xc}(r_s, s, \alpha) d^3r, \quad (3)$$

with the Wigner-Seitz radius $r_s = (4\pi n/3)^{-1/3}$.

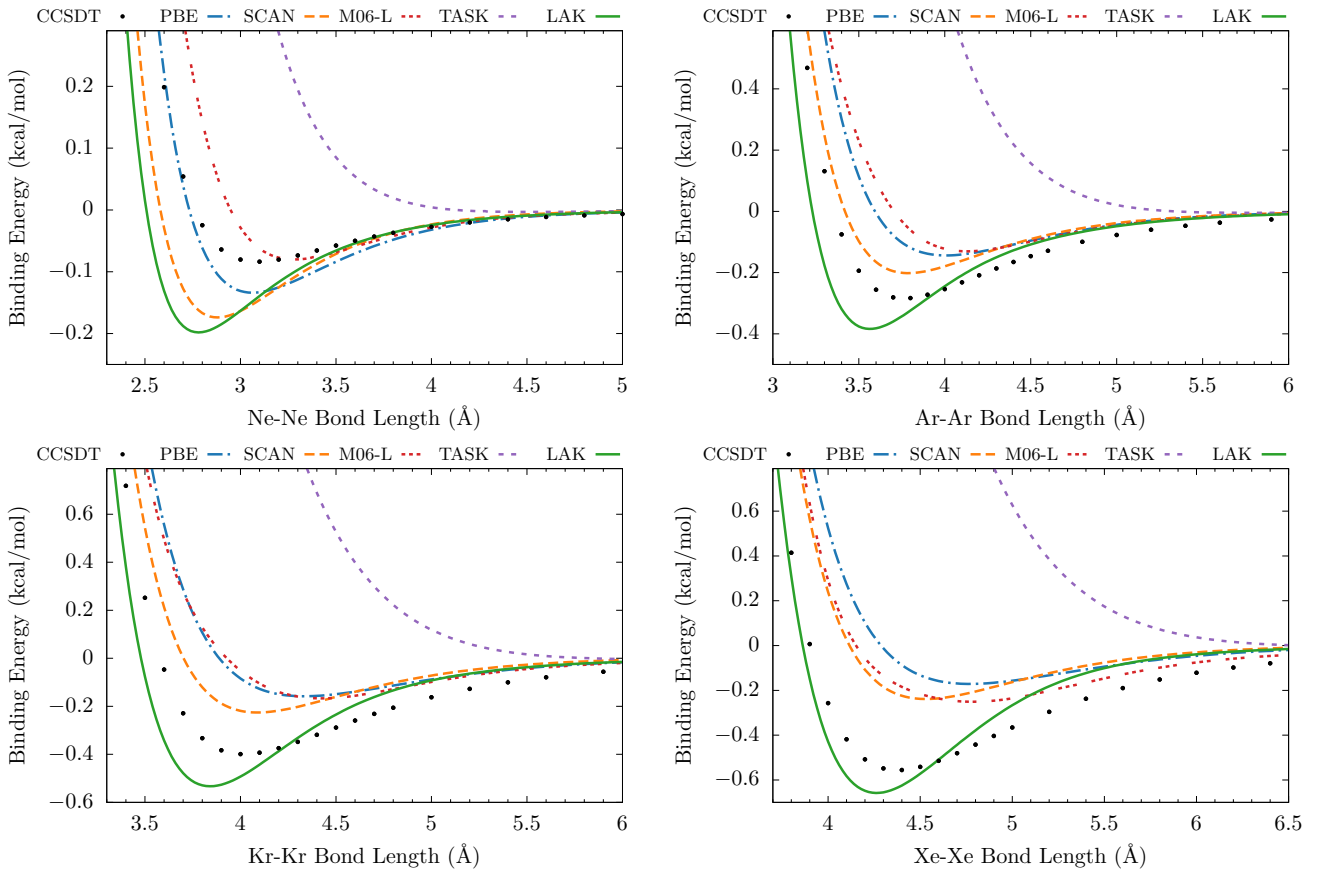


FIG. 1. Rare gas dimer binding curves of LAK compared to selected semilocal density functionals and CCSDT reference values [41–44].

The mechanisms of how and to what extent GGAs can model noncovalent interactions have been discussed in the Literature [3, 45, 59–61]. However, little is known for meta-GGAs. While the ability of α to recognize regions of noncovalent bonds is well-established [27, 28], the influence of α on the description of noncovalent interactions is not yet clear [62]. Thus, to understand noncovalent interactions in meta-GGAs, especially with respect to the α -dependence, we compare the (exchange) enhancement factors of SCAN, TASK, and LAK in Figure 2. For the sake of transparency we first base the following arguments on only the exchange part of the functionals, but it is clear that only exchange and correlation together provide the correct description of weak bonds. Figure 2a shows F_x^{SCAN} , F_x^{TASK} , and F_x^{LAK} (all scaled by a factor of 10) along the bond axis z of the argon dimer at the experimental equilibrium bond length 3.758 Å [63] (solid lines) and the argon atom (dotted lines). Each enhancement factor is obtained from a self-consistent all-electron calculation with the respective functional in the DARSEC code [64, 65], a real-space code for diatomic molecules and atoms. Additionally, we show r_s and the meta-GGA ingredients s and α , as obtained from the calculation with LAK. As discussed above, α becomes zero in single-

orbital regions and thus at the position of the nucleus, whereas it becomes large in regions of density overlap between closed shells such as at the bond center of Ar_2 and in the asymptotic tail of the density far from the nucleus. The gradient of the density, and thus also s , vanishes at the bond center. Except for the binding region, s and α are undistinguishable for the atom and the dimer. Therefore, the same holds for the enhancement factors.

Figure 2b shows the exchange enhancement factors F_x^{SCAN} , F_x^{TASK} , and F_x^{LAK} as functions of s for $\alpha = 0$, $\alpha = 1$, and $\alpha \rightarrow \infty$. All three enhancement factors share the same limit for $\alpha = 0$. Additionally, all three functionals share the same asymptotic decay as $s^{-1/2}$ for $s \rightarrow \infty$. Therefore, all three enhancement factors are very similar for the asymptotic tail of the density, especially LAK and TASK, compare the large z limit of Figure 2a. Because the enhancement factors of LAK and TASK therefore only show significant differences both between each other and between atom and molecule in the binding region, the decisively different binding behavior of LAK and TASK for rare gas dimers must be due to their different behavior in this region. Figure 2c therefore shows a version of Figure 2a zoomed in on the binding region.

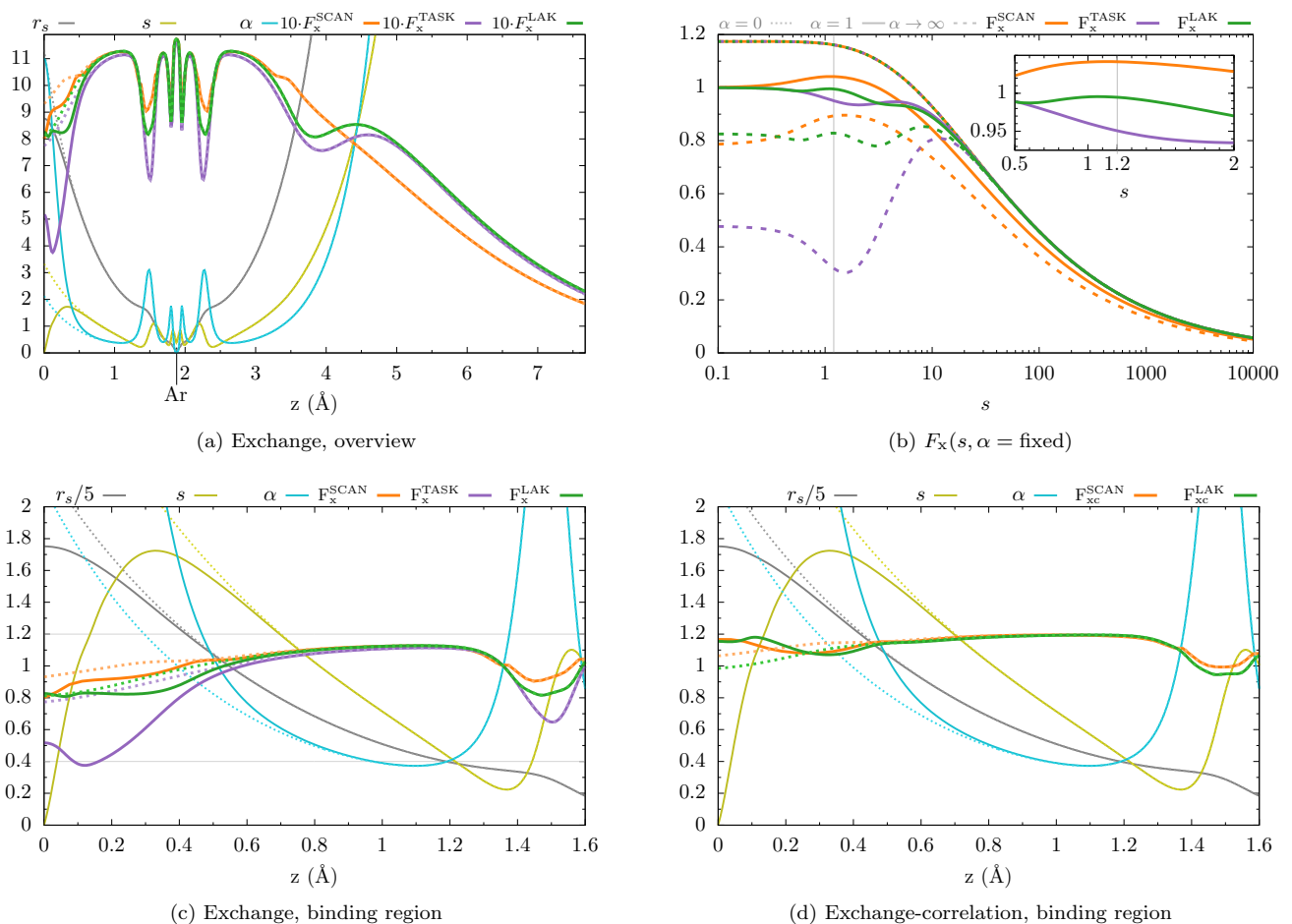


FIG. 2. (a), (c), and (d): Enhancement factors of SCAN, TASK, and LAK along the bond axis z of the argon dimer at equilibrium distance (solid lines) and for the argon atom (dotted lines). The position of the nuclei is -1.879 \AA and 1.879 \AA for the dimer and 1.879 \AA for the atom. The horizontal gray lines in (c) mark $\alpha = 0.4$ and $s = 1.2$. (b): Exchange enhancement factors of SCAN, TASK, and LAK as functions of the reduced density gradient s for $\alpha = 0$ (dotted), $\alpha = 1$ (solid), $\alpha \rightarrow \infty$ (dashed). The vertical gray lines mark $s = 1.2$. Since all three exchange enhancement factors are equivalent for $\alpha = 0$, the lines for $\alpha = 0$ coincide.

Since the binding region is only present in the dimer, s and α in this region differ decisively between atom and dimer. In fact, starting from the nucleus, first α becomes different at $\alpha \approx 0.4$, rising much faster for the dimer due to the increased density overlap between the two atoms. Slightly closer to the center of the bond, also s starts to differ. Starting from $s \approx 1.2$, the reduced density gradient of the atom increases faster than that of the dimer. In the latter, s reaches a peak value of $s \approx 1.7$, begins to decrease and eventually becomes zero at the center of the bond. Thus, regions of $s \lesssim 1.2$ are more energetically relevant in the dimer, whereas regions of $s \gtrsim 1.2$ are more energetically relevant in the atom. This finding is in line with the analysis of Jenkins and coworkers [60, 61], which showed that in GGAs regions with $\partial F_x / \partial s > 0$ contribute attractively to the binding if $s \lesssim 1.2$ and repulsively if $s \gtrsim 1.2$. Consequently, semilocal density functionals predict a stronger binding

of weakly interacting systems if they have a local maximum in s near $s = 1.2$. Our results are further consistent with Ref. 13, where the authors point out that inflection points in the s -dependence of the enhancement factor are important for the description of weakly interacting systems. Ultimately, these insights have been the basis of the second construction principle of LAK [36].

Additionally, Figure 2c clarifies the situation regarding the α -dependence, as it suggests a similar criterion for α : regions of $\partial F_x / \partial \alpha > 0$ contribute attractively to the exchange binding for $\alpha \gtrsim 0.4$, because they energetically favor the dimer [66]. It is questionable if the α -dependence for $\alpha \lesssim 0.4$ plays any role at all for the binding, because, except for the core region, α rarely becomes smaller than 0.4 in both the argon atom and dimer.

Inspection of Figure 2b shows that F_x^{LAK} has a local maximum at $s = 1.2$ for the relevant values of $\alpha > 0.4$, while F_x^{SCAN} has a local maximum and F_x^{TASK} a lo-

cal minimum at slightly larger reduced density gradients. While the local maxima of SCAN and LAK are attractive, the local minimum of TASK is repulsive. Additionally, all three enhancement factors decrease with α [36, 67] and this decrease is much more pronounced in LAK and TASK than in SCAN (this essentially reflects the construction principle of TASK and construction principle one of LAK). Thus, the α -dependence of all three functionals contributes repulsively. Especially for $\alpha > 1$, $\partial F_x/\partial\alpha$ of TASK is clearly the most negative, as can be seen by comparing SCAN, TASK, and LAK for $\alpha = 1$ and $\alpha \rightarrow \infty$ in Figure 2b. As a result, TASK acts extremely repulsively, since both its s - and its α -dependence are strongly repulsive and F_x^{TASK} is therefore significantly smaller in the dimer around the center of the bond. Consequently, TASK penalizes the bond energetically and avoids the accumulation of density between the two closed-shell systems.

SCAN and LAK have a more balanced binding behavior. This is reflected in Figure 2c in the fact that F_x^{TASK} is much smaller in the dimer near the bond center of the dimer than in the corresponding distance from the nucleus of the single atom, whereas there is almost no difference for F_x^{SCAN} and only a small difference for F_x^{LAK} . Although this makes LAK exchange and SCAN exchange significantly less repulsive than TASK exchange, neither just by itself predicts binding at the equilibrium distance. Instead, only the inclusion of the correlation parts in LAK and SCAN leads to the appropriate binding. Therefore, we now extend the analysis to exchange and correlation together in Figure 2d. For exchange and correlation together, the differences between SCAN and LAK are much smaller than for their exchange parts alone. This is because, on the one hand, SCAN is constructed such that all its derivatives with respect to α vanish at $\alpha = 1$, giving rise to small kinks in $F_x^{\text{SCAN}}(z)$ and $F_{xc}^{\text{SCAN}}(z)$ whenever $\alpha = 1$. LAK correlation, on the other hand, counteracts the α -dependence of exchange (a condition required for the expected signs of the exchange and correlation contributions to the derivative discontinuity [58]) and therefore increases the binding of the argon dimer.

Our results regarding the s -dependence might seem to be in conflict with earlier studies that argue that for GGAs the large-gradient behavior of exchange would be decisive for the description of weakly interacting systems [3, 10, 14, 45, 59, 68]. However, our results are in line with other studies [7, 31] that attributed the above-mentioned finding to the fact that the small-gradient behavior of GGAs is typically determined by the gradient expansion and therefore usually very similar. Thus, the description of *weak* interactions in GGAs can be modified by their behavior for large s . Meta-GGAs, on the other hand, provide an additional degree of freedom in the gradient expansion, allowing a much greater variety of small s behaviors to be compatible with the gradient expansion [36]. Therefore, the actually dominant influence of s around 1.2 [60, 61] becomes more important in meta-GGAs.

In summary, our analyses for the argon dimer con-

firm the findings of Refs. 13, 60, and 61: Local maxima and inflection points in the s -dependence of the enhancement factor are decisive for correctly describing weakly interacting systems with semilocal DFT. More precisely, $\partial F_{xc}/\partial s > 0$ increases the binding if $s \lesssim 1.2$ and decreases the binding if $s \gtrsim 1.2$. Furthermore, our analyses suggest a similar criterion for α : $\partial F_{xc}/\partial\alpha < 0$ for $\alpha \gtrsim 0.4$ decreases the binding of weakly interacting systems.

IV. LAK FOR GENERAL THERMOCHEMISTRY

We are aware that good results for the rare gas binding curves do not guarantee good results for dispersion interactions in general, in particular for organic and biological systems [31]. Moreover, good results for dispersion interactions alone are not sufficient in typical applications, but the accurate description of both, noncovalent and covalent interactions is important. To this end, we test LAK on the large GMTKN55 (General Main-group Thermochemistry, Kinetics, and Noncovalent interactions) database [37].

The GMTKN55 database includes basic properties and reaction energies of small molecules, reaction energies for large systems and isomerization reactions, barrier heights, and inter- and intramolecular noncovalent interactions. To make these different quantities comparable, density functionals are typically benchmarked on GMTKN55 using the weighted total mean absolute deviation WTMAD-2 [69]. Table I summarizes the WTMAD-2 of several nonempirical semilocal density functionals, including LAK and the best-performing dispersion corrected semilocal density functionals for the GMTKN55 database and its subcategories. We have not included TASK in Table I because TASK is not particularly well suited for the description of energetic bonds [40, 70] and, as explained above, noncovalent interactions (WTMAD-2 of 48.24 kcal/mol). The results for the pure density functionals, i.e., density functionals without additional dispersion correction, were obtained from fully self-consistent all-electron calculations in ADF [55, 56]. We use the QZ4P basis set except for the anions in the GMTKN55 database, which require more diffuse basis functions. Therefore, we use the AUG/ATZ2P augmented basis set for all anions. We ensure benchmarking accuracy by using excellent numerical accuracy and a radial grid boost of 3. Our results for PBE and SCAN are in line with those of Ref. 37, given that a different code is used. The results for the dispersion corrected methods are from the Literature. The detailed data for all subsets is provided in the Supplemental Material [71].

It is worth noting that both LAK and TASK did not show any convergence issues for any of the 2462 single-point calculations of the GMTKN55 database. The numerical stability of LAK and TASK is supported by recent findings [36, 57, 70, 72, 73], and is in contrast to the often-cited convergence issues of several other popular

meta-GGAs [50, 57]. Regarding convergence with respect to the numerical settings, e.g., the number of grid points, however, LAK is often more challenging than TASK and r2SCAN. Nevertheless, also in this respect LAK converges faster than M06-L and SCAN and does not show any artificial oscillations [36]. Investigating what makes a meta-GGA numerically stable is a further worthwhile task for future work.

Table I reveals a central result of this work. It shows that LAK is, to the best of the authors’ knowledge, the best-performing pure semilocal density functional on the GMTKN55 database. In Ref. 37 from 2017, a large number of density functionals were tested on GMTKN55, and the best-performing semilocal density functionals were M06-L (WTMAD-2 of 8.67 kcal/mol) and SCAN (8.72 kcal/mol). To the best of our knowledge, r2SCAN with a WTMAD-2 of 8.49 kcal/mol is the only semilocal density functional that has been able to surpass this value since then. LAK improves this with a WTMAD-2 of 7.77 kcal/mol.

Taking a look at the subcategories of GMTKN55 in Figure 3 reveals that LAK achieves this improvement by matching the accuracy of r2SCAN for the covalent interactions of small and large molecules, while improving upon r2SCAN for barrier heights and noncovalent interactions.

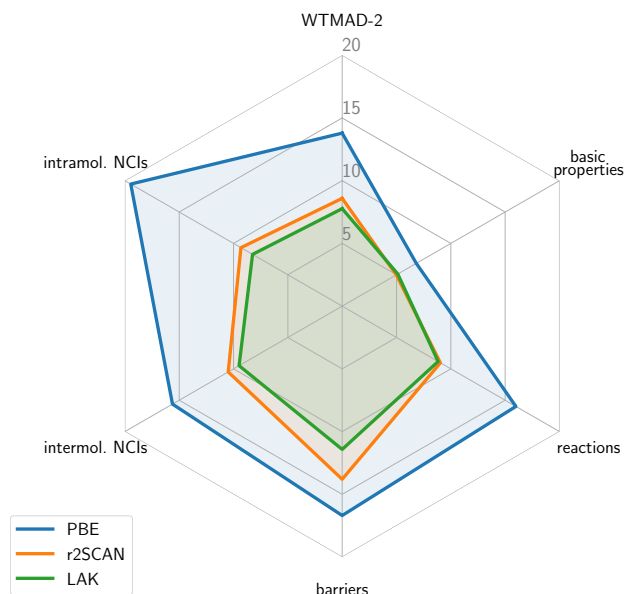


FIG. 3. WTMAD-2 in kcal/mol for the GMTKN55 database and its subcategories for selected nonempirical semilocal density functionals: the GGA PBE, the meta-GGA r2SCAN, and the meta-GGA LAK.

LAK reaches an accuracy that is comparable even to the best dispersion-corrected semilocal density functionals for GMTKN55, and is more accurate than all dispersion-corrected semilocal density functionals reported in Ref. 37. Only SCAN-D3 with an WTMAD-2 of

7.86 reaches a similar accuracy as LAK. Since 2017, only r2SCAN-D4 [74] with a WTMAD-2 of 7.54 kcal/mol, and the semi-empirical B97M-V [34] with a WTMAD-2 of 5.46 kcal/mol [75] (and their respective r2SCAN+rVV10 [76], r2SCAN-3c [77], B97M-D3, and B97M-D4 [78] variants) have improved upon SCAN-D3. Figure 3 compares LAK with the best-performing dispersion-corrected semilocal methods B97M-V and r2SCAN-D4. While LAK and r2SCAN are on par for the WTMAD-2 database as a whole, their performance for the subcategories differs. While LAK is more accurate for the barrier heights, r2SCAN-D4 is more accurate for the noncovalent interactions. The latter finding is expected, as the parameters of the D4 dispersion correction of r2SCAN-D4 are fitted to subsets of GMTKN55 for noncovalent interactions, whereas LAK is a nonempirical pure density functional.

B97M-V shows a significant improvement over LAK and r2SCAN-D4 for all quantities except for the reaction energies and for the intramolecular noncovalent interactions of r2SCAN-D4. Given that B97M-V is constructed semi-empirically based on parts of the GMTKN55 database, this is not too surprising. Nevertheless, the amount of improvement indicates that the additional flexibility of the combined approach of B97M-V, namely designing the semilocal density functional together with a dispersion correction [33, 34], can yield improved results for thermochemistry and kinetics. A nonempirical meta-GGA based on a partitioning of the gradient expansion similar to LAK, but designed together with a dispersion correction, and consequently most likely therefore dropping the second construction principle of LAK, thus represents an interesting target for future research.

It is worth looking at two specific subsets of the GMTKN55. The major shortcoming of semilocal density functionals is their fundamental inability to fully cancel the Hartree self-energy. This can be seen from the SIE4x4 set of self-interaction error related problems, for which LAK has a mean absolute deviation (MAD) of 17.29 kcal/mol, r2SCAN of 17.90 kcal/mol, and M06-L of 17.94 kcal/mol. This indicates that LAK improves only marginally upon other popular meta-GGAs for self-interaction problems. Another noteworthy subset is the MB16-43 set of decomposition energies of artificial molecules [79]. Due to its “mindless” design, it can serve as an indicator of the transferability of a density functional to novel chemistry [80]. It is often reported that nonempirical density functionals are more transferable than empirical ones, and their respective performance on MB16-43 supports this view [74, 77]: While the MADs of the empirical M06-L (64.05 kcal/mol) and the semi-empirical B97M-V (35.35 kcal/mol [75]) are high, the nonempirical functionals PBE (23.34 kcal/mol), SCAN (15.74 kcal/mol), and r2SCAN (12.83 kcal/mol) are systematically and significantly more accurate for MB16-43. LAK has a MAD of 16.36 kcal/mol on MB16-43, similar to the MAD of SCAN, emphasizing its nonempirical

TABLE I. WTMAD-2 in kcal/mol for the GMTKN55 database [37] and its subcategories. Upper half of the table: Nonempirical semilocal density functionals; data from this work. Lower half of the table: Semilocal density functionals with dispersion correction optimized for (parts of) GMTKN55; data from the Literature. The Supplemental Material [71] reports the error statistics for the subsets of GMTKN55.

	Basic	Large	BHs	Intermol. NCIs	Intramol. NCIs	All NCIs	GMTKN55
PBE	6.82	15.99	16.69	15.62	19.46	17.50	13.79
SCAN	5.28	8.76	14.88	10.24	8.20	9.24	8.65
r2SCAN	4.98	9.04	13.80	10.49	8.10	9.32	8.49
LAK	5.12	8.83	11.42	9.49	6.95	8.25	7.77
SCAN-D3 [37]	5.31	7.86	14.94	8.50	6.61	7.58	7.86
r2SCAN-D4 [74]	5.55	8.26	14.29	7.46	5.74	6.62	7.54
B97M-V [75]	3.68	9.30	7.52	3.56	5.76	4.64	5.46

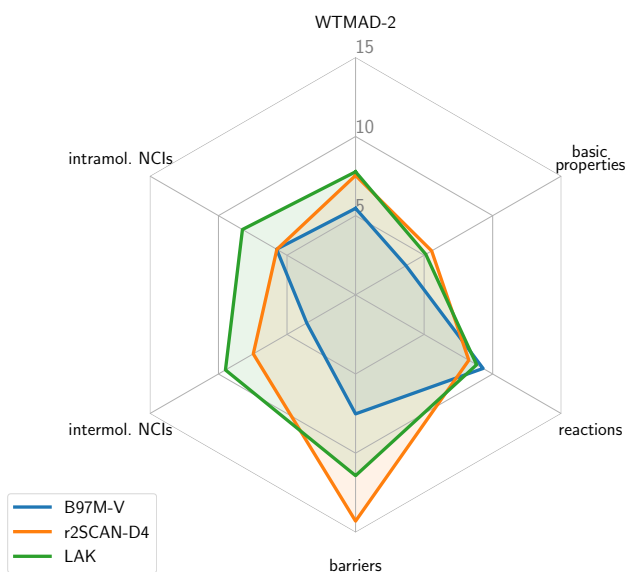


FIG. 4. WTMAD-2 in kcal/mol for the GMTKN55 database and its subcategories: LAK compared with the best-performing dispersion-corrected semilocal functionals B97M-V and r2SCAN-D4.

nature and suggesting a similar transferability to novel chemistry as SCAN. Finally, it is worth to mention that compared to other semilocal-cost functionals, LAK has the additional advantage of considerably improving the prediction of band gaps, as detailed in Ref. 36.

V. ENHANCEMENT FACTOR ENGINEERING: DENSITY FUNCTIONALS BASED ON INSIGHTS FROM MATHEMATICS, PHYSICS, AND CHEMISTRY

In the construction of LAK [36], we extended the successful design strategy for nonempirical density functionals (e.g. Refs. [38–40, 81–84]) of combining exact con-

straints with exactness for model systems, so-called appropriate norms, by the further nonempirical concept of construction principles. In the following we explain the idea behind this strategy of designing exchange-correlation functionals.

A semilocal exchange-correlation functional, and thus the approximation to all electron-electron interactions, is completely defined by its enhancement factor. On the one hand, the exact constraints and model systems restrict the enhancement factor through inequalities, scaling relations, and exact limits [84]. On the other hand, the degree of nonlocality of a density functional depends to a large extent on the details of its enhancement factor in between these limits. However, the exact constraints and model systems provide only limited information on how the enhancement factor should be modeled in this intermediate range. Therefore, the construction principles guide the enhancement factor in the intermediate range to ensure proper nonlocality. In the case of LAK, these are the ultranonlocality associated with the derivative discontinuity and the short- and intermediate-range van der Waals interactions.

Importantly, we consider the *graph* of the enhancement factor the decisive property that should be obtained in a nonempirical fashion. The graph defines the enhancement factor and thus the density functional uniquely. Experience has shown that a lot of information about the performance of a functional can be obtained just from the graph [67]. Furthermore, all exact constraints, appropriate norms, and construction principles also apply to the graph. In addition, we aim for a smooth enhancement factor, a condition found to be important for more accurate densities and the numerical stability of density functional approximations [85]. Given these conditions, it is then up to us to find a suitable representation of the graph in terms of functions. While Occam’s razor advises us to find the simplest possible representation of the graph, it remains a mathematical problem to find functions that can generate this graph.

Following the argumentation above, the construction principles thus guide the graph of the enhancement factor in a range in which the graph was not previously

determined by physical reasons. In other words, the construction principles are additional conditions that tailor the choice of mathematical functions that satisfy the exact constraints and appropriate norms, based on chemical and physical insights. Because we design our functional via conditions on the graph of its enhancement factor, we call this design strategy “enhancement factor engineering”.

Notably, using a *limited* number of parameters to represent the graph can make it easier to find a suitable representation of the graph in terms of functions. We want to emphasize that the parameters introduced in this way are only a means to the end of representing the graph, and are therefore fundamentally different from parameters determined, e.g., by fitting to databases. Moreover, the use of too many parameters is prevented by the condition of a smooth enhancement factor. At this point, we want to emphasize that parameters in a method are not empirical per se, but that it depends on how they are fixed. If they are fixed by fitting to databases, they are empirical. In contrast, if they are fixed by mathematical constraints, we regard them as nonempirical. However, for a given enhancement factor, one can always find more general functions from which one can obtain this enhancement factor by fixing several parameters (e.g., quasi-trivially by setting them to zero or one) [86]. The *graph* of the enhancement factor, however, is independent of its parametrization and thus of any parameters.

The motivation for the design strategy of enhancement factor engineering emerges from the following considerations. From a mathematical point of view, we desire the enhancement factor to satisfy as many analytical conditions as possible that we know about from the exact exchange-correlation functional. This is achieved by adhering to the exact constraints. From a physical point of view, we additionally want the enhancement factor to be correct for certain model systems, such as the homogeneous electron gas. These are the appropriate norms. Finally, from a chemical point of view, we wish to include existing chemical intuition into the enhancement factor. From the authors’ point of view, taking into account existing knowledge about electronic structure or chemical intuition does not mean fitting parameters to large databases, but rather incorporating known facts about the electronic structure of certain types of systems into the design of the graph of the enhancement factor. This leads to the construction principles. In this sense, the strategy of enhancement factor engineering combines the insights from mathematics, physics, and chemistry.

VI. WHEN TO CHOOSE THE LAK EXCHANGE-CORRELATION FUNCTIONAL?

The zoo of density functionals is constantly growing and it is often hard to choose an appropriate functional for a given task. Therefore, we provide our current view of the advantages and disadvantages of LAK, and high-

light areas where LAK could be an attractive choice.

Figure 5 summarizes the performance of LAK reported in Ref. 36, complemented by the performance of LAK for the S22 set of weak interactions [87, 88]. As in Section II, we compare LAK with PBE, SCAN, and M06-L. However, due to its inadequacy with respect to weak interactions, we replace TASK with the range-separated hybrid HSE06 [89, 90], which has become the de-facto standard for DFT band structure prediction, and is therefore often used in materials simulations. The left-hand side shows the mean absolute deviation relative to the worst performing density functional in the respective category. LAK performs best or almost best for all properties except for the lattice constants. To estimate the importance of LAKs attractive accuracy for band gaps, covalent and weak interactions against its relatively less accurate lattice constants, we compare the mean absolute relative deviation from the reference values on the right-hand side of Figure 5. While the relative error in the lattice constants is below 2% for all tested functionals, LAK is the only functional that achieves relative errors of about 10% for band gaps and weak interactions. Although highly accurate lattice constants are critical in some applications, the broad spectrum of properties that LAK can accurately predict makes it an attractive choice for large-scale materials simulations that require high accuracy for a large variety of properties at low computational cost.

In the following, we highlight several areas where we consider LAK a possible improvement over existing density functionals by providing either higher accuracy at similar computational cost, or similar accuracy at strongly reduced computational cost. We write this at a time when LAK has not yet been tested extensively, i.e., the following statements are to be seen as “hopefully educated guesses”. Its balanced accuracy for band gaps and energetic binding together with its reasonable description of noncovalent interactions makes LAK a promising functional for surface and interface problems, as well as biological systems in which covalent and weak interactions play together. Last but not least, LAK (and equally well TASK for this task) can predict the band structure of semiconductors with a similar quality as HSE, but at a fraction of HSE’s computational cost [58].

VII. CODE AVAILABILITY STATEMENT

The LAK meta-GGA is available in AMS, in particular in ADF and BAND, (in the trunk and since AMS2025), as well as in VASP (since version 6.5.0).

ACKNOWLEDGMENTS

The authors thank Jianwei Sun for helpful discussions on the rare gas dimers. We appreciate financial support from the Deutsche Forschungsgemeinschaft, DFG projectnumber 457582427, from the Bavarian State Ministry

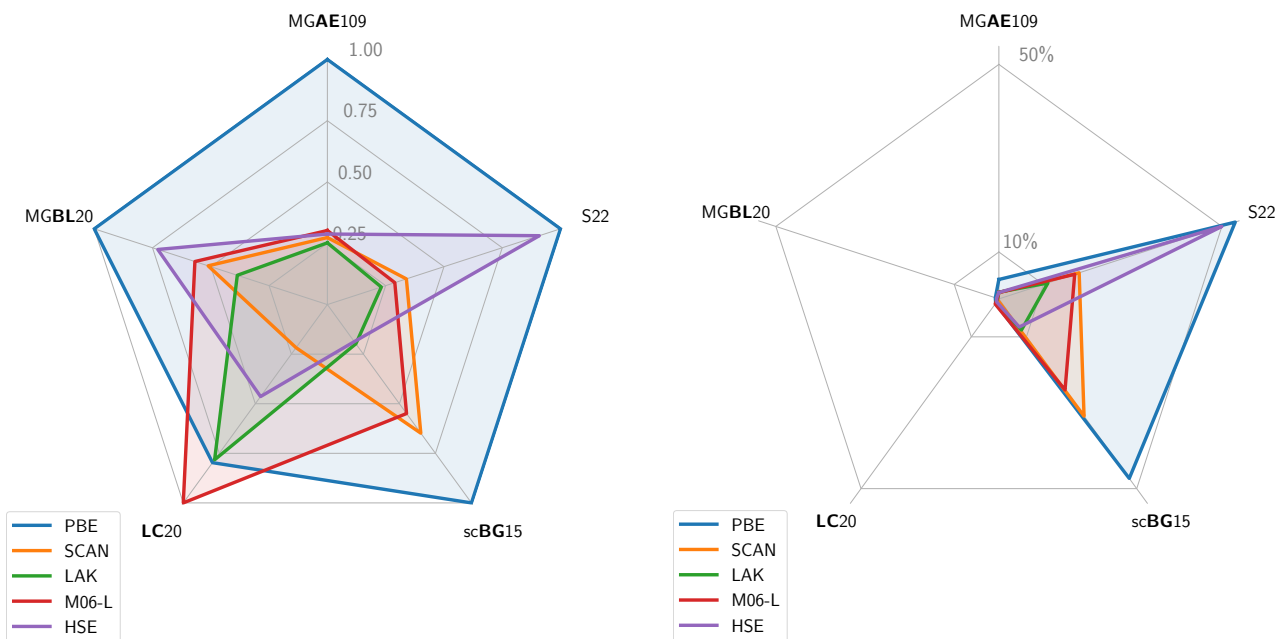


FIG. 5. General performance of selected density functionals for Main-Group Atomization energies (MGAE109) [91], Main-Group Bond Lengths (MGBL20) [92], Lattice Constants (LC20) [93], semi-conductor Band Gaps (scBG15) [36], and weak interactions (S22) [87, 88]. Left: MAD relative to the worst performing functional for each category. Right: mean absolute relative deviation from the reference values.

of Science, Research, and the Arts for the Collaborative Research Network “Solar Technologies go Hybrid”, and from the Elite Study Program “Biological Physics” of the Elite Network of Bavaria.

TL and SK conceptualized the work. TL performed

the research, wrote the required routines, ran the calculations, and analyzed the results. TL wrote the first draft of the manuscript. TL and SK worked out the final manuscript.

-
- [1] A. J. Cohen, P. Mori-Sánchez, and W. Yang, Challenges for density functional theory, *Chem. Rev.* **112**, 289 (2012).
 - [2] B. I. Lundqvist, Y. Andersson, H. Shao, S. Chan, and D. C. Langreth, Density functional theory including van der Waals forces, *Int. J. Quantum Chem.* **56**, 247 (1995).
 - [3] Y. Zhang, W. Pan, and W. Yang, Describing van der Waals Interaction in diatomic molecules with generalized gradient approximations: The role of the exchange functional, *J. Chem. Phys.* **107**, 7921 (1997).
 - [4] W. Kohn, Y. Meir, and D. E. Makarov, Van der Waals energies in density functional theory, *Phys. Rev. Lett.* **80**, 4153 (1998).
 - [5] M. Lein, J. F. Dobson, and E. K. U. Gross, Toward the description of van der Waals interactions within density functional theory, *J. Comput. Chem.* **20**, 12 (1999).
 - [6] T. Van Mourik and R. J. Gdanitz, A critical note on density functional theory studies on rare-gas dimers, *J. Chem. Phys.* **116**, 9620 (2002).
 - [7] J. Tao and J. P. Perdew, Test of a nonempirical density functional: Short-range part of the van der Waals interaction in rare-gas dimers, *J. Chem. Phys.* **122**, 114102 (2005).
 - [8] I. C. Gerber and J. G. Ángyán, London dispersion forces by range-separated hybrid density functional with second order perturbational corrections: The case of rare gas complexes, *J. Chem. Phys.* **126**, 044103 (2007).
 - [9] K. Pernal, R. Podeszwa, K. Patkowski, and K. Szalewicz, Dispersionless density functional theory, *Phys. Rev. Lett.* **103**, 263201 (2009).
 - [10] F. O. Kannemann and A. D. Becke, Van der Waals interactions in density-functional theory: Rare-gas diatomics, *J. Chem. Theory Comput.* **5**, 719 (2009).
 - [11] J. P. Perdew, J. Sun, R. M. Martin, and B. Delley, Semilocal density functionals and constraint satisfaction, *Int. J. Quantum Chem.* **116**, 847 (2016).
 - [12] H. Peng, Z.-H. Yang, J. P. Perdew, and J. Sun, Versatile van der Waals density functional based on a meta-generalized gradient approximation, *Phys. Rev. X* **6**, 041005 (2016).
 - [13] J. H. Yang, D. A. Kitchaev, and G. Ceder, Rationalizing accurate structure prediction in the meta-GGA SCAN functional, *Phys. Rev. B* **100**, 035132 (2019).
 - [14] A. J. A. Price, K. R. Bryenton, and E. R. Johnson, Requirements for an accurate dispersion-corrected density functional, *J. Chem. Phys.* **154**, 230902 (2021).
 - [15] K. R. Bryenton, A. A. Adeleke, S. G. Dale, and E. R.

- Johnson, Delocalization error: The greatest outstanding challenge in density-functional theory, *Wiley Interdiscip. Rev. Comput. Mol. Sci.* **13**, e1631 (2023).
- [16] M. Dion, H. Rydberg, E. Schröder, D. C. Langreth, and B. I. Lundqvist, Van der Waals density functional for general geometries, *Phys. Rev. Lett.* **92**, 246401 (2004); *Phys. Rev. Lett.* **95**, 109902 (2005).
- [17] O. A. Vydrov and T. Van Voorhis, Nonlocal van der Waals density functional: The simpler the better, *J. Chem. Phys.* **133**, 244103 (2010).
- [18] R. Sabatini, T. Gorni, and S. De Gironcoli, Nonlocal van der Waals density functional made simple and efficient, *Phys. Rev. B* **87**, 041108 (2013).
- [19] S. Grimme, Accurate description of van der Waals complexes by density functional theory including empirical corrections, *J. Comp. Chem.* **25**, 1463 (2004).
- [20] A. D. Becke and E. R. Johnson, A density-functional model of the dispersion interaction, *J. Chem. Phys.* **123**, 154101 (2005).
- [21] A. Tkatchenko and M. Scheffler, Accurate molecular Van der Waals interactions from ground-state electron density and free-atom reference data, *Phys. Rev. Lett.* **102**, 073005 (2009).
- [22] S. Grimme, Density functional theory with london dispersion corrections, *Wiley Interdiscip. Rev. Comput. Mol. Sci.* **1**, 211 (2011).
- [23] S. Grimme, A. Hansen, J. G. Brandenburg, and C. Bannwarth, Dispersion-corrected mean-field electronic structure methods, *Chem. Rev.* **116**, 5105 (2016).
- [24] H. Eshuis and F. Furche, A parameter-free density functional that works for noncovalent interactions, *J. Phys. Chem. Lett.* **2**, 983 (2011).
- [25] E. Trushin, A. Thierbach, and A. Görling, Toward chemical accuracy at low computational cost: Density-functional theory with σ -functionals for the correlation energy, *J. Chem. Phys.* **154**, 014104 (2021).
- [26] Y. Zhao and D. G. Truhlar, A new local density functional for main-group thermochemistry, transition metal bonding, thermochemical kinetics, and noncovalent interactions, *J. Chem. Phys.* **125**, 194101 (2006).
- [27] G. K. H. Madsen, L. Ferrighi, and B. Hammer, Treatment of layered structures using a semilocal meta-GGA density functional, *J. Phys. Chem. Lett.* **1**, 515 (2010).
- [28] J. Sun, B. Xiao, Y. Fang, R. Haunschuld, P. Hao, A. Ruzsinszky, G. I. Csonka, G. E. Scuseria, and J. P. Perdew, Density functionals that recognize covalent, metallic, and weak bonds, *Phys. Rev. Lett.* **111**, 106401 (2013).
- [29] J. Sun, R. C. Remsing, Y. Zhang, Z. Sun, A. Ruzsinszky, H. Peng, Z. Yang, A. Paul, U. Waghmare, X. Wu, *et al.*, Accurate first-principles structures and energies of diversely bonded systems from an efficient density functional, *Nat. Chem.* **8**, 831 (2016).
- [30] M. J. Allen and D. J. Tozer, Eigenvalues, integer discontinuities and nmr shielding constants in kohn-sham theory, *Mol. Phys.* **100**, 433 (2002).
- [31] A. Ruzsinszky, J. P. Perdew, and G. I. Csonka, Binding energy curves from nonempirical density functionals II. van der Waals bonds in rare-gas and alkaline-earth diatomics, *J. Phys. Chem. A* **109**, 11015 (2005).
- [32] A. Patra, J. E. Bates, J. Sun, and J. P. Perdew, Properties of real metallic surfaces: Effects of density functional semilocality and van der Waals nonlocality, *PNAS* **114**, E9188 (2017).
- [33] S. Grimme, Semiempirical gga-type density functional constructed with a long-range dispersion correction, *J. Comp. Chem.* **27**, 1787 (2006).
- [34] N. Mardirossian and M. Head-Gordon, Mapping the genome of meta-generalized gradient approximation density functionals: The search for B97M-V, *J. Chem. Phys.* **142**, 074111 (2015).
- [35] N. Mardirossian and M. Head-Gordon, ω B97M-V: A combinatorially optimized, range-separated hybrid, meta-GGA density functional with VV10 nonlocal correlation, *J. Chem. Phys.* **144**, 214110 (2016).
- [36] T. Lebeda, T. Aschebrock, and S. Kümmel, Balancing the contributions to the gradient expansion: Accurate binding and band gaps with a nonempirical Meta-GGA, *Phys. Rev. Lett.* **133**, 136402 (2024).
- [37] L. Goerigk, A. Hansen, C. Bauer, S. Ehrlich, A. Najibi, and S. Grimme, A look at the density functional theory zoo with the advanced GMTKN55 database for general main group thermochemistry, kinetics and noncovalent interactions, *Phys. Chem. Chem. Phys.* **19**, 32184 (2017).
- [38] J. P. Perdew, K. Burke, and M. Ernzerhof, Generalized gradient approximation made simple, *Phys. Rev. Lett.* **77**, 3865 (1996).
- [39] J. Sun, A. Ruzsinszky, and J. P. Perdew, Strongly constrained and appropriately normed semilocal density functional, *Phys. Rev. Lett.* **115**, 036402 (2015).
- [40] T. Aschebrock and S. Kümmel, Ultranonlocality and accurate band gaps from a meta-generalized gradient approximation, *Phys. Rev. Res.* **1**, 033082 (2019).
- [41] R. Hellmann, E. Bich, and E. Vogel, Ab initio potential energy curve for the neon atom pair and thermophysical properties of the dilute neon gas. i. neon-neon interatomic potential and rovibrational spectra, *Mol. Phys.* **106**, 133 (2008).
- [42] B. Jäger, R. Hellmann, E. Bich, and E. Vogel, Ab initio pair potential energy curve for the argon atom pair and thermophysical properties of the dilute argon gas. I. Argon-argon interatomic potential and rovibrational spectra, *Mol. Phys.* **107**, 2181 (2009).
- [43] B. Jäger, R. Hellmann, E. Bich, and E. Vogel, State-of-the-art ab initio potential energy curve for the krypton atom pair and thermophysical properties of dilute krypton gas, *J. Chem. Phys.* **144**, 114304 (2016).
- [44] R. Hellmann, B. Jäger, and E. Bich, State-of-the-art ab initio potential energy curve for the xenon atom pair and related spectroscopic and thermophysical properties, *J. Chem. Phys.* **147**, 034304 (2017).
- [45] D. J. Lacks and R. G. Gordon, Pair interactions of rare-gas atoms as a test of exchange-energy-density functionals in regions of large density gradients, *Phys. Rev. A* **47**, 4681 (1993).
- [46] D. C. Patton and M. R. Pederson, Application of the generalized-gradient approximation to rare-gas dimers, *Phys. Rev. A* **56**, R2495 (1997); *Phys. Rev. A* **71**, 019906 (2005).
- [47] D. C. Patton and M. R. Pederson, A theoretical study of rare-gas diatomic molecules with the generalized-gradient approximation to density functional theory, *Int. J. Quantum Chem.* **69**, 619 (1998).
- [48] E. R. Johnson, R. A. Wolkow, and G. A. DiLabio, Application of 25 density functionals to dispersion-bound homomolecular dimers, *Chem. Phys. Lett.* **394**, 334 (2004).
- [49] Y. Zhao and D. G. Truhlar, Comparative assessment of density functional methods for 3d transition-metal chem-

- istry, *J. Chem. Phys.* **124**, 224105 (2006).
- [50] E. R. Johnson, A. D. Becke, C. D. Sherrill, and G. A. DiLabio, Oscillations in meta-generalized-gradient approximation potential energy surfaces for dispersion-bound complexes, *J. Chem. Phys.* **131**, 034111 (2009).
- [51] K. E. Yousaf and E. N. Brothers, Applications of screened hybrid density functionals with empirical dispersion corrections to rare gas dimers and solids, *J. Chem. Theory Comput.* **6**, 864 (2010).
- [52] F. Tran and J. Hutter, Nonlocal van der Waals functionals: The case of rare-gas dimers and solids, *J. Chem. Phys.* **138**, 204103 (2013).
- [53] L. Goerigk, Treating London-dispersion effects with the latest Minnesota density functionals: problems and possible solutions, *J. Phys. Chem. Lett.* **6**, 3891 (2015).
- [54] J. P. Perdew and Y. Wang, Accurate and simple analytic representation of the electron-gas correlation energy, *Phys. Rev. B* **45**, 13244 (1992).
- [55] SCM, Theoretical Chemistry, Vrije Universiteit, Amsterdam, The Netherlands, *ADF 2023.104 (a modified version is used)* (2023).
- [56] G. te Velde, F. M. Bickelhaupt, E. J. Baerends, C. Fonseca Guerra, S. J. A. van Gisbergen, J. G. Snijders, and T. Ziegler, Chemistry with ADF, *J. Comput. Chem.* **22**, 931 (2001).
- [57] S. Lehtola and M. A. L. Marques, Many recent density functionals are numerically ill-behaved, *J. Chem. Phys.* **157**, 174114 (2022).
- [58] T. Lebeda, T. Aschebrock, J. Sun, L. Leppert, and S. Kümmel, Right band gaps for the right reason at low computational cost with a meta-GGA, *Phys. Rev. Mater.* **7**, 093803 (2023).
- [59] É. D. Murray, K. Lee, and D. C. Langreth, Investigation of exchange energy density functional accuracy for interacting molecules, *J. Chem. Theory Comput.* **5**, 2754 (2009).
- [60] T. Jenkins, K. Berland, and T. Thonhauser, Reduced-gradient analysis of van der Waals complexes, *Electron. Struct.* **3**, 034009 (2021).
- [61] T. Jenkins, D. Chakraborty, K. Berland, and T. Thonhauser, Reduced-gradient analysis of molecular adsorption on graphene with nonlocal density functionals, *Phys. Rev. B* **109**, 035427 (2024).
- [62] An earlier study on the influence of the α -dependence on the description of weakly interacting systems reported findings that are not fully conclusive [28]: While the authors rationalize why a monotonically decreasing dependence on α could explain the increased binding of weakly interacting systems for one density functional, they note in the supplementary material that another functional with stronger decrease in α predicts less binding.
- [63] R. D. Johnson III, ed., *NIST Computational Chemistry Comparison and Benchmark Database*, Available online: (accessed on November 1 2024) (NIST Standard Reference Database Number 101, 2022).
- [64] A. Makmal, S. Kümmel, and L. Kronik, Fully numerical all-electron solutions of the optimized effective potential equation for diatomic molecules, *J. Chem. Theory Comput.* **5**, 1731 (2009).
- [65] The DARSEC grid does not reach the z-axis exactly due to the use of prolate spheroidal coordinates, but one can use an elliptical line very close to the z-axis.
- [66] This criterion is in line with the more direct observation noted in the supplementary material of Ref. 28.
- [67] T. Aschebrock, T. Lebeda, M. Brütting, R. Richter, I. Schelter, and S. Kümmel, Exact exchange-like electric response from a meta-generalized gradient approximation: A semilocal realization of ultranonlocality, *J. Chem. Phys.* **159**, 234107 (2023).
- [68] V. R. Cooper, Van der Waals density functional: An appropriate exchange functional, *Phys. Rev. B* **81**, 161104 (2010).
- [69] Note that the energy factor in the original definition of the WTMAD-2 has been updated to 57.816 due to a correction of the MB16-43 average energy.
- [70] T. Lebeda, T. Aschebrock, and S. Kümmel, First steps towards achieving both ultranonlocality and a reliable description of electronic binding in a meta-generalized gradient approximation, *Phys. Rev. Res.* **4**, 023061 (2022).
- [71] See Supplemental Material at [URL will be inserted by publisher] for the detailed results for the subsets of the GMTKN55 database.
- [72] F. Hofmann, I. Schelter, and S. Kümmel, Molecular excitations from meta-generalized gradient approximations in the Kohn–Sham scheme, *J. Chem. Phys.* **153**, 114106 (2020).
- [73] R. Richter, T. Aschebrock, I. Schelter, and S. Kümmel, Meta generalized gradient approximations in time dependent generalized kohn sham theory: Importance of the current-density correction, *J. Chem. Phys.* **159**, 124117 (2023).
- [74] S. Ehlert, U. Huniar, J. Ning, J. W. Furness, J. Sun, A. D. Kaplan, J. P. Perdew, and J. G. Brandenburg, r2scan-d4: Dispersion corrected meta-generalized gradient approximation for general chemical applications, *J. Chem. Phys.* **154**, 061101 (2021).
- [75] A. Najibi and L. Goerigk, The nonlocal kernel in van der Waals density functionals as an additive correction: An extensive analysis with special emphasis on the B97M-V and ω B97M-V approaches, *J. Chem. Theory Comput.* **14**, 5725 (2018).
- [76] J. Ning, M. Kothakonda, J. W. Furness, A. D. Kaplan, S. Ehlert, J. G. Brandenburg, J. P. Perdew, and J. Sun, Workhorse minimally empirical dispersion-corrected density functional with tests for weakly bound systems: r2scan+rvv10, *Phys. Rev. B* **106**, 075422 (2022).
- [77] S. Grimme, A. Hansen, S. Ehlert, and J.-M. Mewes, r2SCAN-3c: A “Swiss army knife” composite electronic-structure method, *J. Chem. Phys.* **154**, 064103 (2021).
- [78] A. Najibi and L. Goerigk, Dft-d4 counterparts of leading meta-generalized-gradient approximation and hybrid density functionals for energetics and geometries, *J. Comput. Chem.* **41**, 2562 (2020).
- [79] M. Korth and S. Grimme, “Mindless” DFT benchmarking, *J. Chem. Theory Comput.* **5**, 993 (2009).
- [80] T. Gould, B. Chan, S. G. Dale, and S. Vuckovic, Identifying and embedding transferability in data-driven representations of chemical space, *Chem. Sci.* **15**, 11122 (2024).
- [81] J. P. Perdew, A. Ruzsinszky, G. I. Csonka, L. A. Constantin, and J. Sun, Workhorse semilocal density functional for condensed matter physics and quantum chemistry, *Phys. Rev. Lett.* **103**, 026403 (2009).
- [82] J. W. Furness, A. D. Kaplan, J. Ning, J. P. Perdew, and J. Sun, Accurate and numerically efficient r2SCAN meta-generalized gradient approximation, *J. Phys. Chem. Lett.* **11**, 8208 (2020).

- [83] J. W. Furness, A. D. Kaplan, J. Ning, J. P. Perdew, and J. Sun, Construction of meta-GGA functionals through restoration of exact constraint adherence to regularized SCAN functionals, *J. Chem. Phys.* **156**, 034109 (2022).
- [84] A. D. Kaplan, M. Levy, and J. P. Perdew, The predictive power of exact constraints and appropriate norms in density functional theory, *Annu. Rev. Phys. Chem.* **74**, 193 (2023).
- [85] M. G. Medvedev, I. S. Bushmarinov, J. Sun, J. P. Perdew, and K. A. Lyssenko, Density functional theory is straying from the path toward the exact functional, *Science* **355**, 49 (2017); K. P. Kepp, Comment on "density functional theory is straying from the path toward the exact functional", *Science* **356**, 496 (2017); M. G. Medvedev, I. S. Bushmarinov, J. Sun, J. P. Perdew, and K. A. Lyssenko, Response to comment on "density functional theory is straying from the path toward the exact functional", *Science* **356**, 496 (2017).
- [86] Similarly, one could argue that even choosing a particular function is empirical, such as choosing to fulfill the gradient expansion by $(1 + At^2)/(1 + At^2 + A^2t^4)$ in PBE correlation versus $(1 + 4At^2)^{-1/4}$ in SCAN correlation.
- [87] P. Jurečka, J. Šponer, J. Černý, and P. Hobza, Benchmark database of accurate (MP2 and CCSD(T) complete basis set limit) interaction energies of small model complexes, DNA base pairs, and amino acid pairs, *Phys. Chem. Chem. Phys.* **8**, 1985 (2006).
- [88] M. S. Marshall, L. A. Burns, and C. D. Sherrill, Basis set convergence of the coupled-cluster correction, $\delta_{MP2}^{CCSD(T)}$: Best practices for benchmarking non-covalent interactions and the attendant revision of the S22, NBC10, HBC6, and HSG databases, *J. Chem. Phys.* **135**, 194102 (2011).
- [89] J. Heyd, G. E. Scuseria, and M. Ernzerhof, Hybrid functionals based on a screened coulomb potential, *J. Chem. Phys.* **118**, 8207 (2003); *J. Chem. Phys.* **124**, 219906 (2006).
- [90] A. V. Krukau, O. A. Vydrov, A. F. Izmaylov, and G. E. Scuseria, Influence of the exchange screening parameter on the performance of screened hybrid functionals, *J. Chem. Phys.* **125**, 224106 (2006).
- [91] R. Peverati and D. G. Truhlar, Communication: A global hybrid generalized gradient approximation to the exchange-correlation functional that satisfies the second-order density-gradient constraint and has broad applicability in chemistry, *J. Chem. Phys.* **135**, 191102 (2011).
- [92] R. Peverati and D. G. Truhlar, Quest for a universal density functional: the accuracy of density functionals across a broad spectrum of databases in chemistry and physics, *Philos. Trans. R. Soc. A* **372**, 20120476 (2014).
- [93] J. Sun, M. Marsman, G. I. Csonka, A. Ruzsinszky, P. Hao, Y.-S. Kim, G. Kresse, and J. P. Perdew, Self-consistent meta-generalized gradient approximation within the projector-augmented-wave method, *Phys. Rev. B* **84**, 035117 (2011).

Supplementary material for “A meta-Generalized Gradient Approximation that describes weak interactions in addition to bond energies and band gaps”

Timo Lebeda* and Stephan Kümmel†
Theoretical Physics IV, University of Bayreuth, 95440 Bayreuth, Germany

Tables I - V provide the mean signed error (MSE), the mean absolute error (MAE), and the root mean square error (RMSE) for the subsets of the GMTKN55 database [1].

TABLE I. Basic properties and reaction energies for small systems.

Subset	PBE			SCAN			r2SCAN			LAK		
	MSE	MAE	RMSE	MSE	MAE	RMSE	MSE	MAE	RMSE	MSE	MAE	RMSE
W4-11	13.10	14.67	18.11	-0.30	3.46	4.87	0.54	3.73	5.12	-1.08	4.16	5.86
G21EA	2.64	3.26	3.99	-0.13	3.65	4.19	-0.00	3.56	4.11	-0.28	3.48	4.09
G21IP	-0.04	3.78	4.85	-0.23	4.89	5.87	-0.37	4.69	5.71	-1.23	5.02	6.11
DIPCS10	-2.20	4.56	5.96	-2.55	4.80	5.86	-2.69	4.96	5.90	-4.26	5.62	7.38
PA26	1.35	2.00	2.71	3.02	3.06	4.01	2.50	2.52	3.31	4.16	4.16	5.00
SIE4x4	23.17	23.17	25.96	17.72	17.72	20.31	17.90	17.90	20.48	17.29	17.29	19.89
ALKBDE10	5.92	6.38	9.96	1.42	5.04	6.99	2.21	5.05	7.47	0.35	4.83	5.88
YBDE18	-2.56	6.04	7.20	-3.42	3.84	4.22	-3.72	4.06	4.56	-3.44	3.65	4.13
AL2X6	-4.37	4.37	5.03	1.04	1.21	1.41	0.27	0.82	1.07	0.43	0.89	1.10
HEAVYSB11	-2.18	4.54	5.28	-3.09	3.09	3.64	-4.43	4.43	5.28	-7.44	7.44	8.46
NBPRC	1.04	2.73	3.41	-1.23	2.05	2.58	-0.34	1.46	1.88	-0.33	2.13	2.55
ALK8	0.44	2.61	3.46	2.17	3.04	4.01	1.77	2.81	3.79	2.59	3.36	4.83
RC21	4.55	5.53	6.40	5.02	5.66	6.27	4.01	4.52	5.04	4.49	4.88	5.37
G2RC	0.94	5.95	7.28	-1.16	5.83	7.18	-0.52	5.08	6.27	-1.41	5.83	7.20
BH76RC	1.14	4.07	5.96	-0.00	3.11	4.17	0.14	2.95	4.02	0.24	2.93	3.89
FH51	1.81	3.28	4.58	-0.56	2.51	3.75	0.07	2.09	3.23	-0.61	2.66	3.76
TAUT15	0.21	1.86	2.36	0.30	1.84	2.40	0.29	1.66	2.18	-0.33	1.43	1.64
DC13	1.88	10.32	13.08	0.18	6.94	10.36	1.81	8.58	11.59	1.27	7.94	11.24
WTMAD-2		6.82			5.28			4.98			5.12	

TABLE II. Reaction energies for large systems and isomerisation reactions.

Subset	PBE			SCAN			r2SCAN			LAK		
	MSE	MAE	RMSE	MSE	MAE	RMSE	MSE	MAE	RMSE	MSE	MAE	RMSE
MB16-43	-11.59	23.34	31.05	9.97	15.74	19.98	4.60	12.83	16.50	-9.21	16.36	20.87
DARC	6.37	6.49	7.31	-0.24	2.12	2.41	2.60	3.11	3.59	0.75	2.28	2.57
RSE43	-3.03	3.03	3.35	-1.31	1.31	1.82	-1.49	1.49	1.79	-0.88	0.98	1.25
BSR36	-7.32	7.32	8.46	-2.57	2.57	3.08	-1.78	1.78	2.11	-3.29	3.29	4.48
CDIE20	1.79	1.79	1.98	1.50	1.50	1.64	1.64	1.64	1.77	1.66	1.66	1.81
ISO34	-0.92	1.76	2.45	-0.29	1.32	1.84	-0.15	1.30	2.02	-0.19	1.33	2.14
ISOL24	-3.30	6.52	9.94	-0.64	3.55	5.19	-1.31	4.42	6.53	-1.34	3.86	5.55
C60ISO	-10.36	10.36	12.45	-6.01	6.10	8.05	-5.10	5.32	7.25	-4.43	4.75	6.56
PArel	0.24	1.82	2.56	0.68	1.49	2.23	0.65	1.54	2.21	0.57	1.35	2.05
WTMAD-2		15.99			8.76			9.04			8.83	

* timo.lebeda@uni-bayreuth.de

† stephan.kuettel@uni-bayreuth.de; <http://tp4.uni-bayreuth.de/en>

TABLE III. Reaction barrier heights.

Subset	PBE			SCAN			r2SCAN			LAK		
	MSE	MAE	RMSE	MSE	MAE	RMSE	MSE	MAE	RMSE	MSE	MAE	RMSE
BH76	-8.85	8.89	10.24	-7.45	7.51	8.28	-6.90	6.95	7.75	-6.17	6.25	7.16
BHPERI	-3.93	3.93	4.37	-4.80	4.80	5.09	-3.90	3.90	4.18	-3.11	3.15	3.43
BHDIV10	-7.75	8.18	9.13	-5.55	6.46	6.95	-4.99	5.91	6.47	-3.23	4.48	5.13
INV24	-2.74	2.99	3.54	0.61	2.50	7.26	0.62	2.69	7.69	1.06	2.06	5.98
BHROT27	0.31	0.44	0.61	0.81	0.83	1.15	0.73	0.74	1.02	0.70	0.73	0.97
PX13	-11.49	11.49	11.66	-8.31	8.31	8.48	-8.90	8.90	9.13	-3.52	3.52	3.71
WCPT18	-8.53	8.53	8.89	-6.14	6.14	6.77	-6.01	6.01	6.62	-3.51	3.56	4.48
WTMAD-2	16.69			14.88			13.80			11.42		

TABLE IV. Intermolecular noncovalent interactions.

Subset	PBE			SCAN			r2SCAN			LAK		
	MSE	MAE	RMSE	MSE	MAE	RMSE	MSE	MAE	RMSE	MSE	MAE	RMSE
RG18	-0.19	0.27	0.39	-0.01	0.20	0.25	-0.07	0.21	0.27	0.19	0.19	0.25
ADIM6	-3.22	3.22	3.58	-1.58	1.58	1.74	-1.84	1.84	2.02	-0.16	0.17	0.19
S22	-2.41	2.42	3.40	-0.46	0.82	1.12	-0.85	0.99	1.34	0.55	0.56	0.72
S66	-2.00	2.02	2.52	-0.46	0.81	0.96	-0.77	0.90	1.11	0.53	0.58	0.68
HEAVY28	-0.45	0.49	0.58	-0.33	0.36	0.41	-0.48	0.48	0.54	0.26	0.33	0.46
WATER27	0.78	2.51	3.60	6.67	7.27	9.70	3.54	4.10	5.23	7.98	7.98	12.47
CARBHB12	0.94	0.99	1.50	1.08	1.10	1.68	0.83	0.92	1.46	1.27	1.27	1.67
PNICO23	-0.10	0.86	1.27	0.64	0.83	1.35	0.31	0.64	1.13	0.98	0.98	1.27
HAL59	-0.07	1.29	1.85	0.73	1.07	1.73	0.28	0.99	1.45	1.23	1.23	1.56
AHB21	0.03	0.83	1.12	-1.11	1.17	1.55	-0.68	0.90	1.26	-0.68	0.72	1.14
CHB6	0.17	0.70	0.97	-0.09	0.39	0.45	0.13	0.44	0.49	0.36	0.56	0.79
IL16	-1.07	2.09	3.25	-2.97	2.97	4.26	-2.55	2.55	4.06	-3.28	3.28	4.57
WTMAD-2	15.62			10.24			10.49			9.49		

TABLE V. Intramolecular noncovalent interactions

Subset	PBE			SCAN			r2SCAN			LAK		
	MSE	MAE	RMSE	MSE	MAE	RMSE	MSE	MAE	RMSE	MSE	MAE	RMSE
IDISP	2.95	10.32	11.91	1.55	4.46	5.74	1.71	5.48	7.15	2.15	4.14	6.14
ICONF	0.14	0.43	0.71	0.25	0.30	0.46	0.23	0.30	0.51	0.19	0.33	0.57
ACONF	0.64	0.64	0.71	0.38	0.38	0.41	0.44	0.44	0.48	0.23	0.23	0.25
Amino20x4	-0.03	0.49	0.62	0.10	0.26	0.34	0.03	0.25	0.31	-0.05	0.19	0.24
PCONF21	-0.82	3.41	3.68	-0.16	0.83	0.92	-0.27	0.97	1.04	0.16	0.78	0.93
MCONF	-1.67	1.75	1.99	-0.27	0.51	0.61	-0.42	0.59	0.71	0.28	0.41	0.50
SCONF	0.15	0.34	0.44	0.41	0.55	0.60	0.32	0.40	0.43	0.10	0.18	0.20
UPU23	1.18	1.80	2.53	0.10	0.65	0.85	0.18	0.78	1.01	-0.41	0.58	0.72
BUT14DIOL	0.11	0.25	0.34	0.31	0.31	0.33	0.14	0.16	0.20	0.33	0.33	0.35
WTMAD-2	19.46			8.20			8.10			6.95		

-
- [1] L. Goerigk, A. Hansen, C. Bauer, S. Ehrlich, A. Najibi, and S. Grimme, A look at the density functional theory zoo with the advanced GMTKN55 database for general main group thermochemistry, kinetics and noncovalent interactions, *Phys. Chem. Chem. Phys.* **19**, 32184 (2017).

Publication 5

Balancing the Contributions to the Gradient Expansion: Accurate Binding and Band Gaps with a Nonempirical Meta-GGA

Physical Review Letters **133**, 136402 (2024)

Timo Lebeda, Thilo Aschebrock, and Stephan Kümmel

Theoretical Physics IV, University of Bayreuth, 95440 Bayreuth, Germany

Publ. 5

Author contributions

All authors together conceptualized the work. T.L. performed the research, wrote the required routines, ran the calculations, and analyzed the results. T.L. wrote the first draft of the manuscript. T.L. and S.K. worked out the final manuscript. All authors discussed the final version.

Publ.5

Balancing the Contributions to the Gradient Expansion: Accurate Binding and Band Gaps with a Nonempirical Meta-GGA

Timo Lebeda^{✉*}, Thilo Aschebrock[✉], and Stephan Kümmel^{✉†}
Theoretical Physics IV, University of Bayreuth, 95440 Bayreuth, Germany

 (Received 7 May 2024; revised 21 July 2024; accepted 21 August 2024; published 26 September 2024)

The gradient expansion has been a long-standing guide rail in density-functional theory. We here demonstrate that for exchange-correlation approximations that depend on the gradient of the density and the kinetic energy density, i.e., for meta-generalized gradient approximations (meta-GGAs), there is a so far unexploited degree of freedom in the gradient expansion that allows to shift the relative weight of gradient and kinetic energy contributions. As the dependence on the kinetic energy density determines the derivative discontinuity, this allows to construct meta-GGAs that adhere to the known exact constraints, yet have new properties. We demonstrate this with the construction of a meta-GGA that describes both electronic bonds and band gaps with remarkable accuracy.

DOI: [10.1103/PhysRevLett.133.136402](https://doi.org/10.1103/PhysRevLett.133.136402)

Computational materials modeling plays an increasingly important role in the search for new energy materials, as it enables the rational design of new compounds [1–5]. Its balance between useful accuracy and reasonable computational cost made density-functional theory very popular for electronic structure calculations. Between the computationally efficient generalized gradient approximations (GGAs) and the overall more accurate, but computationally much more demanding hybrid functionals, there is the class of meta-generalized gradient approximations (meta-GGAs) [6–15].

Meta-GGAs have conceptual limitations that they share with the local density approximation and GGAs. In particular, they are not one-electron self-interaction free and thus suffer from a delocalization error [16]. Overcoming this limitation requires nonlocality as realized, e.g., in different types of hybrid functionals; see, e.g., [17–21].

However, over the past decade, meta-GGAs have made great progress [13–15,22–25], offering almost hybrid accuracy for electronic bonds at almost GGA computational cost. For example, meta-GGAs made considerable progress on solving the dilemma [26] of choosing between accurate electronic bonds for either molecules or solids [10,14,27,28] and they improved the description of weakly bound systems, both alone [11,14,29] and in combination with dispersion corrections [13,30]. More recently, meta-GGAs were shown to capture the (ultra)nonlocality and derivative discontinuity that are required to accurately predict band gaps [15,31–35].

For many applications, it would be very advantageous to combine high accuracy for both electronic bonds *and* band

gaps within a *single* computationally efficient meta-GGA [36–42]. So far, however, there is no meta-GGA that offers state-of-the-art accuracy for both. Here, we aim to close this gap.

The key idea behind the new construction is to exploit the fact that in meta-GGAs both the density gradient and the kinetic energy density contribute to the gradient expansion of the exchange-correlation energy. Thus, via a partial integration, one can make them contribute with different relative weights [15,43], while maintaining the integrity of the gradient expansion. Since the dependence on the kinetic energy density determines the degree of nonlocality in a meta-GGA [15,34,35,44], adjustment of the relative contributions from the density gradient and the kinetic energy density allows to reach a new, careful balance between energetic binding and (ultra)nonlocal features of the potential.

In our construction, this balanced treatment is guided by fulfilling the exact constraints that a meta-GGA can satisfy [14,45] on the one hand, and on the other hand by insights that emerged from analyzing existing GGAs and meta-GGAs [29,46–55].

As the first step of the derivation, we discuss the general gradient expansion of exchange and correlation with contributions from the density gradient and the kinetic energy density. We consider the exchange-correlation energy of a meta-GGA in its usual form $E_{xc} = E_x + E_c$ with

$$E_x[n] = A_x \int n^{4/3} F_x(s, \alpha) d^3r, \quad (1a)$$

$$E_c[n_\uparrow, n_\downarrow] = \int n \varepsilon_c(r_s, \zeta, s, \alpha) d^3r. \quad (1b)$$

*Contact author: timo.lebeda@uni-bayreuth.de

†Contact author: stephan.kuemmel@uni-bayreuth.de

Here, F_x is the enhancement factor of exchange, ϵ_c is the correlation energy density per particle, and $A_x = -(3/4)(3/\pi)^{1/3}$. We use atomic units throughout. The spin dependence of the exchange energy can be obtained via the exact spin-scaling relation [56]. Semilocal functionals can be parametrized in different variables [19,50,57]. We here use the Wigner-Seitz radius $r_s = (4\pi n/3)^{-1/3}$, the spin polarization $\zeta = (n_\uparrow - n_\downarrow)/(n_\uparrow + n_\downarrow)$, the reduced density gradient s , and the iso-orbital indicator α . These are

$$s = |\nabla n|/[2(3\pi^2)^{1/3}n^{4/3}], \quad \alpha = (\tau - \tau^W)/\tau^{\text{unif}}. \quad (2)$$

Here, n is the electron density, $\tau = (1/2) \sum_{\sigma,i}^{\text{occ}} |\nabla \varphi_{i\sigma}|^2$ is the noninteracting kinetic energy density, $\{\varphi_{i\sigma}\}$ are the (generalized) Kohn-Sham orbitals, $\tau^W = |\nabla n|^2/8n$ is the single-orbital limit of τ , and $\tau^{\text{unif}} = (3/10)(3\pi^2)^{2/3}n^{5/3}$ is the uniform electron gas limit of τ [58].

The dimensionless parameters s and α ensure the correct uniform density scaling behavior of the exchange energy [59]. Furthermore, we choose α as the τ -dependent variable because of its ability to recognize different types of orbital overlap [50,60,61]. While α was reported to lead to numerical instabilities [62,63], more recent meta-GGAs, especially TASK [15], whose construction is strongly based on α , demonstrate that a balanced dependence on α can lead to numerically very stable meta-GGAs [34,63–67].

For a weakly inhomogeneous electron gas, the gradient corrections to the exchange-correlation energy are known to second order [68,69],

$$E_{\text{xc}}^{\text{GE2}}[n] = A_x \int n^{4/3} C_s(r_s) \mu_s^2 d^3 r, \quad (3)$$

with $\mu = 10/81$ the gradient expansion coefficient of exchange. The density dependence of C_s is known numerically from the random phase approximation [68,70–72] and has been parametrized by Rasolt and Geldart [72].

Meta-GGAs depend on two variables that contribute to the gradient expansion, in our parametrization s and α . Consequently, there is a freedom to fulfill the gradient expansion with different relative contributions from s and α . To date, nonempirical meta-GGAs have been constructed based on the gradient expansion of exchange using only s [14], only α [43], or both [15]. So far, only s has been used for the gradient expansion of correlation [14]. We note that r2SCAN [24] uses both s and α for the respective separate gradient expansions of exchange and correlation. There, however, the α dependence is only introduced *a posteriori* for numerical reasons [24,73,74]. As pointed out in Ref. [74], this causes numerical problems if the gradient expansion of exchange is satisfied to fourth order.

Here, we present the general gradient expansion of exchange and correlation using both variables s and α . To this end, we write Eq. (3) in the more general form

$$E_{\text{xc}}^{\text{GE2}}[n] = A_x \int n^{4/3} C_{\mu_\alpha}(r_s) [\mu_s s^2 + \mu_\alpha (\alpha - 1)] d^3 r. \quad (4)$$

μ_s and μ_α are only defined up to multiplication with a constant, which we fix by $C_{\mu_\alpha}(0) = C_s(0)$. Then μ_s is uniquely determined by μ_α and the gradient expansion. The explicit dependency will be derived in Eq. (9). Consequently, μ_α controls the relative contributions from s and α to the gradient expansion.

The density dependence of C_{μ_α} , which depends parametrically on μ_α , is obtained as follows. First, we expand the noninteracting kinetic energy density τ to second order in ∇n [75,76],

$$\tau = \tau^{\text{unif}} [1 + (5/27)s^2 + (20/9)q] + \mathcal{O}(\nabla^4), \quad (5)$$

with $q = \nabla^2 n / [4(3\pi)^{2/3}n^{5/3}]$ the reduced Laplacian of the density. Thus,

$$\alpha = 1 - (40/27)s^2 + (20/9)q + \mathcal{O}(\nabla^4). \quad (6)$$

Inserting Eq. (6) into Eq. (4), transforming the terms in q to terms in s^2 by partial integration and keeping only terms up to second order in ∇n , we obtain

$$\begin{aligned} & \int n^{4/3} C_{\mu_\alpha}(r_s) [\mu_s s^2 + \mu_\alpha (\alpha - 1)] d^3 r \\ & \stackrel{p.l.}{=} \int n^{4/3} \left[C_{\mu_\alpha}(r_s) \mu_s + \frac{20}{27} [r_s C'_{\mu_\alpha}(r_s) - C_{\mu_\alpha}(r_s)] \mu_\alpha \right] s^2 d^3 r. \end{aligned} \quad (7)$$

Consequently, the partitioned gradient expansion of Eq. (4) yields the same energy as the common one of Eq. (3) to second order if

$$\mu C_s(r_s) = \mu_s C_{\mu_\alpha}(r_s) + 6\mu\mu_\alpha [r_s C'_{\mu_\alpha}(r_s) - C_{\mu_\alpha}(r_s)], \quad (8)$$

which is a differential equation that connects C_{μ_α} to C_s . Since $C_{\mu_\alpha}(0) = C_s(0)$, the high-density limit of Eq. (8) yields $\mu = \mu_s - 6\mu\mu_\alpha$. Consequently, μ_s is uniquely determined by μ_α via

$$\mu_s = (1 + 6\mu_\alpha)\mu. \quad (9)$$

Inserting Eq. (9) into Eq. (8) yields

$$C_s(r_s) = C_{\mu_\alpha}(r_s) + 6\mu_\alpha r_s C'_{\mu_\alpha}(r_s). \quad (10)$$

For $\mu_\alpha = 0$, this restores the common gradient expansion in s , while for $\mu_\alpha \neq 0$ this differential equation allows to determine C_{μ_α} from C_s . The general solution of Eq. (10) and a computationally efficient approximation to it are given in the Supplemental Material [77,78]. Thus, the

derivation of the general gradient expansion in s and α now is in principle complete.

For using this general gradient expansion in specific, constraint-guided functional construction, it is advisable to look at exchange and correlation separately, as they are governed by different constraints. In analogy to Eq. (4), we define partitionings of the gradient expansions for exchange-only and correlation-only by

$$E_{x|c}^{\text{GE2}}[n] = A_x \int n^{4/3} [\mu_{s,x|c} s^2 + \mu_{\alpha,x|c} (\alpha - 1)] d^3 r. \quad (11)$$

Inserting the gradient expansion of exchange-only yields that $\mu_{s,x}$ is uniquely determined by $\mu_{\alpha,x}$ via [15]

$$\mu_{s,x} = (1 + 6\mu_{\alpha,x})\mu. \quad (12)$$

Finally, the gradient expansion of correlation is $E_c^{\text{GE2}}[n] = E_{xc}^{\text{GE2}}[n] - E_x^{\text{GE2}}[n]$, i.e., Eq. (4) minus Eq. (11) for exchange. This leads to

$$\mu_{\alpha,c}(r_s) = C_{\mu_\alpha}(r_s)\mu_\alpha - \mu_{\alpha,x}, \quad (13a)$$

$$\mu_{s,c}(r_s) = \mu [C_{\mu_\alpha}(r_s)(1 + 6\mu_\alpha) - (1 + 6\mu_{\alpha,x})]. \quad (13b)$$

Two free parameters remain, $\mu_{\alpha,x}$ and μ_α . While μ_α controls the contribution of α —and thus the kinetic energy density—to the gradient expansion of exchange and correlation together, $\mu_{\alpha,x}$ controls the one of exchange-only. Since the α dependence of the enhancement factor determines its degree of ultranonicity [15,23,34,35], $\mu_{\alpha,x}$ and μ_α control the ultranonicity of a meta-GGA.

We now use these concepts to derive a new meta-GGA, for brevity denoted as LAK (initials of the authors), that is based on the above introduced partitioning of the gradient expansion and on fulfilling the exact constraints that a meta-GGA can fulfill [14]. Furthermore, we use the strategy of interpolating between the iso-orbital limit $\alpha = 0$ and the homogeneous electron gas limit $\alpha = 1$ [14,15,43,50,51] in both exchange and correlation. This method led to the successful meta-GGAs SCAN [14] and TASK [15]. However, we fix the problem of a too small derivative discontinuity in SCAN and a too weak binding in TASK by choosing the particular factors in this interpolation distinctly differently. In the following, we emphasize the general ideas, whereas the Supplemental Material [77] reports the arguments and mathematical steps in detail.

We determine μ_α based on the following four conditions for the enhancement factor F_{xc} : (i) $\partial F_{xc}/\partial\alpha < 0$ to ensure a positive derivative discontinuity [15,34]. This implies $\mu_\alpha > 0$. (ii) The α dependence of exchange should exceed that of correlation to reflect that the contribution of exchange to the derivative discontinuity typically exceeds that of correlation. This implies $\mu_{\alpha,x} < 0$. (iii) As we have argued recently [34], there are many reasons to expect that correlation alone has a negative contribution to the derivative discontinuity, corresponding to $\partial F_c/\partial\alpha > 0$.

Consequently, the fact that C_{μ_α} is of the order of -1 in the most relevant density range for $\mu_\alpha > 0$ [77] implies $\mu_\alpha < -\mu_{\alpha,x}$. (iv) F_{xc} has a monotonic and smooth dependence on α .

The value $\mu_\alpha = -\mu_{\alpha,x}/2$ that emerges as the natural average suggested by conditions (i) and (iii) meets all of these requirements. Therefore, we adopt it in the following.

Next, we introduce the exchange part of LAK. We use Eq. (1a) with the enhancement factor

$$F_x^{\text{LAK}}(s, \alpha) = h_x^0 g_x(s) + [1 - f_x(\alpha)](h_x^1(s) - h_x^0) g_{\text{num}}(s) \quad (14)$$

because the separation of variables allows to conveniently fix $\mu_{\alpha,x}$ via the fourth-order gradient expansion of exchange [15]. Applying the strongly tightened bound for $\alpha = 0$ ($F_x \leq 1.174$) [79] leads to $\mu_{\alpha,x} = -0.209897$. g_x ensures the exact hydrogen atom energy to reduce one-electron self-interaction [14,15].

f_x and h_x^1 are guided by the gradient expansion of exchange to fourth order [80] with contributions from s and α [15]. This particularly makes F_x recover the exact homogeneous electron gas limit. The forms of f_x and h_x^1 are further tightened by the following two constraints: negativity of the exchange energy (locally via $F_x > 0$) and nonuniform density scaling [81,82] (via $F_x \propto s^{-1/2}$ for $s \rightarrow \infty$ [79]). Additionally, we extend the strongly tightened bound for $\alpha = 0$ to all α , as suggested in Ref. [79].

While the exact constraints allow to fix F_x in several limits and by upper and lower bounds, there is still much freedom in how to interpolate between these limits. One way to fix the enhancement factor in this intermediate range is the use of so-called appropriate norms [14,45], i.e., nonbonded model systems. LAK exchange uses the hydrogen atom as an appropriate norm. However, we are not aware of a suitable appropriate norm for the (ultra)nonlocality that we aim for. Therefore, we use two construction principles to guide the enhancement factor of LAK. First, we demand the following extension of condition (ii):

$$\frac{\partial F_x}{\partial\alpha} \begin{cases} < 0, & \text{everywhere} \\ \text{roughly constant} & \text{for } 0.2 \lesssim \alpha \lesssim 1.5 \end{cases}. \quad (15)$$

This condition is known to be important for a sizeable positive (exchange) derivative discontinuity across a wide range of systems [15,34]. It is related to the *nonlocal constraint* n3 of Ref. [45]. Condition (15) determines the form of f_x . Second, we demand

$$\left. \frac{\partial F_{xc}}{\partial s} \right|_{\alpha=1} \begin{cases} > 0 & \text{for } 0.5 \lesssim s \lesssim 1.2 \\ < 0 & \text{for } s \gtrsim 1.2 \end{cases}, \quad (16)$$

a condition known to increase the binding of weakly bound systems [53,54]. The latter is important because condition (15) severely weakens the binding of such systems [83]. Condition (16) determines the form of h_x^1 .

Finally, g_{num} reduces the α dependence for large values of s , which helps to resolve the convergence issues of meta-GGAs [15,24]. The form of g_{num} is chosen such that the numerical stability is improved, but the predicted total energies remain unchanged.

Next, we build the correlation based on Eq. (1b) and our partitioning of the gradient expansion. Like exchange, it is based on the successful idea of interpolating between $\alpha = 0$ and $\alpha = 1$,

$$\begin{aligned} \varepsilon_c^{\text{LAK}}(r_s, \zeta, s, \alpha) &= \varepsilon_c^0(r_s, \zeta, s) + [1 - f_c(r_s, \alpha)] \\ &\times [\varepsilon_c^1(r_s, \zeta, s) - \varepsilon_c^0(r_s, \zeta, s)]g_{\text{num}}(s). \end{aligned} \quad (17)$$

The interpolation function f_c and the GGA terms ε_c^1 and ε_c^0 are introduced below.

The important new insight from our partitioning of the gradient expansion is that the interpolation function f_c should depend not only on α or some other iso-orbital indicator, but also explicitly on r_s and thus on the density. Taking into account this dependence is a new feature that arises naturally from our realization of the gradient expansion as follows. Combine Eqs. (1b), (11), and (13) to obtain the gradient expansion coefficients

$$(\partial\varepsilon_c/\partial\alpha)|_{\zeta=0, s=0, \alpha=1}(r_s) = A_c\mu_{\alpha,c}(r_s)/r_s, \quad (18a)$$

$$(\partial\varepsilon_c/\partial s^2)|_{\zeta=0, s=0, \alpha=1}(r_s) = A_c\mu_{s,c}(r_s)/r_s, \quad (18b)$$

with $A_c = (4\pi/3)^{-1/3}A_x$. The $1/r_s$ in Eq. (18b) is typically accounted for by using $t^2 = c_t s^2/r_s$ with (for $\zeta = 0$) $c_t = (3\pi^2/16)^{2/3}$ as the reduced gradient for correlation [14,84]. Equation (18a) implies to analogously replace $(\alpha - 1)$ by $(\alpha - 1)/r_s$ near $\alpha = 1$. We therefore suggest the iso-orbital indicator for correlation

$$\tilde{\alpha} = (\alpha - 1)/(r_s\alpha). \quad (19)$$

In addition to its proper density dependence near $\alpha = 1$, $\tilde{\alpha} \rightarrow -\infty$ in the iso-orbital limit independently of r_s . Thus, $\tilde{\alpha}$ takes unique values for both $\alpha = 0$ and $\alpha = 1$. Transforming Eq. (18) to t and $\tilde{\alpha}$ yields the gradient expansion coefficients

$$\beta_t(r_s) = (A_c/c_t)\mu_{s,c}(r_s), \quad \beta_{\tilde{\alpha}}(r_s) = -A_c\mu_{\alpha,c}(r_s). \quad (20)$$

For the complete definition of Eq. (17), we still need to define f_c , ε_c^0 , and ε_c^1 . For these, we use the forms

$$f_c(r_s, \alpha) = \frac{2}{\pi} \arctan \left[\frac{\pi}{2} f_c^{\text{GE2}}(r_s) \tilde{\alpha}(r_s, \alpha) \right], \quad (21a)$$

$$\varepsilon_c^0(r_s, \zeta, s) = G_c(\zeta) [\varepsilon_c^{\text{LDA0}}(r_s) + H^0(r_s, s)], \quad (21b)$$

$$\varepsilon_c^1(r_s, \zeta, s) = \varepsilon_c^{\text{LSDA}}(r_s, \zeta) + H^1(r_s, \zeta, t(r_s, s)). \quad (21c)$$

For f_c , we use the iso-orbital indicator $\tilde{\alpha}$ suggested in Eq. (19) and determine f_c^{GE2} by the gradient expansion, Eq. (20). The form of f_c is chosen for consistency with exchange and guarantees $f_c|_{\alpha=0} = 1$ and $f_c|_{\alpha=1} = 0$, regardless of $r_s > 0$.

We take the general idea for the forms of ε_c^0 and ε_c^1 from SCAN [14], but determine the functions distinctly differently using our new strategy.

For the correlation energy density per particle of the homogeneous electron gas $\varepsilon_c^{\text{LSDA}}$, we use the parametrization of Perdew and Wang [85]. The basic idea in the construction of H^1 is to satisfy our partitioning of the gradient expansion and all exact constraints relevant to H^1 with a form that is similar to the respective construction in PBE and SCAN. As for exchange, the condition (16) determines the form of H^1 in the intermediate range.

Importantly, H^1 is subject to the only exact constraint for which LAK and SCAN differ, the Lieb-Oxford bound. LAK satisfies the recently improved bound $F_{xc} \leq 2.1346$ [86], whereas SCAN satisfies the previous best bound $F_{xc} \leq 2.215$ [87]. Note that, strictly speaking, the Lieb-Oxford bound is a bound on the exchange-correlation energy. However, to guarantee it for all possible densities, it is usually applied locally [79].

In the iso-orbital limit $\alpha = 0$, we adopt G_c from SCAN to make the correlation free from one-electron self-interaction. For the term $\varepsilon_c^{\text{LDA0}}$, we use the coupled cluster-motivated correlation of Ref. [88], but modified in order to satisfy the lower bound on the exchange-correlation energies of two-electron systems ($F_{xc} \leq 1.67082$) [89] and the helium iso-electronic series norm [88]. For H^0 , we adopt the form from SCAN to ensure consistency with H^1 . In contrast to SCAN, however, we use the correlation energy of the high-density limit of the two-electron ion with the nucleus number $Z \rightarrow \infty$ [90] as the appropriate norm for H^0 .

This completes the construction of LAK. In the following, we assess its performance for energetic binding and the band gaps of semiconductors. To this end, we compare LAK to the two nonempirical functionals whose construction principles we have followed as close as possible, the GGA PBE [84] and the meta-GGA SCAN [14,24]. Additionally, we compare to the range-separated hybrid HSE06 [91–93] that has become a standard for band gap prediction based on density-functional theory [94].

We have implemented LAK in the codes ADF [95–97] and BAND [96,98–104] of the Amsterdam Modeling Suite. As common for meta-GGAs, these implementations within a generalized Kohn-Sham scheme [105] follow the method of Ref. [106]. Except for the HSE lattice constants, all results shown here were obtained from fully self-consistent all-electron calculations. Computational details, detailed data, and the working equations of LAK are reported in the Supplemental Material [77].

Table I in very compact form summarizes the striking result that our construction makes accessible. It shows that

TABLE I. Mean absolute error of PBE, SCAN, LAK, and HSE06 for the MGAE109 [108] set of 109 main-group atomization energies, the MGBL20 [109] set of 20 main-group bond lengths, the LC20 [110] set of 20 solid lattice constants, and the SCBG15 set of 15 semiconductor band gaps (SCBG15 is defined in the Supplemental Material [77]). All calculations are fully self-consistent all-electron calculations in ADF [97] and BAND [104], except for the lattice constants of HSE06 [94,111]. The Supplemental Material [77] reports the computational details and the detailed data.

	MGAE109 (kcal/mol)	MGBL20 (Å)	LC20 (Å)	SCBG15 (eV)
PBE	13.9	0.009	0.055	0.91
SCAN	3.8	0.005	0.015	0.59
LAK	3.5	0.003	0.054	0.18
HSE06	4.0	0.006	0.032	0.17

LAK has energetics as good as SCAN, but band gaps as good as HSE, yet without exact exchange. We discuss noncovalently bound systems in the Supplemental Material [77,107].

Figure 1 shows the fundamental band gaps of semiconductors as obtained in a generalized Kohn-Sham formalism [105]. The latter takes into account the effects of the derivative discontinuity [34,112,113]. We deliberately focus on semiconductors with a band gap in the technologically relevant range of 0.5 to 4.0 eV. The striking observation is that the band gaps calculated with LAK are in good agreement with the experimental gaps, and in fact,

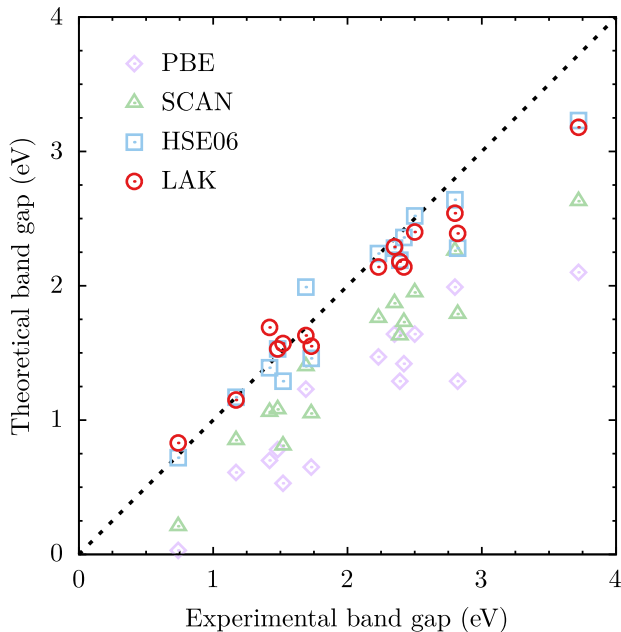


FIG. 1. Calculated vs experimental band gaps of 15 semiconductors (SCBG15). The dotted line illustrates exact agreement with the reference values.

close to the ones found with HSE. That this is a nontrivial achievement is seen in the comparison to SCAN, which closes only about half of the gap between the PBE gaps and the experimental gaps.

These results underscore the potential of the meta-GGA class of exchange-correlation functionals. The remarkable overall performance of LAK is achieved through a well-balanced interplay between s and α in both exchange and correlation.

In summary, we have shown how the gradient expansion for exchange and correlation can be naturally partitioned with contributions from the gradient of the density and from the kinetic energy density. Inspired by the constructions of the nonempirical meta-GGAs SCAN, which is very accurate for energetic bonds but systematically underestimates band gaps, and TASK, which is very accurate for band gaps but strongly underbinding, we constructed a best of both worlds meta-GGA that combines their respective state-of-the-art accuracy for both.

The resulting meta-GGA LAK appears as an attractive alternative to computationally demanding hybrid functionals for large scale applications, e.g., in the realm of energy relevant materials, where the interaction of molecules and solids, interfaces, and band gaps play a prominent role. Furthermore, we are convinced that the new partitioning of the gradient expansion, combined with the constantly emerging further insights on meta-GGAs [33–35,86,114–118], will help to guide and improve the construction of further meta-GGAs and meta-GGA hybrid functionals in the future.

Acknowledgments—T. L. and S. K. appreciate financial support from the Deutsche Forschungsgemeinschaft, DFG Project No. 457582427, from the Bavarian State Ministry of Science, Research, and the Arts for the Collaborative Research Network “Solar Technologies go Hybrid,” and from the Elite Study Program “Biological Physics” of the Elite Network of Bavaria.

All authors together conceptualized the work. T. L. performed the research, wrote the required routines, ran the calculations, and analyzed the results. T. L. wrote the first draft of the manuscript. T. L. and S. K. worked out the final manuscript. All authors discussed the final version.

- [1] A. Jain, Y. Shin, and K. A. Persson, Computational predictions of energy materials using density functional theory, *Nat. Rev. Mater.* **1**, 15004 (2016).
- [2] C. Curutchet and B. Mennucci, Quantum chemical studies of light harvesting, *Chem. Rev.* **117**, 294 (2017).
- [3] B. W. J. Chen, L. Xu, and M. Mavrikakis, Computational methods in heterogeneous catalysis, *Chem. Rev.* **121**, 1007 (2021).

- [4] D. Adekoya, S. Qian, X. Gu, W. Wen, D. Li, J. Ma, and S. Zhang, DFT-guided design and fabrication of carbon-nitride-based materials for energy storage devices: A review, *Nano-Micro Lett.* **13**, 13 (2021).
- [5] E. Olsson, J. Yu, H. Zhang, H.-M. Cheng, and Q. Cai, Atomic-scale design of anode materials for alkali metal (Li/Na/K)-ion batteries: Progress and perspectives, *Adv. Energy Mater.* **12**, 2200662 (2022).
- [6] A. D. Becke, Density-functional thermochemistry. IV. A new dynamical correlation functional and implications for exact-exchange mixing, *J. Chem. Phys.* **104**, 1040 (1996).
- [7] T. Van Voorhis and G. E. Scuseria, A novel form for the exchange-correlation energy functional, *J. Chem. Phys.* **109**, 400 (1998).
- [8] J. P. Perdew, S. Kurth, A. Zupan, and P. Blaha, Accurate density functional with correct formal properties: A step beyond the generalized gradient approximation, *Phys. Rev. Lett.* **82**, 2544 (1999).
- [9] A. D. Boese and N. C. Handy, New exchange-correlation density functionals: The role of the kinetic-energy density, *J. Chem. Phys.* **116**, 9559 (2002).
- [10] J. Tao, J. P. Perdew, V. N. Staroverov, and G. E. Scuseria, Climbing the density functional ladder: Nonempirical meta-generalized gradient approximation designed for molecules and solids, *Phys. Rev. Lett.* **91**, 146401 (2003).
- [11] Y. Zhao and D. G. Truhlar, A new local density functional for main-group thermochemistry, transition metal bonding, thermochemical kinetics, and noncovalent interactions, *J. Chem. Phys.* **125**, 194101 (2006).
- [12] R. Peverati and D. G. Truhlar, An improved and broadly accurate local approximation to the exchange-correlation density functional: The MN12-L functional for electronic structure calculations in chemistry and physics, *Phys. Chem. Chem. Phys.* **14**, 13171 (2012).
- [13] N. Mardirossian and M. Head-Gordon, Mapping the genome of meta-generalized gradient approximation density functionals: The search for B97M-V, *J. Chem. Phys.* **142**, 074111 (2015).
- [14] J. Sun, A. Ruzsinszky, and J. P. Perdew, Strongly constrained and appropriately normed semilocal density functional, *Phys. Rev. Lett.* **115**, 036402 (2015).
- [15] T. Aschebrock and S. Kümmel, Ultranonlocality and accurate band gaps from a meta-generalized gradient approximation, *Phys. Rev. Res.* **1**, 033082 (2019).
- [16] K. R. Bryenton, A. A. Adeleke, S. G. Dale, and E. R. Johnson, Delocalization error: The greatest outstanding challenge in density-functional theory, *Comput. Mol. Sci.* **13**, e1631 (2023).
- [17] A. D. Becke, Density-functional thermochemistry. V. Systematic optimization of exchange-correlation functionals, *J. Chem. Phys.* **107**, 8554 (1997).
- [18] J. Jaramillo, G. E. Scuseria, and M. Ernzerhof, Local hybrid functionals, *J. Chem. Phys.* **118**, 1068 (2003).
- [19] A. D. Boese and J. M. Martin, Development of density functionals for thermochemical kinetics, *J. Chem. Phys.* **121**, 3405 (2004).
- [20] M. Brütting, H. Bahmann, and S. Kümmel, Hybrid functionals with local range separation: Accurate atomization energies and reaction barrier heights, *J. Chem. Phys.* **156**, 104109 (2022).
- [21] M. Kaupp, A. Wodyński, A. V. Arbuznikov, S. Fürst, and C. J. Schattenberg, Toward the next generation of density functionals: Escaping the zero-sum game by using the exact-exchange energy density, *Acc. Chem. Res.* **57**, 1815 (2024).
- [22] J. Tao and Y. Mo, Accurate semilocal density functional for condensed-matter physics and quantum chemistry, *Phys. Rev. Lett.* **117**, 073001 (2016).
- [23] B. Patra, S. Jana, L. A. Constantin, and P. Samal, Relevance of the Pauli kinetic energy density for semilocal functionals, *Phys. Rev. B* **100**, 155140 (2019).
- [24] J. W. Furness, A. D. Kaplan, J. Ning, J. P. Perdew, and J. Sun, Accurate and numerically efficient r2SCAN meta-generalized gradient approximation, *J. Phys. Chem. Lett.* **11**, 8208 (2020).
- [25] P. Kovács, F. Tran, P. Blaha, and G. K. H. Madsen, What is the optimal mGGA exchange functional for solids?, *J. Chem. Phys.* **157**, 094110 (2022).
- [26] J. P. Perdew, A. Ruzsinszky, G. I. Csonka, O. A. Vydrov, G. E. Scuseria, L. A. Constantin, X. Zhou, and K. Burke, Restoring the density-gradient expansion for exchange in solids and surfaces, *Phys. Rev. Lett.* **100**, 136406 (2008).
- [27] J. P. Perdew, A. Ruzsinszky, G. I. Csonka, L. A. Constantin, and J. Sun, Workhorse semilocal density functional for condensed matter physics and quantum chemistry, *Phys. Rev. Lett.* **103**, 026403 (2009).
- [28] J. Sun, R. C. Remsing, Y. Zhang, Z. Sun, A. Ruzsinszky, H. Peng, Z. Yang, A. Paul, U. Waghmare, X. Wu *et al.*, Accurate first-principles structures and energies of diversely bonded systems from an efficient density functional, *Nat. Chem.* **8**, 831 (2016).
- [29] G. K. H. Madsen, L. Ferrighi, and B. Hammer, Treatment of layered structures using a semilocal meta-GGA density functional, *J. Phys. Chem. Lett.* **1**, 515 (2010).
- [30] H. Peng, Z.-H. Yang, J. P. Perdew, and J. Sun, Versatile van der Waals density functional based on a meta-generalized gradient approximation, *Phys. Rev. X* **6**, 041005 (2016).
- [31] V. U. Nazarov and G. Vignale, Optics of semiconductors from meta-generalized-gradient-approximation-based time-dependent density-functional theory, *Phys. Rev. Lett.* **107**, 216402 (2011).
- [32] P. Borlido, J. Schmidt, A. Huran, F. Tran, M. Marques, and S. Botti, Exchange-correlation functionals for band gaps of solids: Benchmark, reparametrization and machine learning, *npj Comput. Mater.* **6**, 96 (2020).
- [33] P. Kovács, P. Blaha, and G. K. H. Madsen, Origin of the success of mGGAs for bandgaps, *J. Chem. Phys.* **159**, 244118 (2023).
- [34] T. Lebeda, T. Aschebrock, J. Sun, L. Leppert, and S. Kümmel, Right band gaps for the right reason at low computational cost with a meta-GGA, *Phys. Rev. Mater.* **7**, 093803 (2023).
- [35] T. Aschebrock, T. Lebeda, M. Brütting, R. Richter, I. Schelter, and S. Kümmel, Exact exchange-like electric response from a meta-generalized gradient approximation: A semilocal realization of ultranonlocality, *J. Chem. Phys.* **159**, 234107 (2023).
- [36] G. Pacchioni, First principles calculations on oxide-based heterogeneous catalysts and photocatalysts: Problems and advances, *Catal. Lett.* **145**, 80 (2015).

- [37] V. Tripkovic, H. A. Hansen, J. M. Garcia-Lastra, and T. Vegge, Comparative DFT + U and HSE study of the oxygen evolution electrocatalysis on perovskite oxides, *J. Phys. Chem. C* **122**, 1135 (2018).
- [38] L. Weston, H. Taylor, K. Krishnaswamy, L. Bjaalie, and C. G. Van de Walle, Accurate and efficient band-offset calculations from density functional theory, *Comput. Mater. Sci.* **151**, 174 (2018).
- [39] Q. He, B. Yu, Z. Li, and Y. Zhao, Density functional theory for battery materials, *Energy Environ. Mater.* **2**, 264 (2019).
- [40] E. B. Isaacs, S. Patel, and C. Wolverton, Prediction of Li intercalation voltages in rechargeable battery cathode materials: Effects of exchange-correlation functional, van der Waals interactions, and Hubbard U, *Phys. Rev. Mater.* **4**, 065405 (2020).
- [41] J. Kang, X. Zhang, and S.-H. Wei, Advances and challenges in DFT-based energy materials design, *Chin. Phys. B* **31**, 107105 (2022).
- [42] H. Xue, J. M. Vicent-Luna, S. Tao, and G. Brocks, Compound defects in halide perovskites: A first-principles study of CsPbI₃, *J. Phys. Chem. C* **127**, 1189 (2023).
- [43] J. Sun, J. P. Perdew, and A. Ruzsinszky, Semilocal density functional obeying a strongly tightened bound for exchange, *Proc. Natl. Acad. Sci. U.S.A.* **112**, 685 (2015).
- [44] F. G. Eich and M. Hellgren, Derivative discontinuity and exchange-correlation potential of meta-ggas in density-functional theory, *J. Chem. Phys.* **141**, 224107 (2014).
- [45] A. D. Kaplan, M. Levy, and J. P. Perdew, The predictive power of exact constraints and appropriate norms in density functional theory, *Annu. Rev. Phys. Chem.* **74**, 193 (2023).
- [46] A. Zupan, K. Burke, M. Ernzerhof, and J. P. Perdew, Distributions and averages of electron density parameters: Explaining the effects of gradient corrections, *J. Chem. Phys.* **106**, 10184 (1997).
- [47] J. P. Perdew, M. Ernzerhof, A. Zupan, and K. Burke, Nonlocality of the density functional for exchange and correlation: Physical origins and chemical consequences, *J. Chem. Phys.* **108**, 1522 (1998).
- [48] P. Haas, F. Tran, P. Blaha, K. Schwarz, and R. Laskowski, Insight into the performance of GGA functionals for solid-state calculations, *Phys. Rev. B* **80**, 195109 (2009).
- [49] G. I. Csonka, J. P. Perdew, A. Ruzsinszky, P. H. T. Philipsen, S. Lebègue, J. Paier, O. A. Vydrov, and J. G. Ángyán, Assessing the performance of recent density functionals for bulk solids, *Phys. Rev. B* **79**, 155107 (2009).
- [50] J. Sun, B. Xiao, and A. Ruzsinszky, Communication: Effect of the orbital-overlap dependence in the meta generalized gradient approximation, *J. Chem. Phys.* **137**, 051101 (2012).
- [51] J. Sun, R. Haunschild, B. Xiao, I. W. Bulik, G. E. Scuseria, and J. P. Perdew, Semilocal and hybrid meta-generalized gradient approximations based on the understanding of the kinetic-energy-density dependence, *J. Chem. Phys.* **138**, 044113 (2013).
- [52] J. H. Yang, D. A. Kitchaev, and G. Ceder, Rationalizing accurate structure prediction in the meta-GGA SCAN functional, *Phys. Rev. B* **100**, 035132 (2019).
- [53] T. Jenkins, K. Berland, and T. Thonhauser, Reduced-gradient analysis of van der Waals complexes, *Electron. Struct.* **3**, 034009 (2021).
- [54] T. Jenkins, D. Chakraborty, K. Berland, and T. Thonhauser, Reduced-gradient analysis of molecular adsorption on graphene with nonlocal density functionals, *Phys. Rev. B* **109**, 035427 (2024).
- [55] P. Kovács, F. Tran, P. Blaha, and G. K. H. Madsen, Comparative study of the PBE and SCAN functionals: The particular case of alkali metals, *J. Chem. Phys.* **150**, 164119 (2019).
- [56] G. L. Oliver and J. P. Perdew, Spin-density gradient expansion for the kinetic energy, *Phys. Rev. A* **20**, 397 (1979).
- [57] J. W. Furness and J. Sun, Enhancing the efficiency of density functionals with an improved iso-orbital indicator, *Phys. Rev. B* **99**, 041119(R) (2019).
- [58] To account for the spin-scaling, τ^{unif} contains the additional factor $d_s(\zeta) = ((1 + \zeta)^{5/3} + (1 - \zeta)^{5/3})/2$ in the case of correlation.
- [59] M. Levy and J. P. Perdew, Hellmann-feynman, virial, and scaling requisites for the exact universal density functionals. Shape of the correlation potential and diamagnetic susceptibility for atoms, *Phys. Rev. A* **32**, 2010 (1985).
- [60] A. D. Becke and K. E. Edgecombe, A simple measure of electron localization in atomic and molecular systems, *J. Chem. Phys.* **92**, 5397 (1990).
- [61] J. Sun, B. Xiao, Y. Fang, R. Haunschild, P. Hao, A. Ruzsinszky, G. I. Csonka, G. E. Scuseria, and J. P. Perdew, Density functionals that recognize covalent, metallic, and weak bonds, *Phys. Rev. Lett.* **111**, 106401 (2013).
- [62] E. R. Johnson, A. D. Becke, C. D. Sherrill, and G. A. DiLabio, Oscillations in meta-generalized-gradient approximation potential energy surfaces for dispersion-bound complexes, *J. Chem. Phys.* **131**, 034111 (2009).
- [63] S. Lehtola and M. A. L. Marques, Many recent density functionals are numerically ill-behaved, *J. Chem. Phys.* **157**, 174114 (2022).
- [64] F. Hofmann, I. Schelter, and S. Kümmel, Molecular excitations from meta-generalized gradient approximations in the Kohn–Sham scheme, *J. Chem. Phys.* **153**, 114106 (2020).
- [65] A. J. A. Price, K. R. Bryenton, and E. R. Johnson, Requirements for an accurate dispersion-corrected density functional, *J. Chem. Phys.* **154**, 230902 (2021).
- [66] R. Kingsbury, A. S. Gupta, C. J. Bartel, J. M. Munro, S. Dwaraknath, M. Horton, and K. A. Persson, Performance comparison of r2SCAN and SCAN metaGGA density functionals for solid materials via an automated, high-throughput computational workflow, *Phys. Rev. Mater.* **6**, 013801 (2022).
- [67] S. Lehtola, Atomic electronic structure calculations with Hermite interpolating polynomials, *J. Phys. Chem. A* **127**, 4180 (2023).
- [68] D. J. W. Geldart and M. Rasolt, Exchange and correlation energy of an inhomogeneous electron gas at metallic densities, *Phys. Rev. B* **13**, 1477 (1976).
- [69] E. Engel and R. M. Dreizler, *Density Functional Theory*, 1st ed., Theoretical and Mathematical Physics (Springer, Berlin, Heidelberg, 2011).

- [70] S.-K. Ma and K. A. Brueckner, Correlation energy of an electron gas with a slowly varying high density, *Phys. Rev.* **165**, 18 (1968).
- [71] C. D. Hu and D. C. Langreth, Beyond the random-phase approximation in nonlocal-density-functional theory, *Phys. Rev. B* **33**, 943 (1986).
- [72] M. Rasolt and D. J. W. Geldart, Exchange and correlation energy in a nonuniform fermion fluid, *Phys. Rev. B* **34**, 1325 (1986).
- [73] A. P. Bartók and J. R. Yates, Regularized SCAN functional, *J. Chem. Phys.* **150**, 161101 (2019).
- [74] J. W. Furness, A. D. Kaplan, J. Ning, J. P. Perdew, and J. Sun, Construction of meta-GGA functionals through restoration of exact constraint adherence to regularized SCAN functionals, *J. Chem. Phys.* **156**, 034109 (2022).
- [75] M. Brack, B. Jennings, and Y. Chu, On the extended thomas-fermi approximation to the kinetic energy density, *Phys. Lett. B* **65**, 1 (1976).
- [76] J. P. Perdew, V. Sahni, M. K. Harbola, and R. K. Pathak, Fourth-order gradient expansion of the fermion kinetic energy: Extra terms for nonanalytic densities, *Phys. Rev. B* **34**, 686 (1986).
- [77] See Supplemental Material at <http://link.aps.org/supplemental/10.1103/PhysRevLett.133.136402> for a summary of the exact constraints, appropriate norms, and construction principles; the comprehensive working equations of LAK; details regarding the construction of LAK; the explicit solution of Eq. (10); reference atomic energies; noncovalent interactions and numerical stability; details on the computational methods; and the full test set data.
- [78] F. Oberhettinger, Hypergeometric functions, in *Handbook of Mathematical Functions with Formulas, Graphs, and Mathematical Tables*, Applied Mathematics Series Vol. 55, edited by M. Abramowitz and I. A. Stegun (US Government printing office, Washington, D.C., 1964), pp. 555–566.
- [79] J. P. Perdew, A. Ruzsinszky, J. Sun, and K. Burke, Gedanken densities and exact constraints in density functional theory, *J. Chem. Phys.* **140**, 18A533 (2014).
- [80] P. S. Svendsen and U. von Barth, Gradient expansion of the exchange energy from second-order density response theory, *Phys. Rev. B* **54**, 17402 (1996).
- [81] M. Levy, Density-functional exchange correlation through coordinate scaling in adiabatic connection and correlation hole, *Phys. Rev. A* **43**, 4637 (1991).
- [82] A. Görling and M. Levy, Requirements for correlation energy density functionals from coordinate transformations, *Phys. Rev. A* **45**, 1509 (1992).
- [83] T. Lebeda, T. Aschbrock, and S. Kümmel, First steps towards achieving both ultranonlocality and a reliable description of electronic binding in a meta-generalized gradient approximation, *Phys. Rev. Res.* **4**, 023061 (2022).
- [84] J. P. Perdew, K. Burke, and M. Ernzerhof, Generalized gradient approximation made simple, *Phys. Rev. Lett.* **77**, 3865 (1996).
- [85] J. P. Perdew and Y. Wang, Accurate and simple analytic representation of the electron-gas correlation energy, *Phys. Rev. B* **45**, 13244 (1992).
- [86] M. Lewin, E. H. Lieb, and R. Seiringer, Improved Lieb–Oxford bound on the indirect and exchange energies, *Lett. Math. Phys.* **112**, 92 (2022).
- [87] G. Kin-Lic Chan and N. C. Handy, Optimized Lieb-Oxford bound for the exchange-correlation energy, *Phys. Rev. A* **59**, 3075 (1999).
- [88] J. T. Margraf, C. Kunkel, and K. Reuter, Towards density functional approximations from coupled cluster correlation energy densities, *J. Chem. Phys.* **150**, 244116 (2019).
- [89] E. H. Lieb and S. Oxford, Improved lower bound on the indirect Coulomb energy, *Int. J. Quantum Chem.* **19**, 427 (1981).
- [90] S. Ivanov and M. Levy, Connections between high-density scaling limits of DFT correlation energies and second-order Z^{-1} quantum chemistry correlation energy, *J. Phys. Chem. A* **102**, 3151 (1998).
- [91] J. Heyd, G. E. Scuseria, and M. Ernzerhof, Hybrid functionals based on a screened Coulomb potential, *J. Chem. Phys.* **118**, 8207 (2003).
- [92] J. Heyd, G. E. Scuseria, and M. Ernzerhof, Erratum: Hybrid functionals based on a screened Coulomb potential, *J. Chem. Phys.* **124**, 219906 (2006).
- [93] A. V. Krukau, O. A. Vydrov, A. F. Izmaylov, and G. E. Scuseria, Influence of the exchange screening parameter on the performance of screened hybrid functionals, *J. Chem. Phys.* **125**, 224106 (2006).
- [94] J. Heyd, J. E. Peralta, G. E. Scuseria, and R. L. Martin, Energy band gaps and lattice parameters evaluated with the heyd-scuseria-ernzerhof screened hybrid functional, *J. Chem. Phys.* **123**, 174101 (2005).
- [95] G. te Velde, F. M. Bickelhaupt, E. J. Baerends, C. Fonseca Guerra, S. J. A. van Gisbergen, J. G. Snijders, and T. Ziegler, Chemistry with ADF, *J. Comput. Chem.* **22**, 931 (2001).
- [96] E. Van Lenthe and E. J. Baerends, Optimized slater-type basis sets for the elements 1–118, *J. Comput. Chem.* **24**, 1142 (2003).
- [97] SCM, Theoretical Chemistry, Vrije Universiteit, Amsterdam, The Netherlands, ADF 2022.102 (a modified version is used) (2022).
- [98] G. te Velde and E. J. Baerends, Precise density-functional method for periodic structures, *Phys. Rev. B* **44**, 7888 (1991).
- [99] G. Wiesenekker and E. J. Baerends, Quadratic integration over the three-dimensional brillouin zone, *J. Phys. Condens. Matter* **3**, 6721 (1991).
- [100] M. Franchini, P. H. T. Philipsen, and L. Visscher, The Becke fuzzy cells integration scheme in the Amsterdam Density Functional program suite, *J. Comput. Chem.* **34**, 1819 (2013).
- [101] M. Franchini, P. H. T. Philipsen, E. van Lenthe, and L. Visscher, Accurate coulomb potentials for periodic and molecular systems through density fitting, *J. Chem. Theory Comput.* **10**, 1994 (2014).
- [102] E. v. Lenthe, E.-J. Baerends, and J. G. Snijders, Relativistic regular two-component Hamiltonians, *J. Chem. Phys.* **99**, 4597 (1993).
- [103] E. S. Kadantsev, R. Klooster, P. L. De Boeij, and T. Ziegler, The formulation and implementation of analytic energy

- gradients for periodic density functional calculations with STO/NAO Bloch basis set, *Mol. Phys.* **105**, 2583 (2007).
- [104] SCM, Theoretical Chemistry, BAND 2023.104 (a modified version is used) (Vrije Universiteit, Amsterdam, The Netherlands, 2023).
- [105] A. Seidl, A. Görling, P. Vogl, J. A. Majewski, and M. Levy, Generalized Kohn-Sham schemes and the band-gap problem, *Phys. Rev. B* **53**, 3764 (1996).
- [106] R. Neumann, R. H. Nobes, and N. Handy, Exchange functionals and potentials, *Mol. Phys.* **87**, 1 (1996).
- [107] B. Jäger, R. Hellmann, E. Bich, and E. Vogel, *Ab initio* pair potential energy curve for the argon atom pair and thermophysical properties of the dilute argon gas. I. Argon–argon interatomic potential and rovibrational spectra, *Mol. Phys.* **107**, 2181 (2009).
- [108] R. Peverati and D. G. Truhlar, Communication: A global hybrid generalized gradient approximation to the exchange–correlation functional that satisfies the second-order density–gradient constraint and has broad applicability in chemistry, *J. Chem. Phys.* **135**, 191102 (2011).
- [109] R. Peverati and D. G. Truhlar, Quest for a universal density functional: The accuracy of density functionals across a broad spectrum of databases in chemistry and physics, *Phil. Trans. R. Soc. A* **372**, 20120476 (2014).
- [110] J. Sun, M. Marsman, G. I. Csonka, A. Ruzsinszky, P. Hao, Y.-S. Kim, G. Kresse, and J. P. Perdew, Self-consistent meta-generalized gradient approximation within the projector-augmented-wave method, *Phys. Rev. B* **84**, 035117 (2011).
- [111] S. Jana, B. Patra, S. Śmiga, L. A. Constantin, and P. Samal, Improved solid stability from a screened range-separated hybrid functional by satisfying semiclassical atom theory and local density linear response, *Phys. Rev. B* **102**, 155107 (2020).
- [112] J. P. Perdew, W. Yang, K. Burke, Z. Yang, E. K. U. Gross, M. Scheffler, G. E. Scuseria, T. M. Henderson, I. Y. Zhang, A. Ruzsinszky, H. Peng, J. Sun, E. Trushin, and A. Görling, Understanding band gaps of solids in generalized Kohn–Sham theory, *Proc. Natl. Acad. Sci. U.S.A.* **114**, 2801 (2017).
- [113] Z. H. Yang, H. Peng, J. Sun, and J. P. Perdew, More realistic band gaps from meta-generalized gradient approximations: Only in a generalized Kohn–Sham scheme, *Phys. Rev. B* **93**, 205205 (2016).
- [114] A. D. Kaplan and J. P. Perdew, Laplacian-level meta-generalized gradient approximation for solid and liquid metals, *Phys. Rev. Mater.* **6**, 083803 (2022).
- [115] C. M. Horowitz, C. R. Proetto, and J. M. Pitarke, Towards a universal exchange enhancement factor in density functional theory, *Phys. Rev. B* **107**, 195120 (2023).
- [116] C. M. Horowitz, C. R. Proetto, and J. M. Pitarke, Construction of a semilocal exchange density functional from a three-dimensional electron gas collapsing to two dimensions, *Phys. Rev. B* **108**, 115119 (2023).
- [117] S. Jana, S. Śmiga, L. A. Constantin, and P. Samal, Semilocal meta-gga exchange–correlation approximation from adiabatic connection formalism: Extent and limitations, *J. Phys. Chem. A* **127**, 8685 (2023).
- [118] R. Pederson and K. Burke, The difference between molecules and materials: Reassessing the role of exact conditions in density functional theory, *J. Chem. Phys.* **159**, 214113 (2023).

Supplementary material for “Balancing the Contributions to the Gradient Expansion: Accurate Binding and Band Gaps with a Nonempirical Meta-GGA”

Timo Lebeda,* Thilo Aschebrock, and Stephan Kümmel†
Theoretical Physics IV, University of Bayreuth, 95440 Bayreuth, Germany

This supplemental material provides a summary of the exact constraints, appropriate norms, and construction principles of the LAK meta-GGA, the comprehensive working equations of LAK, details regarding the construction of LAK, the explicit solution of equation (10) of the main text, reference atomic energies, a numerical stability analysis for the argon dimer, details on the computational methods, and the full test set data.

EXACT CONSTRAINTS, APPROPRIATE NORMS, AND CONSTRUCTION PRINCIPLES

Here, we summarize the exact constraints that LAK fulfills and the appropriate norms and construction principles used for the construction of LAK. We have checked LAK for all the exact constraints listed in the Supplemental Material of Ref. 1. Note that, in contrast to Ref. 1, we list the second-order gradient expansion as an exact constraint for exchange and correlation together instead of for correlation alone, because strictly speaking the second-order gradient expansion holds for exchange and correlation together [2].

Exact Constraints for Exchange

- (x1) Negativity of the exchange energy
- (x2) Exact spin-scaling relation
- (x3) Uniform density scaling
- (x4) Fourth-order gradient expansion
- (x5) Non-uniform density scaling
- (x6) Strongly tightened bound for two-electron densities

Exact Constraints for Correlation

- (c1) Non-positivity of the correlation energy
- (c2) Uniform density scaling to the high-density limit
- (c3) Uniform density scaling to the low-density limit
- (c4) Zero correlation energy for any one-electron spin-polarized density (no self-correlation)
- (c5) Non-uniform density scaling

Exact Constraints for Exchange and Correlation

- (xc1) Size extensivity
- (xc2) Second-order gradient expansion
- (xc3) General Lieb-Oxford bound (as tightened by Lewin, Lieb, and Seiringer (LLS) [3])
- (xc4) Weak dependence upon relative spin polarization in the low-density limit
- (xc5) Static linear response of the uniform electron gas
- (xc6) Lieb-Oxford bound for two-electron densities

Appropriate Norms

- (n1) Uniform and slowly-varying densities
- (n2) The hydrogen atom
- (n3) The helium iso-electronic series
- (n4) The $Z \rightarrow \infty$ limit of the two-electron ion

Construction Principles

- (p1) $\frac{\partial F_x}{\partial \alpha} \begin{cases} < 0, \text{ everywhere} \\ \text{roughly constant for } 0.2 \lesssim \alpha \lesssim 1.5 \end{cases}$
- (p2) $\frac{\partial F_{xc}}{\partial s} \Big|_{\alpha=1} \begin{cases} > 0 \text{ for } 0.5 \lesssim s \lesssim 1.2 \\ < 0 \text{ for } s \gtrsim 1.2 \end{cases}$

LAK satisfies all the exact constraints that SCAN satisfies. Additionally, LAK satisfies a newer, stronger version of the general Lieb-Oxford bound and the gradient expansions in a balanced way. SCAN does not use the appropriate norm (n3), but instead the jellium surface energy, the helium atom, the limit of large atomic number for the rare-gas atoms, and the compressed argon dimer. In SCAN, 10 parameters are fitted to these appropriate norms, whereas in LAK only 3 parameters (b_x , b_{1c} , and χ_0) are determined by appropriate norms and 2 parameters (a_x and a_c) by the construction principles.

LAK WORKING EQUATIONS

Here, we summarize the equations required to conveniently implement LAK. In many modern electronic structure codes, exchange and correlation are implemented separately. We therefore split $E_{xc} = E_x + E_c$ with

$$E_x[n] = A_x \int n^{4/3} F_x(s, \alpha) d^3r, \quad (1a)$$

$$E_c[n_\uparrow, n_\downarrow] = \int n \varepsilon_c(r_s, \zeta, s, \alpha) d^3r, \quad (1b)$$

like in Eq. (1) of the main text and give the definitions for $F_x(s, \alpha)$ and $\varepsilon_c(r_s, \zeta, s, \alpha)$.

Exchange

$$F_x^{\text{LAK}}(s, \alpha) = h_x^0 g_x(s) + (1 - f_x(\alpha)) (h_x^1(s) - h_x^0) g_{\text{num}}(s) \quad (2)$$

$$A_x = -(3/4)(3/\pi)^{1/3} \quad (3)$$

$$g_x(s) = 1 - e^{-b_x s^{-1/2}} \quad (4)$$

$$f_x(\alpha) = \frac{2}{\pi} \arctan \left[\frac{\pi}{2} \left(c_1 \frac{\alpha - 1}{\alpha} + c_2 (\alpha - 1)^2 \right) \right] \quad (5)$$

$$c_1 = \mu_{\alpha, x} / (h_x^0 - 1) \quad (6)$$

$$c_2 = (\mu_{\alpha, x} + \nu_\alpha) / (h_x^0 - 1) \quad (7)$$

$$h_x^1(s) = h_x^{\text{GE4}}(s) + k_x(s) (a_x - h_x^{\text{GE4}}(s)) \quad (8)$$

$$h_x^{\text{GE4}}(s) = 1 + \mu_{s, x} s^2 + \nu_s s^4 + h_x^0 [1 - g_x(s)] \quad (9)$$

$$k_x(s) = \exp(-1 / [(s/a_x)^2 (1 + s^2)]) \quad (10)$$

$$g_{\text{num}}(s) = 1 - e^{-(a_{\text{num}}/s)^2} \quad (11)$$

In the following, we list all parameters appearing in the exchange part of LAK and how they were determined.

$$\begin{aligned}
h_x^0 &= 1.174 & (\text{x6}) \\
\mu_{\alpha,x} &= -\left(97 + 3h_x^0 + [(3h_x^0)^2 + 74166h_x^0 - 64175]^{1/2}\right)/1200 & (\text{x4}) \\
\nu_\alpha &= (73 - 50\mu_{\alpha,x})/5000 & (\text{x4}) \\
\mu_{s,x} &= (10 + 60\mu_{\alpha,x})/81 & (\text{x4}) \\
\nu_s &= -(1606 - 50\mu_{\alpha,x})/18225 & (\text{x4}) \\
b_x &= 4.9479 & (\text{n2}) \\
a_x &= 1.1 & (\text{p2}) \\
a_{\text{num}} &= 5 & (\text{numerical stability})
\end{aligned}$$

Correlation

$$\varepsilon_c^{\text{LAK}}(r_s, \zeta, s, \alpha) = \varepsilon_c^0(r_s, \zeta, s) + [1 - f_c(r_s, \alpha)] [\varepsilon_c^1(r_s, \zeta, s) - \varepsilon_c^0(r_s, \zeta, s)] g_{\text{num}}(s) \quad (12)$$

$$\varepsilon_c^0(r_s, \zeta, s) = [\varepsilon_c^{\text{LDA0}}(r_s) + H^0(r_s, s)] G_c(\zeta) \quad (13)$$

$$\varepsilon_c^{\text{LDA0}}(r_s) = -\frac{b_{1c}}{1 + b_{2c}r_s} \quad (14)$$

$$H^0(r_s, s) = b_{1c} \ln \left[1 + w_0(r_s) \left(1 - [1 + 4\chi_0 s^2]^{-1/4} \right) \right] \quad (15)$$

$$w_0(r_s) = \exp \left[-\varepsilon_c^{\text{LDA0}}(r_s)/b_{1c} \right] - 1 \quad (16)$$

$$G_c(\zeta) = [1 - 2.3631 [d_x(\zeta) - 1]] (1 - \zeta^{12}) \quad (17)$$

$$d_x(\zeta) = \frac{1}{2} \left[(1 + \zeta)^{4/3} + (1 - \zeta)^{4/3} \right] \quad (18)$$

$$f_c(r_s, \alpha) = \frac{2}{\pi} \arctan \left[\frac{\pi}{2} f_c^{\text{GE2}}(r_s) \tilde{\alpha}(r_s, \alpha) \right] \quad (19)$$

$$\tilde{\alpha}(r_s, \alpha) = \frac{\alpha - 1}{r_s \alpha} \quad (20)$$

$$f_c^{\text{GE2}}(r_s) = \frac{\beta_{\tilde{\alpha}}(r_s)}{\varepsilon_c^1(r_s, 0, 0) - \varepsilon_c^0(r_s, 0, 0)} \quad (21)$$

$$\beta_{\tilde{\alpha}}(r_s) = -A_c \mu_{\alpha,c}(r_s) \quad (22)$$

$$\mu_{\alpha,c}(r_s) = C_{\mu_\alpha}(r_s) \mu_\alpha - \mu_{\alpha,x} \quad (23)$$

$$\varepsilon_c^1(r_s, \zeta, s) = \varepsilon_c^{\text{LSDA}}(r_s, \zeta) + H^1(r_s, \zeta, t(r_s, s)) \quad (24)$$

$$H^1(r_s, \zeta, t(r_s, s)) = \begin{cases} H_+^1(r_s, \zeta, t(r_s, s)), & \beta_t(r_s) \geq 0 \\ H_-^1(r_s, \zeta, t(r_s, s)), & \beta_t(r_s) < 0 \end{cases} \quad (25)$$

$$t^2(r_s, \zeta, s) = c_t(\zeta) s^2 / r_s \quad (26)$$

$$c_t(\zeta) = (3\pi^2/16)^{2/3} / \phi^2(\zeta) \quad (27)$$

$$\phi(\zeta) = \frac{1}{2} \left[(1 + \zeta)^{2/3} + (1 - \zeta)^{2/3} \right] \quad (28)$$

$$\beta_t(r_s) = \frac{A_c}{c_t} \mu_{s,c}(r_s) \quad (29)$$

$$A_c = (4\pi/3)^{-1/3} A_x \quad (30)$$

$$\mu_{s,c}(r_s) = \mu [C_{\mu_\alpha}(r_s)(1 + 6\mu_\alpha) - (1 + 6\mu_{\alpha,x})] \quad (31)$$

$$(32)$$

$$H_+^1(r_s, \zeta, t(r_s, s)) = \gamma \phi^3 \ln [1 + w_1 (1 - g_1^+) (1 - g_2^+ + g_3^+)] \quad (33)$$

$$H_-^1(r_s, \zeta, t(r_s, s)) = \gamma \phi^3 \ln [1 + w_1 (1 - g_1^-) (1 - g_2^- - g_3^-)] \quad (34)$$

$$\gamma = (1 - \ln(2))/\pi^2 \quad (35)$$

$$w_1(r_s, \zeta) = \exp [-\varepsilon_c^{\text{LSDA}}(r_s, \zeta)/(\gamma \phi \zeta)^3] - 1 \quad (36)$$

$$g_1^\pm(r_s, t) = [1 \pm 4A(r_s, \zeta)t^2]^{-1/4} \quad (37)$$

$$g_2^\pm(r_s, t) = [1 + (A(r_s, \zeta)t^2)^2]^{-1} \quad (38)$$

$$g_3^+(r_s, t) = [1 + a_c A(r_s, \zeta)t^2]^{-1} \quad (39)$$

$$g_3^-(r_s, t) = [1 - (w_1(r_s, \zeta) + b_{3c})A(r_s, \zeta)t^2]^{-1} \quad (40)$$

$$A(r_s, \zeta) = \frac{\beta_t(r_s)}{\gamma w_1(r_s, \zeta)} \quad (41)$$

$$g_{\text{num}}(s) = 1 - e^{-(a_{\text{num}}/s)^2} \quad (42)$$

For $\varepsilon_c^{\text{LSDA}}$, we use the parametrization of Perdew and Wang [4]. $C_{\mu_\alpha}(r_s)$ is defined in Eq. (62) below. In the following, we list all parameters appearing in the correlation part of LAK and how they were determined.

$\mu_\alpha = -\mu_{\alpha,x}/2$	(ultranonlocality and smoothness; see main text)
$b_{1c} = 0.0468$	(n3)
$b_{2c} = 0.205601$	(xc6)
$\chi_0 = 1.55344$	(n4)
$b_{3c} = 2.85$	(p2)
$a_c = 10$	(numerical stability; identical to exchange)
$a_{\text{num}} = 5$	

DETAILED CONSTRUCTION OF THE LAK FUNCTIONAL

In this section, we explain technical details in the construction of the meta-GGA LAK that we omitted in the main text for the sake of clarity.

Details about LAK exchange

Here, we detail the exchange part of LAK. As noted in the main text, we use the enhancement factor

$$F_x^{\text{LAK}}(s, \alpha) = h_x^0 g_x(s) + (1 - f_x(\alpha)) (h_x^1(s) - h_x^0) g_{\text{num}}(s), \quad (43)$$

because the separation of variables allows to conveniently fix $\mu_{\alpha,x}$ via the fourth-order gradient expansion of exchange. Applying the strongly tightened bound for $\alpha = 0$, $F_x \leq 1.174 =: h_x^0$ [5], leads to $\mu_{\alpha,x} = -0.209897$ [6]. Like in SCAN and TASK, $g_x(s) = 1 - e^{-b_x s^{-1/2}}$ with $b_x = 4.9479$ ensures the exact hydrogen atom energy to reduce one-electron self-interaction [1, 6].

Guided by the gradient expansion of exchange to fourth order with contributions from s and α [6], we define

$$h_x^1(s) = h_x^{\text{GE4}}(s) + k_x(s) (a_x - h_x^{\text{GE4}}(s)), \quad (44a)$$

$$f_x(\alpha) = \frac{2}{\pi} \arctan \left(\frac{\pi}{2} \left(c_1 \frac{\alpha - 1}{\alpha} + c_2 (\alpha - 1)^2 \right) \right). \quad (44b)$$

Here, $h_x^{\text{GE4}}(s) = 1 + \mu_{s,x} s^2 + \nu_s s^4 + h_x^0 [1 - g_x(s)]$, $c_1 = \mu_{\alpha,x}/(h_x^0 - 1)$, and $c_2 = (\mu_{\alpha,x} + \nu_\alpha)/(h_x^0 - 1)$ are determined by the gradient expansion. In particular, the last term of h_x^{GE4} cancels a small contribution from the first term of F_x^{LAK} . The term

$$k_x(s) = \exp(-1/[(s/a_x)^2(1+s^2)]) \quad (45)$$

compensates for the divergence of the gradient expansion as $s \rightarrow \infty$, thus ensuring the negativity of the exchange energy density.

As emphasized in the main text, these considerations fix f_x and h_x^1 in several limits (in particular for $s \rightarrow 0$, $s \rightarrow \infty$, $\alpha = 0$, $\alpha \approx 1$) and by upper and lower bounds. To determine them in the intermediate range, we apply the construction principles. Following this strategy, we use the arctan in f_x because it allows us to fulfill the required limits for $\alpha = 0$, $\alpha = 1$, and $\alpha \rightarrow \infty$ and at the same time satisfy the first construction principle, Eq. (15) of the main text (construction principle (p1) above), compare Figure 1b. Similarly, $a_x = 1.1$ and the form of k_x are determined by the second construction principle, Eq. (16) of the main text (construction principle (p2) above), compare Figure 1a.

Finally, $g_{\text{num}}(s) = 1 - e^{-(a_{\text{num}}/s)^2}$ reduces the α -dependence for large values of s . This has been shown to reduce the convergence issues of meta-GGAs [6, 7]. We choose $a_{\text{num}} = 5$ to improve the numerical stability without changing the predicted total energies.

Figure 1 shows the exchange enhancement factor of LAK (a) as a function of the reduced density gradient s for several values of α and (b) as a function of α for several values of s .

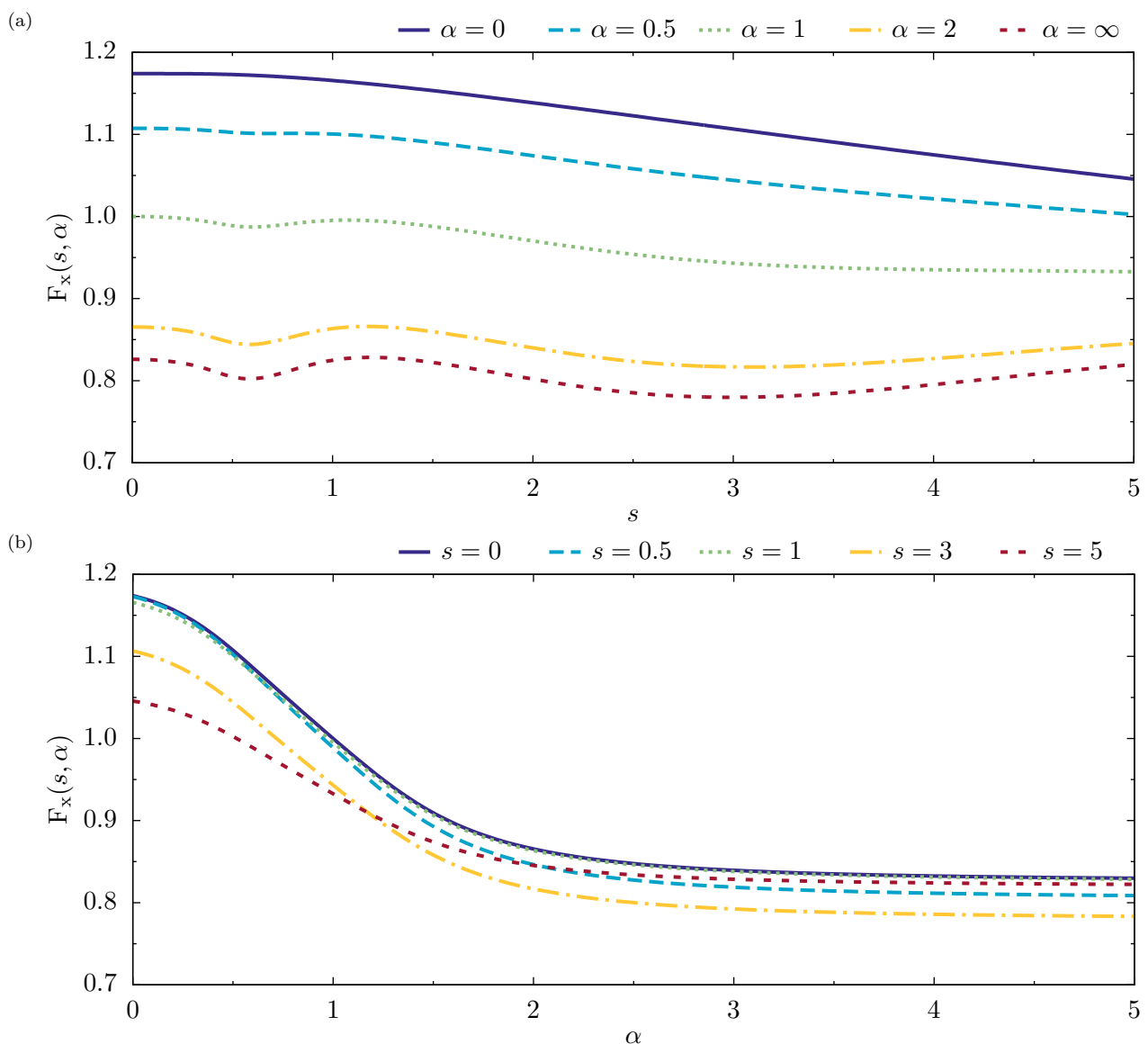


FIG. 1. The LAK exchange enhancement factor F_x^{LAK} of Eq. (2) for a spin-unpolarized system (a) as a function of s for several values of α and (b) as a function of α for several values of s .

Details about LAK correlation

Here, we detail the correlation part of LAK. Like exchange, it is based on a balanced treatment of the gradient expansion and on the successful idea of interpolating between $\alpha = 0$ and $\alpha = 1$,

$$\begin{aligned} \varepsilon_c^{\text{LAK}}(r_s, \zeta, s, \alpha) &= \varepsilon_c^0(r_s, \zeta, s) + [1 - f_c(r_s, \alpha)] \\ &\times [\varepsilon_c^1(r_s, \zeta, s) - \varepsilon_c^0(r_s, \zeta, s)] g_{\text{num}}(s). \end{aligned} \quad (46)$$

As outlined in the main text, we use the interpolation function

$$f_c(r_s, \alpha) = \frac{2}{\pi} \arctan \left[\frac{\pi}{2} f_c^{\text{GE2}}(r_s) \tilde{\alpha}(r_s, \alpha) \right] \quad (47)$$

with the iso-orbital indicator $\tilde{\alpha} = (\alpha - 1)/(r_s \alpha)$. Further, $f_c^{\text{GE2}}(r_s) = \beta_{\tilde{\alpha}}(r_s) / [\varepsilon_c^1(r_s, 0, 0) - \varepsilon_c^0(r_s, 0, 0)]$ is determined by the gradient expansion (the density-dependence of the gradient expansion coefficient $\beta_{\tilde{\alpha}}$ is derived in Eq. (20) of the main text, ε_c^0 and ε_c^1 are defined below). As in f_x and for the same reasons, we also use the arctan in f_c . This additionally ensures the consistency of exchange and correlation.

Next, we detail the correlation term for the iso-orbital limit $\alpha = 0$,

$$\varepsilon_c^0(r_s, \zeta, s) = G_c(\zeta) [\varepsilon_c^{\text{LDA0}}(r_s) + H^0(r_s, s)]. \quad (48)$$

We adopt G_c from SCAN to make the correlation free from one-electron self-interaction via $f_c(r_s, 0) = 1$ and $G_c(|\zeta| = 1) = 0$ [1]. For the term $\varepsilon_c^{\text{LDA0}}$ that depends only on the local density, we modify the coupled cluster-motivated correlation from Ref. 8,

$$\varepsilon_c^{\text{LDA0}}(r_s) = -b_{1c}/(1 + b_{2c}r_s). \quad (49)$$

As in Ref. 8, we use $b_{1c} = 0.0468$, which is fit to the helium iso-electronic series norm. In contrast to Ref. 8, we determine $b_{2c} = 0.205601$ by the lower bound on the exchange-correlation energies of two-electron systems, $F_{xc} \leq 1.67082$ [9]. For H^0 , we adopt only the form from SCAN,

$$H^0(r_s, s) = b_{1c} \ln \left[1 + w_0(r_s) \left(1 - [1 + 4\chi_0 s^2]^{-1/4} \right) \right], \quad (50)$$

but determine $\chi_0 = 1.55344$ from fitting to the correlation energy $E_c = -0.0467$ Ha of the high-density limit of the two-electron ion with the nucleus number $Z \rightarrow \infty$ [10]. Here, $w_0(r_s) = \exp[-\varepsilon_c^{\text{LDA0}}(r_s)/b_{1c}] - 1$.

Finally, we detail the correlation term for the homogeneous electron gas limit $\alpha = 1$,

$$\varepsilon_c^1(r_s, \zeta, s) = \varepsilon_c^{\text{LSDA}}(r_s, \zeta) + H^1(r_s, \zeta, t(r_s, s)). \quad (51)$$

Here, $\varepsilon_c^{\text{LSDA}}$ denotes the correlation energy density per particle of the homogeneous electron gas. The construction of H^1 is somewhat more involved, as detailed below. As noted in the main text, the basic idea is to satisfy our partitioning of the gradient expansion and all exact constraints relevant to H^1 in a way that is similar to the respective construction in PBE and SCAN. Like for exchange, we use the second construction principle, Eq. (16) of the main text (construction principle (p2) above), to determine the form of H^1 in the intermediate range.

Compared to the respective constructions in PBE and SCAN, the detailed construction of H^1 is somewhat more involved for the following reason. According to Eq. (13) of the main text, there exist combinations of μ_α and $\mu_{\alpha,x}$ such that $\mu_{\alpha,c}$ and $\mu_{s,c}$ can have a zero in r_s . For the values used in LAK, $\mu_\alpha = 0.1049487$ and $\mu_{\alpha,x} = -0.2098974$, $\mu_{\alpha,c}$ does not have a zero, but $\mu_{s,c}$ does have a zero at $r_s \approx 50$. Consequently, also β_t does have a zero and changes its sign from positive to negative at $r_s \approx 50$. While such a change in sign *can* become important for specific combinations of μ_α and $\mu_{\alpha,x}$, this is of minor importance for the values used in LAK. Densities corresponding to $r_s \gtrsim 50$ are so small that the region where β_t is negative has almost no influence on the predicted energies. However, the change in sign causes a negative argument in a logarithm if used in the PBE or SCAN construction without modification.

Consequently, to obtain a well-defined functional everywhere that fulfills all the desired exact constraints, we define $H^1(r_s, \zeta, t)$ piecewise in r_s via

$$H^1 = \begin{cases} \gamma \phi^3 \ln [1 + w_1 (1 - g_1^+) (1 - g_2^+ + g_3^+)], & \beta_t(r_s) \geq 0, \\ \gamma \phi^3 \ln [1 + w_1 (1 - g_1^-) (1 - g_2^- - g_3^-)], & \beta_t(r_s) < 0, \end{cases} \quad (52)$$

with γ , $\phi(\zeta)$, and $w_1(r_s, \zeta)$ adopted from PBE [11] and SCAN [1]. We also adopt $A(r_s, \zeta) = \beta_t(r_s)/(\gamma w_1(r_s, \zeta))$ from SCAN, but with β_t according to Eq. (20) of the main text. Further, we take g_1 from SCAN and expand the SCAN expression for H^1 by the term $(1 - g_2 - g_3)$ with

$$g_1(x) = \frac{1}{(1+4x)^{1/4}}, \quad g_2(x) = \frac{1}{1+x^2}, \quad g_3(x) = \frac{1}{1+x}, \quad (53)$$

where we distinguish the cases $\beta_t > 0$ and $\beta_t < 0$ by

$$\begin{aligned} g_1^+(r_s, \zeta, t) &= g_1(At^2), & g_1^-(r_s, \zeta, t) &= g_1(-At^2), \\ g_2^+(r_s, \zeta, t) &= g_2(At^2), & g_2^-(r_s, \zeta, t) &= g_2(-At^2), \\ g_3^+(r_s, \zeta, t) &= g_3(a_c At^2), & g_3^-(r_s, \zeta, t) &= g_3(-[w_1(r_s, \zeta) + b_{3c}] At^2). \end{aligned} \quad (54)$$

Eqs. (53) and (54) follow from the following considerations, which conclude the construction of H^1 .

- i) To ensure smoothness at the zero of β_t , we aim at analogous definitions for $\beta_t > 0$ and $\beta_t < 0$.
- ii) To make correlation properly scale to a finite negative value per electron under uniform density scaling to the high-density limit [12], all functions are defined in terms of At^2 .
- iii) To avoid a zero in the denominator, all functions for $\beta_t < 0$ use $-At^2$, since this is positive for $\beta_t < 0$.
- iv) Like in SCAN, using $(1 - g_1^+)$ alone would fulfill all exact constraints relevant to H^1 for $\beta_t > 0$, in particular the gradient expansion. $(1 - g_1^-)$ is defined analogously to $(1 - g_1^+)$, but with a different sign of At^2 to avoid a zero in the denominator. As a consequence, however, using $(1 - g_1^-)$ alone would fulfill the gradient expansion with the wrong sign. Therefore, $g_2^-(t=0) = g_3^-(t=0) = 1$ to restore the correct sign of the gradient expansion via multiplication by $(1 - g_2^- - g_3^-)$ in H^1 . Following consideration i), we analogously have $g_2^+(t=0) = g_3^+(t=0) = 1$. Thus, $(1 - g_2^+ + g_3^+)$ in H^1 maintains the correct sign of the gradient expansion for $\beta_t > 0$.
- v) g_2 and g_3 must tend to zero faster than g_1 to maintain the correct non-uniform density scaling via $\varepsilon_c \propto s^{-1/2}$ for $s \rightarrow \infty$. We choose the simplest functions that fulfill this requirement for g_2 and g_3 .
- vi) The argument of the logarithm in Eq. (52) must remain positive for all r_s . Since w_1 is unbounded for $r_s \rightarrow 0$ and $0 \leq (1 - g_1^-) \leq 1$, the term $(1 - g_2^- - g_3^-)$ must become less negative with decreasing r_s at the same rate as w_1 increases, in order to avoid a negative argument of the logarithm. This is ensured by the term w_1 in the denominator of g_3^- .
- vii) To ensure the LLS-bound $F_{xc} \leq 2.1346$ [3], we introduce the parameter b_{3c} in g_3^- that we determine to $b_{3c} = 2.85$ using this constraint, compare Figure 2.
- ix) For smoothness at the zero of β_t , the definitions of g_2^+ and g_3^+ follow those of g_2^- and g_3^- as closely as possible. Additionally, g_3^+ is tailored towards fulfilling the second construction principle, Eq. (16) of the main text (construction principle (p2) above). These considerations lead to $a_c = 10 \approx w_1(1, 0) + b_{3c}$.

Note that one could alternatively stick with the simpler PBE or SCAN form for H^1 and let β_t smoothly tend to zero for $r_s \gtrsim 50$ to avoid the change in sign in β_t . Such a procedure could be motivated by the limited accuracy of the parametrization of C_s for such low densities. However, this procedure would result in correlation having a different gradient expansion coefficient than exchange in the low-density limit of the homogeneous electron gas. But the cancellation of the exchange and correlation gradient expansions in the homogeneous electron gas limit is important for a static linear response of the uniform electron gas [13]. Consequently, removing the zero in β_t is in contradiction with our nonempirical construction strategy and the form of H^1 in LAK, although somewhat more involved, is a consequence of our nonempirical construction strategy.

Figure 2 shows the exchange-correlation enhancement factor $F_{xc} = F_x + F_c$ of LAK in the low-density limit $r_s \rightarrow \infty$. Note that the enhancement factor of correlation is $F_c(r_s, \zeta, s, \alpha) = A_c r_s \varepsilon_c(r_s, \zeta, s, \alpha)$.

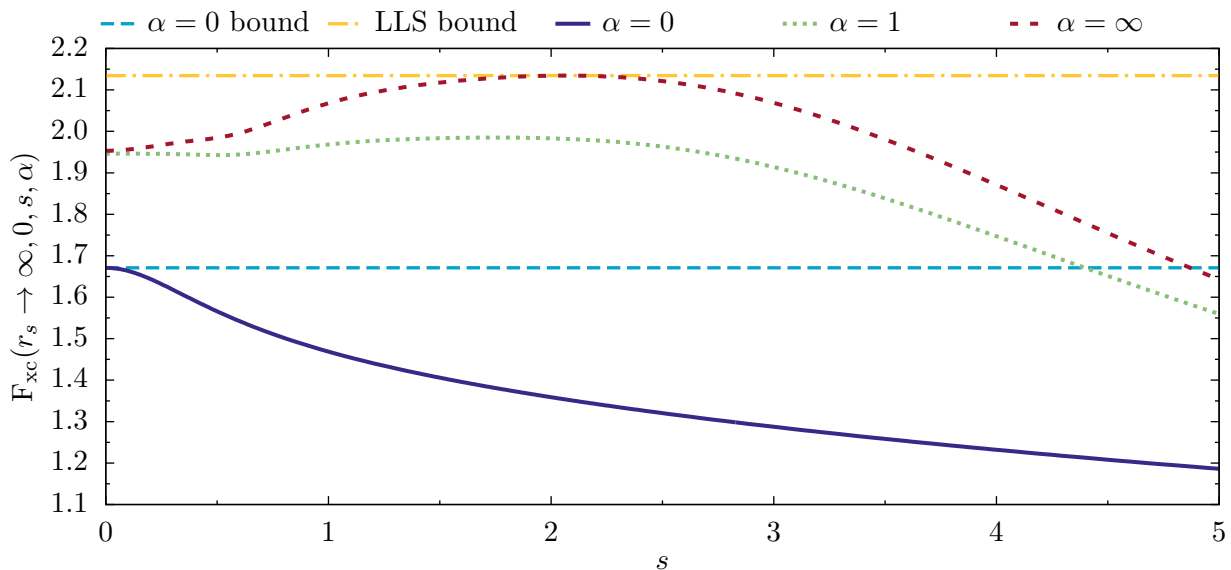


FIG. 2. The LAK enhancement factor F_{xc}^{LAK} in the low-density limit $r_s \rightarrow \infty$ for a spin-unpolarized system as a function of s for several values of α . The LLS bound is the global bound $F_{xc} \leq 2.1346$ as tightened by Lewin, Lieb, and Seiringer [3]. The $\alpha = 0$ bound is the bound for two-electron systems, $F_{xc|\alpha=0} \leq 1.67082$ [9].

EXPLICIT SOLUTION OF EQUATION (10) OF THE MAIN TEXT

As discussed in the main text, shifting the contributions to the gradient expansion between s and α leads to a transformed density-dependent coefficient C_{μ_α} for the gradient expansion. C_{μ_α} depends parametrically on μ_α . For fixed μ_α , the density dependence of C_{μ_α} is determined by C_s via the differential equation (Eq. (10) of the main text)

$$C_s(r_s) = C_{\mu_\alpha}(r_s) + 6\mu_\alpha r_s C'_{\mu_\alpha}(r_s). \quad (55)$$

For $\mu_\alpha = 0$, this restores the common gradient expansion coefficient C_s of the gradient expansion in s -only. For $\mu_\alpha > 0$, the general solution to this differential equation is given by

$$C_{\mu_\alpha}(r_s) = c_\kappa r_s^{-\kappa} + \kappa r_s^{-\kappa} \int_0^{r_s} C_s(x) x^{\kappa-1} dx, \quad (56)$$

while for $\mu_\alpha < 0$ it is given by

$$C_{\mu_\alpha}(r_s) = c_\kappa r_s^{-\kappa} - \kappa r_s^{-\kappa} \int_{r_s}^{\infty} C_s(x) x^{\kappa-1} dx, \quad (57)$$

with $\kappa = 1/(6\mu_\alpha)$. In both cases $c_\kappa = 0$ corresponds to the only solution that behaves regularly both in the high- and low-density limit. We use C_s in the parametrization by Rasolt and Geldart [14]

$$C_s(r_s) = -\frac{16\pi(3\pi^2)^{1/3}}{3000\mu} \frac{2.568 + 23.266r_s + 0.007389r_s^2}{1 + 9.723r_s + 0.472r_s^2 + 0.07389r_s^3}, \quad (58)$$

where $\mu = 10/81$. The solutions to Eqs. (56) and (57) can be represented using hypergeometric functions [15]. Since LAK uses a positive μ_α , we restrict the following discussion to the case $\mu_\alpha > 0$. For $\mu_\alpha < 0$ similar expressions can be derived.

For any $\mu_\alpha > 0$, and thus $\kappa > 0$, the solution to Eq. (56) can be expressed as

$$\begin{aligned}
C_{\mu_\alpha}(r_s) = \frac{1}{\pi} \text{Re} \left[& -3.40792 {}_2F_1(1, \kappa; 1 + \kappa; -8.66954r_s) \right. \\
& + (0.0103142 + 0.015838i) {}_2F_1(1, \kappa; 1 + \kappa; z_1 r_s) \\
& + (0.0103142 - 0.015838i) {}_2F_1(1, \kappa; 1 + \kappa; z_1^* r_s) \\
& + \frac{\kappa r_s}{(1 + \kappa)(2 + \kappa)} \left[-30.8756(2 + \kappa) {}_2F_1(1, 1 + \kappa; 2 + \kappa; -8.66954r_s) \right. \\
& \quad + (0.0934461 + 0.143483i) {}_2F_1(1, 1 + \kappa; 2 + \kappa; z_1 r_s) \\
& \quad + (0.0934461 - 0.143483i) {}_2F_1(1, 1 + \kappa; 2 + \kappa; z_1^* r_s) \\
& \quad - 0.00980572\kappa r_s {}_2F_1(1, 2 + \kappa; 3 + \kappa; -8.66954r_s) \\
& \quad + (0.0000296774 + 0.0000455685i)(1 + \kappa)r_s {}_2F_1(1, 2 + \kappa; 3 + \kappa; z_1 r_s) \\
& \quad \left. \left. + (0.0000296774 - 0.0000455685i)(1 + \kappa)r_s {}_2F_1(1, 2 + \kappa; 3 + \kappa; z_1^* r_s) \right] \right]
\end{aligned} \tag{59}$$

with $z_1 = -(0.0267302 + 0.0883654i)$ and the Gaussian (or ordinary) hypergeometric function [15]

$${}_2F_1(a, b; c; z) = \sum_{n=0}^{\infty} \frac{(a)_n (b)_n}{(c)_n} \frac{z^n}{n!}. \tag{60}$$

Here, $(q)_n$ denotes the (rising) Pochhammer symbol

$$(q)_n = \begin{cases} 1 & , n = 0, \\ \prod_{k=0}^{n-1} (q + k) & , n > 0. \end{cases} \tag{61}$$

As hypergeometric functions are unpractical for numerical calculations, it is advisable to approximate them in a suitable way, as detailed in the next section.

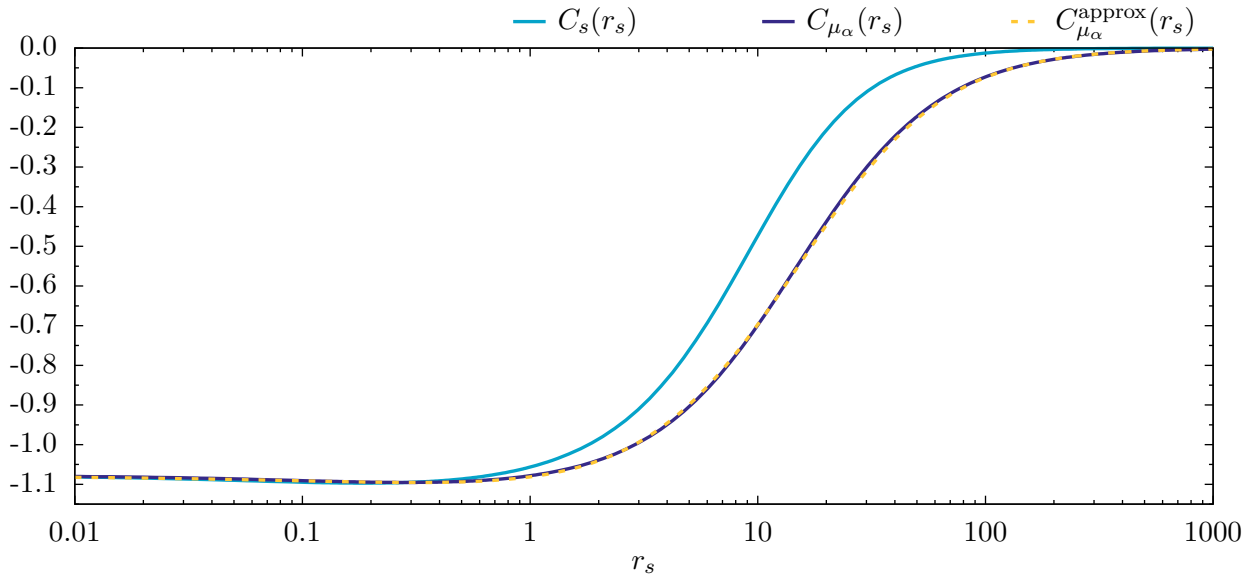


FIG. 3. Comparison of C_s , C_{μ_α} , and $C_{\mu_\alpha}^{\text{approx}}$ for $\mu_\alpha = 0.1049487$.

Parametrization of C_{μ_α}

For convenient implementation, we approximate the analytical solution, Eq. (59), for the value used in LAK, $\mu_\alpha = 0.1049487$, by

$$C_{\mu_\alpha}^{\text{approx}}(r_s) = C_s(0) \frac{1 + 0.1r_s^{0.65}}{(1 + 0.065r_s^{0.9})(1 + 0.03r_s^{1.2})}. \quad (62)$$

Here, $C_s(0) = -16\pi(3\pi^2)^{1/3}2.568/(3000\mu)$ is the high-density ($r_s \rightarrow 0$) limit of Eqs. (58) and (59). The other six parameters are obtained by fitting to the analytical solution for C_{μ_α} as given in Eq. (59) in the energetically important region $0 < r_s < 10$. In this region, the relative deviation $|C_{\mu_\alpha}^{\text{approx}} - C_{\mu_\alpha}|/C_{\mu_\alpha}$ remains well below 1%. Figure 3 shows the untransformed coefficient C_s , the transformed coefficient C_{μ_α} , and the approximated transformed coefficient $C_{\mu_\alpha}^{\text{approx}}$ as functions of the Wigner-Seitz radius r_s , i.e., their density dependence. As noted in the main text, C_s and C_{μ_α} are of the order of -1 in the energetically important region. Since C_s itself is a parametrization of numerical data, Eq. (62) is merely a parametrization of the transformed numerical data by simple functions that does not introduce additional noteworthy uncertainties.

REFERENCE TOTAL ATOMIC ENERGIES

In this section, we report LAK atomic energies. These are calculated self-consistently in ADF [16] with the numerical settings of Table III. To obtain total energies with ADF, we calculate the bare cores (no electrons) such that the ADF fragment is the sum of the core and the free electrons. Additionally, we apply the key `FragMetaGGAToten` to apply the accurate grid also to the fragment. Note, however, that ADF is tailored towards binding energies and not towards highly accurate total energies.

Table I reports reference total, exchange-correlation, exchange, and correlation energies for the nitrogen and neon atom, respectively. These can be used to check future implementations of LAK, with the above mentioned caveat about the accuracy of ADF for total energies.

Table II reports total atomic energies and corresponding exchange-correlation, exchange, and correlation energies of the rare gas atoms neon, argon, krypton, and xenon. For comparison, we also list the respective values for SCAN. Note that the limit of large atomic number for the rare-gas atoms is used as an appropriate norm in the construction of SCAN, but not in LAK. Table II shows that the exchange and correlation energies of LAK are nevertheless reasonable.

TABLE I. Reference total atomic energies and corresponding exchange(-correlation) energies in Hartree for the nitrogen and neon atom calculated self-consistently in ADF. LAKx denotes LAK exchange-only.

	LAK		LAKx	
	E	E_{xc}	E	E_x
N	-54.4406058165	-6.5385912464	-54.2056308070	-6.2961690583
Ne	-129.0724611872	-12.3982382510	-128.6846406935	-12.0028303080

TABLE II. Total atomic energies and corresponding exchange-correlation, exchange, and correlation energies in Hartree for the rare gas atoms Ne, Ar, Kr, and Xe calculated self-consistently in ADF. The reference values are from Ref. [1].

	Ne			Ar			Kr			Xe		
	E_{xc}	E_x	E_c	E_{xc}	E_x	E_c	E_{xc}	E_x	E_c	E_{xc}	E_x	E_c
SCAN	-12.507	-12.163	-0.344	-31.115	-30.424	-0.691	-97.466	-95.709	-1.757	-189.002	-186.102	-2.900
LAK	-12.398	12.010	-0.388	-30.751	-29.948	-0.803	-95.090	-93.950	-2.039	-186.138	-182.805	-3.333
Ref	-12.499	-12.108	-0.391	-30.911	-30.188	-0.723	-95.740	-93.890	-1.850	-182.200	-179.200	-3.000

NONCOVALENT INTERACTIONS AND NUMERICAL STABILITY

Figure 4 shows the potential energy curve of the argon dimer with LAK for different settings of `NumericalAccuracy` in ADF. For comparison, we also show the binding curves of M06-L [17] and a highly accurate CCSDT reference [18]. We recognize that LAK shows a minimum and thus binds the argon dimer. Similar binding curves are obtained for other noncovalently bound systems.

Regarding numerical stability, we observe that LAK does *not* show any oscillatory behavior like M06-L if the numerical accuracy is reduced. Instead, LAK is nicely converged in ADF with `Good` numerical accuracy. If, as recommended for many Meta-GGAs in ADF, the radial grid is boosted by a factor of three, even `Basic` (the lowest) numerical accuracy is sufficient for a converged Ar_2 binding curve. Therefore, we conclude that LAK is numerically stable and does not suffer from the long-standing numerical issues of other popular Meta-GGAs.

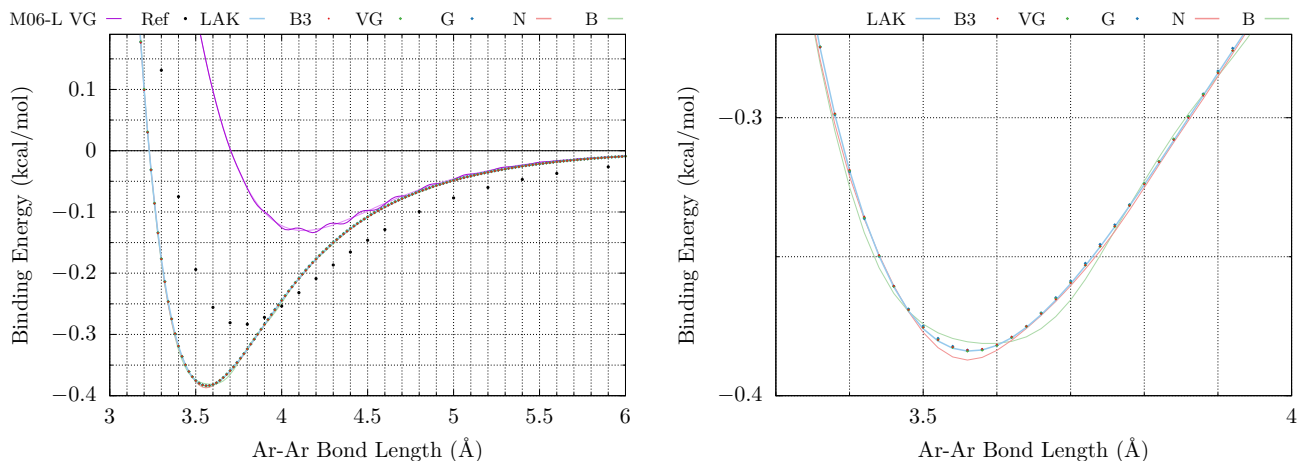


FIG. 4. Ar_2 potential energy curve for different settings of `NumericalAccuracy` in ADF [16]. B: `Basic`, N: `Normal`, G: `Good`, VG (and M06-L VG): `VeryGood`, B3: `Basic with RadialGridBoost 3.0`, LAK and M06-L: `Excellent with RadialGridBoost 3.0`. Ref denotes the CCSDT values from Ref. [18]. The right-hand side shows a zoom on the LAK equilibrium bond length.

COMPUTATIONAL DETAILS

In this Section we list the numerical settings that we have used to calculate the data reported in the main text. For the atomization energies, the interaction energies, and the bond lengths we used the code ADF [16, 19, 20] of the Amsterdam Modeling Suite. Our numerical settings are listed in Table III. These settings are extremely accurate in order to ensure highly accurate results. In practice, `Good` numerical accuracy and no radial grid boost (`RadialGridBoost 1.0`) should be sufficient, as we have shown at the example of the Ar_2 binding curve in the previous section.

TABLE III. Numerical settings used in the calculations for the MGAE109 [21] and MGBL20 [22] sets using the ADF package of the Amsterdam Modeling Suite.

key	MGAE109	MGBL20
NumericalQuality	Excellent	Excellent
BeckeGrid		
RadialGridBoost	3.0	3.0
Basis		
Type	QZ4P	QZ4P
Core	None	None
Relativity		
Level	Scalar	Scalar

For the lattice constants and band gaps we used the code BAND [20, 24–30] of the Amsterdam Modeling Suite. Our numerical settings are listed in Table IV. To check that these are sufficient, we compare them with results

TABLE IV. Numerical settings used in the calculations for the LC20 [23] and SCBG15 (defined below) sets using the BAND package of the Amsterdam Modeling Suite.

key	LC20	SCBG15
NumericalQuality	Good	Good
KSpace		
Type	Regular	Regular
Quality	Good	Good
BeckeGrid		
RadialGridBoost	1.0	1.0
Basis		
Type	QZ4P	TZ2P
Relativity		
Level	Scalar	Scalar
BandStructure		
Enabled	-	True
Automatic	-	False
DeltaK	-	0.02

obtained using increased numerical accuracy in Table V. There, we show the band gaps obtained for LAK with the default settings, with Spin-Orbit coupling (SOC) in the ZORA approximation, with the largest available basis set QZ4P, and with a RadialGridBoost (RGB) of 3 (which is the default for many meta-GGAs in ADF and BAND). It is well-established that (scalar) relativistic effects are important for calculations of lattice constants and band gaps for elements in the fourth row and below [31–33]. Additionally, for some systems studied here, the computationally much more expensive spin-orbit coupling is also important. It has the largest effect for systems that contain heavy elements. Within the SCBG15 set, systems with Te are most affected by Spin-Orbit coupling with differences to the scalar relativistic calculations of up to 0.28 eV for BeTe. While its effect is typically very similar for different functionals [33], we have included the results with scalar relativistic effects in the main text, because hybrid functionals with Spin-Orbit coupling are not available in BAND. Thus, we have to stick with scalar relativistic effects to make the results of the semilocal functionals comparable to HSE. Note that although the LC20 set contains several systems with heavy elements, the Spin-Orbit coupling appears to be less important for the lattice parameters than for the band gaps.

TABLE V. SCBG15 band gaps in eV with LAK for different computational settings. See text for explanations of the settings.

System	default	SOC	QZ4P	GB3	Expt.
Ge	0.83	0.74	0.84	0.83	0.74
Si	1.15	1.13	1.12	1.14	1.17
InP	1.69	1.67	1.68	1.69	1.42
CdTe	1.53	1.27	1.55	1.54	1.48
GaAs	1.57	1.47	1.57	1.57	1.52
AlSb	1.63	1.44	1.64	1.64	1.69
CdSe	1.55	1.43	1.55	1.55	1.73
AlAs	2.14	2.05	2.15	2.14	2.23
GaP	2.29	2.27	2.26	2.29	2.35
ZnTe	2.18	1.91	2.18	2.18	2.39
SiC	2.14	2.14	2.12	2.15	2.42
AIP	2.40	2.39	2.36	2.40	2.50
BeTe	2.54	2.26	2.53	2.54	2.80
ZnSe	2.39	2.27	2.38	2.39	2.82
ZnS	3.18	3.16	3.15	3.17	3.72
MSE	-0.12	-0.23	-0.13	-0.12	
MAE	0.18	0.26	0.19	0.18	
RMSE	0.23	0.32	0.24	0.23	
rel. MAE	8	11	9	8	%

Regarding the numerical accuracy, we observe that using a larger basis set or a finer radial Becke grid does not change the calculated band gaps significantly. The largest single difference is only 0.03 eV with the QZ4P basis set for the band gap of Si. We therefore conclude that our default settings are appropriate. Note that we did not use the QZ4P basis set for all calculations, because HSE with QZ4P is computationally extremely demanding and we chose to make different functionals directly comparable by using identical numerical settings whenever possible.

For the LC20 set calculations with HSE are computationally extremely demanding. Using a smaller basis set than TZ2P appears to give results far from the basis set limit. We therefore draw on literature data for the LC20 set with HSE and use the QZ4P basis set for all other functionals. A finer radial Becke grid (RGB of 3) does not change the lattice constants obtained with LAK by more than 0.001 Å. In Ref. 34 values for the MSE and MAE of HSE for the LC20 set are given. Unfortunately, it remains unclear how relativistic effects were taken into account there and no values for the individual systems are provided. Therefore, we take the values for the individual systems from Ref. 31. These are calculated with small-core relativistic effective core potentials. In Ref. 31 it is estimated that they differ from all-electron scalar-relativistic values by about 0.02 Å. Unfortunately, Ca, Sr, and Ba are not considered in Ref. 31. We therefore provide the error measures for both the full LC20 set and LC20 without Ca, Sr, and Ba in Table VII.

DETAILED RESULTS

Tables VI–IX list the detailed values of the bond lengths, atomization energies, lattice parameters, and band gaps discussed in the main text. RMSE denotes the root mean square error and rel. MAE the mean absolute error relative to the reference values. Table VIII defines the SCBG15 set of semiconductors with band gaps in the technologically relevant range of 0.5 to 4.0 eV. Figure 5 shows the limitations of semilocal DFT for systems where freedom from self-interaction is important at the examples of the H_2^+ and He_2^+ potential energy curves.

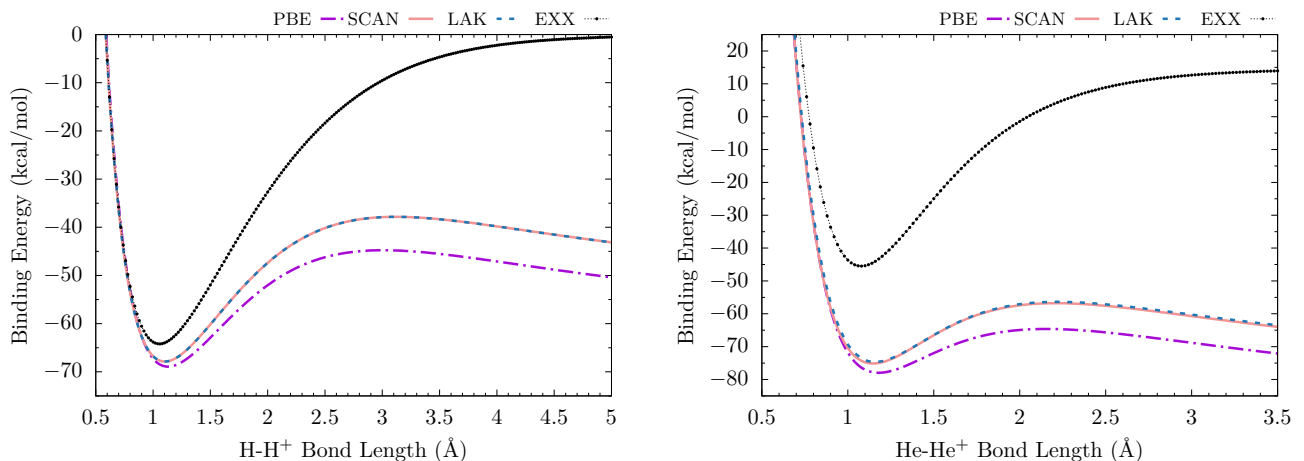


FIG. 5. Potential energy curves for H_2^+ and He_2^+ . All results calculated self-consistently in ADF [16] with QZ4P basis set.

* timo.lebeda@uni-bayreuth.de

† stephan.kuemmel@uni-bayreuth.de; <http://tp4.uni-bayreuth.de/en>

- [1] J. Sun, A. Ruzsinszky, and J. P. Perdew, Strongly constrained and appropriately normed semilocal density functional, *Phys. Rev. Lett.* **115**, 036402 (2015).
- [2] E. Engel and R. M. Dreizler, *Density Functional Theory*, 1st ed., Theoretical and Mathematical Physics (Springer, Berlin, Heidelberg, 2011).
- [3] M. Lewin, E. H. Lieb, and R. Seiringer, Improved Lieb–Oxford bound on the indirect and exchange energies, *Lett. Math. Phys.* **112**, 92 (2022).
- [4] J. P. Perdew and Y. Wang, Accurate and simple analytic representation of the electron-gas correlation energy, *Phys. Rev. B* **45**, 13244 (1992).

TABLE VI. MGBL20 [22] main group bond lengths in Å.

Molecule	PBE	SCAN	LAK	HSE	Ref.
H ₂	0.750	0.741	0.741	0.744	0.741
CH ₄ (C–H)	1.095	1.087	1.089	1.088	1.086
NH ₃ (N–H)	1.021	1.012	1.014	1.011	1.012
H ₂ O (O–H)	0.969	0.960	0.960	0.958	0.957
HF	0.931	0.920	0.920	0.918	0.917
OH	0.983	0.974	0.975	0.971	0.970
C ₂ H ₂ (C–H)	1.070	1.061	1.063	1.063	1.063
C ₂ H ₂ (C–C)	1.206	1.196	1.199	1.195	1.203
HCN (C–H)	1.074	1.066	1.067	1.067	1.065
HCN (C–N)	1.157	1.147	1.150	1.144	1.153
H ₂ CO (C–H)	1.117	1.107	1.110	1.107	1.102
H ₂ CO (C–O)	1.208	1.197	1.201	1.195	1.203
CO	1.135	1.125	1.129	1.122	1.128
N ₂	1.102	1.092	1.095	1.088	1.098
F ₂	1.414	1.400	1.403	1.379	1.412
CO ₂	1.171	1.158	1.162	1.156	1.160
N ₂ O (N–N)	1.137	1.125	1.128	1.117	1.128
N ₂ O (N–O)	1.190	1.180	1.183	1.175	1.184
Cl ₂	2.006	1.997	1.993	1.982	1.988
MgS	2.151	2.130	2.131	2.134	2.143
MSE	0.009	-0.002	-0.000	-0.005	
MAE	0.009	0.005	0.003	0.006	
RMSE	0.010	0.006	0.005	0.009	

- [5] J. P. Perdew, A. Ruzsinszky, J. Sun, and K. Burke, Gedanken densities and exact constraints in density functional theory, *J. Chem. Phys.* **140**, 18A533 (2014).
- [6] T. Aschebrock and S. Kümmel, Ultranonlocality and accurate band gaps from a meta-generalized gradient approximation, *Phys. Rev. Res.* **1**, 033082 (2019).
- [7] J. W. Furness, A. D. Kaplan, J. Ning, J. P. Perdew, and J. Sun, Accurate and numerically efficient r2SCAN meta-generalized gradient approximation, *J. Phys. Chem. Lett.* **11**, 8208 (2020).
- [8] J. T. Margraf, C. Kunkel, and K. Reuter, Towards density functional approximations from coupled cluster correlation energy densities, *J. Chem. Phys.* **150**, 244116 (2019).
- [9] E. H. Lieb and S. Oxford, Improved lower bound on the indirect coulomb energy, *Int. J. Quantum Chem.* **19**, 427 (1981).
- [10] S. Ivanov and M. Levy, Connections between high-density scaling limits of DFT correlation energies and second-order Z^{-1} quantum chemistry correlation energy, *J. Phys. Chem. A* **102**, 3151 (1998).
- [11] J. P. Perdew, K. Burke, and M. Ernzerhof, Generalized gradient approximation made simple, *Phys. Rev. Lett.* **77**, 3865 (1996).
- [12] S.-K. Ma and K. A. Brueckner, Correlation energy of an electron gas with a slowly varying high density, *Phys. Rev.* **165**, 18 (1968).
- [13] J. P. Perdew, A. Ruzsinszky, G. I. Csonka, O. A. Vydrov, G. E. Scuseria, L. A. Constantin, X. Zhou, and K. Burke, Restoring the density-gradient expansion for exchange in solids and surfaces, *Phys. Rev. Lett.* **100**, 136406 (2008).
- [14] M. Rasolt and D. J. W. Geldart, Exchange and correlation energy in a nonuniform fermion fluid, *Phys. Rev. B* **34**, 1325 (1986).
- [15] F. Oberhettinger, Hypergeometric functions, in *Handbook of Mathematical Functions with Formulas, Graphs, and Mathematical Tables*, Applied Mathematics Series, Vol. 55, edited by M. Abramowitz and I. A. Stegun (US Government printing office, Washington, D.C., 1964) pp. 555–566.
- [16] SCM, Theoretical Chemistry, Vrije Universiteit, Amsterdam, The Netherlands, *ADF 2022.102 (a modified version is used)* (2022).
- [17] Y. Zhao and D. G. Truhlar, A new local density functional for main-group thermochemistry, transition metal bonding, thermochemical kinetics, and noncovalent interactions, *J. Chem. Phys.* **125**, 194101 (2006).
- [18] B. Jäger, R. Hellmann, E. Bich, and E. Vogel, Ab initio pair potential energy curve for the argon atom pair and thermophysical properties of the dilute argon gas. I. Argon–argon interatomic potential and rovibrational spectra, *Mol. Phys.* **107**, 2181 (2009).
- [19] G. te Velde, F. M. Bickelhaupt, E. J. Baerends, C. Fonseca Guerra, S. J. A. van Gisbergen, J. G. Snijders, and T. Ziegler, Chemistry with ADF, *J. Comput. Chem.* **22**, 931 (2001).
- [20] E. Van Lenthe and E. J. Baerends, Optimized slater-type basis sets for the elements 1–118, *J. Comput. Chem.* **24**, 1142 (2003).

TABLE VII. LC20 [23] lattice constants in Å. *Individual values taken from Ref. 31. There, HSE values for all systems except for Ca, Sr, and Ba are available. These are calculated with a small-core relativistic effective core potential. **Taken from Ref. 34. There, no individual values are given and it remains unclear, if relativistic effects are taken into account.

System	PBE	SCAN	LAK	HSE*	Ref.
Li	3.444	3.476	3.482	3.460	3.453
Na	4.214	4.215	4.214	4.225	4.214
Ca	5.513	5.543	5.554	-	5.553
Sr	6.022	6.047	6.087	-	6.045
Ba	5.021	5.029	5.161	-	4.995
Al	4.033	4.018	3.989	4.022	4.018
Cu	3.584	3.496	3.623	3.638	3.595
Rh	3.848	3.784	3.874	3.783	3.794
Pd	3.929	3.873	4.013	3.921	3.876
Ag	4.114	4.080	4.246	4.142	4.062
C	3.572	3.548	3.574	3.549	3.553
SiC	4.383	4.355	4.376	4.347	4.346
Si	5.467	5.430	5.455	5.435	5.421
Ge	5.741	5.650	5.747	5.682	5.644
GaAs	5.783	5.632	5.724	5.687	5.640
LiF	4.064	3.966	3.989	4.018	3.972
LiCl	5.139	5.101	5.129	5.115	5.070
NaF	4.708	4.576	4.561	4.650	4.582
NaCl	5.692	5.574	5.570	5.659	5.569
MgO	4.256	4.195	4.207	4.210	4.189
LC20:					
MSE	0.047	-0.000	0.049	0.029**	
MAE	0.055	0.015	0.054	0.032**	
RMSE	0.069	0.026	0.076	-	
without Ca, Sr, and Ba:					
MSE	0.057	-0.002	0.046	0.032	
MAE	0.060	0.015	0.051	0.034	
RMSE	0.073	0.027	0.071	0.043	

- [21] R. Peverati and D. G. Truhlar, Communication: A global hybrid generalized gradient approximation to the exchange-correlation functional that satisfies the second-order density-gradient constraint and has broad applicability in chemistry, *J. Chem. Phys.* **135**, 191102 (2011).
- [22] R. Peverati and D. G. Truhlar, Quest for a universal density functional: the accuracy of density functionals across a broad spectrum of databases in chemistry and physics, *Philos. Trans. R. Soc. A* **372**, 20120476 (2014).
- [23] J. Sun, M. Marsman, G. I. Csonka, A. Ruzsinszky, P. Hao, Y.-S. Kim, G. Kresse, and J. P. Perdew, Self-consistent meta-generalized gradient approximation within the projector-augmented-wave method, *Phys. Rev. B* **84**, 035117 (2011).
- [24] G. te Velde and E. J. Baerends, Precise density-functional method for periodic structures, *Phys. Rev. B* **44**, 7888 (1991).
- [25] G. Wiesenekker and E. J. Baerends, Quadratic integration over the three-dimensional brillouin zone, *J. Phys. Condens. Matter* **3**, 6721 (1991).
- [26] M. Franchini, P. H. T. Philipsen, and L. Visscher, The Becke fuzzy cells integration scheme in the Amsterdam Density Functional program suite, *J. Comput. Chem.* **34**, 1819 (2013).
- [27] M. Franchini, P. H. T. Philipsen, E. van Lenthe, and L. Visscher, Accurate coulomb potentials for periodic and molecular systems through density fitting, *J. Chem. Theory Comput.* **10**, 1994 (2014).
- [28] E. v. Lenthe, E.-J. Baerends, and J. G. Snijders, Relativistic regular two-component Hamiltonians, *J. Chem. Phys.* **99**, 4597 (1993).
- [29] E. S. Kadantsev, R. Klooster, P. L. De Boeij, and T. Ziegler, The formulation and implementation of analytic energy gradients for periodic density functional calculations with STO/NAO Bloch basis set, *Mol. Phys.* **105**, 2583 (2007).
- [30] SCM, Theoretical Chemistry, Vrije Universiteit, Amsterdam, The Netherlands, *BAND 2023.104 (a modified version is used)* (2023).
- [31] J. Heyd, J. E. Peralta, G. E. Scuseria, and R. L. Martin, Energy band gaps and lattice parameters evaluated with the heyd-scuseria-ernzerhof screened hybrid functional, *J. Chem. Phys.* **123**, 174101 (2005).
- [32] Z. H. Yang, H. Peng, J. Sun, and J. P. Perdew, More realistic band gaps from meta-generalized gradient approximations: Only in a generalized Kohn-Sham scheme, *Phys. Rev. B* **93**, 205205 (2016).

TABLE VIII. SCBG15 band gaps of semiconductors in eV.

System	PBE	SCAN	LAK	HSE	Expt.
Ge	0.03	0.21	0.83	0.72	0.74
Si	0.61	0.85	1.15	1.17	1.17
InP	0.70	1.06	1.69	1.39	1.42
CdTe	0.78	1.08	1.53	1.53	1.48
GaAs	0.53	0.81	1.57	1.29	1.52
AlSb	1.23	1.40	1.63	1.99	1.69
CdSe	0.65	1.05	1.55	1.46	1.73
AlAs	1.47	1.76	2.14	2.24	2.23
GaP	1.64	1.87	2.29	2.28	2.35
ZnTe	1.29	1.63	2.18	2.19	2.39
SiC	1.42	1.73	2.14	2.36	2.42
AlP	1.64	1.95	2.40	2.52	2.50
BeTe	1.99	2.26	2.54	2.64	2.80
ZnSe	1.29	1.79	2.39	2.28	2.82
ZnS	2.10	2.63	3.18	3.23	3.72
MSE	-0.91	-0.59	-0.12	-0.11	
MAE	0.91	0.59	0.18	0.17	
RMSE	0.96	0.64	0.23	0.24	
rel. MAE	47	31	8	7	%

- [33] T. Lebeda, T. Aschebrock, J. Sun, L. Leppert, and S. Kümmel, Right band gaps for the right reason at low computational cost with a meta-GGA, *Phys. Rev. Mater.* **7**, 093803 (2023).
- [34] S. Jana, B. Patra, S. Śmiga, L. A. Constantin, and P. Samal, Improved solid stability from a screened range-separated hybrid functional by satisfying semiclassical atom theory and local density linear response, *Phys. Rev. B* **102**, 155107 (2020).

TABLE IX. MGAE109 [21] main group atomization energies in kcal/mol.

Molecule	PBE	SCAN	LAK	HSE	Expt.
CH	84.6	82.2	81.4	82.8	84.2
CH ₂ (3B1.)	194.4	197.1	196.3	193.2	190.8
CH ₂ (1A1.)	178.8	175.8	177.0	175.9	181.5
CH ₃	309.8	312.7	312.3	307.6	307.9
CH ₄	419.8	420.0	421.6	416.6	420.4
C ₂ H ₂	414.7	402.5	398.7	403.2	405.5
C ₂ H ₄	571.1	563.4	562.5	562.0	563.7
C ₂ H ₆	716.3	713.9	715.2	709.7	713.0
HCO	294.6	282.4	280.2	279.0	279.4
H ₂ CO	385.2	373.6	373.0	370.7	374.7
CH ₃ OH	519.3	513.1	513.3	507.8	513.5
HCN	326.0	307.5	303.7	310.0	313.4
NH ₂ NH ₂	452.4	433.9	433.1	436.2	438.6
CH ₃ Cl	399.5	395.9	397.2	393.7	396.4
CH ₃ SH	477.7	474.9	477.8	471.2	474.5
C ₃ H ₄ (pro.)	720.5	705.5	701.5	705.5	705.1
C ₄ H ₄ O	1029.7	1002.9	993.1	1000.3	994.3
C ₄ H ₄ S	995.4	971.5	965.4	971.3	963.6
C ₄ H ₅ N	1109.6	1078.9	1068.5	1081.6	1071.9
C ₄ H ₆ (tra.)	1033.5	1016.1	1012.5	1014.4	1012.7
C ₄ H ₆ (yne.)	1024.9	1006.9	1002.7	1006.4	1004.5
C ₅ H ₅ N	1283.5	1247.2	1236.3	1250.1	1238.1
CCH	276.7	266.5	261.8	265.6	265.3
CH ₂ OH	421.0	414.9	413.4	409.1	410.1
CH ₃ CN	635.0	613.9	609.8	615.7	616.0
CH ₃ NH ₂	590.4	580.7	580.4	579.2	582.3
CH ₃ NO ₂	640.2	607.1	605.8	601.8	601.8
CHCl ₃	358.2	346.3	347.5	345.4	345.8
CHF ₃	477.0	459.9	455.7	455.6	458.7
CH ₂ CH	457.5	451.3	448.5	448.3	446.1
HCOOCH ₃	809.6	791.5	788.1	782.4	785.9
HCOOH	521.1	503.8	501.9	497.6	501.5
C ₂ H ₅	611.5	611.0	610.3	605.3	603.9
C ₄ H ₆ (bic.)	1010.9	992.6	988.5	993.6	987.6
C ₄ H ₆ (cyc.)	1023.2	1005.5	1000.5	1005.2	1002.0
HCOCOH	661.7	636.3	633.4	631.8	634.0
CH ₃ CHO	693.5	679.7	678.8	675.3	677.4
C ₂ H ₄ O	669.1	655.2	653.1	651.0	651.1
C ₂ H ₅ O	709.6	703.1	701.3	695.4	699.0
CH ₃ OCH ₃	808.8	801.4	800.3	793.4	798.5
CH ₃ CH ₂ OH	820.5	812.3	812.3	805.5	810.8
C ₃ H ₄ (all.)	723.4	707.5	703.9	707.0	703.5
C ₃ H ₄ (cyc.)	701.1	683.7	680.8	686.0	683.0
CH ₃ COOH	826.5	807.8	805.5	800.1	803.7
CH ₃ COCH ₃	998.8	983.4	982.2	977.3	978.5
C ₃ H ₆	867.6	857.3	855.8	856.1	853.7
CH ₃ CHCH ₂	872.9	862.9	861.7	860.2	860.9
C ₃ H ₈	1014.3	1009.9	1010.8	1004.4	1007.1
C ₂ H ₅ OCH ₃	1110.0	1100.6	1099.3	1091.2	1095.6
C ₄ H ₁₀ (iso.)	1313.1	1307.2	1307.9	1299.8	1303.4
C ₄ H ₁₀ (anti.)	1312.3	1305.9	1306.5	1299.0	1301.7
C ₄ H ₈ (cyc.)	1166.5	1154.8	1152.1	1151.5	1149.4
C ₄ H ₈ (iso.)	1174.5	1162.7	1161.2	1158.4	1159.0
C ₅ H ₈ (spi.)	1314.6	1293.7	1289.5	1294.1	1284.7
C ₆ H ₆	1408.0	1378.7	1369.2	1379.9	1368.1
CH ₃ CO	602.8	588.2	585.4	583.6	582.0
CH ₃ CHCH ₃	913.6	910.3	909.3	903.6	901.0
C ₄ H ₉ (t.)	1215.6	1209.9	1208.8	1201.9	1199.7
CH ₂ CO	557.4	538.5	535.1	535.8	532.7

Continued on next page.

Molecule	PBE	SCAN	LAK	HSE	Expt.
CN	196.9	177.4	172.1	177.8	181.4
CO	268.4	254.7	253.1	254.1	259.7
N ₂	243.0	218.6	215.5	224.3	228.5
NO	171.4	150.7	149.3	151.8	152.8
O ₂	142.9	127.6	130.0	122.7	120.8
F ₂	52.7	36.9	38.0	34.4	39.0
CO ₂	415.1	393.3	391.2	389.3	390.2
Si ₂	79.3	75.5	70.6	73.2	76.4
P ₂	120.9	111.3	107.2	111.0	117.6
S ₂	114.5	108.5	110.0	105.9	104.2
Cl ₂	65.2	57.4	59.1	58.7	59.8
SiO	196.4	187.8	184.8	182.7	193.1
SC	179.4	167.5	166.7	167.2	171.8
SO	140.6	131.9	132.2	126.0	126.5
ClO	81.1	69.6	68.9	66.3	65.5
CIF	72.0	60.9	61.4	60.4	62.8
SO ₂	279.5	260.7	260.2	251.5	260.6
AlCl ₃	304.5	310.7	314.1	302.4	312.6
AlF ₃	426.6	422.3	423.4	412.9	430.9
BCl ₃	334.3	330.9	333.3	326.5	325.4
BF ₃	480.2	469.7	468.6	464.5	471.0
C ₂ Cl ₄	499.5	475.8	474.1	476.5	469.8
C ₂ F ₄	628.2	595.3	586.2	592.0	591.1
CCl ₄	332.3	316.4	317.6	315.5	316.2
CF ₃ CN	678.7	640.5	631.0	640.0	641.2
CF ₄	500.7	479.1	473.7	474.5	477.9
CIF ₃	165.0	138.6	135.8	129.4	127.3
NF ₃	243.4	209.9	208.4	207.0	205.7
PF ₃	373.8	360.6	356.1	354.3	365.0
SiCl ₄	383.5	386.7	388.7	378.1	388.7
SiF ₄	570.3	565.6	564.2	554.2	576.3
NH	88.4	84.9	82.7	85.1	83.1
NH ₂	188.5	184.4	183.6	182.7	182.6
NH ₃	301.7	294.4	295.1	294.1	298.0
OH	109.8	109.0	109.6	105.3	107.2
H ₂ O	234.0	229.3	231.2	226.2	233.0
HF	141.9	136.8	137.8	136.4	141.6
SiH ₂ (1A1.)	147.6	149.1	150.0	147.0	152.2
SiH ₂ (3B1.)	131.1	137.9	139.5	131.5	131.5
SiH ₃	221.8	230.0	232.5	222.7	228.0
SiH ₄	312.8	322.8	324.8	314.4	324.9
PH ₂	154.1	156.2	156.9	152.6	153.2
PH ₃	238.6	241.1	242.5	236.5	242.3
H ₂ S	181.7	181.8	185.0	179.1	183.9
HCl	106.2	105.2	107.1	104.4	107.5
NH ₂ NH ₂	452.4	433.9	433.1	436.2	438.6
H ₂ O ₂	281.5	267.4	269.5	261.6	269.0
Si ₂ H ₆	518.8	534.6	537.8	520.8	535.9
HOCl	174.9	164.1	165.9	161.7	166.2
H ₂	104.6	107.7	108.9	104.3	109.5
SH	87.8	88.4	90.1	86.4	87.0
MSE	12.4	1.4	-0.0	-1.9	
MAE	13.9	3.8	3.5	4.0	
RMSE	17.4	4.6	4.5	5.5	

Acknowledgments

I owe my deepest gratitude to numerous people that accompanied me during the process of creating this thesis. In particular, I wish to thank:

- **Stephan Kümmel** for being a great supervisor both from a scientific and human point of view. I am deeply grateful for his unwavering support and confidence in me and my work, especially in difficult times during the Covid epidemic, and for providing me extensive freedom in choosing the direction of my research.
- **Jianwei Sun** for his support, many fruitful discussions and his warm welcome into his working group during my research stay in New Orleans.
- **All former and current members of the Theoretical Physics IV group** for the great atmosphere and the unconditional mutual helpfulness. In particular, I would like to thank **Moritz Brütting, Sophie Meißner, Alexander Kaiser, Thomas Trepl, and Rian Richter** for carefully proofreading the manuscript of this dissertation. Moreover, it has been a pleasure to share an office first with **Julian Garhammer** and **Fabian Hofmann** and later with **Sophie Meißner** and **Matthias Knodt**.
- All the lovely people who made my time in Bayreuth such a wonderful time, especially **Rebecca Benelli, Sebastian Krauß, and Michael Cosacchi**.
- **Rebecca** for being the best friend I could have ever imagined.
- My parents **Ursula** and **Norbert** for always supporting me throughout the years in every possible way.
- My wife **Flora** for her love and support in good and in difficult times.
- My children **Janus** and **Luna** for just being who they are and for always being a source of joy and motivation for me :)

Eidesstattliche Versicherung

Hiermit versichere ich an Eides statt, dass ich die vorliegende Arbeit selbstständig verfasst und keine anderen als die von mir angegebenen Quellen und Hilfsmittel verwendet habe.

Weiterhin erkläre ich, dass ich die Hilfe von gewerblichen Promotionsberatern bzw. -vermittlern oder ähnlichen Dienstleistern weder bisher in Anspruch genommen habe, noch künftig in Anspruch nehmen werde.

Zusätzlich erkläre ich hiermit, dass ich keinerlei frühere Promotionsversuche unternommen habe.

Bayreuth, den 13.12.2024

Timo Lebeda